Universität Rostock Traditio et Innovatio

Kumulative Dissertation
zur
Erlangung des akademischen Grades
doctor rerum naturalium (Dr. rer. nat.)
der Mathematisch-Naturwissenschaftlichen Fakultät
der Universität Rostock

Benchmarking time-dependent renormalized natural orbital theory with exact solutions for a laser-driven model helium atom

vorgelegt von

Mārtiņš Brics

geb. am 23.10.1985 in Riga

aus Riga, Lettland

Rostock, 24.08.2016
angefertigt an der
Universität Rostock, Institut für Physik
AG Quantentheorie und Vielteilchensysteme

urn:nbn:de:gbv:28-diss2017-0008-7

Adresse: Universität Rostock
Institut für Physik
18051 Rostock
Tel: +49 381 498-6955
Fax: +49 381 498-6942
Internet: http://www.physik.uni-rostock.de/qtmps/

E-Mail des Betreuers: dieter.bauer@uni-rostock.de
E-Mail des Authors: martins.brics2@uni-rostock.de

1. **Gutachter:** Prof. Dr. Dieter Bauer
Institut für Physik, Universität Rostock

2. **Gutachter:** Prof. Dr. Neepa T. Maitra
Department of Physics and Astronomy,
Hunter College of the City University of New York

Datum der Einreichung: 26.08.2016
Datum der Verteidigung: 09.12.2016

Abstract

Intense, ultra-short laser pulses interacting with atoms, molecules, clusters, and solids give rise to many new fascinating phenomena, not at all accessible to quantum mechanics textbook perturbation theory. A full numerical solution of the time-dependent Schrödinger equation (TDSE) for such strong-field problems is also impossible for more than two electrons. Hence, powerful time-dependent quantum many-body approaches need to be developed. Unfortunately, efficient methods such as time-dependent density functional theory (TDDFT) fail in reproducing experimental observations, in particular if strong correlations are involved. In TDDFT, the approximation not only lies in the so-called exchange correlation potential but also in the density functionals for the observables of interest. In fact, with just the single-particle density alone it is unclear how to calculate, e.g., multiple-ionization probabilities or photoelectron spectra, or, even worse, correlated photoelectron spectra, as measured in nowadays experiments.

In general, the simple structure of the time-dependent many-body Schrödinger equation for a highly-dimensional many-body wavefunction can only be traded for more complicated equations of motion for simpler quantities. In this thesis, a theory is examined that goes one step beyond TDDFT as far as the complexity of the propagated quantity is concerned. In time-dependent renormalized natural orbital theory (TDRNOT), the basic quantities that are propagated in time are the eigenvalues and eigenstates of the one-body reduced density matrix (1-RDM). The eigenstates are called natural orbitals (NOs), the eigenvalues are the corresponding occupation numbers (ONs). Compared to TDDFT, the knowledge of the NOs and the ONs relax the problem of calculating observables in practice because they can be used to construct the 1-RDM and the two-body reduced density matrix (2-RDM).

After the derivation of the equations of motion for a combination of NOs and ONs, the so-called renormalized natural orbitals (RNOs), TDRNOT is benchmarked with the help of a numerically exactly solvable model helium atom in laser fields. In the special case of time-dependent two-electron systems the two-particle density matrix in terms of ONs and NOs is known exactly. Hence, in this case TDRNOT is exact, apart from the unavoidable truncation of the number of RNOs per particle taken into account in the simulation.

It is shown that, unlike TDDFT, TDRNOT is able to describe doubly-excited states, Fano profiles in electron and absorption spectra, auto-ionization, Rabi oscillations, high harmonic generation, non-sequential ionization, and single-photon double ionization in excellent agreement with the corresponding TDSE results.

Zusammenfassung

Die Wechselwirkung intensiver, ultrakurzer Laserpulse mit Atomen, Molekülen, Clustern und Festkörpern bringt viele neue, faszinierende Phänomene hervor, die nicht den aus Quantenmechaniklehrbüchern bekannten Näherungsverfahren zugänglich sind. Auch eine volle, numerische Lösung der zeitabhängigen Schrödinger-Gleichung (TDSE) für solche Starkfeldprobleme ist für mehr als zwei Elektronen nicht möglich. Daher müssen mächtige zeitabhängige Quantenvielteilchenmethoden entwickelt werden. Leider sind effiziente Verfahren wie zeitabhängige Dichtefunktionaltheorie (TDDFT) nicht in der Lage die experimentellen Beobachtungen zu reproduzieren, insbesondere wenn starke Korrelationen involviert sind. Die Näherung in TDDFT besteht nicht nur im sog. Austauschkorrelationspotential, sondern auch in den Dichtefunktionalen für die interessierenden Observablen. In der Tat ist unklar, wie man mit der Einteilchendichte alleine beispielsweise Vielfachionisationswahrscheinlichkeiten oder Photoelektronenspektren berechnen kann. Noch schwieriger wird dies bei differentielleren Observablen, wie z.B. bei den heutzutage messbaren korrelierten Photoelektronenspektren.

Im Allgemeinen handelt man sich im Gegensatz zur einfachen Struktur der zeitabhängigen Vielteilchen-Schrödinger-Gleichung für eine hochdimensionale Vielteilchenwellenfunktion eine kompliziertere Bewegungsgleichung ein, wenn man eine einfachere Größe zeitentwickeln möchte. In dieser Arbeit wird eine Theorie untersucht, die einen Schritt über TDDFT hinsichtlich der zu propagierenden Größe hinausgeht. In der Theorie der zeitabhängigen, renormalisierten natürlichen Orbitale (TDRNOT) werden die Eigenwerte und die Eigenvektoren der reduzierten Einteilchendichtematrix (1-RDM) in der Zeit propagiert. Die Eigenvektoren heißen natürliche Orbitale (NOs), die Eigenwerte sind die zugehörigen Besetzungszahlen (ONs). Die Kenntnis der NOs und ONs entspannt im Vergleich zu TDDFT in der Praxis das Problem, Observable zu berechnen, da sie zur Konstruktion der 1-RDM und der reduzierten Zweiteilchendichtematrix (2-RDM) verwendet werden können.

Nach der Herleitung der Bewegungsgleichung für eine Kombination aus NOs und ONs, den sog. renormalisierten natürlichen Orbitalen (RNOs), wird TDRNOT mithilfe eines numerisch exakt lösbaren Modellheliumatoms in Laserfeldern getestet. Im Spezialfall von zeitabhängigen Zweielektronensystemen ist die Zweiteilchendichtematrix, ausgedrückt durch ONs und NOs, exakt bekannt. Daher ist in diesem Fall TDRNOT exakt, abgesehen von der unvermeidlichen Beschränkung in der Anzahl der RNOs pro Teilchen, die in der Simulation berücksichtigt werden.

Es wird gezeigt, dass im Unterschied zu TDDFT, TDRNOT in der Lage ist, doppelt angeregte Zustände, Fano-Profile in Elektronen- und Absorptionsspektren, Autoionisation, Rabi-Oszillationen, die Erzeugung hoher Harmonischer, nichtsequentielle Ionisation sowie Einphotonen-Doppelionisation in exzellenter Übereinstimmung mit den entsprechenden TDSE-Resultaten zu beschreiben.

Contents

List of Abbreviations

APSGs	anti-symmetrized product of strongly orthogonal geminals
DFT	density functional theory
DM	density matrix
EOM	equation of motion
GGA	generalized gradient approximation
HHG	high harmonic generation
HF	Hartree–Fock
KS	Kohn–Sham
LDA	local density approximation
LSDA	local spin-density approximation
MCHF	multiconfiguration Hartree-Fock
MCTDHF	multiconfiguration time-dependent Hartree-Fock
NO	natural orbital
NSDI	non-sequential double ionization
ON	occupation number
PNOF	Piris natural orbital functional
RDM	reduced density matrix
RK	Runge-Kutta
RK4	Runge-Kutta's fourth order method
RK54	adaptive Runge-Kutta's fifth order method (4th order for error estimation)
RNO	renormalized natural orbital
SPDI	single-photon double ionization
TDDFT	time-dependent density functional theory
TDHF	time-dependent Hartree–Fock
TDKS	time-dependent Kohn–Sham
TDRNOT	time-dependent renormalized natural orbital theory
TDSE	time-dependent Schrödinger equation
m-RNO	TDRNOT calculation with m RNOs
n-RDM	n-body reduced density matrix

1. Introduction

If one wants to describe an atom or molecule interacting with light "exactly" one has to solve the time-dependent Schrödinger, or, in the relativistic case, Dirac, Pauli, or Klein-Gordon equation, possibly in second quantization and with a quantized electromagnetic field. Unfortunately, in full dimensionality and with strong, long-wavelength lasers even the simplest case of the time-dependent Schrödinger equation (TDSE) and non-quantized, linearly polarized electromagnetic field in dipole approximation is solvable at most for two particles [102]. However, most experiments in the intense-laser, ultra-short pulse regime are performed on many-electron targets [85, 93]. Thus, efficient time-dependent many-body methods are in great demand.

In practice, there are approximate methods like time-dependent density functional theory (TDDFT) which allows to treat moderate-sized molecules interacting with strong and short laser pulses [93]. However, there are several effects which are not properly described in practice within TDDFT. One example is that doubly excited states [68] are missing with standard exchange-correlation functionals available in the literature. There are other wavefunction-based approaches which perform generally better [45, 49]. However, such methods are more demanding. One of them is multi-configurational time-dependent Hartree-Fock (MCTDHF) [46, 101], or variants of it, which allow to treat small molecules made of few-electron atoms (in Born-Oppenheimer approximation) [82, 84]. Another one is time-dependent configuration interaction (TDCI) [38, 50, 74] and related approaches [6, 44, 47].

In this thesis, we introduce time-dependent renormalized natural orbital theory (TDRNOT) as a novel method. TDRNOT is based on the propagation of the one-body reduced density matrix (1-RDM), more precisely its eigenvalues and eigenstates. TDRNOT is also an in principle exact method. One can formally relate this method to TDCI and MCTDHF, as one can always formally expand any wavefunction in terms of the eigenstates of the 1-RDM. Thus TDRNOT should perform quite similar to TDCI and MCTDHF. It could be more efficient though because natural orbitals should be a particularly adequate single-particle basis [35].

This cumulative thesis is outlined as follows: after a brief introduction of (TD)DFT in Sec. 1.1, reduced density matrices and their equations of motion are discussed in Sec. 1.2. Renormalized natural orbitals (RNOs) are introduced in Sec. 1.3. In this section, also equations of motion for RNOs are derived, and known approximations for the two-body reduced density matrix in terms of these RNOs are given. The model helium atom, its ground state and the linear response spectrum are described in Sec. 1.4. There are also

TDRNOT results for the helium model presented that are not included in the published papers, summarized in Sec. 1.5. A conclusion and an outlook is given in Sec. 1.6.

Atomic units (a.u.) are used throughout, unless noted otherwise.

1.1. Density functional theory

Nobel prize-winning [54] density functional theory (DFT) has become the most utilized method for groundstate property calculations of many-body systems such as atoms and molecules [24]. The main advantage over earlier techniques, such as Hartree–Fock (HF) and other approaches based on the many-body wavefunction, is the lower computational cost, which allows to treat much larger systems.

DFT is based on the Hohenberg-Kohn theorem [48], published in 1964, which states that, for a given particle interaction, the external potential $V_{\mathrm{ext}}(\boldsymbol{r})$ determines uniquely the single-particle groundstate density $n_0(\boldsymbol{r})$. As a consequence, all observables are, in principle, determined by $n_0(\boldsymbol{r})$. Kohn and Sham [55] proposed a practical scheme to calculate $n_0(\boldsymbol{r})$ by introducing a fictitious non-interacting system, generating the same single-particle density.

Suppose we have a system of N interacting particles with the Hamiltonian

$$\hat{H} = \sum_{i=1}^{N} \hat{T}_i + \sum_{i=1}^{N} V_{\mathrm{ext}}(\hat{\boldsymbol{r}}_i) + \sum_{i<j}^{N} V_{\mathrm{ee}}(\hat{\boldsymbol{r}}_i, \hat{\boldsymbol{r}}_j), \tag{1.1}$$

where $\hat{T}_i$ is kinetic energy of the i-th electron, $V_{\mathrm{ext}}(\hat{\boldsymbol{r}}_i)$ is the external potential, and $V_{\mathrm{ee}}(\hat{\boldsymbol{r}}_i, \hat{\boldsymbol{r}}_j)$ is the electron-electron interaction potential. The Hohenberg-Kohn theorem states that for any such system—given the particle interaction $V_{\mathrm{ee}}(\hat{\boldsymbol{r}}_i, \hat{\boldsymbol{r}}_j)$—the external potential $V_{\mathrm{ext}}(\hat{\boldsymbol{r}}_i)$ is determined uniquely (up to a constant) by the groundstate single-particle density $n_0(\boldsymbol{r})$, and vice versa. This means that the single-particle density of the groundstate determines the Hamiltonian up to a constant energy shift. Therefore the single-particle density of the groundstate uniquely determines all properties of the system completely, and any groundstate observable is a functional of the single-particle density.

Following Kohn and Sham, we assume that one can construct a system without electron-electron interaction that generates the same single-particle density. The problem then separates into N single-electron TDSE-like equations

$$\left(-\frac{1}{2}\nabla^2 + \hat{V}_{\mathrm{KS}}(\boldsymbol{r})\right)\varphi_i(\boldsymbol{r}) = \varepsilon_i \varphi_i(\boldsymbol{r}), \quad \text{for } i = 1, 2, \ldots, N. \tag{1.2}$$

Here, $\hat{V}_{\mathrm{KS}}(\boldsymbol{r})$ is the Kohn-Sham potential, i.e., the external potential for this fictitious system, ε_i is the eigenvalue, called the Kohn-Sham orbital energy, and $\varphi_i(\boldsymbol{r})$ is the eigenfunction, known as the Kohn-Sham orbital. The single-particle density in terms of the

Kohn-Sham orbitals reads

$$n_0(\boldsymbol{r}) = \sum_{i=1}^{N} |\varphi_i(\boldsymbol{r})|^2. \tag{1.3}$$

The "task" of the Kohn-Sham potential is to yield the same groundstate density $n_0(\boldsymbol{r})$ as the original, interacting system. Unfortunately, it is unknown how to calculate the Kohn-Sham potential in general. Formally it is defined as

$$\hat{V}_{\mathrm{KS}}(\boldsymbol{r}) = V_{\mathrm{ext}}(\boldsymbol{r}) + V_{\mathrm{H}}(\boldsymbol{r}) + \hat{V}_{\mathrm{xc}}(\boldsymbol{r}), \tag{1.4}$$

where $V_{\mathrm{ext}}(\boldsymbol{r})$ is the external potential of the original system,

$$V_{\mathrm{H}}(\boldsymbol{r}) = \int \mathrm{d}^3 r' \frac{n_0(\boldsymbol{r}')}{|\boldsymbol{r} - \boldsymbol{r}'|} \tag{1.5}$$

is the Hartree potential, and the exchange-correlation potential is the variational derivative of the exchange-correlation energy density functional $E_{\mathrm{xc}}[n_0(\boldsymbol{r})]$,

$$\hat{V}_{\mathrm{xc}}(\boldsymbol{r}) = \frac{\delta E_{\mathrm{xc}}[n(\boldsymbol{r})]}{\delta n_0(\boldsymbol{r})}. \tag{1.6}$$

The exact exchange-correlation energy functional is unknown so that one has to use approximations in practice. This is the point where, although DFT in principle is exact, in practice it becomes an approximation.

1.1.1. Time-dependent density functional theory

Since DFT is so successful in describing groundstate properties, a natural question arises regarding whether this concept is also extendable to time-dependent problems. This question is answered affirmatively by the Runge-Gross theorem [80], which led to time-dependent density functional theory (TDDFT) [92, 94].

The Runge-Gross theorem shows that, given an initial state $|\Phi(0)\rangle$, there exists a unique one-to-one mapping between the external potential $V_{\mathrm{ext}}(\boldsymbol{r}, t)$ and the single-particle density $n(\boldsymbol{r}, t)$ if the external potential $V_{\mathrm{ext}}(\boldsymbol{r}, t)$ can be expanded in a Taylor series around the initial time t_0,

$$V_{\mathrm{ext}}(\boldsymbol{r}, t) = \sum_{i=0}^{\infty} \frac{v_i(\boldsymbol{r})}{i!} \left(t - t_0\right)^k. \tag{1.7}$$

If the system is initially in the groundstate, then the initial-state dependence simplifies to a groundstate-density dependence, thanks to the Hohenberg-Kohn theorem.

Also the Kohn-Sham approach can be extended to the time-dependent case. This is possible due to the van-Leeuwen theorem [62], which states that for every density $n(\boldsymbol{r}, t)$, evolving from a given initial state $|\Phi(0)\rangle$ under a given electron-electron interaction V_{ee}

and external potential $V_{\mathrm{ext}}(\boldsymbol{r},t)$, there exists another external potential $V'_{\mathrm{ext}}(\boldsymbol{r},t)$, another particle interaction V'_{ee}, and some initial state $|\Phi'(0)\rangle$ leading to the same density $n(\boldsymbol{r},t)$. This is a generalization of the Runge-Gross theorem, but it requires that not only the external potential but also the density is expandable in a Taylor series around the initial time t_0. One may argue that densities $n(\boldsymbol{r},t)$ which cannot be expanded in a Taylor series around the initial time t_0 can be considered as pathological cases. However, it turns out that this situation is actually common in real-world systems [66, 99] so that a more general proof would be desirable. Ignoring these mathematical subtleties for the moment, the time-dependent Kohn-Sham approach amounts to solve the equations

$$i\partial_t\varphi_j(\boldsymbol{r},t) = \left[-\frac{\nabla^2}{2} + \hat{V}_{\mathrm{KS}}(\boldsymbol{r},t)\right]\varphi_j(\boldsymbol{r},t), \tag{1.8}$$

with

$$\hat{V}_{\mathrm{KS}}[n(\boldsymbol{r}',t'),\,\Phi_0,\,\Phi'_0](\boldsymbol{r},t) = V_{\mathrm{ext}}(\boldsymbol{r},t) + V_{\mathrm{H}}(\boldsymbol{r},t) + \hat{V}_{\mathrm{xc}}[n(\boldsymbol{r}',t'),\,\Phi_0,\,\Phi'_0](\boldsymbol{r},t), \tag{1.9}$$

and

$$n(\boldsymbol{r},t) = \sum_{i=1}^{N}|\varphi_i(\boldsymbol{r},t)|^2. \tag{1.10}$$

Here, Φ_0 is the initial state of the interacting system and Φ'_0 is the initial state of the Kohn-Sham system. The exchange-correlation potential $\hat{V}_{\mathrm{xc}}[n(\boldsymbol{r}',t')](\boldsymbol{r},t)$ is, in general, onlocal in space and time, as indicated by different time and space arguments $\boldsymbol{r}'$, t'. If one starts from the groundstate the situation is simplified as the exchange-correlation functional can be written as a density functional only, $\hat{V}_{\mathrm{xc}}[n(\boldsymbol{r}',t')](\boldsymbol{r},t)$. However, even for this case the exact exchange-correlation functional is unknown and one has to apply approximations.

In the so-called adiabatic approximation nonlocality in time is ignored, i.e.,

$$\hat{V}_{\mathrm{xc}}[n(\boldsymbol{r}',t')](\boldsymbol{r},t) = \hat{V}^{gs}_{\mathrm{xc}}[n_0(\boldsymbol{r}')]\Big|_{n_0(\boldsymbol{r}')=n(\boldsymbol{r}',t')}. \tag{1.11}$$

$\hat{V}^{gs}_{\mathrm{xc}}$ is the groundstate exchange-correlation potential, evaluated at the instantaneous density. However, adiabatic approximations are known to have certain deficiencies, e.g., a lack of doubly-excited states [68], improper charge transfer [29, 31], or Rabi oscillations [30, 43, 79]. There are very few functionals with memory effects, i.e., with dependence on density (or Kohn-Sham orbitals) at earlier times [58, 59, 95, 96], which illustrates the difficulty in "designing" such functionals. As there is the more memory involved the more reduced quantities are propagated [67], the obvious idea would be to propagate less reduced quantities than Kohn-Sham orbitals. The most obvious candidates are reduced density matrices.

1.2. Reduced density matrices

Even if one could solve the N-particle TDSE

$$i\partial_t |\Phi(t)\rangle = \hat{H}(t)|\Phi(t)\rangle \tag{1.12}$$

of a large system, it is not desirable in practice as the wavefunction is a by far too high-dimensional object to store and analyze for larger N.

The N-particle density matrix (DM) of a pure state is defined as

$$\hat{\gamma}_N(t) = |\Phi(t)\rangle\langle\Phi(t)|. \tag{1.13}$$

Assuming that all particles are of the same type, the q-th order RDM (q-RDM) for $0 < q < N$ is

$$\hat{\gamma}_q(t) = \binom{N}{q} \mathrm{Tr}_{q+1,\ldots,N} \hat{\gamma}_n(t), \tag{1.14}$$

where $\mathrm{Tr}_{q+1,\ldots,N}$ means that all degrees of freedom of particles $q+1,\ldots,N$ are traced out. Note that the (1.14) implies a recurrence relation between RDMs,

$$\hat{\gamma}_{q-1}(t) = \frac{q}{N-q+1} \mathrm{Tr}_q \hat{\gamma}_q(t). \tag{1.15}$$

RDMs are especially useful in calculations of observables. For example, the energy of the system's groundstate can be expressed as

$$E = \mathrm{Tr}\left(\hat{H}\hat{\gamma}_N\right), \tag{1.16}$$

where Tr means that all degrees of freedom are traced out. Equation (1.16) simplifies if the Hamiltonian contains up to q-particle interactions. Then knowledge of the q-RDM is sufficient to calculate the energy. In fact, this statement can be generalized. If a q-RDM originates from the non-degenerate groundstate of a system whose Hamiltonian contains at most q-particle interactions, the q-RDM is sufficient to determine the groundstate wavefunction uniquely (up to a phase) and therefore also all groundstate observables. The last statement is known as Rosina's theorem [78]. We will demonstrate it on a simple example of a system with N identical particles with two-particle interactions (e.g., electrons with Coulomb interaction). The corresponding Hamiltonian can be written as

$$\hat{H}(t) = \sum_{i=1}^{N} \hat{h}^{(i)}(t) + \sum_{i<j=2}^{N} \hat{V}_{\mathrm{ee}}^{(i,j)}, \tag{1.17}$$

where $\hat{h}$ is the single-particle Hamiltonian, and $\hat{V}_{\mathrm{ee}}$ is the two-particle interaction potential. The superscript indices in brackets indicate the particles on which the operator is

acting. Then the total energy of the system in the groundstate is

$$E = \mathrm{Tr}\left(\hat{H}\hat{\gamma}_N\right) = N\mathrm{Tr}\left(\hat{h}\hat{\gamma}_N\right) + \frac{N(N-1)}{2}\mathrm{Tr}\left(\hat{V}_{\mathrm{ee}}\hat{\gamma}_N\right), \tag{1.18}$$

which, with help of (1.14), simplifies to

$$E = \mathrm{Tr}\left(\hat{h}\hat{\gamma}_1\right) + \mathrm{Tr}\left(\hat{V}_{\mathrm{ee}}\hat{\gamma}_2\right). \tag{1.19}$$

This, and more generally, Rosina's theorem shows the importance of 1-RDM and 2-RDM in physics as systems with 2-particle interactions are most abundant. Also despite the fact that all observables are, in principle, functionals of the single-particle density (i.e., the diagonal of the 1-RDM), it is much easier to calculate observables if one has access to the 2-RDM.

As $\hat{\gamma}_1$, with the help of (1.15), can be expressed in terms of $\hat{\gamma}_2$, one can consider (1.19) as a functional of $\hat{\gamma}_2$, and thus perform a variational calculus to find the groundstate. In fact, this was already proposed in 1955 by Mayer [69] and Löwdin [65] independently. However, only a couple of years later [4, 10, 72, 91] it was noted that such variational calculus leads to energies which are significantly below the experimental values. The reason for this is that not all possible 2-RDMs which are encountered in a variational minimization of the groundstate energy correspond to an N-particle DM that originates from a pure fermionic state. Therefore one has to add non-trivial constraints to the variation, in order to ensure that $\hat{\gamma}_2$ is representable by a pure-state N-particle DM. These constraints are known as N-representability conditions [21]. Despite the fact that formal solutions of the N-representability problem were developed already in the 1960s [32, 57], practically they require knowledge of the N-particle DM [21, 70]. Although for pure states not all N-representability conditions in terms of $\hat{\gamma}_2$ are known, a systematic classification of N-representability conditions has been developed [71] for ensemble-representable RDMs [60]. Applying these constraints for moderate-sized molecules one obtains only slightly lower-than-experimental energies [81] and provides a lowest energy bound.

1.2.1. EOM for RDMs

Applying the time derivative to both sides of (1.13) one obtains,

$$\partial_t\hat{\gamma}_N(t) = |\dot{\Phi}(t)\rangle\langle\Phi(t)| + |\Phi(t)\rangle\langle\dot{\Phi}(t)|, \tag{1.20}$$

which, with the help of the TDSE (1.12) and the Hamiltonian (1.17), can be written as

$$i\partial_t\gamma_N(t) = \left[\sum_{i=1}^{N}\hat{h}^{(i)}(t) + \sum_{i<j}^{N}\hat{V}_{\mathrm{ee}}^{(i,j)}, \hat{\gamma}_N(t)\right]. \tag{1.21}$$

Similarly, the EOM for the q-RDM can be obtained by applying the time derivative to both sides of (1.14) and performing partial traces. Alternatively one can also perform partial traces of (1.21). Using either method, one attains

$$\begin{aligned}
i\partial_t\gamma_1(t) &= \left[\hat{h}(t),\hat{\gamma}_1(t)\right] + 2\mathrm{Tr}_2\left[\hat{V}_{\mathrm{ee}},\hat{\gamma}_2(t)\right],\\
i\partial_t\gamma_2(t) &= \sum_{i=1}^{2}\left[\hat{h}^{(i)}(t),\hat{\gamma}_2(t)\right] + \left[\hat{V}_{\mathrm{ee}},\hat{\gamma}_2(t)\right] + 3\sum_{i=1}^{2}\mathrm{Tr}_3\left(\left[\hat{V}_{\mathrm{ee}}^{(i,3)},\hat{\gamma}_3(t)\right]\right),\\
&\vdots \qquad \vdots\\
i\partial_t\gamma_q(t) &= \sum_{i=1}^{q}\left[\hat{h}^{(i)}(t),\hat{\gamma}_q(t)\right] + \sum_{i<j}^{q}\left[\hat{V}_{\mathrm{ee}}^{(i,j)},\hat{\gamma}_q(t)\right] + (q+1)\sum_{i=1}^{q}\mathrm{Tr}_{q+1}\left(\left[\hat{V}_{\mathrm{ee}}^{(i,q+1)},\hat{\gamma}_{q+1}(t)\right]\right),\\
&\vdots \qquad \vdots\\
i\partial_t\gamma_N(t) &= \sum_{i=1}^{N}\left[\hat{h}^{(i)}(t),\hat{\gamma}_N(t)\right] + \sum_{i<j}^{N}\left[\hat{V}_{\mathrm{ee}}^{(i,j)},\hat{\gamma}_N(t)\right].
\end{aligned} \tag{1.22}$$

This system of coupled equations is called BBGKY (Bogoliubov, Born, Green, Kirkwood, Yvon) hierarchy [8, 9, 11, 51, 52, 100]. Any application in practice aims at truncating the hierarchy at some level $q \ll N$. The most obvious truncation is to consider only the first equations of the hierarchy up to level q and to set $\hat{\gamma}_r$ with $r \geq q+1$ equal to zero. However, this provides only a very crude approximation. A much better approach is to express $\hat{\gamma}_{q+1}$ as functional of $\hat{\gamma}_q$. Often the BBGKY is truncated by making an approximation for $\hat{\gamma}_3$ [1, 60], e.g., via the so-called cluster expansion [16–19, 88].

There is also an option to close the hierarchy after the first equation, although one finds only very few attempts in the literature. Quite recently, P. Elliot and N.T. Maitra [25] demonstrated a method to truncate this hierarchy after the first equation using the semi-classical approximation for electron correlations and time-dependent Hartree-Fock (TDHF) for propagation. In this way, however, N-representability was violated in the test case of a 1D helium model atom.

The reason why it is not an easy task to close the BBGKY hierarchy after the first equation is that the functional for $\hat{\gamma}_2$ in terms of $\hat{\gamma}_1$ is unknown. It is definitely a non-adiabatic one, and may not even exist. The Runge-Gross theorem [80] of TDDTF ensures that, given an initial state, the single-particle density determines the many-electron wavefunction up to a purely time-dependent phase and therefore, using (1.13) and (1.14), one is able to determine the 2-RDM. The problem with this statement is that the Runge-Gross theorem requires that time evolution of the single-particle density occurs in a potential that is local in position space. The one-to-one mapping between potentials and 1-RDMs only holds if one allows for non-local potentials as well [34, 36]. The van-Leeuwen theorem is not applicable in this case as well. Therefore currently there is no proof in the literature that such functional has to exist. But there is a formal way to overcome this problem, even if such a functional does not exist. It can be overcome by replacing the 1-

RDM propagation with the propagation of its eigenstates and eigenvalues. This approach is explained in the following section.

1.3. Renormalized natural orbitals

The natural orbitals (NOs) $|k(t)\rangle$ and occupation numbers (ONs) $n_k(t)$ are defined as eigenstates and eigenvalues of the 1-RDM, respectively,

$$\hat{\gamma}_1(t)|k(t)\rangle = n_k(t)|k(t)\rangle. \tag{1.23}$$

As $\hat{\gamma}_1(t)$ is hermitian, the $n_k(t)$ are real, and the $|k(t)\rangle$ are orthogonal. If one requests that the $|k(t)\rangle$ are normalized to unity, then $\{|k(t)\rangle\}$ forms a complete, orthonormal basis. The ensemble N-representability conditions for the 1-RDM can be easily expressed via ONs [20],

$$\sum_k n_k(t) = N, \tag{1.24}$$

$$0 \leq n_k(t) \leq 1, \quad \forall k. \tag{1.25}$$

Since 2006, due to work of A. Klyachko [53], also N-representability conditions of 1-RDM for pure states are known. Compared to the ensemble N-representability conditions there are additional linear inequality constraints, and geometrically these constraints define a convex polytope. Unfortunately, the number of constraints grows exponentially with the number of NOs, therefore in practice they are still not very useful. Fortunately, due to the minimization principle, the ensemble N-representability conditions are sufficient to guarantee that the minimizing 1-RDM corresponds to a pure state, i.e. the ground state, in all cases without ground-state degeneracy [90].

The 1-RDM expressed in NOs reads

$$\hat{\gamma}_1(t) = \sum_{k=1}^{\infty} n_k |k(t)\rangle\langle k(t)|. \tag{1.26}$$

As NOs form a complete basis set, one can formally express not only the 1-RDM but any p-RDM ($0 < p \leq N$) in terms of NOs [3]. For example, expansion of the 2-RDM reads

$$\hat{\gamma}_2(t) = \sum_{ijkl} \gamma_{2,ijkl}(t)|i(t)j(t)\rangle\langle k(t)l(t)|, \tag{1.27}$$

where the shorthand notation for tensor products $|i(t)j(t)\rangle = |i(t)\rangle^{(1)}|j(t)\rangle^{(2)} = |i(t)\rangle^{(1)} \otimes |j(t)\rangle^{(2)}$ is used, and a superscript index indicates the particle to which states

refers. The expansion coefficients

$$\gamma_{2,ijkl}(t) = \langle k(t)l(t)| \, \hat{\gamma}_2(t) \, |i(t)j(t)\rangle \,, \tag{1.28}$$
$$\gamma_{2,ijkl}(t) = \gamma^*_{2,klij}(t), \tag{1.29}$$

are generally unknown, apart from two-particle systems like the two-electron case of interest of this thesis.

By inserting (1.28) and (1.26) into (1.22) one is able to derive EOMs for NOs and ONs (illustrated in Sec. A.1 of the Appendix). However, it appears that the EOM for renormalized NOs (RNOs) is numerically more stable. The RNO $|\tilde{k}(t)\rangle$ is the corresponding NO, normalized to its occupation number,

$$|\tilde{k}(t)\rangle = \sqrt{n_k}|k(t)\rangle, \quad \langle\tilde{k}(t)|\tilde{k}(t)\rangle = n_k(t). \tag{1.30}$$

The expansion of the 1-RDM and 2-RDM in RNOs reads

$$\hat{\gamma}_1(t) = \sum_{k=1}^{\infty} |\tilde{k}(t)\rangle\langle\tilde{k}(t)| \tag{1.31}$$

and

$$\hat{\gamma}_2(t) = \sum_{ijkl} \tilde{\gamma}_{2,ijkl}(t)|\tilde{i}(t)\tilde{j}(t)\rangle\langle\tilde{k}(t)\tilde{l}(t)|, \tag{1.32}$$

where the expansion coefficients

$$\tilde{\gamma}_{2,ijkl}(t) = \frac{\gamma_{2,ijkl}(t)}{\sqrt{n_i(t)n_j(t)n_k(t)n_l(t)}} \tag{1.33}$$

have the same symmetry property (1.29) and are formally defined as

$$\tilde{\gamma}_{2,ijkl}(t) = \frac{\left\langle \tilde{k}(t)\tilde{l}(t)\right| \hat{\gamma}_2(t) \left|\tilde{i}(t)\tilde{j}(t)\right\rangle}{n_i(t)n_j(t)n_k(t)n_l(t)}. \tag{1.34}$$

Note that there is a problem when the ON number of some NO becomes exactly zero, leading to ill-defined $\tilde{\gamma}_{2,ijkl}$ involving that orbital. This is a direct consequence of the fact that $\left\{|\tilde{k}(t)\rangle\right\}$ does not form a complete orthogonal basis, when at least one ON is equal to zero. The fact that $\left\{|\tilde{k}(t)\rangle\right\}$ is not a complete basis, however, does not matter if there is an infinite number of NOs with non-zero ONs.

For an electronic groundstate there exists a proof [28] that there is an infinite number of NOs with non-zero ONs. However, to the best of our knowledge there is no proof in the literature for NOs during time propagation. Fortunately, in all NO propagations [12–14, 42, 77, 83] and TDSE propagations in which ONs were calculated [2], until now

no indications were observed. Clearly, if one uses the HF approximation for $\tilde{\gamma}_{2,ijkl}(t)$ or any other approximation, which results in pinned ONs (ONs $\in \{0;1\}$) one should not use RNOs.

1.3.1. EOM for RNOs

NOs as eigenstates of the 1-RDM are defined only up to a phase. However, if one wants to propagate NOs, one has to fix the phase for each NO, otherwise the time-derivative of an NO is not defined. The means to fix the phase convention is to choose some possibly time-dependent real value for $i\langle k(t)|\dot{k}(t)\rangle(t)$, or $i\langle\tilde{k}(t)|\dot{\tilde{k}}(t)\rangle(t)$ in case of RNOs. One option is to set this value to zero, as in [12], which means that in free evolution NOs do not change. By choosing the particular phase convention introduced in [77] (see also Appendix A.1) and inserting (1.31) and (1.34) into (1.22) one obtains

$$i\partial_t|\tilde{n}(t)\rangle = \hat{h}(t)|n(t)\rangle + \tilde{\mathcal{A}}_n(t)|\tilde{n}(t)\rangle + \sum_{k\neq n}\tilde{\mathcal{B}}_{nk}(t)|\tilde{k}(t)\rangle + \sum_k \hat{\tilde{\mathcal{C}}}_{nk}(t)|\tilde{k}(t)\rangle, \tag{1.35}$$

with

$$\tilde{\mathcal{A}}_n(t) = -\frac{1}{n_n(t)}\Re\sum_{jkl}\tilde{\gamma}_{2,njkl}(t)\langle\tilde{k}\tilde{l}|\hat{V}_{\mathrm{ee}}|\tilde{n}\tilde{j}\rangle, \tag{1.36}$$

$$\tilde{\mathcal{B}}_{nk}(t) = \frac{2}{n_k(t)-n_n(t)}\sum_{jpl}\Big[\tilde{\gamma}_{2,kjpl}(t)\langle\tilde{p}\tilde{l}|\hat{V}_{\mathrm{ee}}|\tilde{n}\tilde{j}\rangle - \tilde{\gamma}_{2,plnj}(t)\langle\tilde{k}\tilde{j}|\hat{V}_{\mathrm{ee}}|\tilde{p}\tilde{l}\rangle\Big], \quad n_k(t)\neq n_n(t) \tag{1.37}$$

and

$$\hat{\tilde{\mathcal{C}}}_{nk}(t) = 2\sum_{jl}\tilde{\gamma}_{2,kjnl}(t)\langle\tilde{l}|\hat{V}_{\mathrm{ee}}|\tilde{j}\rangle. \tag{1.38}$$

Here, the time dependence of RNOs is suppressed for brevity. One also readily observes that matrices $\tilde{\mathcal{A}}_n(t)$, $\tilde{\mathcal{B}}_{nk}(t)$ and $\hat{\tilde{\mathcal{C}}}_{nk}(t)$ are hermitian, which is ideal for unitary-time propagation.

Besides the problem of ONs in the denominator, now a vanishing denominator in (1.37) may also arise if two ONs become equal. The reason for this is that if at time t two orbitals are degenerate one has the freedom to choose any orthogonal pair from the subspace they span. Suggestions of what to do in this case are provided in [14].

1.3.2. Approximations for expansion coefficients $\tilde{\gamma}_{2,ijkl}(t)$

The EOM for RNOs is quite useless unless the expansion coefficients $\tilde{\gamma}_{2,ijkl}(t)$ are known. As already noted previously they are known exactly only for systems with up to two particles. Therefore if one wants to investigate larger systems, one has to use approximations. In this section, we will examine functionals $\tilde{\gamma}_{2,ijkl}(t)$ that are available in the literature.

Hartree-Fock (HF) functional

One of the simplest approximations is the HF functional. The HF functional reads

$$\gamma_{2,ijkl}(t) = \frac{1}{2} n_i(t) n_j(t) \left(\delta_{ik}\delta_{jl} - \delta_{il}\delta_{jk}\right); \quad \tilde{\gamma}_{2,ijkl}(t) = \frac{1}{2}\left(\delta_{ik}\delta_{jl} - \delta_{il}\delta_{jk}\right). \tag{1.39}$$

The advantage is that this functional is N-representable as there is the HF wavefunction which generates this 2-RDM. Another positive property, which surprisingly is not fulfilled by the majority of functionals in the literature, is contraction consistency, i.e, by tracing out all degrees of freedom of the second particle and using proper normalization, one recovers the 1-RDM as

$$\begin{aligned}
\hat{\gamma}_1 =& \frac{2}{N-1}\mathrm{Tr}_2\hat{\gamma}_2 = \frac{2}{N-1}\sum_n \langle n|\,\hat{\gamma}_2\,|n\rangle \\
=& \frac{1}{N-1}\sum_{ij} n_i n_j |i\rangle\langle i| - \frac{1}{N-1}\sum_i n_i^2 |i\rangle\langle i| \\
=& \frac{N}{N-1}\sum_i n_i |i\rangle\langle i| - \frac{1}{N-1}\sum_i n_i^2 |i\rangle\langle i| \\
=& \sum_i n_i |i\rangle\langle i|,
\end{aligned} \tag{1.40}$$

where it was used that $n_i^2 = n_i$ since $n_i \in \{0;1\}$. However, one finds that ONs are pinned: $n_i(t) = 1$ if $i \leq N$ and $n_i(t) = 0$ if $i > N$. Therefore this functional ignores correlations completely, as the amount of correlation can be characterized with correlation entropy [3, 103]

$$s(t) = \frac{1}{N}\sum_i n_i(t)\log n_i(t), \tag{1.41}$$

which vanishes if $n_i \in \{0;1\}$. Also $\mathcal{B}_{nk}(t) = 0$ in (A.7) is zero. Further, one can choose the phase convention

$$i\langle n|\dot{n}\rangle = \langle n|\,\hat{h}(t)\,|n\rangle + \sum_{j=1}^{N}\left[\langle nj|\,\hat{V}_{\mathrm{ee}}\,|nj\rangle - \langle nj|\,\hat{V}_{\mathrm{ee}}\,|jn\rangle\right] \tag{1.42}$$

such that $\mathcal{A}_n(t) = 0$, and the TDHF equations are recovered.

Müller functional

A frequently used functional leading to non-pinned ONs was introduced by Müller [73] and Buijse and Baerends [15]. The Müller functionals for NOs and RNOs read

$$\begin{aligned}\gamma_{2,ijkl}(t) &= \frac{1}{2}n_i(t)n_j(t)\delta_{ik}\delta_{jl} - \frac{1}{2}\sqrt{n_i(t)n_j(t)}\delta_{il}\delta_{jk},\\ \tilde{\gamma}_{2,ijkl}(t) &= \frac{1}{2}\delta_{ik}\delta_{jl} - \frac{1}{2\sqrt{n_i(t)n_j(t)}}\delta_{il}\delta_{jk}.\end{aligned} \tag{1.43}$$

It is also contraction consistent as

$$\begin{aligned}\hat{\gamma}_1 =& \frac{2}{N-1}\mathrm{Tr}_2\hat{\gamma}_2 = \frac{2}{N-1}\sum_n \langle n|\,\hat{\gamma}_2\,|n\rangle\\ =& \frac{1}{N-1}\sum_{ij} n_i n_j |i\rangle\langle i| - \frac{1}{N-1}\sum_i n_i |i\rangle\langle i|\\ =& \sum_i n_i |i\rangle\langle i|.\end{aligned} \tag{1.44}$$

Occupation numbers are not pinned, but as $\dot{n}_i(t) = 0$, as follows from (A.5), i.e., they remain constant during propagation. The Müller functional is not N-representable except the case where one truncates EOMs after N NOs, thus obtaining the HF functional. As a consequence one obtains energies significantly below the true value. In fact, there is a proposal [27] to correct Müller's functional by adding a correction of $\frac{N}{8}$ to the energy, although for helium and hydrogen this correction is overestimated.

Power functional and other corrections to the Müller functional

The HF functional provides too high energies and the Müller functional provides too low energies. Actually both of them belong to a larger class of functionals of the form

$$\gamma_{2,ijkl}(t) = \frac{1}{2}n_i(t)n_j(t)\delta_{ik}\delta_{jl} - \frac{1}{2}\left[n_i(t)n_j(t)\right]^{\alpha}\delta_{il}\delta_{jk}. \tag{1.45}$$

For the HF case, $\alpha = 1$ and for the Müller case, $\alpha = \frac{1}{2}$. Therefore, as energy values for both cases are quite far from the exact one, one may conclude that with some values $\frac{1}{2} < \alpha \leq 1$ one will obtain better results. The functional (1.45) with $\frac{1}{2} \leq \alpha \leq 1$ is called the power functional [87]. However, the optimal value of α will differ from system to system. In practice it has been optimized for some groups of molecules. The power functional is neither contraction consistent nor N-representable. ONs do not change over time.

The Goedecker and Umrigar functional [37] is a self-interaction-corrected version of Müller's functional where all terms $\gamma_{2,iiii}(t)$ are set to zero. In corrections BBC1–3 [39]

of the Müller functional the sign or power of α is changed from $\frac{1}{2}$ to 1 in (1.43) for some NOs. Note that these functionals are optimized to produce better energy values and thus may perform worse than the Müller functional for other variables.

Piris natural orbital functionals

Piris' natural orbital functionals (PNOFs) and anti-symmetrized products of strongly orthogonal geminals (APSGs) [89] are the only classes of functionals for which ONs can change with time. Moreover, it turns out that these functionals are N-representable and contraction consistent. The most recent functionals are PNOF5e [76] and PNOF6(N_c) [64]. These functionals utilize an orbital pairing approach. They divide all electrons in pairs with opposite spins and require that the sum of occupation numbers for each pair is 2. Therefore, it can be applied only to systems with an even number of electrons in a singlet state. PNOF5e describes only correlations within an electron pair and ignores correlations with all other electrons. PNOF6 can describe both intra-pair and inter-pair correlations. As both functionals match with APSGs and the exact functional in the helium case anyway we will not examine them deeper in this thesis.

1.4. TDRNOT applied to helium model atom

If one desires to test a new theory, it is always advisable to benchmark it on models for which one does not need to do too many approximations. Ideally, the "exact" solution for the model is available for comparison. The perfect test object for our purpose is a few-electron model atom for which we can solve the TDSE. The two-electron He case is especially attractive as the expansion coefficients $\gamma_{2,ijkl(t)}$ are exactly known.

1.4.1. Helium

A helium atom or helium-like ions are composed of two electrons and a nucleus. The electronic Hamiltonian reads

$$\hat{H}^{(1,2)}(t) = \hat{h}^{(1)}(t) + \hat{h}^{(2)}(t) + \hat{V}_{\mathrm{ee}}^{(1,2)}, \tag{1.46}$$

where $\hat{h}(t)$ is the single-particle Hamiltonian consisting of kinetic energy, electron-nucleus interaction and electron interaction with external fields, e.g. the laser field. The $\hat{V}_{\mathrm{ee}}$ is the electron-electron interaction potential, and the upper indices indicate that the operator is acting on either electron 1, electron 2, or both.

The two-electron state $|\Phi(t)\rangle$ is antisymmetric under particle exchange and therefore

can be expanded in a single particle basis as [77]

$$|\Phi(t)\rangle = \sum_{k=1}^{\infty} d_k(t)|k(t)\rangle|k'(t)\rangle = \sum_{k\ \text{odd}} d_k(t)\left[|k(t)\rangle|k'(t)\rangle - |k'(t)\rangle|k(t)\rangle\right], \tag{1.47}$$

where $|k(t)\rangle$ are NOs, the "prime operator" acting on a positive integer k is given as

$$k' = \begin{cases} k+1 & \text{if } k \text{ odd} \\ k-1 & \text{if } k \text{ even,} \end{cases} \qquad k > 0, \tag{1.48}$$

and the expansion coefficients have the property $d_{i'}(t) = -d_i(t)$.

If one now calculates the 1-RDM and compares with (1.23), one finds that

$$2|d_k(t)|^2 = n_k(t); \qquad d_k(t) = \sqrt{\frac{n_k(t)}{2}}\mathrm{e}^{i\varphi_k(t)}, \tag{1.49}$$

where $\varphi_k(t) = \pi + \varphi_{k'}(t)$ is some real function which depends on the phase convention for the NOs. For a specific phase convention it is actually possible to choose $\varphi_k(t) = \varphi_k(0)$ and thus write

$$|\Phi(t)\rangle = \sum_{k=1}^{\infty} \sqrt{\frac{n_k(t)}{2}}\mathrm{e}^{i\varphi_k(0)}|k(t)\rangle|k'(t)\rangle. \tag{1.50}$$

By inserting (1.50) into (1.13), one obtains the 2-DM expansion in NOs from which one immediately finds

$$\tilde{\gamma}_{2,ijkl}(t) = (-1)^{k+j}\frac{\mathrm{e}^{i[\varphi_i(0)-\varphi_k(0)]}}{2\sqrt{n_i(t)n_k(t)}}\delta_{ij'}\delta_{kl'}. \tag{1.51}$$

If one requests that RNOs for groundstates are real, then one obtains the phase factors for He-like ions

$$\mathrm{e}^{i\varphi_k(0)} = \pm(2\delta_{1k} + 2\delta_{2k} - 1). \tag{1.52}$$

For the choice $\mathrm{e}^{i\varphi_k(0)} = 1$ the groundstate RNOs will be complex. This choice is useful for, e.g., the H_2 molecule in Born-Oppenheimer approximation where the phase factors change as a function of the internuclear distance.

Note that explicit expressions for $\tilde{\gamma}_{2,ijkl}(t)$ as in (1.51) are only known for two-particle systems.

Model atom

To perform the benchmarking test, the widely used one-dimensional helium model atom was used [7, 40, 41, 61, 63, 97, 98]. The Hamiltonian of the model helium atom has the

form (1.46). The single-particle Hamiltonian in dipole approximation and length gauge reads

$$\hat{h}_{\mathrm{E}} = \frac{\hat{p}^2}{2} - \frac{2}{\sqrt{\hat{x}^2 + \varepsilon_{\mathrm{ne}}}} + E(t)\hat{x} - i\hat{\Gamma}, \tag{1.53}$$

and in velocity gauge, with the purely time-dependent $A^2(t)$ term transformed away,

$$\hat{h}_{\mathrm{L}} = \frac{\hat{p}^2}{2} - \frac{2}{\sqrt{\hat{x}^2 + \varepsilon_{\mathrm{ne}}}} + A(t)\hat{p} - i\hat{\Gamma}. \tag{1.54}$$

The electron-electron interaction reads

$$V_{\mathrm{ee}}^{(1,2)} = \frac{1}{\sqrt{\left(\hat{x}^{(1)} - \hat{x}^{(2)}\right)^2 + \varepsilon_{\mathrm{ee}}}}. \tag{1.55}$$

We used two different values for parameters $\varepsilon_{\mathrm{ne}}$ and $\varepsilon_{\mathrm{ee}}$. In the first two papers [12, 77], where the main purpose was to demonstrate the capabilities of the method, the values $\varepsilon_{\mathrm{ne}} = \varepsilon_{\mathrm{ee}} = 1$ were used. In the papers [13, 14] the values $\varepsilon_{\mathrm{ne}} = 0.50$ and $\varepsilon_{\mathrm{ee}} = 0.33$ were chosen to match the real, three-dimensional He and He^+ ionization potentials. The latter will be used for all examples in the introductory part of this thesis. The imaginary potential $-i\hat{\Gamma}$ is introduced to absorb outgoing electron flux [14].

1.4.2. Groundstate

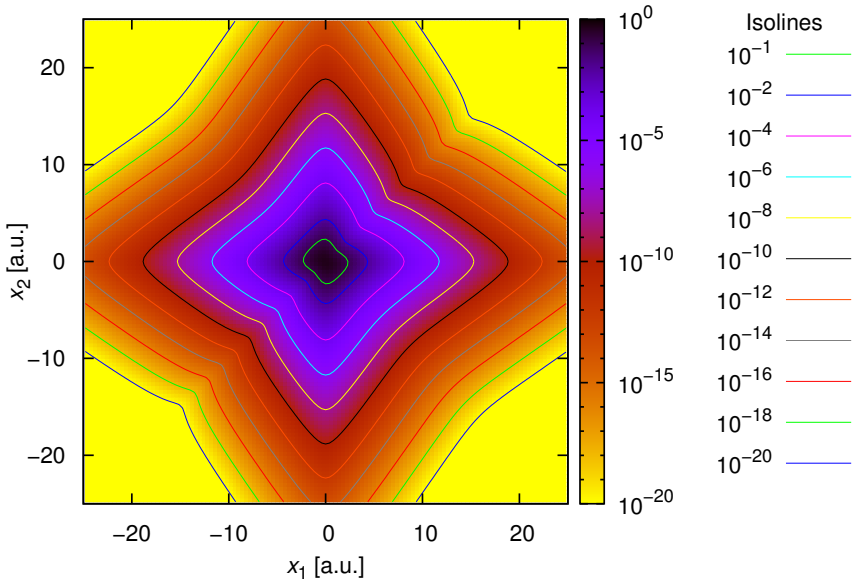

Figure 1.1.: Groundstate wavefunction of the helium model atom. The calculations were performed on a square grid with $N_x = N_y = 1000$ spacial gridpoints and a resolution $dx = dy = 0.4$.

The TDSE (1.12) governs the time evolution of a state $|\Phi(t)\rangle$ given an initial state $|\Phi(t=t_0)\rangle$. In all examples of this thesis the groundstate is used as the initial state. To find the groundstate one can apply imaginary-time propagation [5] where time is replaced by imaginary time, $t \to -i\tau$, and the wavefunction is renormalized after each time step. Starting with a guess at $\tau = 0$ one attains the groundstate of the system in the limit $\tau \to \infty$. By applying this procedure to our helium model atom one finds the groundtate state wavefunction presented in Figure 1.1 with energy $E_0 = -2.9$. To obtain excited states one additionally projects out all states with lower energy after each time step.

One can apply the imaginary-time propagation also to TDRNOT for the $\bar{N}_\circ$ RNOs with highest ONs. Apart from renormalization after each imaginary time step (making sure that $\sum_i n_i = 2$) one has to perform Gram-Schmidt orthogonalization of the RNOs. The helium singlet RNOs $|\tilde{i}(t)\rangle$ and $|\tilde{i}'(t)\rangle$ have the same spatial part but opposite spins. Thus numerically one needs to propagate only $N_\circ = \frac{1}{2}\bar{N}_\circ$ RNOs.

Table 1.1.: Groundstate energy convergence with increasing number m of RNOs in the propagation. For the calculation of the error the energy obtained with m RNOs (labeled m-RNO) was compared with the one obtained by the TDSE.

$N_\circ$	ΔE [a.u.]	rel. err.	$N_\circ$	ΔE [a.u.]	rel. err.
1	$3.7{\cdot}10^{-2}$	$1.3{\cdot}10^{-2}$	13	$5.3{\cdot}10^{-8}$	$1.8{\cdot}10^{-8}$
2	$6.7{\cdot}10^{-3}$	$2.3{\cdot}10^{-3}$	16	$7.8{\cdot}10^{-9}$	$2.7{\cdot}10^{-9}$
3	$7.9{\cdot}10^{-4}$	$2.7{\cdot}10^{-4}$	19	$1.2{\cdot}10^{-9}$	$4.2{\cdot}10^{-10}$
4	$2.7{\cdot}10^{-4}$	$9.2{\cdot}10^{-5}$	22	$2.6{\cdot}10^{-10}$	$9.1{\cdot}10^{-11}$
5	$5.9{\cdot}10^{-5}$	$2.0{\cdot}10^{-5}$	25	$5.0{\cdot}10^{-11}$	$1.7{\cdot}10^{-11}$
6	$2.4{\cdot}10^{-5}$	$8.3{\cdot}10^{-6}$	28	$9.9{\cdot}10^{-12}$	$3.4{\cdot}10^{-12}$
7	$7.2{\cdot}10^{-6}$	$2.5{\cdot}10^{-6}$	31	$1.5{\cdot}10^{-12}$	$5.2{\cdot}10^{-13}$
8	$3.3{\cdot}10^{-6}$	$1.1{\cdot}10^{-6}$	34	$2.7{\cdot}10^{-13}$	$9.4{\cdot}10^{-14}$
9	$1.2{\cdot}10^{-6}$	$4.0{\cdot}10^{-7}$	37	$4.1{\cdot}10^{-14}$	$1.4{\cdot}10^{-14}$
10	$5.7{\cdot}10^{-7}$	$2.0{\cdot}10^{-7}$	39	$<1.0{\cdot}10^{-15}$	$<1.0{\cdot}10^{-15}$

By applying the imaginary-time propagation to TDRNOT using the exact functional for $\tilde{\gamma}_{2,ijkl}(t)$ (1.51) for different number $N_\circ$ of NOs one finds that the groundstate energy monotonously converges with increasing $N_\circ$ to the value obtained from the TDSE calculation. This convergence is shown in Table 1.1. The ONs rapidly drop, as shown in Figure 1.2. Unfortunately, it is not an easy task to find excited states with TDRNOT. The difference to the TDSE case is that groundstate RNOs are not orthogonal to excited state RNOs, which means one has to add nontrivial constraints.

The groundstate obtained via imaginary-time propagation applied to TDRNOT does not depend on the imaginary time step as long as it is small enough such that results converge at all. Starting from a reasonable initial guess the results converge for $N_\circ < 40$ with $d\tau \leq 0.05$ and $N_\circ \leq 80$ with $d\tau \leq 0.005$ using 4-th order Runge-Kutta propagation.

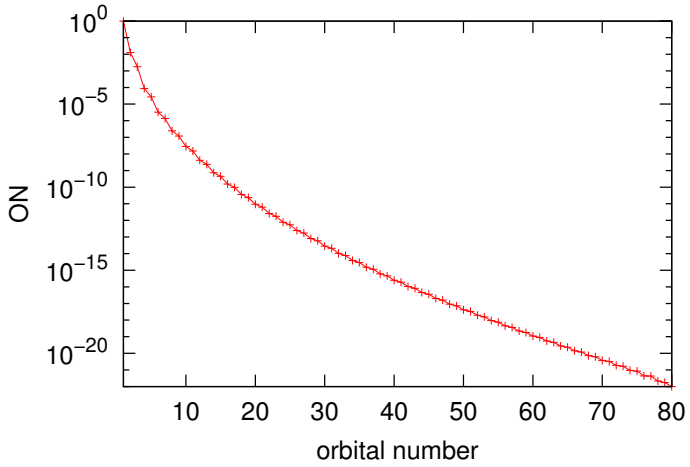

Figure 1.2.: ONs of TRNOT groundstate with $N_\circ = 80$ RNOs.

Also the 2-DM converges monotonously with increasing number of RNOs so that every groundstate observable also converges. The convergence of the 2-particle density (diagonal part of the 2-DM) is shown in Figure 1.3. $N_\circ = 39$ is sufficient to reach the point where the TDRNOT results for the 2-DM match those of the TDSE up to a machine precision. Figure 1.3 also demonstrates how correlations build up with increasing number of RNOs.

Müller functional

As the exact functional is known only for the two-particle case it is interesting to investigate what happens when one uses an approximate function instead, e.g., Müller functional (see Sec. 1.3.2 for definition). The first noticeable difference is that the EOM in imaginary time is less stable with the Müller functional. Thus one has to use smaller time steps in order to achieve convergence. The energy of the Müller-functional groundstate also converges monotonously with increasing $N_\circ$, but it does not converges to the TDSE result. It converges to a value which is significantly (0.7%) below the TDSE result. Already the 3-RNO calculation provides an energy which is below the TDSE value. Even worse with the 2-DM: there are regions where the 2-particle density becomes negative for TDRNOT calculations with $N_\circ > 3$. The size of those regions increases with increasing $N_\circ$.

1.4.3. Linear response

The next step after finding the groundstate is to examine the excited states which can be populated by laser excitations. To determine those states, one can apply a small, perturbing field (hence, "linear response") which contains all frequencies and then analyze which

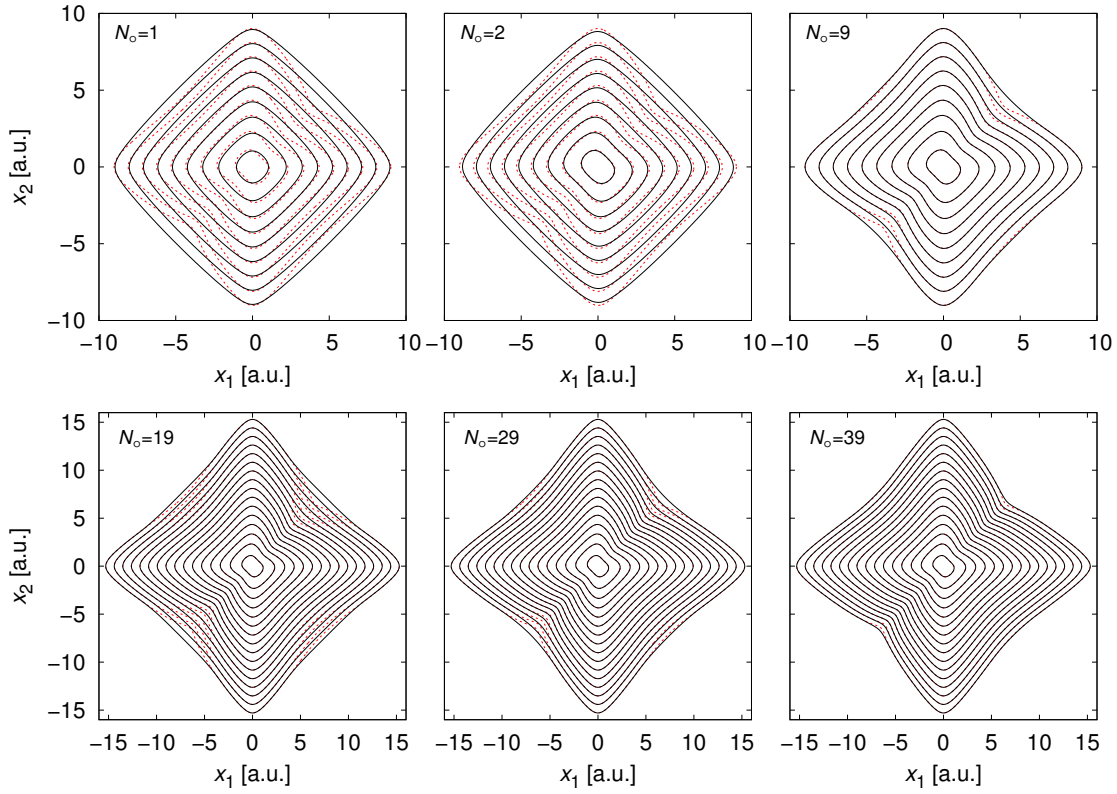

Figure 1.3.: Isolines of the 2-particle density of the helium groundstate. The red dashed isolines indicate the TDSE solution while the solid black isolines represent the TDRNOT solution with $N_\circ$ =1, 2, 9, 19, 29, 39 RNOs. On the top panel the isolines have the values 10^{-1}, 10^{-2}, ...,10^{-9}, on the bottom panel 10^{-1}, 10^{-2}, ...,10^{-16}.

states are populated. An example for such a perturbation is a vector potential of the form

$$A(t) = \hat{A}\,\Theta(t - t_0) \tag{1.56}$$

where $\Theta(x)$ is the Heaviside step function. The electric field $E(t) = -\partial_t A(t)$ then is a δ-like kick. To analyze which states are populated one can use the fact that during field-free evolution all populated states evolve $\sim \exp(-iE_i t)$, where E_i is the eigenenergy of state i. Thus, to find the energies E_i one may Fourier-transform the auto-correlation function [26]. Excitation energies, i.e., energy differences $E_i - E_0$ in the linear-response regime, can be inferred from the Fourier transform of the dipole or dipole acceleration. The expectation value of the acceleration is computationally preferable, as the results converge on smaller grids [14]. By applying a perturbation (1.56) with $\hat{A} = 10^{-5}$ and propagating the system until $t = t_0 + 5000$ the linear response spectra in Figure 1.4 is obtained. To eliminate box states due to the finite grid size an imaginary potential was used. Because of this imaginary potential the Hamiltonian is not hermitian anymore. Thus we cannot use the EOM (1.35) but have to use the ammended EOM which was derived

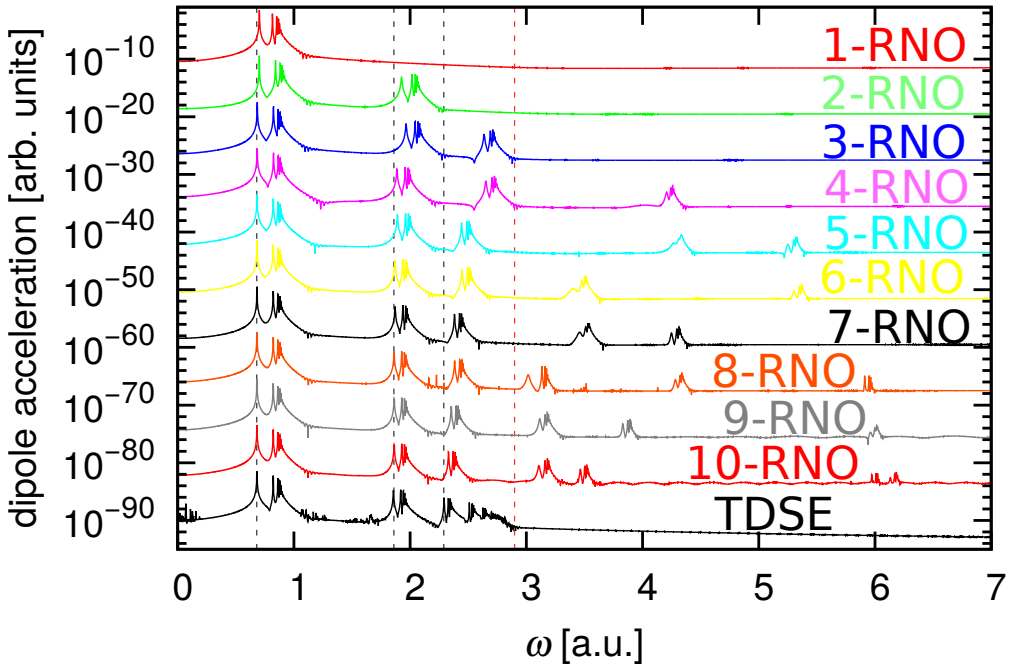

Figure 1.4.: Comparison of linear response spectra calculated with TDSE and TDRNOT with 1 to 10 RNOs. For the purpose of easier comparison, the spectra are vertically shifted. The dashed black lines indicate the positions of the first, second, and third series of peaks from the TDSE. The dashed red line shows the frequency corresponding to the fully ionized ion, therefore one would not expect any peaks with larger frequencies. However, they are present in the TDRNOT case with more than three RNOs. The low-intensity peaks in the TDSE spectrum (around the first series) are caused by splitting errors in the numerical solution of TDSE. The positions correspond to frequency differences between high intensity peaks visible in the graph.

in [14]. Alternative methods to suppress box states are mask functions [56] or complex exterior scaling [86]. For the mask function case one may still use (1.35), but for complex exterior scaling one has to modify the EOM as well.

The TDSE spectrum in Figure 1.4 shows several series of peaks. The positions where the first three series start are indicated by dashed black lines. Five series of peaks (of the infinitely many) are resolved up to the frequency $\omega = 2.9$ that is sufficient to fully ionize the helium atom. This is indicated by the dashed red line in Figure 1.4. The first series of peaks corresponds to single excitations where one electron stays in the groundstate and the other electron ends up in some excited state. The second series corresponds to the transition to a final state where one electron is in the first excited state and the other electron is in a higher excited state. The third series of peaks correspond to the situation where the lowest electron is in the second excited state, and so forth. Thus, all series except the first one represent transitions to doubly-excited states. If we look

at the 1-RNO calculation, which is equivalent to TDHF or TDDFT in exact exchange-only approximation, we notice that the double-excitations are missing. However, if we increase the number of RNOs in the TDRNOT propagation, we observe additional series of peaks. The positions of the previous peaks improve by adding extra orbitals, although not monotonously. The position of the first series is already well described with the 3-RNO calculation, and the second series with the 6-RNO calculation. The problem, however, is that each new series appears at increasingly larger frequencies. Already the 4-RNO calculation shows peaks in the double-ionization continuum (dashed red line) in Figure 1.4). Thus one has to be cautios in simulations of He in laser fields using TDRNOT, as one may excite these artificial states, which then can auto-ionize, altering observables of interest in an unphysical way.

Müller functional

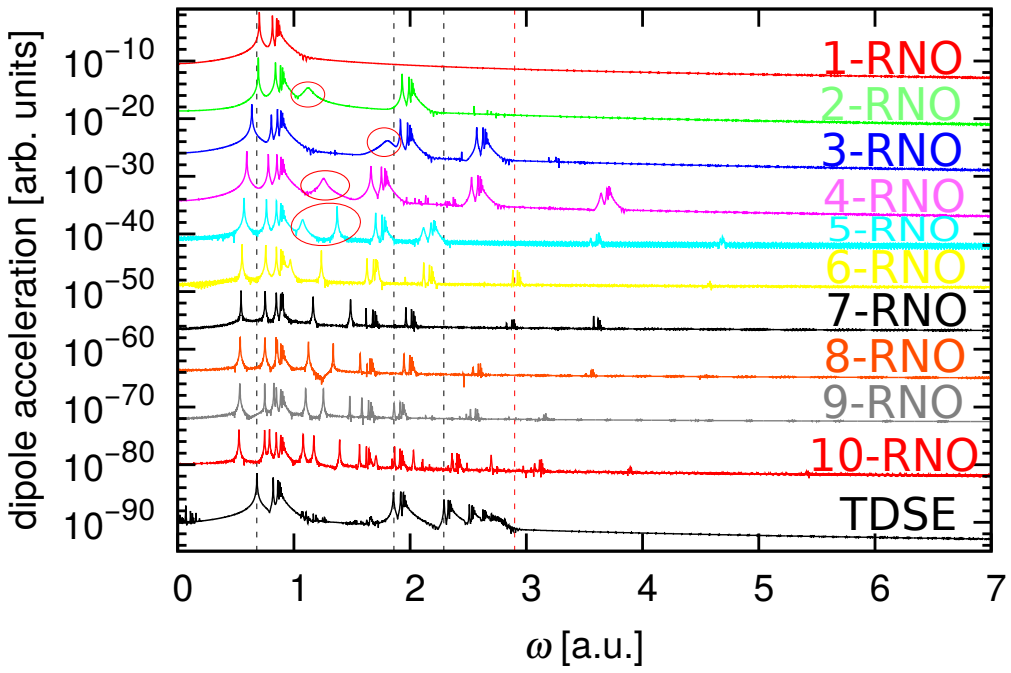

Figure 1.5.: Comparison of the linear response spectra calculated with TDSE and TDRNOT using the Müller functional with 1–10 RNOs. The vertical lines have the same meaning as in Figure 1.4. The red ellipses mark extra peaks in the calculation for 2-5 RNOs.

Using the Müller functional (1.43) instead of the exact (1.51) the linear response spectrum in Figure 1.5 is obtained. Compared to Figure 1.4 obtained using the exact functional, we observe a higher noise level for the Müller functional, despite the fact that a more then ten times smaller time steps were used. There are also additional peaks, which are quite similar to the results obtained using the "frozen" approximation [12]. But the

main difference is that the series of peaks converge to lower frequencies than in the TDSE case. Only the first ionization continuum is well described. Given the fact that the TDSE can be considered exact here, this means that the Müller functional does not work for many RNOs.

1.4.4. Peak shifting problem

One artifact generated by all widely applied exchange-correlation functionals for (TD)DFT available in the literature is that photoelectron peaks shift towards smaller energies as ionization proceeds during the laser pulse. The time-dependent ionization degree in TDDFT corresponds to a variation of the fractional occupation numbers in DFT [75], and most of the exchange-correlation potentials applied in practice vary smoothly as a function of these fractional occupations. However, the exact exchange-correlation functional is known to have so-called "derivative discontinuities" [63, 75]. Figure 1.6 shows the total energy and the Kohn-Sham orbital energies as functions of the occupation for the He model in exchange-only approximation.

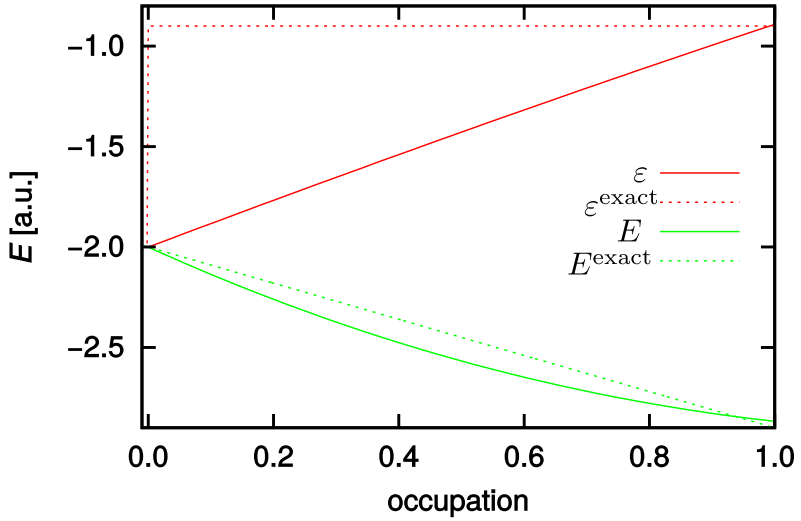

Figure 1.6.: Total (green) and Kohn-Sham orbital energies (red) as functions of the orbital occupation for the helium model atom in exchange-only approximation (solid). Corresponding dashed lines show how the exact result should look like.

If the Kohn-Sham orbital energy decreases monotonously with increasing ionization probability, the kinetic energy of emitted photoelectrons decreases monotonously as well. Thus, when we apply laser pulses of different intensities in TDDFT calculations, we observe photoelectron peaks at different positions. Consider, for instance, $|E_0^{\mathrm{He}^+}| > \hbar\omega > E_0^{\mathrm{He}^+} - E_0^{\mathrm{He}}$, where E_0^{He} and $E_0^{\mathrm{He}^+}$ are groundstate energies of He and He^+ and a laser intensity that is small such that multi-photon processes are very improbable. Then, as

ionization proceeds, at some time during the interaction, single-photon ionization is not possible anymore because the Kohn-Sham orbital energy drops below $\hbar\omega$.

The 1-RNO calculation is equivalent to TDDFT with exchange-only approximation. Hence, for TRNOT with one RNO in Figure 1.7 we observe strong peak shifting. For the 3-RNO calculations we can still observe peak shifting, although less pronounced than in the TDDFT case. The situation continues to improves if one adds more RNOs. For the 6-RNO calculations there is no peak shift on the energy scale shown in the plots.

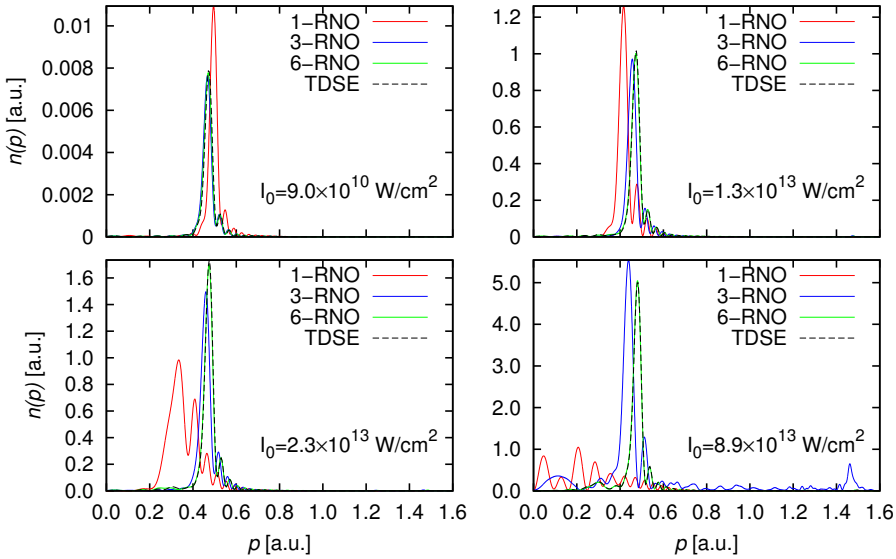

Figure 1.7.: Comparison of photoelectron momentum spectra calculated with TDSE and TDRNOT using one, three, and six RNOs. A 50-cycle trapezoidal (2-cycle linear up-ramping and down-ramping) laser pulse with $\omega = 1$ and different peak intensities I_0 was used. The 1-RNO result is equivalent to the TDHF and TDDFT using exchange-only approximation.

Müller functional

The position of the first ionization continuum is well described by the TDRNOT with the Müller functional. Thus one may hope that the peak positions will improve as well if one adds more RNOs in propagation, although probably more then six RNOs are required to cure this effect. Unfortunately, in practice, one is not able to notice any improvement at all. The shift is quite similar for 1-RNO, 2-RNO, 3-RNO, and 20-RNO calculations. Thus, there is no point of using TDRNOT with the Müller functional, as we cannot go beyond TDDFT, and TDDFT calculations are faster. Therefore, a good functional is essential for TDRNOT, and probably the N-representability is the crucial property that must be satisfied in order to improve on TDDFT.

1.4.5. Single-photon double ionization

Single-photon double ionization (SPDI) is another effect where TDDFT does not work in practice, especially if one is interested in correlated photoelectron spectra, for which no density functional is known.

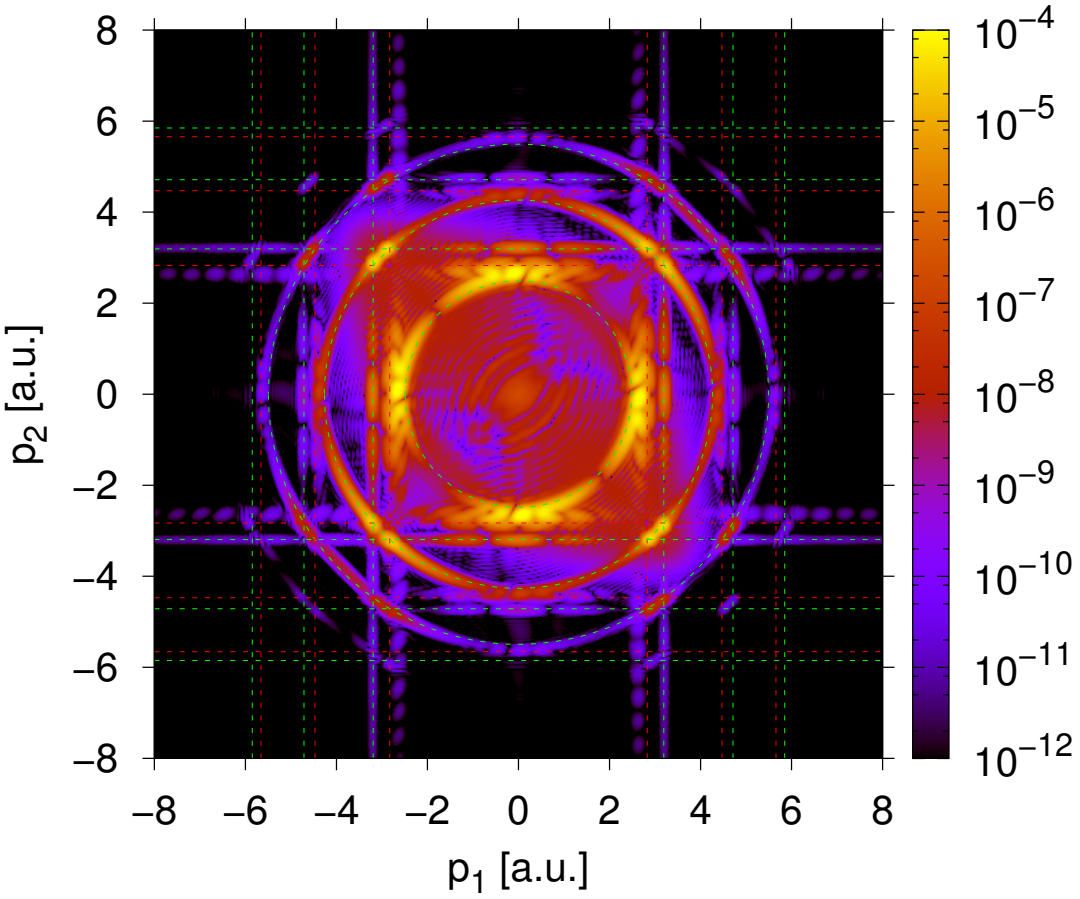

Figure 1.8.: Correlated photoelectron momentum spectrum calculated with the TDSE. A 7.6-nm 20-cycle $\sin^2$-shaped laser pulse of peak intensity $I_0 = 2.4 \times 10^{14}\,\mathrm{W/cm^2}$ was used. The dashed green vertical and horizontal lines indicate the photoelectron momenta after single ionization of He by absorbing one, two, and three photons. The dashed red vertical and horizontal lines indicate the photoelectron momenta after ionization of He^+ by absorbing one, two, and three photons. The dashed green circles are explained in the text.

If $\hbar\omega > |E_0^{\mathrm{He}}|$ then one photon can fully ionize a helium atom. However, electron-electron interaction is required, as the photon energy, absorbed by one electron, has to be shared with the other electron. From energy conservation, one obtains

$$E_{kin}^{(1)} + E_{kin}^{(2)} = \hbar\omega + E_0^{\mathrm{He}}, \tag{1.57}$$

where $E_{kin}^{(i)}$ is the kinetic energy of the i-th photoelectron. As a consequence, one expects a ring with radius $p = \sqrt{2\left(\hbar\omega + E_0^{\mathrm{He}}\right)}$ in correlated photoelectron momentum spectra. If both electrons are emitted in the same direction it is very improbable that one will measure both electrons with the same kinetic energy due to Coulomb repulsion. It is more likely that one electron will have a higher kinetic energy than the other. Due to Coulomb repulsion the second electron accelerates the first and slows down. Thus, we expect the probability along the SPDI-ring to vary. In fact, this is seen in Figure 1.8. There is a minimum on the inner SPDI-ring if both photoelectrons have the same energy and are emitted in the same direction.

An atom can simultaneously absorb also two and more photons. If n is the number of photons which are simultaneously absorbed then the atom can be fully ionized if $n\hbar\omega > |E_0^{\mathrm{He}}|$. Thus, if the photon energy $\hbar\omega > |E_0^{\mathrm{He}}|$, rings of radius $p = \sqrt{2\left(m\hbar\omega + E_0^{\mathrm{He}}\right)}$ with $m \in \{1, 2, 3, ...\}$ are expected in correlated photelectron momentum spectra. The probability to simultaneous absorb multiple photons decreases exponentially with the number of photons. Three rings can be identified in Figure 1.8, and some traces of a fourth one. In order to observe more rings one has to increase the laser intensity.

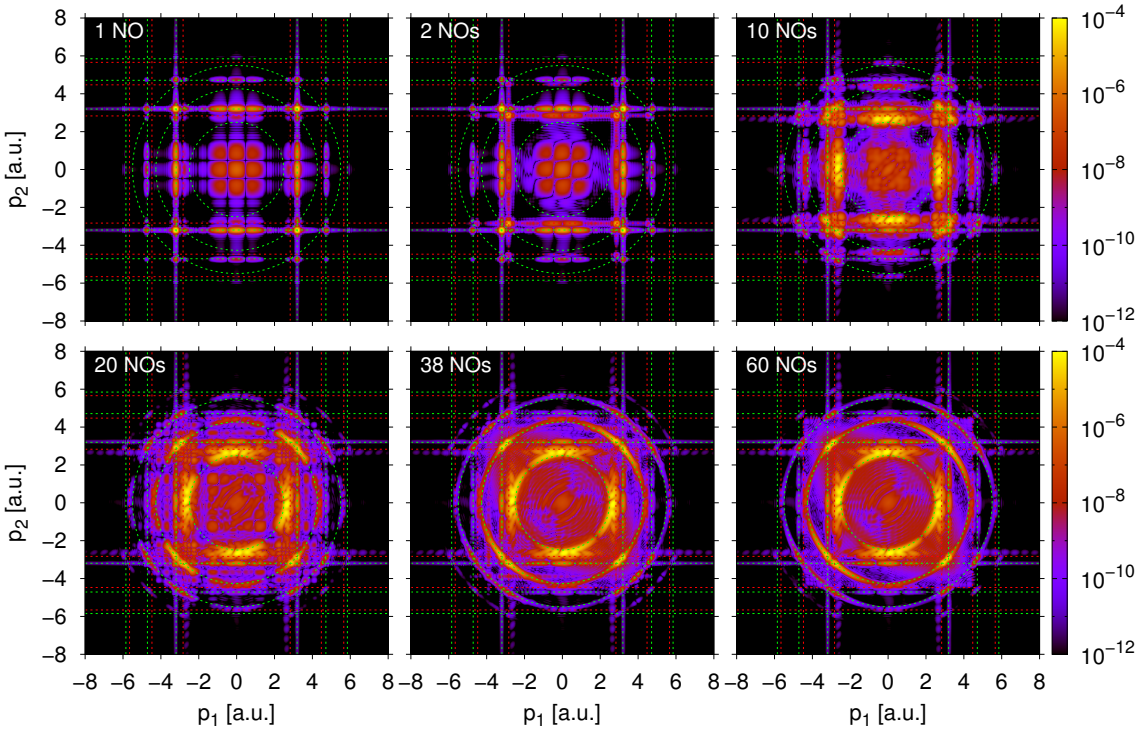

Figure 1.9.: Correlated photoelectron momentum spectra obtained from the first 60 NOs (not all are shown) calculated from the TDSE wavefunction. The same laser pulse was used as in Figure 1.8. The dashed lines also have the same meaning as in Figure 1.8.

The vertical and horizontal lines in features in Figures 1.8 and 1.9 indicate the photoelectron momenta after single ionization of He (green) and He^+ (red) by one, two, three

photons. An enhanced ionization probability is observed when lines of different color cross the higher-order rings ($m = 2, 3, \ldots$), corresponding to sequential double ionization. The probability is "smeared out" due to electron-electron interaction, especially if the electrons are emitted in the same direction. The correlated photoelectron momentum spectra were calculated by applying a filtering method in position-space [13, 98] instead of projecting out all bound and singly ionized states. As this is not a rigorous approach to calculate photoelectron spectra, traces of bound and singly excited states are still visible in Figure 1.8.

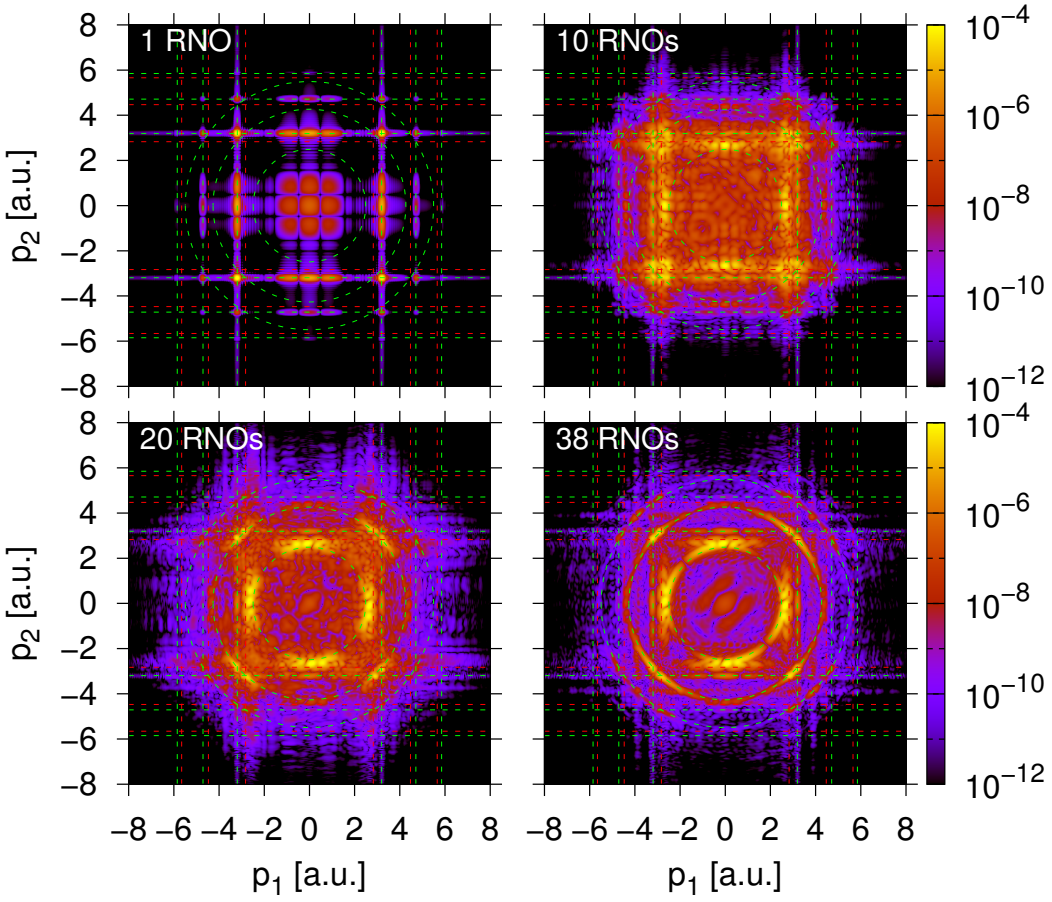

Figure 1.10.: Correlated photoelectron momentum spectrum obtained by TDRNOT with one to 38 RNO (not all are shown). The laser pulse has the same parameters and dashed lines have the same meaning as in Figure 1.8

The correlation entropy (1.41) may be used to quantify the amount of correlation. However, to get a rough estimate, one can also examine how many NOs are needed (calculated from TDSE) to describe a particular feature in the spectra. For instance, 60 NOs are needed to reproduce the spectrum in Figure 1.8. Reproducing the SPDI-ring ($m = 1$) requires 38 NOs. Clearly, SPDI is a very correlated process. Thus, it is interesting to investigate how many RNOs are necessary for TDRNOT to describe SPDI. In actual TDRNOT

calculations one has to restrict the number of NOs, which introduces the so-called "truncation error" [13, 14, 42, 77]. Hence, more NOs are needed to reproduce the correlated photoelectron spectra with TDRNOT than in Figure 1.9 where the NOs were calculated from the TDSE wavefunction. Such TDRNOT calculations of correlated photoelectron spectra in the context of nonsequential double ionization were pursued in Ref. [13]. TDRNOT results for SPDI are shown in 1.10. 38 RNOs are sufficient to describe SPDI well.

1.5. Overview of the published results

In this section the key points of papers 1-5 are summarized.

1.5.1. Paper 1 - Time-dependent renormalized natural orbital theory applied to the two-electron spin-singlet case: Ground state, linear response, and autoionization[12]

In Paper 1, we introduced time-dependent renormalized natural orbital theory (TDRNOT), derived equations of motion and tested the new theory on the two-electron spin-singlet case. We calculate the groundstate RNOs but used just the groundstate $\gamma_{2,ijkl}(t = 0)$ for time propagation, which is an approximation. This approximation is similar to "freezing" the ground-state Kohn-Sham potential during time propagation in time-dependent Kohn-Sham (TDKS) calculations. This is not uncommon and occasionaly phrased "bare" Kohn-Sham response in the literature. Using $\gamma_{2,ijkl}(t = 0)$, we calculated the linear response spectrum and demonstrated that the method is able of describing doubly-exited states. Moreover, those doubly-excited states autoionize, leading to Fano line-shapes in photoelectron momentum spectra. Thereby we showed that TDRNOT is capable to describe effects which are missing in TDDFT with adiabatic exchange-correlation functionals.

1.5.2. Paper 2 - Equations of motion for natural orbitals of strongly driven two-electron systems [77]

In Paper 2, we present the derivation for the exact function $\gamma_{2,ijkl}(t)$ in the two-electron case. We compared results calculated with the exact functional $\gamma_{2,ijkl}(t)$ and with the "frozen" approximation from Paper 1. Unfortunately, it was revealed that the "frozen" approximation becomes worse if we add more RNOs. There are extra peaks in the linear response and peaks are shifted towards lower energy (similar to the results obtained with the Müller functional in Sec. 1.4.3). In addition, we also showed that TDRNOT with the exact functional is able to describe Rabi oscillations, unlike TDDFT. In this paper we also discussed the effect of truncation errors in TDRNOT for the first time.

1.5.3. Papers 3 and 4 - Nonsequential double ionization and strong-field absorption and emission of radiation in two-electron systems calculated with time-dependent natural orbitals [13, 14]

In Papers 3 and 4, we went one step further and investigated the performance of TDRNOT for processes which involve more than two RNOs. To achieve this, we optimized propagations of RNOs. We abandoned the split-operator technique [26], as the splitting error increased if one increased the number of RNOs in the propagation. In Paper 4, we also replaced the unitary Crank–Nicolson [22] propagation with the Dormand–Prince RK54 method [23]. It turned out that the error for orthogonality of RNOs plays a much larger role than the error in the norm. The error for the norm using Dormand–Prince RK54 method is still small (10^{-12}). With this, as one can see from Secs. 1.4.5 and A.3, we were able to propagate more than 38 RNOs. We also extended TDRNOT to non-hermitian potentials to allow imaginary potentials to reduce the grid sizes. Having optimized TDRNOT propagation we tested it on non-sequential double ionization, Fano profiles in absorption spectra, and high-order harmonic spectra. TDRNOT was able to describe all those effects. The number of RNOs required depends on how correlated the process is. For more differential observables one typically needs more RNOs. The effect of the truncation error on the relevant observables was investigated in all cases.

1.5.4. Paper 5 - TDRNOT applied to laser-driven H_2^+ [42]

For Paper 5, we extended the TDRNOT to multicomponent systems. The exact expressions $\gamma_{2,iJkL}(t)$ for the case of (effectively) two distinguishable particles was employed. The extended theory was tested on a 1D model of the H_2^+ hydrogen molecular ion beyond the Born-Oppenheimer approximation. In order to benchmark the extended theory, groundstate properties, linear response spectra, fragmentation, and high-order harmonic generation were investigated. The exact groundstate energy was achieved with very few orbitals. However, the linear response spectra were plagued by multiple sharp peaks that only for very many orbitals would reproduce the correct, broad structure caused by bound-continuum transitions. It was found that TDRNOT was able to reproduce dissociation and Coulomb explosion, and high-harmonics spectra. In the case of high-order harmonics spectra, it was found that 8 RNOs per particle yielded very good agreement with the benchmark result from the TDSE. Here, similarly as in Paper 4, we noticed that the noise level got larger if the number of RNOs in the propagation is increased.

1.6. Conclusion and outlook

We introduced TDRNOT and benchmarked it on a numerically exactly solvable helium model atom. As the exact functional $\gamma_{2,ijkl}(t)$ is known for two electrons, no approximations were necessary, apart from the necessarily truncated number of RNOs considered in the simulations. For two electrons, in the limit of one RNO per spin, TDDFT in exchange-only approximation is recovered. Adding more RNOs per spin is similar to adding Slater determinants in MCTDHF.

We showed that the method correctly describes doubly-excited states, auto-ionization, Fano profiles in photoelectron and absorption spectra, Rabi oscillations, single-photon double ionization, and non-sequential double ionization. Depending on the observable of interest, for some effects, as, e.g., single-photon double ionization, as many as 38 RNOs are required.

Obvious next steps are (i) applying TDRNOT to "real" helium in three dimensions, and (ii) extending TDRNOT to more than two particles. Step (i) is already taken by another PhD student in the group, Julius Rapp. The exact knowledge of the 2-DM in terms of RNOs holds in 3D as well. However, one RNO in the 1D He model corresponds to an entire shell in 3D He, making TDRNOT simulations significantly more demanding in 3D. Selection rules and sum rules can be used to reduce the computational cost. In the two-electron case, TDRNOT should be less demanding than MCDTHF.

Concerning step (ii), the EOM derived in this thesis actually applies to an arbitrary number of electrons. The problem with more than two electrons will be to find a good approximation for the $\tilde{\gamma}_{2,ijkl}(t)$ coefficients, i.e., the 2-RDM. A first, explorative investigation in this derection was pursued in the BSc thesis of Nicolas Künzel in 2014, where the ground state of a one-dimensional Li atom was studied. It was found that the exact $\tilde{\gamma}_{2,ijkl}(t)$ obtained from the solution of the Schrödinger equation (which is possible for this model) has a complicated structure, but an approximation based on an MCHF ansatz for the wavefunction might be a reasonable. However, when it comes to the time evolution of driven three or more electron systems it is not clear at that point whether there is a phase convention that renders $\tilde{\gamma}_{2,ijkl}(t)$ adiabatic.

The success of TDRNOT will rise and fall with the availability of approximate functionals for $\tilde{\gamma}_{2,ijkl}(t)$ that are able to capture the phenomena of interest. Tests of the functionals already available in the literature (see Sec. 1.3) should be performed. Certainly, a promising functional must be N-representable, and, for strong-field applications, the ONs must not be constant.

2. Publications

2.1. Paper 1

Time-dependent renormalized natural orbital theory applied to the two-electron spin-singlet case: Ground state, linear response, and autoionization

Physical Review A 88, 052514:1–14 (2013)

DOI:http://dx.doi.org/10.1103/PhysRevA.88.052514

Author contributions

Martins Brics	Co-development of theory, programming, calculations, figure preparation.
Dieter Bauer	Development of theory, preparation of manuscript, verification of results, figure preparation, supervision.

PHYSICAL REVIEW A **88**, 052514 (2013)

Time-dependent renormalized natural orbital theory applied to the two-electron spin-singlet case: Ground state, linear response, and autoionization

M. Brics and D. Bauer*
Institut für Physik, Universität Rostock, 18051 Rostock, Germany
(Received 6 September 2013; published 19 November 2013)

Favorably scaling numerical time-dependent many-electron techniques such as time-dependent density functional theory (TDDFT) with adiabatic exchange-correlation potentials typically fail in capturing highly correlated electron dynamics. We propose a method based on natural orbitals, i.e., the eigenfunctions of the one-body reduced density matrix, that is almost as inexpensive numerically as adiabatic TDDFT, but which is capable of describing correlated phenomena such as doubly excited states, autoionization, Fano profiles in the photoelectron spectra, and strong-field ionization in general. Equations of motion (EOMs) for natural orbitals and their occupation numbers have been derived earlier. We show that by using renormalized natural orbitals (RNOs) both can be combined into one equation governed by a hermitian effective Hamiltonian. We specialize on the two-electron spin-singlet system, known as being a "worst case" testing ground for TDDFT, and employ the widely used, numerically exactly solvable, one-dimensional helium model atom (in a laser field) to benchmark our approach. The solution of the full, nonlinear EOMs for the RNOs is plagued by instabilities, and resorting to linear response is not an option for the ultimate goal to study nonperturbative dynamics in intense laser fields. We therefore make two rather bold approximations: we employ the initial-state-"frozen" effective RNO Hamiltonian for the time propagation and truncate the number of RNOs to only two per spin. Surprisingly, it turns out that even with these strong approximations we obtain a highly accurate ground state, reproduce doubly excited states, and autoionization.

DOI: 10.1103/PhysRevA.88.052514 PACS number(s): 31.15.ee, 31.70.Hq, 32.80.Zb

I. INTRODUCTION

The "holy grail" of computational many-body theory is to overcome the so-called "exponential wall," i.e., the exponentially increasing numerical effort as a function of the particle number to solve the many-body Schrödinger equation [1]. It is an obvious idea that one should try to replace the high-dimensional many-body wave function by some simpler, lower-dimensional quantity, and then derive equations governing this quantity because the "many-electron wave function tells us more than we need to know" [2]. Reduced density matrices (RDMs) appear to be most suitable for that purpose. In fact, extensive research has been devoted to the properties and applications of RDMs, starting with the classic work by Löwdin [3], already early summarized in [4], and meanwhile covered in books and reviews [5–9], and excellent thesis works [10,11].

For systems with two-body interactions, any observable can be *explicitly* written down in terms of the two-body reduced density matrix (2RDM). The Hohenberg-Kohn theorem [12] of density functional theory (DFT) (see, e.g., [13]) even ensures that any observable (of a system governed by a Hamiltonian with a scalar, local, external potential) is *in principle* a functional of the single-particle density, i.e., the diagonal of the (spin-integrated) one-body reduced density matrix (1RDM). However, these functionals are not known for all observables of interest so that approximations have to be made in practice. Quite reasonably, it seems that the more reduced the quantity employed is, the more approximations have to be made in the governing equations (such as the intricate exchange-correlation (xc) potential in the Kohn-Sham scheme [14]), and for the observables. Employing the 1RDM as the basic "variable" instead of the single-particle density brings us to reduced density-matrix functional theory (RDMFT) [3–8,10,11]. In RDMFT, the Bogoliubov-Born-Green-Kirkwood-Yvon chain of equations needs to be truncated by a (sufficiently accurate) approximation of the 2RDM as a functional of the 1RDM. In the simplest form, this leads just to the Hartree-Fock (HF) equations. Expressions for the 2RDM beyond HF have been devised and applied (see, e.g., [15–19]), although relatively few compared to the abundant literature on xc potentials in DFT. Approaches using directly the 2RDM as the basic variable have been proposed and applied as well [9]. A naive minimization of the energy as a functional of the 2RDM will, however, yield too low energy values, as not all two-matrices (2Ms) originate from an N-electron state. Recent progress in the solution of this so-called N-representability problem has been made by formulating a hierarchy of conditions a 2M has to fulfill in order to be a proper 2RDM (without resorting to higher-order RDMs) [20].

It is computationally beneficial to expand the 1RDM and 2RDM in 1RDM eigenfunctions, the so-called natural orbitals (NOs) [3], as they form the best possible basis set (in a well-defined mathematical sense; see, e.g., [5,11] for details). The resulting equations for these NOs form a set of coupled, nonlinear Schrödinger-like equations [21], as in configuration interaction calculations. The eigenvalue of the 1RDM to which a NO belongs can be interpreted as its occupation number (OCN). Unlike in, e.g., Hartree-Fock, these OCNs are, in general, fractional $\in]0,1[$ in correlated fermionic systems (unless they are "pinned" to 0 or 1 [22,23]).

In this work, we investigate whether NOs can be efficiently employed to describe the correlated *dynamics* of a two-electron

*Corresponding author: dieter.bauer@uni-rostock.de

spin-singlet system in an external, driving field such as that of a laser. Of course, the study of the *structure* of correlated two-electron systems has a long history that started soon after the "invention" of quantum mechanics. In view of a NO description it has been analyzed by Löwdin and Shull in 1956 [24]. The two-electron spin-singlet ground-state wave function has an exceptionally simple structure when expanded in NOs, as the coefficient matrix turns out to be diagonal. This means that the ground-state two-body density matrix (2DM) needs not be approximated in terms of the NOs but is known exactly in the two-electron case.

One may think that the two-electron case is a bit (too) trivial to test a novel time-dependent *many*-body method. However, this is not the case. While electronic structure calculations are difficult enough, time-dependent quantum dynamics beyond linear response with nonperturbative drivers is by far more challenging. In fact, from a computational point of view it is orders of magnitude more demanding because on top of the ground-state problem one, subsequently, needs to propagate the system for typically 10^3–10^4 time steps on numerical grids typically 10^2–10^3 times larger than that for the ground state. It is thus even more important to develop efficient numerical methods capable of describing such strongly driven quantum dynamics. Time-dependent density functional theory (TDDFT) [25,26] works well in many cases but fails (with known and practicable adiabatic xc potentials) whenever the processes to be described rely on strong correlation or involve resonant interaction [27–35]. As the correlation energy (relative to the total energy) typically increases as the number of electrons decreases (down to 2), it is the *few*-body correlated electron dynamics that serve as "worst case" benchmarks for methods beyond TDDFT with adiabatic xc potentials. For instance, autoionization in strong laser fields is currently investigated experimentally [36,37] and particularly challenging for theory because it involves multiply excited states. As multiply excited states are absent in TDDFT using adiabatic xc potentials [25,38] it serves as an ideal testing ground for novel *ab initio* methods going beyond "standard" TDDFT.

An algorithm for propagating NOs and OCNs for two coupled nonlinear oscillators has been proposed in [39]. The general equations of motion (EOM) for the NOs and their OCNs have been derived in [40] (see also [10]). However, the volume of published work on *time-dependent* density matrix functional theory (TDDMFT) is still very limited. Different adiabatic approximations to TDDMFT have been derived and applied to molecules [41–44] and a two-site Hubbard model [45], respectively. Exact time-dependent NO occupations have been investigated [46] using the same numerically exactly solvable model atom employed in the current work. It was found that common approximations for the 2RDM functional render the OCN constant, which is incorrect for, e.g., atoms in strong laser pulses or resonant interactions [33]. A semiclassical approach to propagate the 1RDM that allows for changing OCNs has been proposed in [47] and applied to Moshinsky's two-electron model atom [48].

Our paper is organized as follows. In Sec. II we review the basic density matrix and NO theory for the two-electron case and introduce renormalized NOs (RNOs), which allow us to unify the EOMs for the OCNs and the NOs. Further, we specialize in the spin-singlet case, briefly discuss the time-dependent Hartree-Fock limit, and derive variationally the equations governing the RNO ground-state configuration. In Sec. III we present results for two RNOs per spin. After the ground state is obtained, the linear-response spectrum and autoionization in a laser field are investigated. We conclude and give an outlook in Sec. IV. Details of the derivation of the EOMs for the NOs are given in Appendix A, the relation between the expansion coefficients of the ground-state 2DM and those of the two-electron spin singlet ground state is given in Appendix B. Atomic units are used throughout.

II. THEORY

The hermitian 2DM for a two-electron system with wave function $\Phi(12;t)$ reads

$$\gamma_2(12,1'2';t) = \Phi^*(1'2';t)\Phi(12;t), \tag{1}$$

where the arguments 1, 2, 1′, etc., comprise spatial and spin degrees of freedom (x_1,σ_1), (x_2,σ_2), $(x_1',\sigma_1')\ldots$. The hermitian 1RDM is

$$\gamma_1(1,1';t) = 2\int d2\,\gamma_2(12,1'2;t). \tag{2}$$

Given a Hamiltonian for the two-electron time-dependent Schrödinger equation (TDSE),

$$i\partial_t\Phi(12;t) = \hat{H}(12;t)\Phi(12;t), \tag{3}$$

of the form

$$\hat{H}(12;t) = \hat{h}_0(1;t) + \hat{h}_0(2;t) + v_{ee}(12), \tag{4}$$

where v_{ee} is the electron-electron interaction, the 2DM fulfills the von Neumann equation, while the 1RDM obeys the EOM

$$-i\partial_t\gamma_1(1,1';t) = [\hat{h}_0(1') - \hat{h}_0(1)]\gamma_1(1,1';t) + 2\int d2\,\{v_{ee}(1'2) - v_{ee}(12)\}\gamma_2(12,1'2;t). \tag{5}$$

The hermitian 1RDM can be written in terms of an orthonormalized set of NOs, ϕ_k, $k = 1,2,3,\ldots$, and real, positive-definite OCNs n_k as

$$\gamma_1(1,1';t) = \sum_k n_k(t)\phi_k^*(1';t)\phi_k(1;t), \tag{6}$$

$$\sum_k n_k(t) = 2, \quad \int d1\,|\phi_k(1;t)|^2 = 1. \tag{7}$$

In other words, ϕ_k is the eigenvector of γ_1 with respect to the eigenvalue n_k,

$$\int d1'\,\gamma_1(1,1';t)\phi_k(1';t) = n_k(t)\phi_k(1;t). \tag{8}$$

As the NOs form a complete basis one can expand the 2DM in them,

$$\gamma_2(12,1'2';t) = \sum_{ijkl}\gamma_{2,ijkl}(t)\phi_i(1;t)\phi_j(2;t)\phi_k^*(1';t)\phi_l^*(2';t). \tag{9}$$

A. Equation of motion for renormalized natural orbitals

We find it numerically beneficial to incorporate the OCNs into the NOs by renormalizing them,

$$\tilde{\phi}_k(1;t) = \sqrt{n_k(t)}\,\phi_k(1;t), \tag{10}$$

$$\int d1\,|\tilde{\phi}_k(1;t)|^2 = n_k(t). \tag{11}$$

Inserting the NO expansions of the density matrices γ_1 and γ_2, (6) and (9), respectively, into the EOM for the 1RDM (5), coupled EOMs for the NOs and OCNs have been derived and reviewed in the literature [10,11,40].

We have derived a single EOM that is particularly useful for our purposes. It has the form

$$i\,\partial_t \tilde{\mathbf{\Phi}}(1;t) = \hat{\mathcal{H}}(1;t)\tilde{\mathbf{\Phi}}(1;t) \tag{12}$$

with a hermitian Hamiltonian $\hat{\mathcal{H}}$ and a column vector $\tilde{\mathbf{\Phi}}(1;t)$ with the RNO $\tilde{\phi}_k(1;t)$ in it. The derivation is given in Appendix A, the result being

$$\begin{aligned} i\,\partial_t\tilde{\phi}_n(1;t) = &-\frac{1}{n_n(t)}\left\{2\,\mathrm{Re}\sum_{jkl}\tilde{\gamma}_{2,njkl}(t)\langle\tilde{k}(t)\tilde{l}(t)|v_{ee}|\tilde{n}(t)\tilde{j}(t)\rangle + \langle\tilde{n}(t)|\hat{h}_0(t)|\tilde{n}(t)\rangle\right\}\tilde{\phi}_n(1;t)\\ &+\sum_{k\neq n}\frac{2}{n_k(t)-n_n(t)}\sum_{jpl}\{\tilde{\gamma}_{2,kjpl}(t)\langle\tilde{p}(t)\tilde{l}(t)|v_{ee}|\tilde{n}(t)\tilde{j}(t)\rangle - [\tilde{\gamma}_{2,njpl}(t)\langle\tilde{p}(t)\tilde{l}(t)|v_{ee}|\tilde{k}(t)\tilde{j}(t)\rangle]^*\}\tilde{\phi}_k(1;t)\\ &+\hat{h}_0(1;t)\tilde{\phi}_n(1;t) + 2\sum_k\sum_{jl}\tilde{\gamma}_{2,kjnl}(t)\langle\tilde{l}(t)|v_{ee}|\tilde{j}(t)\rangle(1;t)\,\tilde{\phi}_k(1;t). \end{aligned} \tag{13}$$

Here, we used the abbreviations

$$\tilde{\gamma}_{2,njkl}(t) = \frac{\gamma_{2,njkl}(t)}{\sqrt{n_n(t)n_j(t)n_k(t)n_l(t)}}, \tag{14}$$

$$\langle\tilde{l}(t)|v_{ee}|\tilde{j}(t)\rangle(1;t) = \int d1'\,\tilde{\phi}_l^*(1';t)v_{ee}(11')\tilde{\phi}_j(1';t), \tag{15}$$

$$\begin{aligned}&\langle\tilde{k}(t)\tilde{l}(t)|v_{ee}|\tilde{n}(t)\tilde{j}(t)\rangle\\ &\quad= \int d1\,\tilde{\phi}_k^*(1;t)\langle\tilde{l}(t)|v_{ee}|\tilde{j}(t)\rangle(1;t)\tilde{\phi}_n(1;t).\end{aligned} \tag{16}$$

With (11), Eq. (13) is a set of coupled EOMs for the RNOs alone.

Multiplication of (13) by $\tilde{\phi}_n^*(1;t)$ and integration $\int d1$ yields

$$\dot{n}_n(t) = -4\ \mathrm{Im}\sum_{jkl}\tilde{\gamma}_{2,njkl}(t)\langle\tilde{k}(t)\tilde{l}(t)|v_{ee}|\tilde{n}(t)\tilde{j}(t)\rangle, \tag{17}$$

which, expressed in terms of NOs instead of RNOs, has been derived earlier [40]. This equation is useful to see whether a certain approximation of $\tilde{\gamma}_{2,njkl}$ will lead to time-varying OCNs or constant OCNs. For instance, common approximations of the form

$$\tilde{\gamma}_{2,njkl}^{(\mathrm{approx})}(t) = f_{njkl}(t)\delta_{nk}\delta_{jl} - g_{njkl}(t)\delta_{nl}\delta_{jk} \tag{18}$$

with $f_{njkl}(t)$ and $g_{njkl}(t)$ real will lead to constant OCNs, $\dot{n}_n(t)\equiv 0$, because all NO phases that could lead to an imaginary part on the right-hand side of (17) cancel. From the exact numerical solution of the two-electron TDSE we know that for, e.g., resonant interactions (Rabi floppings) and in other scenarios, the OCNs *do* change in time [33,46,47].

If the total number of particles is conserved,

$$0 = \mathrm{Im}\sum_{njkl}\tilde{\gamma}_{2,njkl}(t)\langle\tilde{k}(t)\tilde{l}(t)|v_{ee}|\tilde{n}(t)\tilde{j}(t)\rangle \tag{19}$$

follows from (17) upon summing over n. Moreover, one finds that the RNOs stay mutually orthogonal if

$$\mathcal{D}_{nm}(t) = \mathcal{D}_{mn}^*(t) \tag{20}$$

holds, where

$$\mathcal{D}_{nm}(t) = \sum_{kjl}\tilde{\gamma}_{2,kjnl}(t)\langle\tilde{m}(t)\tilde{l}(t)|v_{ee}|\tilde{k}(t)\tilde{j}(t)\rangle. \tag{21}$$

As the RNOs, being $\forall t$ eigenfunctions of a hermitian matrix, *should* stay orthogonal, Eq. (20) poses a condition any approximation of $\tilde{\gamma}_{2,kjnl}(t)$ has to fulfill.

B. Two-electron spin-singlet case

If the two-electron wave function is $\forall t$ of the spin-singlet form

$$\Phi(12;t) = \Phi(x_1x_2;t)\frac{1}{\sqrt{2}}(\delta_{\sigma_1+}\delta_{\sigma_2-} - \delta_{\sigma_1-}\delta_{\sigma_2+}), \tag{22}$$

$\Phi(x_1x_2;t) = \Phi(x_2x_1;t)$ (with "+" and "−" for "spin up" and "spin down," respectively), we have with (1) and

$$\gamma_1(x_1,x_1';t) = 2\int dx_2\,\Phi^*(x_1'x_2;t)\Phi(x_1x_2;t) \tag{23}$$

that

$$\gamma_1(1,1';t) = \tfrac{1}{2}\gamma_1(x_1,x_1';t)(\delta_{\sigma_1+}\delta_{\sigma_1'+} + \delta_{\sigma_1-}\delta_{\sigma_1'-}). \tag{24}$$

We switch temporarily back to NOs normalized to unity. Making the ansatz

$$\phi_k(x\sigma;t) = \phi_k(x;t)\,(a_k\delta_{\sigma+} + b_k\delta_{\sigma-}), \tag{25}$$

$$|a_k|^2 + |b_k|^2 = 1, \quad \int dx\,|\phi_k(x;t)|^2 = 1, \tag{26}$$

one simply finds the same form for the spin-reduced 1RDM as in (6),

$$\gamma_1(x,x';t) = \sum_k n_k(t)\phi_k^*(x';t)\phi_k(x;t). \tag{27}$$

Because of orthonormality of the NOs, for $k \neq k'$

$$(a_k^* a_k + b_{k'}^* b_k) \int dx\, \phi_{k'}^*(x;t)\phi_k(x;t) = 0 \tag{28}$$

need to be fulfilled so that either the spatial part of the NOs must be orthogonal or the spin part. For a given spin part of ϕ_k with coefficients a_k and b_k one can always find (up to an irrelevant phase factor) a normalized spin part $(a_{k'}\delta_{\sigma+} + b_{k'}\delta_{\sigma-})$ of $\phi_{k'}$ that is orthogonal to $(a_k\delta_{\sigma+} + b_k\delta_{\sigma-})$. A convenient choice is $a_k = 1$, $b_k = 0$, $a_{k'} = 0$, $b_{k'} = 1$ while $\phi_{k'}(x;t) = \phi_k(x;t)$. In other words, the spatial NOs appear *pairwise* equal, with opposite spin parts. This is probably the most trivial example of a *pairing* phenomenon. One may order the NOs such that for odd k the following equations hold:

$$\phi_k(x\sigma;t) = \phi_k(x;t)\,\delta_{\sigma+}, \quad k = 1,3,5,\ldots, \tag{29}$$

$$\phi_k(x;t) = \phi_{k+1}(x;t), \tag{30}$$

$$\phi_{k+1}(x\sigma;t) = \phi_{k+1}(x;t)\,\delta_{\sigma-} = \phi_k(x;t)\,\delta_{\sigma-}. \tag{31}$$

Then we can write instead of (27)

$$\gamma_1(x,x';t) = 2\sum_{k\ \mathrm{odd}} n_k(t)\phi_k^*(x';t)\phi_k(x;t), \tag{32}$$

and we need to consider only half of the NOs (i.e., those with, e.g., the odd indices, i.e., spin up) in the following.

Because the spatial spin-singlet wave function is symmetric it can be shown [11] that its expansion in NOs is diagonal,

$$\Phi(x_1x_2;t) = \sum_{i\ \mathrm{odd}} D_i(t)\,\phi_i(x_1;t)\phi_i(x_2;t), \tag{33}$$

where, because of (23) and (27),

$$|D_i(t)|^2 = n_i(t). \tag{34}$$

We can thus use the NO expansion coefficients for the wave function $D_i(t)$ instead of resorting to the NO expansion coefficients $\gamma_{2,njkl}(t)$ for the 2DM. How both are connected is discussed in Appendix B. Formally, in Eq. (33) the time-dependent spatial two-electron wave function is written as a single *geminal* [49], expanded in time-dependent NOs.

The EOMs for the spatial RNOs in terms of the time-dependent geminal expansion coefficients D_i can be written as (from now on all time arguments are suppressed for brevity)

$$i\,\partial_t\tilde{\phi}_n(x) = \hat{\mathcal{H}}_n^0(x)\tilde{\phi}_n(x) + \sum_{k\ \mathrm{odd}\neq n} \mathcal{H}_{nk}^1(x)\tilde{\phi}_k(x), \tag{35}$$

where

$$\hat{\mathcal{H}}_n^0(x) = A_n + \hat{\mathcal{K}}_n^0(x), \tag{36}$$

$$\mathcal{H}_{nk}^1(x) = B_{nk} + \mathcal{K}_{nk}^1(x) \tag{37}$$

with

$$A_n = -\frac{1}{n_n}\left[\mathrm{Re}\left(\sum_{k\ \mathrm{odd}} \frac{D_n D_k^*}{n_n n_k}\langle\tilde{k}\tilde{k}|v_{ee}|\tilde{n}\tilde{n}\rangle_x\right) + \langle\tilde{n}|\hat{h}_0|\tilde{n}\rangle_x\right],$$

$$\hat{\mathcal{K}}_n^0(x) = \hat{h}_0(x) + \frac{\langle\tilde{n}|v_{ee}|\tilde{n}\rangle_x(x)}{n_n}, \tag{38}$$

$$B_{nk} = \frac{1}{n_k - n_n}\sum_{p\ \mathrm{odd}}\left(\frac{D_k\,D_p^*}{n_k n_p}\langle\tilde{p}\tilde{p}|v_{ee}|\tilde{n}\tilde{k}\rangle_x - \left[\frac{D_n\,D_p^*}{n_n n_p}\langle\tilde{p}\tilde{p}|v_{ee}|\tilde{k}\tilde{n}\rangle_x\right]^*\right),$$

$$\mathcal{K}_{nk}^1(x) = \frac{D_k\,D_n^*}{n_k n_n}\langle\tilde{n}|v_{ee}|\tilde{k}\rangle_x(x), \tag{39}$$

and the potentials $\langle\tilde{n}|v_{ee}|\tilde{k}\rangle_x(x)$ and matrix elements $\langle\tilde{p}\tilde{p}|v_{ee}|\tilde{n}\tilde{k}\rangle_x$ defined as in (15) and (16) but all integrals with respect to position space only. Here we exploit that the electron-electron interaction does not directly involve the spin degrees of freedom.

C. Time-dependent Hartree-Fock limit

Equations (35)–(39) reduce to the two-electron spin-singlet Hartree-Fock limit for $n_1 = n_2 = 1$, $\tilde{\phi}_1(x) = \phi_1(x) = \tilde{\phi}_2(x) = \phi_2(x)$, and all other OCNs (and thus RNOs) zero. The (in the NO index) off-diagonal part of the Hamiltonian $\mathcal{H}_{nk}^1(x)$ in (35) therefore vanishes, and

$$A_1 = -\langle 11|v_{ee}|11\rangle_x - \langle 1|\hat{h}_0|1\rangle_x,$$

$$\hat{\mathcal{K}}_1^0(x) = \hat{h}_0(x) + \langle 1|v_{ee}|1\rangle_x(x)$$

so that

$$i\,\partial_t\phi_1(x) = [\hat{h}_0(x) + \langle 1|v_{ee}|1\rangle_x(x) + A_1]\phi_1(x),$$

which is indeed the time-dependent Hartree-Fock (TDHF) equation for the two-electron spin-singlet system (where the Fock term cancels half of the Hartree). In the case of the two-electron spin-singlet system TDHF is equivalent to a time-dependent Kohn-Sham (TDKS) treatment in "exact-exchange approximation" (EXA) and the correlation potential set to zero. Note that, unlike in the general case with more than one NO per spin, the purely time-dependent term A_1 can be eliminated via a contact transformation $\phi_1(x) \to \phi_1(x)\,\exp[-i\int^t A_1(t')\,dt']$ here.

D. Ground state

A time-dependent calculation most often starts from the ground state. As we need anyway a code that propagates the RNOs in time according (35) it would be convenient to use imaginary-time propagation for finding the ground state, as is commonly done in TDSE solvers. On the other hand, it must be possible to derive the ground state in terms of RNOs via a minimization approach. We show now that both ways will indeed lead to the same result.

The ground-state energy to be minimized is

$$E = \int d1[\hat{h}_0(1')\gamma_1(1',1)]_{1'=1} + \int d1 \int d2\, v_{ee}(|1-2|)\gamma_2(12,12). \quad (40)$$

Expressed in RNOs, the energy becomes

$$E = 2\sum_{i\ \mathrm{odd}}\langle\tilde{i}|\hat{h}_0|\tilde{i}\rangle_x + \sum_{i\ \mathrm{odd}}\sum_{j\ \mathrm{odd}}\frac{e^{i(\varphi_j-\varphi_i)}}{\sqrt{\langle\tilde{i}|\tilde{i}\rangle_x\langle\tilde{j}|\tilde{j}\rangle_x}}\langle\tilde{i}\tilde{i}|v_{ee}|\tilde{j}\tilde{j}\rangle_x, \quad (41)$$

where we introduced the phases φ_i via [cf. Eq. (34)]

$$D_i = \sqrt{n_i}\, e^{i\varphi_i} \quad (42)$$

and explicitly write

$$n_i = \langle\tilde{i}|\tilde{i}\rangle_x. \quad (43)$$

We define a functional $\tilde{E}[\{|\tilde{i}\rangle\},\{\langle\tilde{i}|\}]$ that takes the constraint $\sum_{i\ \mathrm{odd}}\langle\tilde{i}|\tilde{i}\rangle = \sum_{i\ \mathrm{odd}} n_i = 1$ via the Lagrange parameter ϵ into account, the orthogonality of the RNOs via λ_{ij}, $\lambda_{ii}=0$, the condition $n_i \geqslant 0$ via ϵ_i^0, and $n_i \leqslant 1$ through ϵ_i^1 (Karush-Kuhn-Tucker conditions, see, e.g., [11,50]),

$$\tilde{E} = 2\sum_{i\ \mathrm{odd}}\langle\tilde{i}|\hat{h}_0|\tilde{i}\rangle + \sum_{i\ \mathrm{odd}}\sum_{j\ \mathrm{odd}}\frac{e^{i(\varphi_j-\varphi_i)}}{\sqrt{\langle\tilde{i}|\tilde{i}\rangle\langle\tilde{j}|\tilde{j}\rangle}}\langle\tilde{i}\tilde{i}|v_{ee}|\tilde{j}\tilde{j}\rangle - \epsilon\left(\sum_{i\ \mathrm{odd}}\langle\tilde{i}|\tilde{i}\rangle - 1\right) - \sum_{i\ \mathrm{odd}}\sum_{j\ \mathrm{odd}\neq i}\lambda_{ij}\langle\tilde{i}|\tilde{j}\rangle - \sum_{i\ \mathrm{odd}}\left[\epsilon_i^0\langle\tilde{i}|\tilde{i}\rangle + \epsilon_i^1(1-\langle\tilde{i}|\tilde{i}\rangle)\right]. \quad (44)$$

Here, we dropped the index x at $\langle\cdot|\cdot\rangle_x$. The "slackness conditions" are [11]

$$\epsilon_i^0 n_i = \epsilon_i^0\langle\tilde{i}|\tilde{i}\rangle = 0, \quad \epsilon_i^1(1-n_i) = \epsilon_i^1(1-\langle\tilde{i}|\tilde{i}\rangle) = 0. \quad (45)$$

Actually, the energy functional $\tilde{E}$ depends not only on the RNOs but also on the phases $\{\varphi_j\}$ of the geminal expansion coefficients. We suppress this dependence here because the values of these phases for the He spin-singlet ground-state case are already known [see Eq. (73) below]. A more general approach to the ground-state problem based on geminals (where these phases are part of the minimization procedure) has been proposed and applied in [49,51].

A variation of $\tilde{E}$ with respect to $\langle\tilde{k}|$ and $|\tilde{k}\rangle$ leads with

$$\epsilon_k = \epsilon + \epsilon_k^0 - \epsilon_k^1 \quad (46)$$

to

$$\epsilon_k|\tilde{k}\rangle = \left\{2\left[\hat{h}_0 + \frac{1}{n_k}\langle\tilde{k}|v_{ee}|\tilde{k}\rangle(x)\right] - \frac{1}{n_k}\mathrm{Re}\left[\sum_{j\ \mathrm{odd}}\frac{D_j D_k^*\langle\tilde{k}\tilde{k}|v_{ee}|\tilde{j}\tilde{j}\rangle}{n_k n_j}\right]\right\}|\tilde{k}\rangle + \sum_{j\ \mathrm{odd}\neq k}\left\{2\frac{D_j D_k^*}{n_j n_k}\langle\tilde{k}|v_{ee}|\tilde{j}\rangle(x) - \lambda_{kj}\right\}|\tilde{j}\rangle, \quad (47)$$

and the hermitian conjugate of it. Multiplying by $\langle\tilde{i}|$ from the left (and the hermitian conjugate by $|\tilde{i}\rangle$ from the right) leads for $i=k$ to

$$\epsilon_i = \frac{1}{n_i}\left(2\langle\tilde{i}|\hat{h}_0|\tilde{i}\rangle + \sum_{j\ \mathrm{odd}}\left\{2\frac{D_j D_i^*}{n_i n_j}\langle\tilde{i}\tilde{i}|v_{ee}|\tilde{j}\tilde{j}\rangle - \mathrm{Re}\left[\frac{D_j D_i^*}{n_i n_j}\langle\tilde{i}\tilde{i}|v_{ee}|\tilde{j}\tilde{j}\rangle\right]\right\}\right), \quad (48)$$

$$\forall i \quad 0 = \mathrm{Im}\sum_{j\ \mathrm{odd}}\frac{D_j D_i^*}{n_j}\langle\tilde{i}\tilde{i}|v_{ee}|\tilde{j}\tilde{j}\rangle, \quad (49)$$

and for $i \neq k$ to

$$\lambda_{ki} = \frac{2}{n_i}\left[\langle\tilde{i}|\hat{h}_0|\tilde{k}\rangle + \sum_{j\ \mathrm{odd}}\frac{D_j D_k^*}{n_k n_j}\langle\tilde{k}\tilde{i}|v_{ee}|\tilde{j}\tilde{j}\rangle\right] = \lambda_{ik}^*, \quad (50)$$

$$\lambda_{ik} = \frac{2}{n_k}\left[\langle\tilde{k}|\hat{h}_0|\tilde{i}\rangle + \sum_{j\ \mathrm{odd}}\frac{D_j D_i^*}{n_i n_j}\langle\tilde{i}\tilde{k}|v_{ee}|\tilde{j}\tilde{j}\rangle\right]. \quad (51)$$

From this follows

$$\langle\tilde{k}|\hat{h}_0|\tilde{i}\rangle = \frac{1}{n_i - n_k}\sum_{j\ \mathrm{odd}}\frac{1}{n_j} \times (D_k D_j^*\langle\tilde{j}\tilde{j}|v_{ee}|\tilde{k}\tilde{i}\rangle - D_j D_i^*\langle\tilde{i}\tilde{k}|v_{ee}|\tilde{j}\tilde{j}\rangle), \quad (52)$$

which can be used to remove $\hat{h}_0$ entirely from the off-diagonal (with respect to the NO index) part of the Hamiltonian.

Putting Eqs. (47)–(52) together we can write

$$0 = \hat{\mathcal{H}}_n^{00}(x)\tilde{\phi}_n(x) + \sum_{k\ \mathrm{odd}\neq n}\mathcal{H}_{nk}^{01}(x)\tilde{\phi}_k(x),$$
$$\hat{\mathcal{H}}_n^{00}(x) = A_n^0 + \hat{\mathcal{K}}_n^{00}(x), \quad (53)$$
$$\mathcal{H}_{nk}^{01}(x) = B_{nk}^0 + \mathcal{K}_{nk}^{01}(x)$$

with

$$A_n^0 = -\frac{1}{n_n}\left(\langle\tilde{n}|\hat{h}_0|\tilde{n}\rangle + \mathrm{Re}\sum_{k\ \mathrm{odd}}\frac{D_k D_n^*}{n_n n_k}\langle\tilde{n}\tilde{n}|v_{ee}|\tilde{k}\tilde{k}\rangle\right),$$
$$\hat{\mathcal{K}}_n^{00}(x) = \hat{h}_0 + \frac{1}{n_n}\langle\tilde{n}|v_{ee}|\tilde{n}\rangle(x), \quad (54)$$
$$B_{nk} = \frac{1}{n_k - n_n}\sum_{p\ \mathrm{odd}}\left(\frac{D_k D_p^*}{n_k n_p}\langle\tilde{p}\tilde{p}|v_{ee}|\tilde{k}\tilde{n}\rangle - \frac{D_p D_n^*}{n_n n_p}\langle\tilde{n}\tilde{k}|v_{ee}|\tilde{p}\tilde{p}\rangle\right),$$
$$\mathcal{K}_{nk}^{01}(x) = \frac{D_k D_n^*}{n_k n_n}\langle\tilde{n}|v_{ee}|\tilde{k}\rangle(x). \quad (55)$$

Hence, we obtain by this variational method indeed the time-independent, ground-state analog of Eqs. (35)–(39). This allows for finding the RNO ground-state configuration (for a given set of OCNs) by imaginary time propagation of the time-dependent Schrödinger-like, nonlinear equation (35) (see Sec. III A below).

The ϵ_k in (47) play the role of orbital energies. Unless the OCNs are pinned to $n_k = 0$ or 1 we have noninteger $0 < n_k < 1$ for correlated systems. In such cases Eqs. (45) imply $\epsilon_k^0 = 0$,

$\epsilon_k^1 = 0$ so that

$$\epsilon_k = \epsilon, \tag{56}$$

i.e., all orbital energies are equal. The ground-state RNOs and wave-function expansion coefficients D_j can be chosen real. Thus we have with (48)

$$\forall i \quad \epsilon = \epsilon_i = \frac{1}{n_i}\left(2\langle\tilde{i}|\hat{h}_0|\tilde{i}\rangle + \sum_{j\ \mathrm{odd}} \frac{D_j D_i}{n_i n_j}\langle\tilde{i}\tilde{i}|v_{ee}|\tilde{j}\tilde{j}\rangle\right) \tag{57}$$

and thus

$$\sum_{i\ \mathrm{odd}} \epsilon_i n_i = \epsilon \sum_{i\ \mathrm{odd}} n_i = \epsilon = E \tag{58}$$

because the total energy is, according to (41),

$$E = 2\sum_{i\ \mathrm{odd}}\langle\tilde{i}|\hat{h}_0|\tilde{i}\rangle + \sum_{i,j\ \mathrm{odd}} \frac{D_j D_i}{n_i n_j}\langle\tilde{i}\tilde{i}|v_{ee}|\tilde{j}\tilde{j}\rangle. \tag{59}$$

As already noticed in [52], the aesthetically appealing result (58) is puzzling, at least at first sight. All orbital energies are equal and equal to the total energy of the system. Only with NOs and their fractional OCNs does the simple additive form $E = \sum_i \epsilon_i n_i$—commonly known only from *noninteracting* systems—persist here for *interacting* systems.

E. Two orbitals per spin

In our code that actually solves (35) we work on a numerical grid representing the discretized space variable x and the RNO index $n = 1,3,\ldots N_{\mathrm{RNO}}$ (see Fig. 1). All sums over the RNO indices have to be terminated at some finite N_{RNO} in practice. Let us consider the simplest yet nontrivial case of two RNOs (per spin), i.e.,

$$n_1 = n_2 \neq 0, \quad n_3 = n_4 \neq 0, \quad n_i = 0 \quad \text{for} \quad i > 4, \tag{60}$$

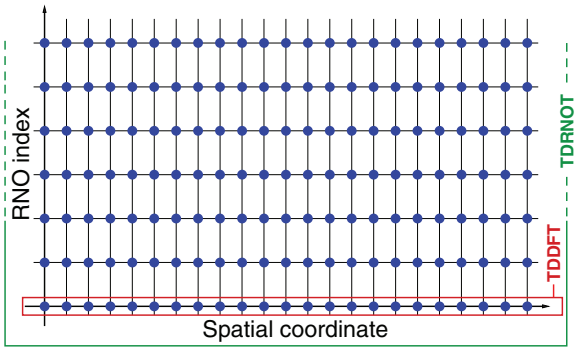

FIG. 1. (Color online) Sketch of the numerical grid. Each row corresponds to one of the RNOs. Horizontal flux of probability density represents motion in position space with the OCNs kept constant. Flux in vertical direction implies a change in the OCNs. Because we work with RNOs instead of NOs, the time evolution on this grid is unitary. In the two-electron spin-singlet case the restriction to a single RNO (per spin) corresponds to TDHF or TDDFT in EXA approximation (red). In time-dependent RNO theory (TDRNOT, green) more than one RNO is allowed.

which implies

$$\tilde{\phi}_1 = \tilde{\phi}_2, \quad \tilde{\phi}_3 = \tilde{\phi}_4, \quad \tilde{\phi}_i \equiv 0 \quad \text{for} \quad i > 4. \tag{61}$$

As a single NO (per spin) is equivalent to TDHF (cf. Sec. II C), allowing for two RNOs per spin is just "one small step beyond TDHF." However, we shall see below that two RNOs per spin are already enough to describe some of the correlated two-electron dynamics completely missed by TDHF (or TDKS in EXA). The relevant terms in (35) in this case are

$$\hat{\mathcal{H}}_1^0(x) = A_1 + \hat{\mathcal{K}}_1^0(x), \quad \hat{\mathcal{H}}_3^0(x) = A_3 + \hat{\mathcal{K}}_3^0(x), \tag{62}$$

$$\mathcal{H}_{13}^1(x) = B_{13} + \mathcal{K}_{13}^1(x), \quad \mathcal{H}_{31}^1(x) = \mathcal{H}_{13}^{1\,*}(x). \tag{63}$$

We find, making use of (34),

$$A_1 = -\frac{1}{n_1}\left[\mathrm{Re}\left(\langle\tilde{1}\tilde{1}|v_{ee}|\tilde{1}\tilde{1}\rangle + \frac{D_1 D_3^*}{n_1 n_3}\langle\tilde{3}\tilde{3}|v_{ee}|\tilde{1}\tilde{1}\rangle\right) + \langle\tilde{1}|\hat{h}_0|\tilde{1}\rangle\right], \quad A_3 = A_1[1 \leftrightarrow 3], \tag{64}$$

$$\hat{\mathcal{K}}_1^0(x) = \hat{h}_0(x) + \frac{\langle\tilde{1}|v_{ee}|\tilde{1}\rangle(x)}{n_1}, \quad \hat{\mathcal{K}}_3^0(x) = \hat{\mathcal{K}}_1^0(x)[1 \leftrightarrow 3], \tag{65}$$

$$B_{13} = \frac{1}{n_3 - n_1}\left(\frac{D_3 D_1^*}{n_1 n_3}\langle\tilde{1}\tilde{1}|v_{ee}|\tilde{1}\tilde{3}\rangle + \frac{\langle\tilde{3}\tilde{3}|v_{ee}|\tilde{1}\tilde{3}\rangle}{n_3} - \left[\frac{D_1 D_3^*}{n_1 n_3}\langle\tilde{3}\tilde{3}|v_{ee}|\tilde{3}\tilde{1}\rangle + \frac{\langle\tilde{1}\tilde{1}|v_{ee}|\tilde{3}\tilde{1}\rangle}{n_1}\right]^*\right), \quad B_{31} = B_{13}^*, \tag{66}$$

$$\mathcal{K}_{13}^1(x) = \frac{D_3 D_1^*}{n_1 n_3}\langle\tilde{1}|v_{ee}|\tilde{3}\rangle(x), \quad \mathcal{K}_{31}^1(x) = \mathcal{K}_{13}^{1\,*}(x), \tag{67}$$

and the equation of motion has the simple structure,

$$i\partial_t\begin{pmatrix}\tilde{\phi}_1(x)\\ \tilde{\phi}_3(x)\end{pmatrix} = \begin{pmatrix}\hat{\mathcal{H}}_1^0(x) & \mathcal{H}_{13}^1(x)\\ \mathcal{H}_{31}^1(x) & \hat{\mathcal{H}}_3^0(x)\end{pmatrix}\begin{pmatrix}\tilde{\phi}_1(x)\\ \tilde{\phi}_3(x)\end{pmatrix}. \tag{68}$$

Here, the off-diagonal elements determine whether or not the OCNs are constant,

$$\dot{n}_1 = 2\,\mathrm{Im}\,\langle\tilde{1}|\mathcal{H}_{13}^1|\tilde{3}\rangle, \quad \dot{n}_3 = 2\,\mathrm{Im}\,\langle\tilde{3}|\mathcal{H}_{13}^{1\,*}|\tilde{1}\rangle. \tag{69}$$

Furthermore, it is easy to show that the RNOs $\tilde{\phi}_1$ and $\tilde{\phi}_3$ stay orthogonal at all times.

III. RESULTS AND DISCUSSION

The results in the following are obtained for the well-known model heliumlike atom introduced in [53] and used extensively ever since (see, e.g., [32,33,46,54]). In the spin-singlet configuration the full two-body TDSE reads

$$i\frac{\partial}{\partial t}\Psi(x_1x_2;t) = \left[\sum_{i=1}^{2}\left(-\frac{1}{2}\frac{\partial^2}{\partial x_i^2} - \frac{2}{\sqrt{x_i^2+1}} - iA(t)\frac{\partial}{\partial x_i}\right) + \frac{1}{\sqrt{(x_1-x_2)^2+1}}\right]\Psi(x_1x_2;t). \quad (70)$$

We employ the velocity gauge to couple an external field with vector potential $A(t)$ in dipole approximation to the model atom (with the purely time-dependent term $\sim A^2$ "transformed away"). The corresponding one-body Hamiltonian for the RNO equations reads accordingly

$$\hat{h}_0 = -\frac{1}{2}\frac{\partial^2}{\partial x^2} - iA(t)\frac{\partial}{\partial x} - \frac{2}{\sqrt{x^2+1}} \quad (71)$$

and

$$v_{ee}(x_1x_2) = \frac{1}{\sqrt{(x_1-x_2)^2+1}}. \quad (72)$$

For the real spin-singlet ground-state wave function of the He atom the geminal expansion coefficients D_i are

$$D_1 = \sqrt{n_1}, \quad D_i = -\sqrt{n_i} \quad \text{for} \quad i = 3,5,7,\ldots, \quad (73)$$

or, in terms of the phases introduced in Sec. II D,

$$\varphi_1 = 0, \quad \varphi_i = \pi \quad \text{for} \quad i = 3,5,7,\ldots. \quad (74)$$

A two-fermion system is the fortunate case where these phases are typically known for stationary configurations. However, it is in general not known how the D_i (or φ_i) change in time with an external driver $A(t)$ switched on (unless we solve the full two-electron TDSE and extract this information).

A. Ground-state RNOs

We applied imaginary-time propagation in combination with Gram-Schmidt orthogonalization to (68) with the D_i according (73) inserted in (64)–(67) in order to find the ground-state configuration for given OCN. A grid with $N_x = 500$ spatial points and a resolution of $\Delta x = 0.4$ was found to be sufficient for that purpose.

From Sec. II D we know that if we try all combinations

$$n_1 = 1.0 - y, \quad n_3 = y, \quad n_1 + n_3 = 1, \quad y \in [0,1], \quad (75)$$

the ground-state configuration will be the one for which

$$\epsilon_1 = \epsilon_3 = \epsilon = E. \quad (76)$$

Figure 2 shows the orbital energies ϵ_1, ϵ_3 and the total energy E according (48) and (59), respectively, vs n_1. Condition (76) is fulfilled for

$$n_1 = 0.991\,27, \quad n_3 = 8.73 \times 10^{-3}, \quad (77)$$

with a total energy

$$E_{N_{\mathrm{RNO}}=2} = -2.2366. \quad (78)$$

The two NOs are shown in Fig. 3.

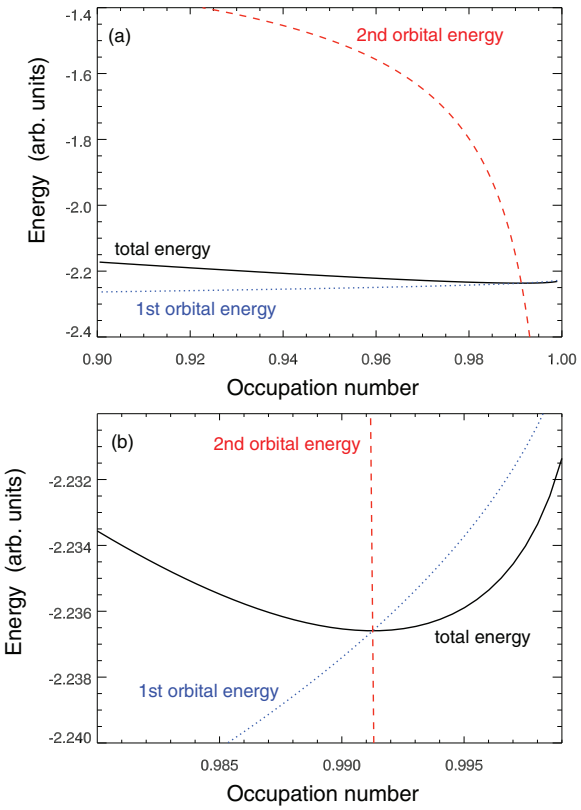

FIG. 2. (Color online) Orbital energies ϵ_1 (dotted blue), ϵ_3 (dashed red), and total energy E (solid black) vs the dominant OCN n_1. The physically relevant RNOs are obtained when the three curves cross [cf. (56) and (58)]. Panel (b) shows a zoom into the narrow n_1 region where all energies cross in one point. The curves cross in the minimum of E.

From the full TDSE solution on a spatial 500×500 grid, also with $\Delta x = 0.4$, we obtain the reference value for the ground-state energy,

$$E_{\mathrm{TDSE}} = -2.2384 \quad (79)$$

and, via diagonalization of the 1RDM calculated from the two-body Schrödinger wave function, for the first five OCNs $n_1 = 0.990\,96$, $n_3 = 8.297 \times 10^{-3}$, $n_5 = 7.063 \times 10^{-4}$, $n_7 = 3.127 \times 10^{-5}$, $n_9 = 7.392 \times 10^{-6}$. The relative error in the total energy is thus only 0.08%. The HF ground-state energy of the system is $E_{\mathrm{HF}} = 2.2243$, i.e., with 0.6% relative error.

The OCNs n_1 and n_3 we obtain for $N_{\mathrm{RNO}} = 2$ are slightly above the exact values because the two alone are already forced to sum up to unity.

The logarithmic ground-state contour plot of the full TDSE two-body electron density $|\Psi(x_1x_2;t)|^2$ shows characteristic kinks along the diagonal $x_1 = x_2$ [see Fig. 6(a) below]. These kinks are not reproduced with only two RNOs since they are visible only on a probability density level governed by higher-order RNOs which have a much smaller OCN and which are spatially more extended. Nevertheless, we will see that two RNOs are already sufficient to describe, e.g., doubly excited

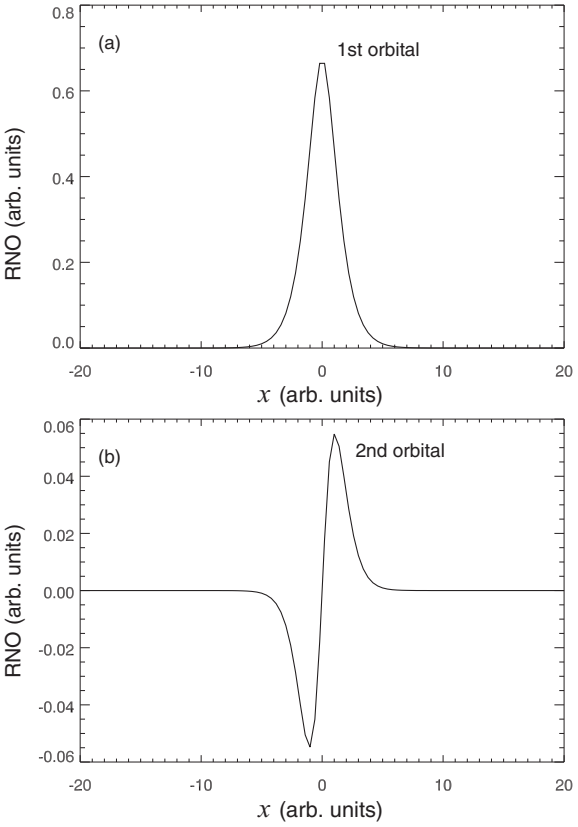

FIG. 3. Ground-state orbitals $\tilde{\phi}_1$ (a) and $\tilde{\phi}_3$ (b) for $N_{\mathrm{RNO}} = 2$.

states and autoionization, not captured by (TD)DFT employing adiabatic xc potentials.

B. "Frozen" Hamiltonian

The full nonlinear system (35) [and even its truncated form (68)] is numerically difficult to handle because of instabilities. The time evolution of the RNOs and the OCNs (i.e., the RNO norms) is extremely sensitive to the phases $\varphi_i(t)$. Although we apply an unconditionally stable (i.e., exactly unitary) propagation algorithm (including predictor-corrector steps) to our Schrödinger-like equation (68) (with a hermitian Hamiltonian), the individual OCNs $n_i(t) = \langle\tilde{i}(t)|\tilde{i}(t)\rangle$—while still adding up to unity—tend to develop an unphysical, rather erratic behavior after some time of propagation. Such a behavior is actually to be anticipated from Eqs. (69): the phases of the D_i *and* the phases of the RNOs determine the changes in the OCNs n_i which, in turn, are fed back into the Hamiltonian. One way to mitigate these instabilities is to make approximations to $\tilde{\gamma}_{2,ijkl}$ that keep the OCNs constant. However, the change of the OCNs is often crucial to capture strongly driven, correlated, or resonant electron dynamics [33,46,47].

In TDKS calculations it is not uncommon to "freeze" the ground-state Kohn-Sham potential during time propagation, leading to the so-called "bare" Kohn-Sham response. The result can be compared to the full TDKS calculation. In this way one may identify the effect of the nonlinearity in the full Kohn-Sham potential. For instance, the peaks in the linear-response spectrum obtained from the bare Kohn-Sham Hamiltonian correspond to the (allowed) transitions between the eigenstates of this Hamiltonian. The nonlinearity in the full Kohn-Sham potential typically moves the peaks from the frozen transition energies towards the correct position (see [32] for the case of the model He atom studied here). We expect something similar for the differences in the linear-response spectrum calculated with the full, nonlinear Hamiltonian in (35) [or, for two RNOs, (68)] and the ground-state RNO-frozen Hamiltonian. Let us denote the ground-state RNOs, OCNs, etc. by the corresponding underlined quantities. Then, for two RNOs per spin, Eqs. (64)–(67) become

$$\underline{A}_1 = -\frac{1}{\underline{n}_1}\left[\langle\tilde{1}\tilde{1}|v_{ee}|\underline{\tilde{1}}\underline{\tilde{1}}\rangle - \frac{1}{\sqrt{n_1 n_3}}\langle\tilde{3}\tilde{3}|v_{ee}|\underline{\tilde{1}}\underline{\tilde{1}}\rangle + \langle\tilde{1}|\hat{h}_0|\underline{\tilde{1}}\rangle\right], \quad \hat{\underline{\mathcal{K}}}^0_1(x) = \hat{h}_0(x) + \frac{\langle\tilde{1}|v_{ee}|\underline{\tilde{1}}\rangle(x)}{\underline{n}_1}, \tag{80}$$

$$\underline{B}_{13} = \frac{1}{\underline{n}_3 - \underline{n}_1}\left(\frac{\langle\tilde{3}\tilde{3}|v_{ee}|\underline{\tilde{1}}\underline{\tilde{3}}\rangle}{\underline{n}_3} + \frac{\langle\tilde{3}\tilde{1}|v_{ee}|\underline{\tilde{3}}\underline{\tilde{3}}\rangle - \langle\tilde{1}\tilde{1}|v_{ee}|\underline{\tilde{1}}\underline{\tilde{3}}\rangle}{\sqrt{\underline{n}_1\underline{n}_3}} - \frac{\langle\tilde{3}\tilde{1}|v_{ee}|\underline{\tilde{1}}\underline{\tilde{1}}\rangle}{\underline{n}_1}\right), \quad \underline{\mathcal{K}}^1_{13}(x) = -\frac{1}{\sqrt{\underline{n}_1\underline{n}_3}}\langle\tilde{1}|v_{ee}|\underline{\tilde{3}}\rangle(x), \tag{81}$$

where we have used (73). The only remaining time dependence in the Hamiltonian in

$$\mathrm{i}\partial_t\begin{pmatrix}\tilde{\phi}_1\\ \tilde{\phi}_3\end{pmatrix} = \begin{pmatrix}\hat{\underline{\mathcal{H}}}^0_1 & \underline{\mathcal{H}}^1_{13}\\ \underline{\mathcal{H}}^1_{31} & \hat{\underline{\mathcal{H}}}^0_3\end{pmatrix}\begin{pmatrix}\tilde{\phi}_1\\ \tilde{\phi}_3\end{pmatrix} \tag{82}$$

then is in $\hat{h}_0$ through the vector potential $A(t)$, i.e., only in the diagonal parts $\hat{\underline{\mathcal{H}}}^0_1$ and $\hat{\underline{\mathcal{H}}}^0_3$.

Equations (82) and (80) and (81) can be easily generalized to more than two RNOs per spin. It is simple to prove that the sum of all OCNs is conserved, $\partial_t \sum_i n_i = 0$. With the frozen Hamiltonian the individual n_i may *not* stay constant, which is a good feature, as remarked on above. A drawback of the frozen Hamiltonian, however, is that $\partial_t\langle\tilde{i}|\tilde{n}\rangle = 0$ is not strictly fulfilled anymore. This means that different RNOs may not stay orthogonal during time propagation although, as eigenfunctions of a hermitian 1RDM, they should.

C. Bare linear response

Figure 4 shows linear-response spectra for the He model system. All spectra were calculated by Fourier transforming the dipole after disturbance of the system with a minute electric-field kick, corresponding to a steplike vector potential.

The exact TDSE result shows the dominating series of peaks starting around a frequency $\omega = 0.5$. In the

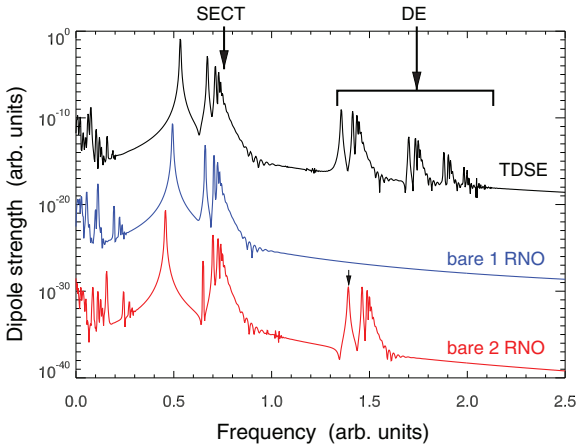

FIG. 4. (Color online) Linear response of the He model system obtained form the full TDSE (70) (upper, black, labeled "TDSE"), with a single RNO per spin, i.e., equivalent to bare TDHF or TDKS in EXA (center, blue, labeled "bare 1 RNO"), and two RNOs (lower, red, labeled "bare 2 RNO"). The single-electron continuum threshold is indicated by "SECT," doubly excited series of peaks by "DE." The little arrow indicates the first double-excitation peak in the bare two-RNO result, discussed in Sec. III D.

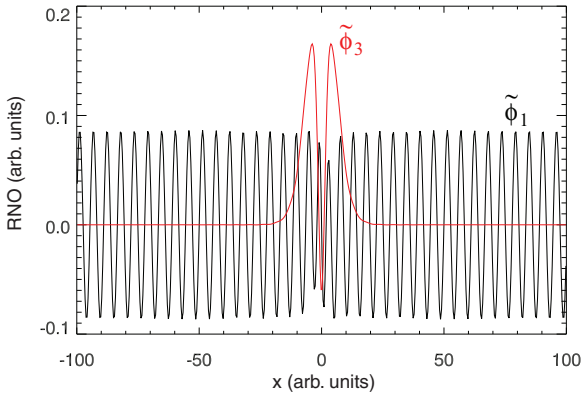

FIG. 5. (Color online) The two RNOs $\tilde{\phi}_1(x)$ and $\tilde{\phi}_3(x)$ of the autoionizing state indicated by the small vertical arrow in Fig. 4 for the bare two-RNO calculation.

independent-electron picture, these peaks correspond to single-electron excitations: one electron stays in its ground state, the other one is excited to the first, second, etc. (dipole-allowed) state, up to the single-electron continuum threshold (SECT). Series of peaks corresponding to doubly excited states follow around $\omega \simeq 1.3$ and greater. As in the "real" He atom, all double excitations are embedded in the single-ionization continuum and thus are autoionizing. Ultimately, with excitations of frequencies $\omega > |E|$, both electrons can be lifted into the two-electron continuum [55].

The linear-response spectrum obtained with just one RNO (per spin) is equivalent to the result of a bare TDHF (or TDKS-EXA) calculation [56]. One can show that doubly excited states are not even covered by full TDDFT (i.e., without frozen Kohn-Sham potential) as long as adiabatic exchange-correlation (xc) potentials are employed (see, e.g., [25]). With a frozen Hamiltonian and just a single RNO it is immediately clear that double excitations cannot exist. And indeed, the peaks corresponding to transitions to doubly excited states are absent for the "bare 1 RNO' result in Fig. 4. The single-excitation series is there but a bit redshifted as compared to the TDSE reference spectrum.

The first main result of this paper is that the first series of double-excitation peaks is present when Eq. (82) is solved. In order to reproduce double excitations in TDDFT one would have to use xc potentials with memory [38]. Even if useful potentials with memory were known they would very likely be computationally expensive. Instead, with our time-dependent RNO theory (TDRNOT) we cover double excitations even with a frozen Hamiltonian and just two RNOs. This is because we allow for more than one orbital per spin (or, in the single-particle picture, per particle), like in a configuration interaction calculation or in multiconfigurational Hartree-Fock. However, the advantage of TDRNOT over such methods is that the RNOs constitute automatically the most adequate time-dependent basis, as mentioned already in the Introduction. This is the reason why we get along with only two RNOs. Thanks to this small number of necessary RNOs we have only little computational overhead compared to the corresponding TDHF or TDKS-EXA simulation.

The single-excitation peaks in the bare two-RNO spectrum are even more redshifted compared to the TDSE than in the bare one-RNO result, while the peaks corresponding to double-excited states are slightly blueshifted. We have checked that with three RNOs the next series of double excitation peaks (seen in the TDSE result starting around $\omega \simeq 1.7$) is also reproduced, although even more blueshifted. "Unfreezing" of the Hamiltonian should cure these shifts and improve the quantitative agreement between TDSE and TDRNOT results but, as mentioned above, we first have to overcome the instability problems before we can check this assertion.

D. Autoionization after excitation by a laser pulse

The small arrow in Fig. 4 indicates the lowest-lying transition to a doubly excited state in the bare TDRNOT He system employing two RNOs. The two RNOs for that particular state were calculated via diagonalization of the bare Hamiltonian in (82) on a grid with 500 spatial grid points. The result is depicted in Fig. 5. The dominating RNO $\tilde{\phi}_1(x)$ has an OCN $n_1 = 0.733$ and is delocalized, thus allowing for outgoing electron flux. Indeed, the spatial oscillations fit to the wave number $k = \sqrt{2(\omega - I_p)} \simeq 1$ expected for the outgoing electron (with $\omega \simeq 1.38$ the energy required to populate the autoionizing state and the ionization potential inferred from the SECT in Fig. 4, $I_p \simeq 0.75$). The second RNO $\tilde{\phi}_3(x)$ is localized close to the origin and has an OCN $n_3 = 0.267$. If one detunes from the autoionizing resonance the OCN of the delocalized NO increases. Hence, the characterizing feature of an autoionizing resonance (as compared to states in a "flat" continuum) is the relative increase of the occupation of localized NOs.

As an example for a TDRNOT calculation beyond linear response we have simulated the interaction of the model He atom with an $N_{cyc} = 30$-cycle $\sin^2$-shaped laser pulse of

frequency ω, i.e.,

$$A(t) = \hat{A}\,\sin^2\left(\frac{\omega t}{2N_{\rm cyc}}\right)\sin\omega t, \tag{83}$$

for $0 < t < N_{\rm cyc}T$ with $T = 2\pi/\omega$, and zero otherwise. The frequency in one calculation was chosen resonant with the transition to the first doubly excited, autoionizing state while in another run, for comparison, we tuned it off-resonant. In all cases the vector potential amplitude was $\hat{A} = 0.01$.

1. TDSE result in position space

Before showing the results obtained with the bare TDRNOT equation (82), let us illustrate the exact dynamics we observe by solving the full two-electron TDSE (70). The same model atom has been employed to study autoionization in the presence of an additional, optical laser pulse in [57].

For the off-resonant case we chose $\omega = 1.25$. In this case, we expect single-photon ionization while the laser is on and no ionization thereafter. In fact, this can be clearly inferred from the (logarithmically scaled) position space probability density plotted in Fig. 6(a) for time $t = 255$, i.e., well after the laser was off at $30T = 151$. Around the origin, the remaining ground-state density is visible. Around $x_1 \simeq 180$, $x_2 = 0$ the laser-generated photoelectron wave packet is seen. It travels to the right with velocity (or wave number) $k = \sqrt{2(\omega - I_{\rm p})} \simeq 1$, where the ionization potential (for the TDSE calculation) is $I_{\rm p} = 0.751$. Analogous wave packets travel in the $-x_1$ and $\pm x_2$ directions (not shown).

The frequency $\omega = 1.36$ for the resonant case can be read off Fig. 4. Figure 6(b) shows the probability density, again at time $t = 255$. Because the frequency is higher than in (a), the photoelectron wave packet is faster and narrower ($N_{\rm cyc}$ was kept constant). The major qualitative differences compared to the off-resonant case is that (i) the system continues to ionize after the laser is off, as is seen from the trailing edge of probability density following the (directly) laser-generated wave packet, and (ii) the different structure in the probability density around the origin. The latter clearly shows that the system is not left in the ground state after the interaction with the laser pulse. Instead, it is in a superposition of ground and autoionizing state. Similar patterns are shown in [57].

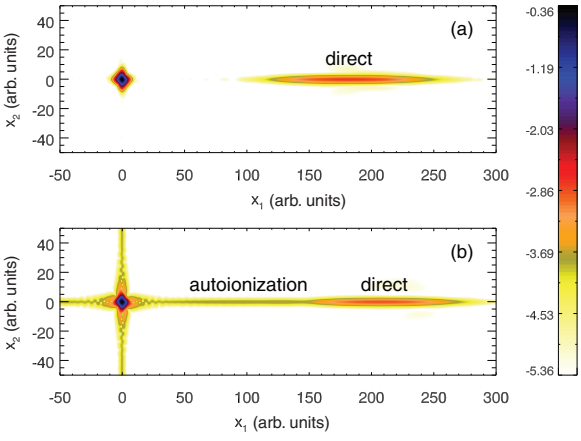

FIG. 6. (Color online) Logarithmic probability density (over five orders of magnitude) from (70) for a $N_{\rm cyc} = 30$-cycle laser pulse with $\hat{A} = 0.01$ at $t = 255$ for the off-resonant case $\omega = 1.25$ (a) and the resonant one $\omega = 1.36$ (b). In (b), ionization continues after the laser pulse, as can be seen from the probability density trailing the (directly) laser-generated photoelectron wave packet.

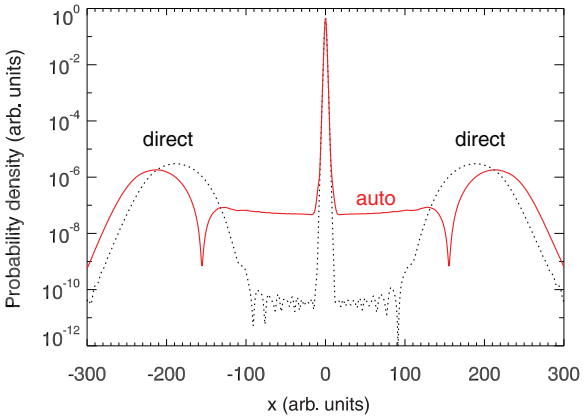

FIG. 7. (Color online) TDRNOT result corresponding to the TDSE two-electron density dynamics in Fig. 6. The off-resonant frequency used was $\omega = 1.28$ (other parameters as in the TDSE runs), leading to the black, dotted density at $t = 255$. The resonant frequency $\omega = 1.38$ yields the red, solid density.

2. Bare two-RNO result in position space

The probability density $|\tilde{\phi}_1(x)|^2 + |\tilde{\phi}_3(x)|^2$ from the bare two-RNO simulation at $t = 255$ is shown in Fig. 7. The laser frequency for the resonant excitation of the autoionizing state was tuned to the respective value $\omega = 1.38$ indicated by an arrow in Fig. 4. For the nonresonant run $\omega = 1.28$ was chosen. Again, left- and right-going photoelectron wave packets (with their maxima at the expected positions) are observed. In the case with autoionization (red, solid) a much higher probability density level between the origin and the wave packets is observed. This is the 1D analog of the TDSE density dynamics in the x_1,x_2 plane in Fig. 6.

3. Momentum spectra

With autoionization involved, the electron spectra should display Fano line shapes [58]. Strictly speaking, one should calculate photoelectron spectra by projecting the final wave function at a time when the laser is off on field-free continuum eigenstates. When the final wave function is not available but only the RNOs, one can, in principle, rewrite the expectation value of the corresponding spectral projection operator in terms of the 2DM γ_2 or the coefficients D_i. The latter need to be approximated anyway in the general TDRNOT approach. Hence, there is no conceptual problem in calculating any observable for systems with two-body interactions because the knowledge of γ_2 suffices. Note that in TDDFT it is not clear how to calculate photoelectron spectra in a rigorous way because the density functional for this observable is unknown [59].

Projection on field-free continuum states is computationally expensive. Hence, it is quite common in practice to project out

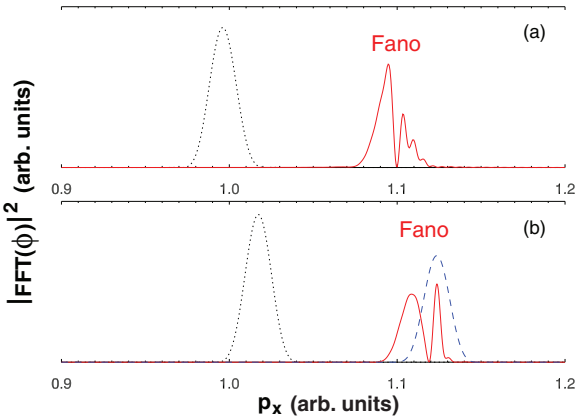

FIG. 8. (Color online) Linearly scaled photoelectron momentum spectra obtained by Fourier transforming (FFT) the outgoing part of the TDSE wave function (a) and RNO (b) for a $N_{\mathrm{cyc}} = 100$ laser pulse of the form (83) with $\hat{A} = 0.01$. The same resonant (solid, red) and off-resonant (dotted, black) frequencies as in Figs. 6 and 7 were chosen. The spectra were obtained at times $t = 750$. Fano profiles are seen in the TDSE result at resonance and the TDRNOT result at resonance when two RNOs are employed (red). In panel (b) the result for a single NO and $\omega = 1.38$ (dashed, blue) is also plotted, showing no Fano profile.

the most populated bound states and Fourier transform the "rest" in order to obtain momentum spectra. Alternatively, one may filter out the region around the origin. While not being a rigorous way to calculate photoelectron spectra, the method yields sufficiently accurate spectra for our purposes. Hence, we pursued the same strategy and Fourier transformed the outgoing part of the wave function. In this way we obtain the momentum spectra shown in Fig. 8.

The TDSE results for the modulus square of the Fourier transform (integrated over p_{x_2}) are presented in Fig. 8(a). The off-resonant excitation by an $N_{\mathrm{cyc}} = 100$ laser pulse of the form (83) (the same frequency $\omega = 1.25$ and field amplitude as in Fig. 6) leads to a peak close to momentum $p_x = 1$, as expected. The resonant excitation leads to a Fano "kink" in the photoelectron peak at $p_x \simeq 1.1$.

Figure 8(b) shows the bare two-RNO TDRNOT results. The second main result of this work—after the existence of doubly excited states—is that our approach also yields a resonance peak with a Fano kink (solid, red). Although the detailed shape of the Fano resonance differs from the TDSE result it is remarkable that it is present at all. As emphasized already, autoionizing states are not captured by a TDHF or TDKS calculation (with adiabatic xc potentials). As a consequence, Fano profiles will not be present there either. The black, dotted peak in Fig. 8(b) is the result for the off-resonant frequency. The dashed blue peak is obtained for $\omega = 1.38$ but with one NO only (equivalent to the bare TDHF result). As there are no doubly excited states with one NO, there is no autoionization and thus no Fano profile.

IV. CONCLUSION AND OUTLOOK

We have introduced time-dependent renormalized natural orbital theory (TDRNOT) and tested it with a numerically exactly solvable model helium atom. The main result is that even with only two renormalized natural orbitals (RNOs) and the bare (i.e., "frozen") effective ground-state Hamiltonian we observe correlation signatures impossible to capture with time-dependent density functional theory (TDDFT) using adiabatic exchange-correlation potentials, namely (i) excitation of doubly excited states in the linear-response spectrum and—beyond linear response—(ii) autoionization and Fano profiles in the photoelectron spectra. The numerical effort scales with the number of RNOs cubed but only linearly with the number of spatial grid points required for one particle. While in TDDFT exchange-correlation potentials with memory are required to capture doubly excited states, the effective Hamiltonian in TDRNOT is local in time. Moreover, the problem in TDDFT concerning density functionals for observables that are not explicitly known in terms of the single-particle density is removed.

Future work will be devoted to other two-electron systems in laser fields (in full dimensionality, spin triplet, H_2), resonant interactions, and three-electron model systems that are still numerically exactly solvable. In full dimensionality, each RNO will be expanded in spherical harmonics and with the radial coordinate discretized as in this work. Then, one may apply analogs of the central field approximation for ground-state calculations and a multipole expansion of the effective Hamiltonian for time-dependent simulations. In the spin-triplet case the algebraic structure of the two-body density matrix (or two-electron wave function) expansion is different from the spin singlet but otherwise the approach is the same. The same holds for H_2. Three-electron systems such as the lithium atom in intense laser fields is of interest as it is the simplest system with "inner" electrons in a closed shell. The time-dependent Schrödinger equation of one-dimensional model Li atoms in intense laser fields is still possible to solve exactly [60] and thus may serve as a benchmark for our method. Another research direction will be the development of density matrix functionals that allow one to go beyond the bare TDRNOT without unleashing instabilities in the RNO equation of motion.

ACKNOWLEDGMENT

This work was supported by the SFB 652 of the German Science Foundation (DFG).

APPENDIX A: DERIVATION OF EOM (13)

Inserting (6) and (9) into (5) yields (suppressing all time arguments)

$$-i\sum_k [\partial_t n_k]\phi_k^*(1')\phi_k(1) - i\sum_k n_k[\partial_t\phi_k^*(1')]\phi_k(1) - i\sum_k n_k\phi_k^*(1')[\partial_t\phi_k(1)]$$
$$= [\hat{h}_0(1') - \hat{h}_0(1)]\sum_k n_k\phi_k^*(1')\phi_k(1) + 2\int d2\,\{v_{ee}(|1'-2|) - v_{ee}(|1-2|)\}\sum_{ijkl}\gamma_{2,ijkl}\phi_i(1)\phi_j(2)\phi_k^*(1')\phi_l^*(2). \quad \text{(A1)}$$

Because the NOs form a complete basis we may introduce time-dependent coefficients $\alpha_{km}(t)$ [10] such that

$$i\,\partial_t \phi_k(t) = \alpha_{kk}(t)\phi_k(t) + \sum_{m\neq k} \alpha_{km}(t)\phi_m(t). \tag{A2}$$

Here we drop the argument 1 as the equation holds for all position and spin degrees of freedom. With the transformation

$$\phi_k(t) = e^{-i\int^t \alpha_{kk}(t')\,dt'}\phi'_k(t) \tag{A3}$$

[where α_{kk} is real because of $\alpha_{km}(t) = \alpha^*_{mk}(t)$] we transform away the diagonal part of α_{km} and obtain

$$i\,\partial_t \phi'_k(t) = \sum_{m\neq k} \alpha'_{km}(t)\phi'_m(t), \quad \alpha'_{km}(t) = \alpha_{km}(t)e^{-i\int^t [\alpha_{mm}(t')-\alpha_{kk}(t')]\,dt'}. \tag{A4}$$

α'_{km} constitutes another hermitian matrix. The NOs are defined as the eigenfunctions of the hermitian 1RDM. We have the freedom to choose the phase in such a way that (A4) holds. This is the analog of switching to the interaction picture, but now for a nonlinear Hamiltonian. Dropping the primes, $\phi' \to \phi$, $\alpha' \to \alpha$, we have for (A1)

$$\begin{aligned} &-i\sum_k [\partial_t n_k]\phi^*_k(1')\phi_k(1) + \sum_{k,m\neq k} n_k \alpha^*_{km}\phi^*_m(1')\phi_k(1) - \sum_{k,m\neq k} n_k \phi^*_k(1')\alpha_{km}\phi_m(1) \\ &= [\hat{h}_0(1') - \hat{h}_0(1)]\sum_k n_k\phi^*_k(1')\phi_k(1) + 2\int d2\,\{v_{ee}(|1'-2|) - v_{ee}(|1-2|)\}\sum_{ijkl}\gamma_{2,ijkl}\phi_i(1)\phi_j(2)\phi^*_k(1')\phi^*_l(2). \end{aligned} \tag{A5}$$

Multiplying by $\phi_n(1')$, $\phi^*_p(1)$, and integrating over 1 and $1'$ gives

$$-i\dot{n}_n\delta_{np} + n_p\alpha^*_{pn} - n_n\alpha_{np} = (n_p - n_n)\langle p|\hat{h}_0|n\rangle + 2\sum_{jkl}\{\gamma_{2,pjkl}\langle kl|v_{ee}|nj\rangle - [\gamma_{2,njkl}\langle kl|v_{ee}|pj\rangle]^*\}. \tag{A6}$$

For $n = p$ we obtain (17)

$$\dot{n}_n = -4\,\mathrm{Im}\sum_{jkl}\gamma_{2,njkl}\langle kl|v_{ee}|nj\rangle. \tag{A7}$$

For $n \neq p$ we have

$$\alpha_{np}(n_p - n_n) = (n_p - n_n)\langle p|\hat{h}_0|n\rangle + 2\sum_{jkl}\{\gamma_{2,pjkl}\langle kl|v_{ee}|nj\rangle - [\gamma_{2,njkl}\langle kl|v_{ee}|pj\rangle]^*\}. \tag{A8}$$

If $n_p \neq n_n$ we can divide by $n_p - n_n$, which gives with (A4)

$$i\,\partial_t\phi_n = \sum_{p\neq n}\left(\langle p|\hat{h}_0|n\rangle + \frac{2}{n_p - n_n}\sum_{jkl}\{\gamma_{2,pjkl}\langle kl|v_{ee}|nj\rangle - [\gamma_{2,njkl}\langle kl|v_{ee}|pj\rangle]^*\}\right)\phi_p. \tag{A9}$$

Equations (A9) and (A6) are EOMs for NOs and OCNs, respectively, but not useful for our purposes because truncating them to a small number of NOs would yield extremely poor results [61]. Instead, it is more suitable to seek an EOM of the form of Eq. (12), $i\,\partial_t\mathbf{\Phi}(1) = \hat{\mathcal{H}}(1)\mathbf{\Phi}(1)$, where $\mathbf{\Phi}(1,t)$ is a vector of NOs $\phi_k(1,t)$ and $\hat{\mathcal{H}}$ acts in NO and position-spin space (see Fig. 1) instead of only in NO space as in (A9). Multiplying (A1) by $\phi_n(1')$ and integrating-out only $1'$ (but not 1) leads to

$$\begin{aligned} i\,\partial_t\phi_n(1) = &\frac{4i}{n_n}\left\{\mathrm{Im}\sum_{jkl}\gamma_{2,njkl}\langle kl|v_{ee}|nj\rangle\right\}\phi_n(1) - \langle n|\hat{h}_0|n\rangle\phi_n(1) \\ &+ \sum_{k\neq n}\frac{2n_k/n_n}{n_k - n_n}\sum_{jpl}\{\gamma_{2,kjpl}\langle pl|v_{ee}|nj\rangle - [\gamma_{2,njpl}\langle pl|v_{ee}|kj\rangle]^*\}\phi_k(1) - \frac{2}{n_n}\sum_{kjpl}\gamma_{2,kjpl}\langle pl|v_{ee}|nj\rangle\,\phi_k(1) \\ &+ \hat{h}_0(1)\phi_n(1) + \frac{2}{n_n}\sum_{kjl}\gamma_{2,kjnl}\langle l|v_{ee}|j\rangle(1)\,\phi_k(1). \end{aligned} \tag{A10}$$

In the first line on the right-hand side there are purely time-dependent coefficients in front of $\phi_n(1)$. This part of the total Hamiltonian $\hat{\mathcal{H}}(1)$ is diagonal in both NO-index and position-spin space. In the second line we have the terms corresponding to the NO-index off-diagonal part of the Hamiltonian. In the third line the first term does the "usual" coupling in position (spin) space due to the single-particle Hamiltonian $\hat{h}_0$. This term is diagonal in NO space. The second term in the third line couples the NOs through space-dependent (though multiplicative) coefficients.

It is simple to rewrite the EOM (A10) in terms of the RNOs (10). Using (A7) and (14), the result (13) is obtained.

APPENDIX B: CONNECTION BETWEEN $\gamma_{2,njkl}$ AND D_i

For the 2DM in the two-electron spin-singlet case we find, using (22),

$$\gamma_2(12,1'2') = \Phi(x_1x_2)\Phi^*(x_1'x_2')\tfrac{1}{2}\left(\delta_{\sigma_1+}\delta_{\sigma_2-} - \delta_{\sigma_1-}\delta_{\sigma_2+}\right) \times \left(\delta_{\sigma_1'+}\delta_{\sigma_2'-} - \delta_{\sigma_1'-}\delta_{\sigma_2'+}\right), \tag{B1}$$

and with (9)

$$\Phi(x_1x_2)\Phi^*(x_1'x_2')\frac{1}{2}\left(\delta_{\sigma_1+}\delta_{\sigma_2-} - \delta_{\sigma_1-}\delta_{\sigma_2+}\right)\left(\delta_{\sigma_1'+}\delta_{\sigma_2'-} - \delta_{\sigma_1'-}\delta_{\sigma_2'+}\right) = \sum_{ijkl}\gamma_{2,ijkl}\phi_i(x_1)\delta_{\sigma_1\sigma_i}\phi_j(x_2)\delta_{\sigma_2\sigma_j}\phi_k^*(x_1')\delta_{\sigma_1'\sigma_k}\phi_l^*(x_2')\delta_{\sigma_2'\sigma_l}. \tag{B2}$$

Multiplication by NOs and integration allows us to solve for the γ_2 expansion coefficients,

$$\gamma_{2,mnop} = \tfrac{1}{2}\left(\delta_{\sigma_o+}\delta_{\sigma_p-} - \delta_{\sigma_o-}\delta_{\sigma_p+}\right) \times \left(\delta_{\sigma_m+}\delta_{\sigma_n-} - \delta_{\sigma_m-}\delta_{\sigma_n+}\right)\ \gamma^{(x)}_{2,mnop} \tag{B3}$$

with the spatial part

$$\begin{aligned}\gamma^{(x)}_{2,mnop} &= \int dx_1 \int dx_2 \int dx_1' \int dx_2'\, \phi_n^*(x_2)\phi_m^*(x_1) \times \Phi(x_1x_2)\Phi^*(x_1'x_2')\phi_o(x_1')\phi_p(x_2') \\ &= \int dx_1 \int dx_2 \int dx_1' \int dx_2'\, \phi_n^*(x_2)\phi_m^*(x_1) \times \sum_{i\ \mathrm{odd}} D_i\, \phi_i(x_1)\phi_i(x_2) \\ &\quad \times \sum_{j\ \mathrm{odd}} D_j^*\, \phi_j(x_1')\phi_j(x_2')\phi_o(x_1')\phi_p(x_2').\end{aligned} \tag{B4}$$

Now, one must not forget that, e.g., not only $m = i$ contributes but also $m = i+1$ because $\phi_i = \phi_{i+1}$ for i odd. Hence

$$\gamma^{(x)}_{2,mnop} = (\delta_{m,i} + \delta_{m,i+1})(\delta_{n,i} + \delta_{n,i+1})D_i\, D_j^*\,(\delta_{o,j} + \delta_{o,j+1}) \times (\delta_{p,j} + \delta_{p,j+1}) \quad \text{for } i,j \text{ odd} \tag{B5}$$

TABLE I. Nonvanishing $\gamma_{2,mnop}$ in the case of two NOs per spin in the two-electron spin-singlet case and for approximations of the form (18).

m	n	o	p	$\gamma_{2,mnop}$	$\gamma^{(\mathrm{approx})}_{2,mnop}$
1	2	1	2	$\frac{1}{2}\lvert D_1\rvert^2 = n_1/2$	f_{1212}
1	2	2	1	$-\frac{1}{2}\lvert D_1\rvert^2 = -n_1/2$	$-g_{1221}$
1	2	3	4	$\frac{1}{2}D_1D_3^* = \frac{1}{2}\sqrt{n_1n_3}\,e^{i\varphi}$	0
1	2	4	3	$-\frac{1}{2}D_1D_3^* = -\frac{1}{2}\sqrt{n_1n_3}\,e^{i\varphi}$	0
2	1	1	2	$-\frac{1}{2}\lvert D_1\rvert^2 = -n_1/2$	$-g_{2112}$
2	1	2	1	$\frac{1}{2}\lvert D_1\rvert^2 = n_1/2$	f_{2121}
2	1	3	4	$-\frac{1}{2}D_1D_3^* = -\frac{1}{2}\sqrt{n_1n_3}\,e^{i\varphi}$	0
2	1	4	3	$\frac{1}{2}D_1D_3^* = \frac{1}{2}\sqrt{n_1n_3}\,e^{i\varphi}$	0
3	4	1	2	$\frac{1}{2}D_3D_1^* = \frac{1}{2}\sqrt{n_1n_3}\,e^{-i\varphi}$	0
3	4	2	1	$-\frac{1}{2}D_3D_1^* = -\frac{1}{2}\sqrt{n_1n_3}\,e^{-i\varphi}$	0
3	4	3	4	$\frac{1}{2}\lvert D_3\rvert^2 = n_3/2$	f_{3434}
3	4	4	3	$-\frac{1}{2}\lvert D_3\rvert^2 = -n_3/2$	$-g_{3443}$
4	3	1	2	$-\frac{1}{2}D_3D_1^* = -\frac{1}{2}\sqrt{n_1n_3}\,e^{-i\varphi}$	0
4	3	2	1	$\frac{1}{2}D_3D_1^* = \frac{1}{2}\sqrt{n_1n_3}\,e^{-i\varphi}$	0
4	3	3	4	$-\frac{1}{2}\lvert D_3\rvert^2 = -n_3/2$	$-g_{4334}$
4	3	4	3	$\frac{1}{2}\lvert D_3\rvert^2 = n_3/2$	f_{4343}

and thus

$$\gamma_{2,mnop} = \tfrac{1}{2}\left(\delta_{\sigma_o+}\delta_{\sigma_p-} - \delta_{\sigma_o-}\delta_{\sigma_p+}\right)\left(\delta_{\sigma_m+}\delta_{\sigma_n-} - \delta_{\sigma_m-}\delta_{\sigma_n+}\right) \times (\delta_{m,i} + \delta_{m,i+1})(\delta_{n,i} + \delta_{n,i+1})D_i\, D_j^*(\delta_{o,j} + \delta_{o,j+1}) \times (\delta_{p,j} + \delta_{p,j+1}) \quad \text{for } i,j \text{ odd}. \tag{B6}$$

Because of the spin part and our indexing (odd index $\leftrightarrow$ spin up, even index $\leftrightarrow$ spin down, see Sec. II B), for $\gamma_{2,mnop}$ not to vanish the index pair (o,p) must be (even, odd) or (odd, even). The same holds for the index pair (m,n).

In the case of two NOs per spin this leads to the nonvanishing $\gamma_{2,mnop}$ summarized in Table I. We not only have the general property $\gamma_{2,mnop} = \gamma^*_{2,opmn}$ here but also $\gamma_{2,mnop} = -\gamma_{2,mnpo} = -\gamma_{2,nmop} = \gamma_{2,nmpo}$. We also show the results for typical approximations of the form (18), which give erroneously zeros for "cross-block" elements like $mnop =$ 1234 or 3421 while they may give erroneously diagonal contributions, e.g., $f_{1111} - g_{1111}$ unless $f_{mnop} = g_{mnop}$, as in Hartree-Fock.

[1] W. Kohn, Rev. Mod. Phys. **71**, 1253 (1999).
[2] C. A. Coulson, Rev. Mod. Phys. **32**, 170 (1960).
[3] P.-O. Löwdin, Phys. Rev. **97**, 1474 (1955).
[4] A. J. Coleman, Rev. Mod. Phys. **35**, 668 (1963).
[5] A. J. Coleman and V. I. Yukalov, *Reduced Density Matrices, Coulson's Challenge*, Lecture Notes in Chemistry (Springer, Berlin, Heidelberg, 2000), Vol. 72.
[6] *Many-electron Densities and Reduced Density Matrices*, edited by J. Cioslowski, Mathematical and Computational Chemistry Series (Kluwer/Plenum, New York, 2000).
[7] *Electron Density, Density Matrix and Density Functional Theory in Atoms, Molecules and the Solid State*, edited by N. I. Gidopoulos and S. Wilson, Progress in Theoretical Chemistry and Physics (Kluwer, Dordrecht, 2003).
[8] *Reduced-Density-Matrix Mechanics*, edited by D. A. Mazziotti, Advances in Chemical Physics (Wiley, Hoboken, NJ, 2007), Vol. 134.
[9] D. A. Mazziotti, Chem. Rev. **112**, 244 (2012).
[10] H. Appel, Ph.D. thesis, Free University Berlin, 2007.
[11] K. J. H. Giesbertz, Ph.D. thesis, Free University Amsterdam, 2010.
[12] P. Hohenberg and W. Kohn, Phys. Rev. **136**, B864 (1964).
[13] R. M. Dreizler and E. K. U. Gross, *Density Functional Theory—An Approach to the Quantum Many-Body Problem* (Springer, Berlin, Heidelberg, 1990).
[14] W. Kohn and L. J. Sham, Phys. Rev. **140**, A1133 (1965).
[15] A. M. K. Müller, Phys. Lett. A **105**, 446 (1984).

[16] S. Goedecker and C. J. Umrigar, Phys. Rev. Lett. **81**, 866 (1998).
[17] O. Gritsenko, K. Pernal, and E. J. Baerends, J. Chem. Phys. **122**, 204102 (2005).
[18] M. Piris, Int. J. Quantum Chem. **113**, 620 (2013).
[19] E. N. Zarkadoula, S. Sharma, J. K. Dewhurst, E. K. U. Gross, and N. N. Lathiotakis, Phys. Rev. A **85**, 032504 (2012).
[20] D. A. Mazziotti, Phys. Rev. Lett. **108**, 263002 (2012).
[21] K. Pernal, Phys. Rev. Lett. **94**, 233002 (2005).
[22] N. Helbig, N. N. Lathiotakis, M. Albrecht, and E. K. U. Gross, Europhys. Lett. **77**, 67003 (2007).
[23] Ch. Schilling, D. Gross, and M. Christandl, Phys. Rev. Lett. **110**, 040404 (2013).
[24] P.-O. Löwdin and H. Shull, Phys. Rev. **101**, 1730 (1956).
[25] C. A. Ullrich, *Time-Dependent Density Functional Theory, Concepts and Applications* (Oxford University Press, Oxford, 2012).
[26] *Fundamentals of Time-Dependent Density Functional Theory*, edited by M. A. L. Marques, N. T. Maitra, F. M. S. Nogueira, E. K. U. Gross, and A. Rubio (Springer, Berlin, Heidelberg, 2012).
[27] M. Lein and S. Kümmel, Phys. Rev. Lett. **94**, 143003 (2005).
[28] F. Wilken and D. Bauer, Phys. Rev. Lett. **97**, 203001 (2006).
[29] F. Wilken and D. Bauer, Phys. Rev. A **76**, 023409 (2007).
[30] M. Thiele, E. K. U. Gross, and S. Kümmel, Phys. Rev. Lett. **100**, 153004 (2008).
[31] A. S. de Wijn, M. Lein, and S. Kümmel, Europhys. Lett. **84**, 43001 (2008).
[32] M. Ruggenthaler and D. Bauer, Phys. Rev. Lett. **102**, 233001 (2009).
[33] N. Helbig, J. I. Fuks, I. V. Tokatly, H. Appel, E. K. U. Gross, and A. Rubio, Chem. Phys. **391**, 1 (2011).
[34] S. Raghunathan and M. Nest, J. Chem. Theor. Comput. **8**, 806 (2012); J. Chem. Phys. **136**, 064104 (2012).
[35] P. Elliott, J. I. Fuks, A. Rubio, and N. T. Maitra, Phys. Rev. Lett. **109**, 266404 (2012).
[36] H. Wang, M. Chini, S. Chen, C.-H. Zhang, F. He, Y. Cheng, Y. Wu, U. Thumm, and Z. Chang, Phys. Rev. Lett. **105**, 143002 (2010).
[37] C. Ott, A. Kaldun, P. Raith, K. Meyer, M. Laux, J. Evers, C. H. Keitel, C. H. Greene, and T. Pfeifer, Science **340**, 716 (2013).
[38] N. T. Maitra, F. Zhang, R. J. Cave, and K. Burke, J. Chem. Phys. **120**, 5932 (2004).
[39] D. A. Portes, Jr., T. Kodama, and A. F. R. de Toledo Piza, Phys. Rev. A **54**, 1889 (1996).
[40] K. Pernal, O. Gritsenko, and E. J. Baerends, Phys. Rev. A **75**, 012506 (2007).
[41] K. Pernal, K. Giesbertz, O. Gritsenko, and E. J. Baerends, J. Chem. Phys. **127**, 214101 (2007).
[42] K. J. H. Giesbertz, E. J. Baerends, and O. V. Gritsenko, Phys. Rev. Lett. **101**, 033004 (2008).
[43] K. J. H. Giesbertz, K. Pernal, O. V. Gritsenko, and E. J. Baerends, J. Chem. Phys. **130**, 114104 (2009).
[44] K. J. H. Giesbertz, O. V. Gritsenko, and E. J. Baerends, J. Chem. Phys. **136**, 094104 (2012).
[45] R. Requist and O. Pankratov, Phys. Rev. A **81**, 042519 (2010).
[46] H. Appel and E. K. U. Gross, Europhys. Lett. **92**, 23001 (2010).
[47] A. K. Rajam, I. Raczkowska, and N. T. Maitra, Phys. Rev. Lett. **105**, 113002 (2010).
[48] M. Moshinsky, Am. J. Phys. **36**, 52 (1968).
[49] D. A. Mazziotti, J. Chem. Phys. **112**, 10125 (2000).
[50] J. Nocedal and S. Wright, *Numerical Optimization*, Springer Series in Operations Research and Financial Engineering (Springer, New York, 2006).
[51] D. A. Mazziotti, Chem. Phys. Lett. **338**, 323 (2001).
[52] T. L. Gilbert, Phys. Rev. B **12**, 2111 (1975).
[53] R. Grobe and J. H. Eberly, Phys. Rev. Lett. **68**, 2905 (1992); S. L. Haan, R. Grobe, and J. H. Eberly, Phys. Rev. A **50**, 378 (1994).
[54] D. Bauer, Phys. Rev. A **56**, 3028 (1997); D. G. Lappas and R. van Leeuwen, J. Phys. B **31**, L249 (1998); D. Bauer and F. Ceccherini, Phys. Rev. A **60**, 2301 (1999); M. Lein, E. K. U. Gross, and V. Engel, Phys. Rev. Lett. **85**, 4707 (2000).
[55] The peaks at frequencies $\omega < 0.3$ correspond to transitions *between* singly excited states and are thus actually of second order in the number of transitions involved (when starting from the ground state). However, these peaks are of about the same dipole strength as the peaks corresponding to *single* transitions to doubly excited states (i.e., involving *two* electrons).
[56] See Fig. 1 in [32] for the full result, i.e., with "unfrozen" TDKS Hamiltonian.
[57] J. Zhao and M. Lein, New J. Phys. **14**, 065003 (2012).
[58] U. Fano, Phys. Rev. **124**, 1866 (1961).
[59] V. Véniard, R. Taïeb, and A. Maquet, Laser Phys. **13**, 465 (2003).
[60] C. Ruiz, L. Plaja, and L. Roso, Phys. Rev. Lett. **94**, 063002 (2005).
[61] This is most obvious in the limit of just one NO where $i\partial_t\phi_1 = 0$ would result. To describe ionization, i.e., an outgoing electron wave packet, as we study it in Sec. III D, a very large set of NOs would be necessary. Instead, (A10) captures outgoing wave packets already with just one NO (and autoionization with two).

2.2. Paper 2

Equations of motion for natural orbitals of strongly driven two-electron systems

Physical Review A 90, 012518:1–11 (2014)

DOI:http://dx.doi.org/10.1103/PhysRevA.90.012518

Author contributions

Julius Rapp	Exact functional, preparation of manuscript, programming, improvements to numerical scheme, calculations, figure preparation.
Martins Brics	Newton scheme for finding ground-state ONs (not necessary for the new phase convention), discussions, suggestions.
Dieter Bauer	Finalization of manuscript, supervision.

PHYSICAL REVIEW A **90**, 012518 (2014)

Equations of motion for natural orbitals of strongly driven two-electron systems

J. Rapp, M. Brics, and D. Bauer*
Institut für Physik, Universität Rostock, 18051 Rostock, Germany
(Received 19 April 2014; published 18 July 2014)

Natural orbital theory is a computationally useful approach to the few- and many-body quantum problems. While natural orbitals have been known and applied for many years in electronic structure applications, their potential for time-dependent problems started being investigated only recently. Correlated two-particle systems are of particular importance because the structure of the two-body reduced density matrix expanded in natural orbitals is known exactly in this case. However, in the time-dependent case the natural orbitals carry time-dependent phases that allow for certain time-dependent gauge transformations of the first kind. Different phase conventions will, in general, lead to different equations of motion for the natural orbitals. A particular phase choice allows us to derive the exact equations of motion for the natural orbitals of any (laser-) driven two-electron system *explicitly*, i.e., without any dependence on quantities that, in practice, require further approximations. For illustration, we solve the equations of motion for a model helium system. Besides calculating the spin-singlet and spin-triplet ground states, we show that the linear response spectra and the results for resonant Rabi flopping are in excellent agreement with the benchmark results obtained from the exact solution of the time-dependent Schrödinger equation.

DOI: 10.1103/PhysRevA.90.012518 PACS number(s): 31.15.ee, 31.70.Hq, 31.15.V−

I. INTRODUCTION

N-electron systems in full dimensionality that are strongly driven by, e.g., an intense laser field, can be simulated on an *ab initio* time-dependent Schrödinger equation (TDSE) level only up to $N = 2$ (see, e.g., [1]). This embarrassingly small number calls for efficient time-dependent "even-not-so-many"-body quantum approaches that are applicable beyond linear response.

In order to overcome the unpleasant exponential complexity scaling of a correlated many-particle state $|\Psi(t)\rangle$, quantities of less dimensionality should be used [2]. An example for such an approach is time-dependent density functional theory (TDDFT). The Runge-Gross theorem of TDDFT [3,4] ensures that the single-particle density $n(\vec{r},t)$ is, in principle, sufficient to calculate all observables of a time-dependent many-body quantum system. However, the—principally exact—equations of motion (EOM) of TDDFT for the auxiliary Kohn-Sham orbitals involve a generally unknown exchange-correlation (XC) functional. It has been shown that the *nonadiabaticity* of the XC functional is essential for the description of correlated dynamics [5]. However, essentially all practicable approximations to the unknown exact XC functional neglect memory effects but make use of the numerically strongly favorable adiabatic approximation. However, even if the exact single-particle density $n(\vec{r},t)$ was reproduced there remains the problem of extracting the relevant observables from $n(\vec{r},t)$ in practice. For instance, it is unknown how multiple ionization probabilities and photoelectron spectra, let alone differential and correlated ones, can be *explicitly* calculated from $n(\vec{r},t)$ alone [6–8].

Because of these practical difficulties with $n(\vec{r},t)$-based TDDFT it is an obvious idea to use less reduced quantities as building bricks, e.g., reduced density matrices (or quantities related to them; see, for instance, [9–19]). In fact, the knowledge of the two-body reduced density matrix (2-RDM) is sufficient to explicitly calculate any observable involving one- and two-body operators. However, as density matrices are still high-dimensional objects, it is not attractive to solve the EOM for them directly. Löwdin introduced so-called natural orbitals (NOs) and occupation numbers (ONs) as eigenfunctions and eigenvalues of the one-body reduced density matrix (1-RDM), respectively [20], and investigated the stationary two-electron case in great detail [21]. NOs have the same dimensionality as single-particle wave functions and may be used as basis functions for configuration interaction (CI) approaches, for instance. In fact, one may hope that NOs form the best possible basis set with respect to some measure, e.g., $\|\Psi - \Phi\|^2$, where Φ is a CI approximation to the exact wave function Ψ. Recently, it has been shown that this is true only for special cases (including two electrons) and how NOs may be used to generate the best basis [22].

In the current paper we derive the general EOM for NOs renormalized to the corresponding ONs [called *time-dependent renormalized natural orbital theory* (TDRNOT)] before we specialize on the time-dependent two-body problem. For the interacting two-body system the structure of the 2-RDM expressed in terms of NOs is exactly known but unique only up to certain combinations of time-dependent NO phases. Different NO phase choices will lead to different EOM. For a particular phase choice [17] the 2-RDM depends only on the time-dependent ONs and NOs but not on additional time-dependent phases, and the TDRNOT Hamiltonian in the EOM is thus *exactly* and *explicitly* known. Hence, solving the EOM for the NOs is equivalent to the solution of the corresponding TDSE. In particular, the N-representability (also called "quantum marginal") problem (see, e.g., [9]) is not an issue in this simplest time-dependent few-body case.

In practice, we wish (and need) to truncate the number of NOs we take into account, which introduces propagation errors in the numerical solution of the TDRNOT EOM. We therefore benchmark our approach with a system for which we can actually solve the TDSE numerically exactly: the

*Corresponding author: dieter.bauer@uni-rostock.de

widely used (laser-) driven one-dimensional helium model atom (see, e.g., [23,24]). It has already been shown in [25] that our approach—even with a ground-state "frozen" effective Hamiltonian—covers highly correlated phenomena such as double excitations and autoionization, both inaccessible by practicable, adiabatic TDDFT [26]. The frozen-Hamiltonian calculations (also known as the "bare" response) was used in [25] because with the phase convention chosen there, the time evolution of the above-mentioned phases, and thus the consistent time-evolution of the 2-RDM, was unknown.

The paper is organized as follows. The basic theory of reduced density matrices and NOs regarding two-electron systems is introduced in Sec. II. The new phase convention is introduced in Sec. II E; the respective EOM for the NOs is discussed in Sec. III. Finally, we benchmark the performance of TDRNOT in Sec. IV, before we conclude and give an outlook in Sec. V. Some of the derivations and details are given in Appendixes A–E.

II. TWO-BODY NATURAL ORBITAL THEORY

Atomic units (a.u.) are used throughout. In some cases, operator hats are used to emphasize the nondiagonality of an operator in some particular space.

A. Density matrices, natural orbitals, and occupation numbers

The starting point in the case of a two-body system is the pure two-body density matrix (2-DM),

$$\hat{\gamma}_2(t) = |\Psi(t)\rangle\langle\Psi(t)|. \tag{1}$$

The 1-RDM $\hat{\gamma}_1(t)$ then reads

$$\hat{\gamma}_1(t) = \sum_{i=1}^{2} \mathrm{Tr}_i\, \hat{\gamma}_2(t) = 2\,\mathrm{Tr}_1\, \hat{\gamma}_2(t) = 2\,\mathrm{Tr}_2\, \hat{\gamma}_2(t), \tag{2}$$

where the partial trace Tr_i means tracing out all degrees of freedom of particle i. Both $\hat{\gamma}_2(t)$ and $\hat{\gamma}_1(t)$ are Hermitian.

The NOs $|k(t)\rangle$ and ONs $n_k(t)$ are defined as eigenstates and eigenvalues of the 1-RDM, respectively,

$$\hat{\gamma}_1(t)|k(t)\rangle = n_k(t)|k(t)\rangle. \tag{3}$$

As $\hat{\gamma}_1(t)$ is Hermitian, the $n_k(t)$ are real, and the $|k(t)\rangle$ are orthogonal. We further assume the $|k(t)\rangle$ to be normalized to unity so that $\{|k(t)\rangle\}$ is a complete, orthonormal basis. With this convention, the spectral decomposition of the 1-RDM reads

$$\hat{\gamma}_1(t) = \sum_{k=1}^{\infty} n_k(t)|k(t)\rangle\langle k(t)|. \tag{4}$$

Because of the normalization of the two-particle state $\langle\Psi(t)|\Psi(t)\rangle = 1$ we have $\mathrm{Tr}\,\hat{\gamma}_2(t) = 1$ and $\mathrm{Tr}\,\hat{\gamma}_1(t) = N = 2$, where $N = 2$ arises as the number of particles in the system, and Tr without subscript is understood to be the trace over whatever degrees of freedom the operator to be traced has. Evaluating the trace of $\hat{\gamma}_1(t)$ leads to

$$\sum_k n_k(t) = N = 2. \tag{5}$$

The 2-DM can be expanded in NOs as well,

$$\hat{\gamma}_2(t) = \sum_{ijkl} \gamma_{2,ijkl}(t)|i(t),j(t)\rangle\langle k(t),l(t)|, \tag{6}$$

where the shorthand notation for tensor products $|i(t),j(t)\rangle = |i(t)\rangle|j(t)\rangle = |i(t)\rangle \otimes |j(t)\rangle$ is used, and the expansion coefficients $\gamma_{2,ijkl}(t)$ formally read

$$\gamma_{2,ijkl}(t) = \langle i(t),j(t)|\hat{\gamma}_2(t)|k(t),l(t)\rangle. \tag{7}$$

B. Renormalized natural orbitals

In TDRNOT, renormalized natural orbitals (RNOs)

$$|\tilde{k}(t)\rangle = \sqrt{n_k(t)}|k(t)\rangle, \quad \langle\tilde{k}(t)|\tilde{k}(t)\rangle = n_k(t), \tag{8}$$

are introduced because it is numerically beneficial to store and *unitarily propagate* the combined quantity $|\tilde{k}(t)\rangle$ instead of using the coupled set of equations for $|k(t)\rangle$ and $n_k(t)$ [25]. In RNOs, the expansions (4) and (6) read

$$\hat{\gamma}_1(t) = \sum_k |\tilde{k}(t)\rangle\langle\tilde{k}(t)|, \tag{9}$$

$$\hat{\gamma}_2(t) = \sum_{ijkl} \tilde{\gamma}_{2,ijkl}(t)|\tilde{i}(t),\tilde{j}(t)\rangle\langle\tilde{k}(t),\tilde{l}(t)|, \tag{10}$$

with renormalized expansion coefficients

$$\tilde{\gamma}_{2,ijkl}(t) = \frac{\gamma_{2,ijkl}(t)}{\sqrt{n_i(t)n_j(t)n_k(t)n_l(t)}}. \tag{11}$$

C. Peculiarities of the two-electron state

Based on the exchange antisymmetry,

$$\hat{\mathcal{P}}^{(1,2)}|\Psi(t)\rangle = -|\Psi(t)\rangle, \tag{12}$$

any two-electron state $|\Psi(t)\rangle$ can be expanded in its RNOs $|\tilde{k}(t)\rangle$ as

$$|\Psi(t)\rangle = \sum_{k\ \mathrm{odd}} \frac{e^{i\varphi_k(t)}}{\sqrt{2n_k(t)}}[|\tilde{k}(t),\tilde{k}'(t)\rangle - |\tilde{k}'(t),\tilde{k}(t)\rangle], \tag{13}$$

with the "prime operator" acting on a positive integer k as

$$k' = \begin{cases} k+1 & \text{if} \quad k \text{ odd}, \\ k-1 & \text{if} \quad k \text{ even}, \end{cases} \qquad k > 0. \tag{14}$$

A proof of (13) is provided in Appendix A. The conditions

$$n_k(t) = n_{k'}(t), \quad n_k(t) \in [0,1], \tag{15}$$

for the ONs follow.

If we require $|\Psi(t)\rangle$ to be an eigenstate of the spin operators $\hat{S}^2$ and $\hat{S}_z$ at all times, we can write

$$|\Psi(t)\rangle = |\Psi(t)\rangle_x \otimes |\Psi\rangle_\sigma, \tag{16}$$

where $|\Psi\rangle_\sigma$ is a time-independent spin component and $|\Psi(t)\rangle_x$ is the spatial part. The spin part needs not to be considered explicitly as long as the Hamiltonian does not act on it. However, it affects the exchange symmetry of $|\Psi(t)\rangle_x$.

1. Spin singlet

In the spin-singlet case,

$$|\Psi\rangle_\sigma = \frac{1}{\sqrt{2}}[|\uparrow\downarrow\rangle_\sigma - |\downarrow\uparrow\rangle_\sigma], \tag{17}$$

so that

$$\hat{\mathcal{P}}^{(1,2)}|\Psi\rangle_\sigma = -|\Psi\rangle_\sigma, \quad \hat{\mathcal{P}}^{(1,2)}|\Psi(t)\rangle_x = +|\Psi(t)\rangle_x.$$

The RNOs $|\tilde{k}(t)\rangle$ may be factorized,

$$|\tilde{k}(t)\rangle = |\tilde{k}(t)\rangle_x \otimes \begin{cases} |\uparrow\rangle_\sigma & \text{if} \quad k \text{ odd}, \\ |\downarrow\rangle_\sigma & \text{if} \quad k \text{ even}, \end{cases} \tag{18}$$

with pairwise equal components,

$$|\tilde{k}(t)\rangle_x = |\tilde{k}'(t)\rangle_x. \tag{19}$$

Insertion into (13) and comparison with (16) and (17) yields

$$|\Psi(t)\rangle_x = \sum_{k \text{ odd}} \frac{e^{i\varphi_k(t)}}{\sqrt{n_k(t)}} |\tilde{k}(t),\tilde{k}(t)\rangle_x, \tag{20}$$

which, indeed, has the desired exchange symmetry.

2. Spin triplet

In the three spin-triplet cases we have

$$\hat{\mathcal{P}}^{(1,2)}|\Psi\rangle_\sigma = +|\Psi\rangle_\sigma, \quad \hat{\mathcal{P}}^{(1,2)}|\Psi(t)\rangle_x = -|\Psi(t)\rangle_x.$$

Each of the three spin-triplet configurations is associated with a different factorization of the RNOs. Consider, e.g.,

$$|\Psi\rangle_\sigma = |\uparrow\uparrow\rangle_\sigma\,. \tag{21}$$

In this case we choose

$$|\tilde{k}(t)\rangle = |\tilde{k}(t)\rangle_x \otimes |\uparrow\rangle_\sigma\,, \tag{22}$$

leading to the correct

$$|\Psi(t)\rangle_x = \sum_{k \text{ odd}} \frac{e^{i\varphi_k(t)}}{\sqrt{2n_k(t)}} [|\tilde{k}(t),\tilde{k}'(t)\rangle_x - |\tilde{k}'(t),\tilde{k}(t)\rangle_x] \tag{23}$$

[without an additional condition like (19)]. The structure (23) of $|\Psi(t)\rangle_x$ also holds for the two remaining triplet configurations, as shown in Appendix B. Moreover, the RNO factorizations in spin and spatial components can be chosen such that $|\tilde{k}(t)\rangle_x$ is invariant when switching between the different spin triplets.

D. Exact 2-DM

The universal expansion (13) of any two-electron state $|\Psi(t)\rangle$ in terms of RNOs $|\tilde{k}(t)\rangle$ implies fundamental knowledge about the connection between the 2-DM $\hat{\gamma}_2(t)$ and the RNOs, as revealed by inserting (13) into (1). As a result, $\tilde{\gamma}_{2,ijkl}(t)$ can be calculated using (7) and (11),

$$\tilde{\gamma}_{2,ijkl}(t) = (-1)^{i-k} \frac{e^{i[\varphi_i(t)-\varphi_k(t)]}}{2\sqrt{n_i(t)n_k(t)}} \delta_{i,j'}\delta_{k,l'}. \tag{24}$$

One sees that the renormalized expansion coefficients $\tilde{\gamma}_{2,ijkl}(t)$ are only nonvanishing for *paired* index combinations. Both the first index pair $\{i,j\}$ and the second index pair $\{k,l\}$ must contain one odd and one even index. Moreover, the "distance" between the paired indices is unity; i.e.,

$$|i-j| = 1, \quad |k-l| = 1, \quad \text{if} \quad \tilde{\gamma}_{2,ijkl}(t) \neq 0. \tag{25}$$

E. Phase conventions

So far, no assumption has been made concerning the phases of the NOs. Any phase transformation according to

$$|\underline{k}(t)\rangle = e^{i\vartheta_k(t)}|k(t)\rangle \tag{26}$$

yields a new set of NOs $\{|\underline{k}(t)\rangle\}$ for the same 1-RDM $\hat{\gamma}_1(t)$ with the same ONs $\{n_k(t)\}$. This phase freedom originates from the definition of NOs as eigenstates of $\hat{\gamma}_1(t)$, allowing for arbitrary time-dependent NO phases because they vanish in (4). However, the expansion (13) of $|\Psi(t)\rangle$ requires phase factors $e^{i\varphi_k(t)}$ in order to compensate for the phase freedom in the NOs. The transformation (26) thus also involves a phase transformation,

$$\underline{\varphi_k}(t) = \varphi_k(t) - \vartheta_k(t) - \vartheta_{k'}(t), \quad k \text{ odd}. \tag{27}$$

This is in analogy of "gauge transformations of the first kind" in field theory. However, the TDRNOT Hamiltonian is, in general, *not* invariant under such phase transformations. Observables *are* invariant.

In order to derive EOM for the NOs, one needs to choose well-defined NO phases. Two choices are presented in the following.

1. Time-dependent phases

In the first publication on TDRNOT [25], the NO phases were fixed by

$$\langle\underline{k}(t)|\partial_t|\underline{k}(t)\rangle = 0, \tag{28}$$

which can formally be fulfilled by the transformation

$$\vartheta_k(t) = i\int^t \langle k(t')|\partial_{t'}|k(t')\rangle dt'. \tag{29}$$

As a result, the phases $\underline{\varphi_k}(t)$ are time-dependent, which requires the solution of coupled EOM for the NOs and $\{\underline{\varphi_k}(t)\}$ because the time evolution of the RNOs depends on these phases via $\tilde{\gamma}_{2,ijkl}(t)$ [see (24) and the EOM in Sec. III below].

2. Phase-including natural orbitals

The phase freedom can be utilized to transform away the time dependence of $\underline{\varphi_k}(t)$. One easily verifies that, e.g., the transformation

$$\vartheta_k(t) = \vartheta_{k'}(t) = \tfrac{1}{2}[\varphi_k(t) - \varphi_{k,0}], \quad k \text{ odd}, \tag{30}$$

yields arbitrarily tunable constant phases $\underline{\varphi_k}(t) \equiv \varphi_{k,0} \in \mathbb{R}$. Depending on the spin configuration [singlet (S) or triplet (T)], we choose the atomic He ground-state phase factors

$$e^{i\varphi_{k,0}^{(\mathrm{S})}} = 2\delta_{k,1} - 1, \quad e^{i\varphi_{k,0}^{(\mathrm{T})}} = 1, \quad k \text{ odd}, \tag{31}$$

so that a real ground-state wave function yields real NOs in position space representation.

Based on this phase convention, one may derive EOM for $|\underline{k}(t)\rangle$ such that all time-dependence is incorporated in the *phase-including* NOs (PINOs) [17,27,28] and the ONs. Note that the transformation (30) does not remove all phase freedom

because one can still distribute the phase between any pair $|\tilde{k}(t),\tilde{k}'(t)\rangle$ in the triplet case. The missing constraint is given by (C9) in the derivation of the respective EOM.

In the following we omit the underline in $|\underline{k}(t)\rangle$ for the phase-including (R)NOs.

III. EQUATIONS OF MOTION FOR RENORMALIZED PHASE-INCLUDING NATURAL ORBITALS

We consider a two-electron Hamiltonian,

$$\hat{H}^{(1,2)}(t) = \hat{h}^{(1)}(t) + \hat{h}^{(2)}(t) + v_{\mathrm{ee}}{}^{(1,2)}, \tag{32}$$

where the single-particle part $\hat{h}(t)$ incorporates kinetic energy, binding potential, and, e.g., the coupling to (time-dependent) external fields, and v_{ee} is the electron-electron interaction. Superscripts indicate the particle indices. The time evolution of the NOs is expanded as

$$i\partial_t|k(t)\rangle = \sum_m \alpha_{km}(t)|m(t)\rangle.$$

We see that the phase convention (28) chosen in [25] is equivalent to setting $\alpha_{kk}(t) \equiv 0$. Instead, for the PINO phase convention of Sec. II E 2 we employ the diagonal elements $\alpha_{kk}(t)$ in order to modify the EOM such that the phases $\{\varphi_k\}$ stay constant. A useful expression for $\alpha_{kk}(t)$ in terms of RNOs is derived in Appendix C for the two-electron case considered here. Adding the new contributions associated with $\alpha_{kk}(t)$ to the EOM for the RNOs derived in [25] yields (time arguments of the RNOs suppressed)

$$\begin{aligned} i\partial_t|\tilde{n}\rangle &= \hat{h}(t)|\tilde{n}\rangle + \mathcal{A}_n(t)|\tilde{n}\rangle \\ &\quad + \sum_{k\neq n}\mathcal{B}_{nk}(t)|\tilde{k}\rangle + \sum_k \hat{\mathcal{C}}_{nk}(t)|\tilde{k}\rangle, \end{aligned} \tag{33}$$

with

$$\mathcal{A}_n(t) = -\frac{1}{n_n(t)}\,\mathrm{Re}\sum_{jkl}\tilde{\gamma}_{2,njkl}(t)\langle\tilde{k}\tilde{l}|v_{\mathrm{ee}}|\tilde{n}\,\tilde{j}\rangle, \tag{34}$$

$$\begin{aligned} \mathcal{B}_{nk}(t) = \frac{2}{n_k(t)-n_n(t)}\sum_{jpl}&[\tilde{\gamma}_{2,kjpl}(t)\langle\tilde{p}\tilde{l}|v_{\mathrm{ee}}|\tilde{n}\,\tilde{j}\rangle \\ &- \tilde{\gamma}_{2,plnj}(t)\langle\tilde{k}\,\tilde{j}|v_{\mathrm{ee}}|\tilde{p}\tilde{l}\rangle], \quad k\neq n', \end{aligned} \tag{35}$$

and

$$\hat{\mathcal{C}}_{nk}(t) = 2\sum_{jl}\tilde{\gamma}_{2,kjnl}(t)\langle\tilde{l}|v_{\mathrm{ee}}|\tilde{j}\rangle. \tag{36}$$

Only $\mathcal{A}_n(t)$ is modified due to $\alpha_{kk}(t) \not\equiv 0$, whereas $\mathcal{B}_{nk}(t)$ and $\hat{\mathcal{C}}_{nk}(t)$ are invariant under the phase transformation.

Special treatment is required regarding the $\mathcal{B}_{nk}(t)$ of the pairs $k = n'$ because of the pairwise degeneracy $n_k(t) = n_{k'}(t)$. Recalling (A8) of [25],

$$\begin{aligned} \alpha_{np}(t)[n_p(t)-n_n(t)] &= [n_p(t)-n_n(t)]\langle p|\hat{h}(t)|n\rangle \\ &\quad + 2\sum_{jkl}\gamma_{2,pjkl}(t)\langle kl|v_{\mathrm{ee}}|nj\rangle \\ &\quad - 2\sum_{jkl}\gamma_{2,klnj}(t)\langle pj|v_{\mathrm{ee}}|kl\rangle, \end{aligned}$$

it follows that $\alpha_{np}(t)$ is undetermined for $n_p(t) = n_n(t)$ so that $\mathcal{B}_{nn'}(t)$ cannot be obtained by following the derivation in [25]. This reflects the fact that, independent of the choice of phase, eigenstates corresponding to degenerate eigenvalues are not uniquely defined. In terms of NOs one finds that $|\underline{k}\rangle$, $|\underline{k}'\rangle$ according to

$$\begin{pmatrix}|\underline{k}\rangle\\|\underline{k}'\rangle\end{pmatrix} = \begin{pmatrix}\cos[\theta_k(t)] & \sin[\theta_k(t)]\\ -\sin[\theta_k(t)] & \cos[\theta_k(t)]\end{pmatrix}\begin{pmatrix}|k\rangle\\|k'\rangle\end{pmatrix} \tag{37}$$

yield the same state $|\Psi(t)\rangle$ for any choice of $\{\theta_k(t)\}$. In practice, this is not an issue for the spin singlet because the additional freedom is removed by the particular choice of the product ansatz (18). For the spin triplet we choose $\alpha_{nn'}(t) \equiv 0$. Hence, we replace the corresponding coefficients $\mathcal{B}_{nn'}(t)$ in the spin-triplet case by

$$\begin{aligned} \mathcal{B}_{nn'}(t) = &-\frac{1}{n_n(t)} \\ &\times\left[\langle\tilde{n}'|\hat{h}(t)|\tilde{n}\rangle + 2\sum_{jpl}\tilde{\gamma}_{2,plnj}(t)\langle\tilde{n}'\,\tilde{j}|v_{\mathrm{ee}}|\tilde{p}\tilde{l}\rangle\right]. \end{aligned} \tag{38}$$

A. Occupation numbers during imaginary-time propagation

It has already been shown [25] that the spin-singlet ground state is a stationary point of the EOM when propagating the RNOs in imaginary time. Unfortunately, using the phase convention of Sec. II E 1 used in [25], the ONs are invariant during imaginary-time propagation. As a consequence, one needs to inject the correct ONs for the ground state. A useful criterion for the ground-state configuration $\{n_k\}$ can be derived by means of variational calculus minimizing the total energy $E \geqslant E_0$. In this work we supplement the variational calculus with an additional constraint for finding the spin-triplet ground state. Details are given in Appendix D. The result for the orbital energies reads

$$\epsilon_k = \frac{1}{n_k}\left[\langle\tilde{k}|\hat{h}_0|\tilde{k}\rangle + \sum_{ijl}\tilde{\gamma}_{2,ijkl}\langle\tilde{k}\tilde{l}|v_{\mathrm{ee}}|\tilde{i}\,\tilde{j}\rangle\right].$$

The ONs in the ground-state configuration have to be such that

$$E = \epsilon_k + \epsilon_{k'}, \tag{39}$$

i.e., each sum of two associated orbital energies in the ground state equals the total energy E. For the spin-singlet ground state all orbital energies are equal; i.e., $\epsilon_k^{(\mathrm{S})} = \epsilon^{(\mathrm{S})}$. In the spin-triplet case, one additional Lagrange parameter ϵ_k^{d} for odd k is introduced to ensure that $n_k = n_{k'}$. Because of ϵ_k^{d}, individual triplet orbital energies are generally not equal,

$$\epsilon_k^{(\mathrm{T})} = \epsilon^{(\mathrm{T})} + \epsilon_k^{\mathrm{d}}\delta_{k\ \mathrm{odd}} - \epsilon_{k-1}^{\mathrm{d}}\delta_{k\ \mathrm{even}}.$$

Using the phase convention of Sec. II E 1, one may tune the ONs n_k such that the orbital energies ϵ_k fulfill (39) when the RNOs $|\tilde{k}\rangle$ are converged to the stationary point of the imaginary-time propagation. For more than four NOs this is a multidimensional problem so that a Newton-Raphson scheme may be employed to find the correct ground-state ONs. Details are given in Appendix E.

Fortunately, using the PINO phase convention of Sec. II E 2 simplifies the ground-state search because the ONs are *not* constant during imaginary-time propagation but adjust themselves. In fact, $\partial_t n_n(t)$ can be calculated using

$$\partial_t n_n(t) = \big[\partial_t \langle\tilde{n}|\big]|\tilde{n}\rangle + \langle\tilde{n}|\big[\partial_t|\tilde{n}\rangle\big]. \tag{40}$$

Replacing $i\,\partial_t|\tilde{n}\rangle$ with $-\partial_t|\tilde{n}\rangle$ on the left-hand side of the EOM (33) one may insert the result and its adjoint into (40) to obtain

$$\partial_t n_n(t) = -2n_n(t)\epsilon_n(t)$$

for real NOs. We conclude that in the desired ground-state configuration, the relative change of ONs is constant for each associated orbital pair, i.e.,

$$\frac{\partial_t\,[n_n(t) + n_{n'}(t)]}{n_n(t) + n_{n'}(t)} = -E_0.$$

As a result, the set of ground-state ONs is a stationary point of the imaginary-time propagation if the restrictions (5) and (15) are enforced after each time step. In practice, we find that the ONs converge to this stationary point when propagating in imaginary time. No additional criterion such as (39) needs to be applied for finding the ground state via imaginary-time propagation with the PINO phase convention.

B. Conservation of occupation-number degeneracies

Let us check whether the pairwise degeneracy of ONs (15) is conserved when propagating the RNOs in real time. As the pairwise degeneracy results from the exchange antisymmetry, a violation of the ON degeneracies would imply a violation of the Fermionic character of the electrons described. In the actual numerical implementation we use an absorbing potential, i.e., $\hat{h}^\dagger(t) \neq \hat{h}(t)$, in order to remove orbital probability density approaching the grid boundaries. One then finds (suppressing time arguments of the RNOs again)

$$\partial_t n_k(t) = 2\,\mathrm{Im}\langle\tilde{k}|\hat{h}(t)|\tilde{k}\rangle + 4\,\mathrm{Im}\sum_{ijl}\tilde{\gamma}_{2,ijkl}(t)\langle\tilde{k}\tilde{l}|v_{\mathrm{ee}}|\tilde{i}\,\tilde{j}\rangle.$$

If the time propagation is performed fully self-consistently, i.e., without freezing the effective Hamiltonian, and absorption is negligible,

$$\partial_t\,[n_k(t) - n_{k'}(t)] = 0,$$

as can be shown by making use of the special structure (24) of $\tilde{\gamma}_{2,ijkl}(t)$ in the case of two electrons.

If the absorbing potential significantly influences the ONs, the condition for the conservation of degeneracies reads

$$\mathrm{Im}\langle\underline{\tilde{k}}|\hat{h}(t)|\underline{\tilde{k}}\rangle = \mathrm{Im}\langle\underline{\tilde{k}}'|\hat{h}(t)|\underline{\tilde{k}}'\rangle. \tag{41}$$

In the singlet case, (41) always holds because the spatial components of the RNOs $|\tilde{k}(t)\rangle$ and $|\tilde{k}'(t)\rangle$ are equal due to the factorization (18). In the triplet case, there is the freedom to use superpositions (37) such that (41) is fulfilled for all k. However, in this paper we do not show results where a significant amount of probability density was absorbed so that the application of criterion (41) was not necessary.

IV. RESULTS

Results are obtained for the one-dimensional helium model atom [23,24] described by the Hamiltonian (32) with

$$\hat{h}(t) = \frac{\hat{p}^2}{2} - \frac{2}{\sqrt{x^2+1}} + A(t)\hat{p},$$

$$v_{\mathrm{ee}}{}^{(1,2)} = \frac{1}{\sqrt{(x^{(1)} - x^{(2)})^2 + 1}}.$$

The interaction with an external (laser) field in dipole approximation is incorporated in velocity gauge via the vector potential $A(t)$, with the purely time-dependent A^2 term transformed away. Numerical results are shown for both the spin singlet and the spin triplet. As a first check, we confirm in Sec. IV A that the EOM for the renormalized PINOs (33)–(36) and (38) yield the exact ground-state energy and correct ONs if enough RNOs are included in the propagation. The second step is to employ the PINO EOM for a propagation in real time in order to evaluate the advantages of the PINO phase convention over the previously used [25] phase convention of Sec. II E 1. For this purpose, linear response spectra considering a different number of RNOs are discussed in Sec. IV B. Rabi oscillations, as a prime example for highly resonant and nonperturbative phenomena that bring quantum systems far away from their ground state, are investigated in Sec. IV C.

In practice, the number of RNOs is truncated in order to allow for a numerical treatment. In the following, N_o denotes the number of spin orbitals so that N_o RNOs correspond to $N_\mathrm{o}/2$ different spatial orbitals for the spin singlet and N_o different spatial orbitals for the spin triplet. Computational details are given in [25].

A. Ground-state calculations

The ground state is obtained via imaginary-time propagation, as discussed in Sec. III A. Both phase conventions yield the same ground-state configurations so that we do not need to distinguish between the two in this section.

The total energy and the dominant ONs for both the spin-singlet and the spin-triplet ground state are presented in Table I. TDRNOT results for different N_o are compared to the exact TDSE results. All TDRNOT results clearly converge to the corresponding exact TDSE value for increasing N_o.

$N_\mathrm{o} = 2$ is equivalent to a time-dependent Hartree-Fock (TDHF) treatment or TDDFT in exact exchange-only approximation. Results very similar to those in Table I have been reported in [29] using a multiconfigurational time-dependent Hartree-Fock (MCTDHF) approach. The strength of two-electron TDRNOT compared to two-electron MCTDHF is the choice of RNOs as a basis, which always guarantees the best approximation to the exact solution $|\Psi(t)\rangle$ for a given number of orbitals [22] *at all times* during real-time propagation.

B. Linear response spectra

Starting from the spin-singlet or spin-triplet ground state, the vector potential is switched to a finite but small value ($A = 0.0005$ was chosen for the results presented in the following), and the RNOs are propagated in real time for $t_\mathrm{max} = 1000$, with an enabled imaginary potential. The Fourier transform

TABLE I. Total energy and ONs of the spin-singlet and spin-triplet ground states, respectively. Exact results obtained from the direct solution of the TDSE are compared to TDRNOT results using different N_o. Converged digits are underlined.

No. N_o of RNOs	Total energy E_0 (a.u.)	Dominant occupation numbers n_1	$n_3/10^{-3}$	$n_5/10^{-5}$
		Spin singlet		
2 (TDHF)	−2.224 318	1.000 000 0		
4 (TDRNOT)	−2.236 595	0.991 266 5	8.7335	
6 (TDRNOT)	−2.238 203	0.990 959 0	8.3142	72.683
8 (TDRNOT)	−2.238 324	0.990 943 8	8.3221	70.229
∞ (TDSE)	−2.238 368	0.990 947 3	8.3053	70.744
		Spin triplet		
2 (TDHF)	−1.812 052 4	1.000 000 00		
4 (TDRNOT)	−1.816 079 8	0.997 640 48	2.359 52	
6 (TDRNOT)	−1.816 187 0	0.997 607 05	2.364 64	2.8298
8 (TDRNOT)	−1.816 194 5	0.997 606 56	2.362 67	2.9581
∞ (TDSE)	−1.816 195 4	0.997 606 77	2.362 20	2.9610

of the dipole expectation value then yields peaks at energy differences $E - E_0$ for all dipole-allowed transitions.

Figure 1 shows that the fully self-consistent TDRNOT time propagation reproduces the exact linear response spectra (solid line; labeled "TDSE") for both the spin singlet (a) and the spin triplet (b) if enough RNOs are taken into account. As

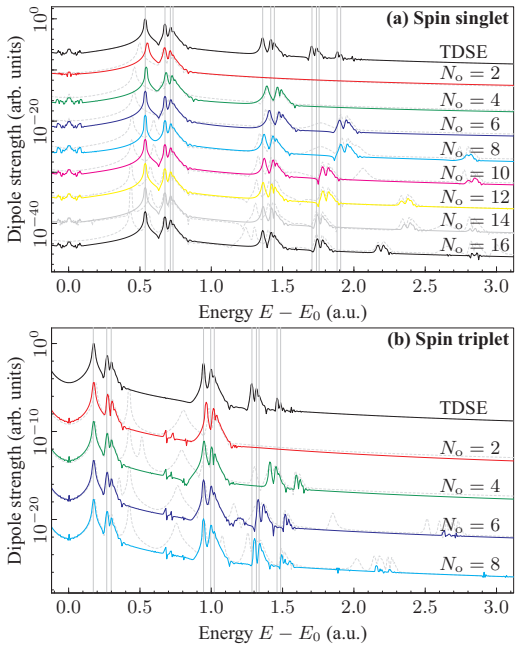

FIG. 1. (Color online) Singlet (a) and triplet (b) linear response spectra for a different numbers of RNOs N_o, compared to the exact TDSE result. For comparison, bare (i.e., with ground-state frozen Hamiltonian) TDRNOT results following the phase convention of Sec. II E 1 are shown with dashed lines. To guide the eyes, vertical lines indicate some of the distinct peaks in the exact TDSE spectrum.

already known from the bare evolution in [25], the description of doubly excited states requires at least $N_o \geqslant 4$ so that the ONs are not pinned to the integers 0 or 1.

As expected, the more series of doubly excited states are sought, the more RNOs are needed. Interestingly, some peak positions of the spin singlet show an alternating convergence if one successively adds two RNOs more. For example, the peak around $E - E_0 \approx 1.35$ is shifted to the wrong direction from $N_o = 4$ to $N_o = 6$ but substantially shifts towards its correct position for $N_o = 8$. Using $N_o = 10$, its peak position again slightly worsens compared to the previous value, whereas for $N_o = 12$ the energy matches almost perfectly with the TDSE peak position.

The fully self-consistent time propagation using the PINO phase convention of Sec. II E 2 (solid line) is clearly superior to the bare evolution with the phase convention of Sec. II E 1 (dashed gray line): erroneous extra peaks are absent, and the physical peaks are shifted to the correct TDSE positions. Both effects are particularly important for more RNOs, say $N_o \geqslant 6$. Especially for the triplet, the full propagation with PINOs leads to much better results. The bare evolution generates erroneous extra peaks for any number of RNOs, corresponding to artificial states with nondegenerate ONs. Since degenerate ONs are a consequence of the exchange antisymmetry, those peaks indicate the breaking of the exchange symmetry by the bare time evolution with the ground-state frozen Hamiltonian. This deficiency is removed by the full propagation using PINOs, as discussed in Sec. III B.

MCTDHF linear response spectra for the same model have been obtained in [29]. Our Fig. 1(a) can be directly compared with Fig. 3 there, where artificial extra peaks just above the first ionization threshold are seen. The reason for the erroneous peaks in the MCTDHF results is unknown to us. The superior performance of our TDRNOT approach using PINOs is presumably due to the built-in optimal choice of basis set functions *at all times*.

It is to be expected that our promising results translate to 3D two-electron systems. In fact, in Refs. [27,28] it has been shown already that only a few of the highest occupied PINOs are sufficient to capture accurately the lowest excitations in the response of the 3D two-electron systems H_2 and HeH^+.

C. Rabi oscillations

Linear response spectra are not enough to study strong-field laser-matter interaction phenomena, which, by definition, are nonperturbative in nature and rely on electron dynamics far away from the ground state. A prime example for nonperturbative laser-matter coupling is Rabi oscillations. It has been shown that Rabi oscillations are not captured within "standard" TDDFT [30] but that XC functionals with memory, i.e., XC functionals beyond the adiabatic approximation, are required [5]. It is important to understand that adiabatic TDDFT applied to Rabi oscillations may reproduce a reasonable looking position expectation value as a function of time [30], even though the time-dependent density is *not* properly described, especially at times of population inversion, e.g., after a π pulse. Instead, the ONs $n_k(t)$ as a function of time are very sensitive entities, which we use for benchmarking our

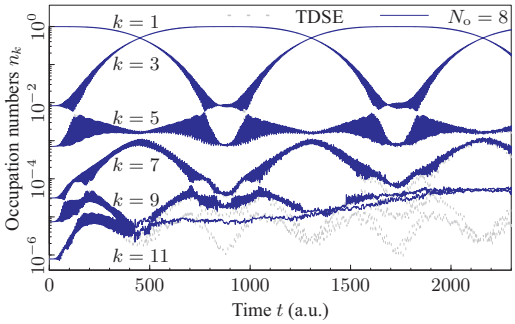

FIG. 2. (Color online) ONs $n_k(t)$ vs time t for the spin singlet in a laser field of frequency $\omega = 0.5337$ resonantly tuned to the first excited state. The four most significant ONs $n_1(t)$,$n_3(t)$,$n_5(t)$,$n_7(t)$ obtained by TDRNOT with $N_o = 16$ RNOs (solid lines) correctly reproduce more than two Rabi cycles of the exact TDSE propagation (dotted lines). Due to the truncation to a finite number of RNOs in TDRNOT, fewer significant orbitals are missing the proper coupling to lower orbitals, leading to erroneous behavior of small ONs over time. For longer propagation times, also higher ONs are affected because the RNOs are coupled.

TDRNOT approach via a comparison with the exact TDSE result.

We consider a Rabi oscillation between the spin-singlet ground state and the first excited state, driven by a laser of resonant frequency $\omega = 0.5337$. The vector potential amplitude $A = 0.0125$ of the flat-top part is linearly ramped up over four periods. Propagating eight different spatial NOs, we have $N_o = 16$. Due to the pairwise degeneracy, it follows that $n_1(t) = n_2(t), \ldots, n_{15}(t) = n_{16}(t)$ so that it is sufficient to discuss $n_{k\,\mathrm{odd}}(t)$.

The six most significant ONs $n_1(t)$,$n_3(t)$, $\ldots$,$n_{11}(t)$ predicted by the TDRNOT propagation (solid lines) are compared with the exact TDSE result (dotted lines) in Fig. 2.

1. Truncation problem

Thanks to the proper ground-state description reported in Sec. IV A, all TDRNOT ONs start on top of the exact TDSE reference for $t = 0$ in Fig. 2. However, already for small times $0 < t \lesssim 200$ ONs $n_{13}(t)$ and $n_{15}(t)$ (not shown) begin to deviate from the correct value. Instead of the periodic oscillation with the Rabi period $2\pi/\Omega_R \approx 850$ and a modulation on the time scale of the laser period $2\pi/\omega \approx 11.8$, they just approach their respective "upper-neighbor" NO's ON. The next ONs $n_{11}(t)$ and $n_9(t)$ become quantitatively distinguishable from their respective TDSE values around $t \gtrsim 400$ and $t \gtrsim 800$. After two Rabi cycles, i.e., $t \gtrsim 1700$, also their qualitative behavior is completely wrong, showing no oscillation on the Rabi time scale any longer. Around that time $t \approx 1700$ the next-higher ON $n_7(t)$ is affected and shows some small quantitative differences compared to the exact solution, although it regains the proper behavior at later times.

The origin of these imperfections regarding the least significant orbitals in the propagation lies in the truncation to a finite number $N_o = 16$ of RNOs taken into account. The EOM in Sec. III have been derived for an infinite number of coupled RNOs. It turns out that the orbital coupling via $\mathcal{B}_{nk}(t)$ is particularly strong for orbitals with nearby ONs so that the truncation of the orbitals $\{|\tilde{17}(t)\rangle, |\tilde{18}(t)\rangle, \ldots\}$ is most severe for the least significant orbitals. Once their dynamics is spoiled, the truncation error subsequently propagates "upwards" due to the coupling to the respective next higher orbitals.

2. Overall performance

The four most significant ONs $n_1(t)$, $n_3(t)$, $n_5(t)$, $n_7(t)$ in Fig. 2 are in striking agreement with the exact TDSE result. Their dynamics during more than two Rabi cycles, i.e., a time period of 2300 atomic units in total, is well described. Overall, the "well-behaved" RNOs represent more than 99.9 % of the 1-RDM so that the significant part of the Rabi dynamics is captured by TDRNOT.

The remarkable gain of TDRNOT compared to, e.g., TDDFT, is that—despite the (numerically strongly favorable) locality in time—TDRNOT is capable of describing the highly resonant dynamics of Rabi oscillations. In fact, the exact two-electron TDRNOT EOM are strictly memory free.

V. CONCLUSION AND OUTLOOK

In the current work, we have extended the previously introduced [25] TDRNOT. We have derived the EOM for RNOs, employing the phase convention in which the entire time-dependence is carried by the NOs themselves. In the two-particle case, this makes it possible to obtain the exact EOM, without making any assumptions about (or any approximations to) the expansion of the time-dependent two-body density matrix in NOs. As an example, we have solved the EOM for a widely used helium model atom. In practical calculations, the number of NOs taken into account should be as small as possible. As a truncation of the number of NOs introduces numerical errors, we have benchmarked our results by the corresponding exact solutions of the TDSE. Excellent agreement has been found for the spin-singlet and spin-triplet ground states (obtained via imaginary-time propagation), linear response spectra, and Rabi flopping dynamics (as an example for a strongly nonperturbative, resonant phenomenon).

We are mainly interested in laser-driven *few*-body correlated quantum dynamics. Besides Rabi flopping, we are currently applying the TDRNOT method successfully to other (strong-field) scenarios where "standard" TDDFT with practicable XC potentials is known to fail, e.g., nonsequential double ionization. Moreover, we are investigating the structure of the exact 2-RDM expansion coefficients $\tilde{\gamma}_{2,ijkl}$ for three-electron systems in order to derive useful expressions that can be used to propagate the respective NOs using TDRNOT.

ACKNOWLEDGMENTS

Fruitful discussions with M. Lein are acknowledged. This work was supported by the SFB 652 of the German Science Foundation (DFG).

APPENDIX A: EXPANSION OF A TWO-FERMION STATE IN RNOS

Let the expansion of a two-fermion state $|\Psi(t)\rangle$ in orthonormal single-particle basis functions $|\psi_i(t)\rangle$ comprising spin and spatial degrees of freedom be

$$|\Psi(t)\rangle = \sum_{ij} \Psi_{ij}(t)|\psi_i(t),\psi_j(t)\rangle,$$
$$\Psi_{ij}(t) = \langle\psi_i(t),\psi_j(t)|\Psi(t)\rangle.$$

Defining a matrix $\boldsymbol{\Psi} = [\Psi_{ij}(t)]$ of expansion coefficients $\Psi_{ij}(t)$, the exchange antisymmetry can be expressed as $\boldsymbol{\Psi}^{\mathrm{T}} = -\boldsymbol{\Psi}$. With

$$\boldsymbol{\psi} = \begin{pmatrix} |\psi_1(t)\rangle \\ |\psi_2(t)\rangle \\ \vdots \end{pmatrix}, \quad \boldsymbol{\psi}^* = \begin{pmatrix} \langle\psi_1(t)| \\ \langle\psi_2(t)| \\ \vdots \end{pmatrix},$$
$$\boldsymbol{\psi}^{\mathrm{T}} = \big(|\psi_1(t)\rangle,|\psi_2(t)\rangle,\dots\big), \quad \boldsymbol{\psi}^\dagger = (\langle\psi_1(t)|,\langle\psi_2(t)|,\dots),$$

such that

$$\boldsymbol{\psi}^*\boldsymbol{\psi}^\dagger = \begin{pmatrix} \langle\psi_1(t)| \\ \langle\psi_2(t)| \\ \vdots \end{pmatrix}(\langle\psi_1(t)|,\langle\psi_2(t)|,\dots)$$
$$= \begin{pmatrix} \langle\psi_1(t),\psi_1(t)| & \langle\psi_1(t),\psi_2(t)| & \dots \\ \langle\psi_2(t),\psi_1(t)| & \langle\psi_2(t),\psi_2(t)| & \dots \\ \vdots & \vdots & \ddots \end{pmatrix}$$

the relation between a two-fermion state $|\Psi(t)\rangle$ and its coefficient matrix $\boldsymbol{\Psi}$ in the basis $\{|\psi_i(t)\rangle\}$ may be written as

$$\boldsymbol{\Psi} = \boldsymbol{\psi}^*\boldsymbol{\psi}^\dagger|\Psi(t)\rangle, \quad |\Psi(t)\rangle = \boldsymbol{\psi}^{\mathrm{T}}\boldsymbol{\Psi}\boldsymbol{\psi}. \tag{A1}$$

The skew-symmetric matrix $\boldsymbol{\Psi} = -\boldsymbol{\Psi}^{\mathrm{T}}$ can be factorized into unitary matrices $\boldsymbol{U},\boldsymbol{U}^\dagger$ and a block-diagonal matrix $\boldsymbol{\Sigma}$ as [31], [Corollary 2.6.6. (b)]

$$\boldsymbol{\Psi} = \boldsymbol{U}\boldsymbol{\Sigma}\boldsymbol{U}^{\mathrm{T}}, \quad \boldsymbol{\Sigma} = \mathrm{diag}(\boldsymbol{\Sigma}_1,\boldsymbol{\Sigma}_3,\boldsymbol{\Sigma}_5,\dots),$$
$$\boldsymbol{\Sigma}_i = \begin{pmatrix} 0 & \xi_i(t) \\ -\xi_i(t) & 0 \end{pmatrix}, \quad i \ \text{ odd}.$$

Inserting this factorization into (A1), one obtains an expansion in the transformed basis $\boldsymbol{\phi} = \boldsymbol{U}^{\mathrm{T}}\boldsymbol{\psi}$,

$$|\Psi(t)\rangle = \boldsymbol{\psi}^{\mathrm{T}}(\boldsymbol{U}\boldsymbol{\Sigma}\boldsymbol{U}^{\mathrm{T}})\boldsymbol{\psi} = \boldsymbol{\phi}^{\mathrm{T}}\boldsymbol{\Sigma}\boldsymbol{\phi}.$$

In other words, any two-fermion state $|\Psi(t)\rangle$ can be written in the form

$$|\Psi(t)\rangle = \sum_{i \text{ odd}} \xi_i(t)[|\phi_i(t),\phi_{i'}(t)\rangle - |\phi_{i'}(t),\phi_i(t)\rangle], \tag{A2}$$

where the prime operator (14) was used. Inserting (A2) into the 1-RDM (2) gives

$$\hat{\gamma}_1(t) = \sum_{k \text{ odd}} 2|\xi_k(t)|^2[|\phi_k(t)\rangle\langle\phi_k(t)| + |\phi_{k'}(t)\rangle\langle\phi_{k'}(t)|],$$

which proves that $|k(t)\rangle = |\phi_k(t)\rangle$; i.e., the set $\{|\phi_k(t)\rangle\}$ *is* a set of NOs. The corresponding eigenvalues $2|\xi_k(t)|^2$ for odd k, i.e., the ONs, are (at least) pairwise degenerate,

$$n_k(t) = n_{k+1}(t) = 2|\xi_k(t)|^2, \quad k \ \text{ odd}.$$

Writing $\xi_k(t) = \frac{1}{\sqrt{2}}e^{i\varphi_k(t)}\sqrt{n_k(t)}$ for odd k, and switching to RNOs $\{|\tilde{k}(t)\rangle\}$, a two-fermion state reads

$$|\Psi(t)\rangle = \sum_{k \text{ odd}} \frac{e^{i\varphi_k(t)}}{\sqrt{2n_k(t)}}[|\tilde{k}(t),\tilde{k}'(t)\rangle - |\tilde{k}'(t),\tilde{k}(t)\rangle]. \tag{A3}$$

APPENDIX B: FACTORIZATION OF RNOS IN THE TRIPLET CASES

Section II C 2 contains a brief discussion of the very simple RNO factorization for the spin-triplet configuration $|\Psi\rangle_\sigma = |\uparrow\uparrow\rangle_\sigma$. The case $|\Psi\rangle_\sigma = |\downarrow\downarrow\rangle_\sigma$ is analogous. The factorization of the NOs for the spin triplet

$$|\Psi\rangle_\sigma = \frac{1}{\sqrt{2}}[|\uparrow\downarrow\rangle_\sigma + |\downarrow\uparrow\rangle_\sigma] \tag{B1}$$

is more involved. Considering both positive and negative indices k, one may define RNOs

$$|\tilde{k}(t)\rangle = \begin{cases} |\tilde{k}(t)\rangle_x & \text{if} \quad k > 0 \\ |-\tilde{k}(t)\rangle_x & \text{if} \quad k < 0 \end{cases}$$
$$\otimes \begin{cases} |\uparrow\rangle_\sigma & \text{if} \quad k > 0, \quad k \text{ odd}, \\ |\downarrow\rangle_\sigma & \text{if} \quad k > 0, \quad k \text{ even}, \\ |\downarrow\rangle_\sigma & \text{if} \quad k < 0, \quad k \text{ odd}, \\ |\uparrow\rangle_\sigma & \text{if} \quad k < 0, \quad k \text{ even}, \end{cases}$$

and a generalized prime operator acting on nonzero integer numbers k according

$$k' = \begin{cases} k+1 & \text{if} \quad k > 0, \quad k \text{ odd}, \\ k-1 & \text{if} \quad k > 0, \quad k \text{ even}, \\ k-1 & \text{if} \quad k < 0, \quad k \text{ odd}, \\ k+1 & \text{if} \quad k < 0, \quad k \text{ even}. \end{cases}$$

Insertion into (13) (where now both positive and negative k have to be considered in the sum) yields, again, the same structure (23) and the same $|\tilde{k}(t)\rangle_x$ as the other triplet configurations. If the Hamiltonian (32) does not act on spin degrees of freedom, as is the case for the model He atom considered, the sole significance of the spin component of the state $|\Psi(t)\rangle$ is its effect on the exchange symmetry of the spatial part, which is the same for each of the three triplet configurations.

APPENDIX C: DERIVATION OF α_{kk} FOR PINOS

Writing (13) as

$$|\Psi(t)\rangle = \sum_{i \text{ odd}} \xi_i(t)[|i,i'\rangle - |i',i\rangle], \quad \xi_i(t) = e^{i\varphi_{i,0}}\sqrt{\frac{n_i(t)}{2}}, \tag{C1}$$

with the phase factors $e^{i\varphi_i}$ given by (31), yields, upon insertion into the right-hand side of the TDSE,

$$\hat{H}(t)|\Psi(t)\rangle = i\,\partial_t|\Psi(t)\rangle,$$
$$\hat{H}(t)|\Psi(t)\rangle = i\sum_{i \text{ odd}}[\dot{\xi}_i(t)(|i,i'\rangle - |i',i\rangle) + \xi_i(t)(|\dot{i},i'\rangle$$
$$- |i',\dot{i}\rangle + |i,\dot{i'}\rangle - |i',\dot{i}\rangle)]. \tag{C2}$$

Multiplying from the left by $\langle k,k'|$ for an odd k gives

$$\langle k,k'|\hat{H}(t)|\Psi(t)\rangle = i\dot{\xi}_k(t) + \xi_k(t)[\langle k|\partial_t|k\rangle + \langle k'|\partial_t|k'\rangle] = i\frac{\dot{n}_k(t)}{2n_k(t)}\xi_k(t) + i\xi_k(t)[\alpha_{kk}(t) + \alpha_{k'k'}(t)]. \tag{C3}$$

Insertion of (C1) into the left-hand side of the TDSE (C2) gives

$$\langle k,k'|\hat{H}(t)|\Psi(t)\rangle = \xi_k(t)[\langle k|\hat{h}(t)|k\rangle + \langle k'|\hat{h}(t)|k'\rangle] + \sum_{i\ \text{odd}}\xi_i(t)[\langle k,k'|v_{\text{ee}}|i,i'\rangle - \langle k,k'|v_{\text{ee}}|i',i\rangle]. \tag{C4}$$

Combination of (C3) and (C4) yields

$$\alpha_{kk}(t) + \alpha_{k'k'}(t) = \langle k|\hat{h}(t)|k\rangle + \langle k'|\hat{h}(t)|k'\rangle + \sum_{i\ \text{odd}}\frac{\xi_i(t)}{\xi_k(t)}[\langle k,k'|v_{\text{ee}}|i,i'\rangle - \langle k,k'|v_{\text{ee}}|i',i\rangle] - i\frac{\dot{n}_k(t)}{2n_k(t)}. \tag{C5}$$

Recasting the sum in (C5) in the form

$$\frac{2}{n_k(t)}\sum_{i\ \text{odd}} e^{i(\varphi_{i,0}-\varphi_{k,0})}\sqrt{\frac{n_i(t)}{2}}\sqrt{\frac{n_k(t)}{2}}[\langle k,k'|v_{\text{ee}}|i,i'\rangle - \langle k,k'|v_{\text{ee}}|i',i\rangle] = \frac{2}{n_k(t)}\sum_{ijl}\tilde{\gamma}_{2,ijkl}(t)\langle\tilde{k}\tilde{l}|v_{\text{ee}}|\tilde{i}\,\tilde{j}\rangle \tag{C6}$$

and making use of the analytically known expression for $\dot{n}_k(t)$ [25],

$$\dot{n}_k(t) = 4\,\text{Im}\sum_{ijl}\tilde{\gamma}_{2,ijkl}(t)\langle\tilde{k}\tilde{l}|v_{\text{ee}}|\tilde{i}\,\tilde{j}\rangle, \tag{C7}$$

gives

$$\alpha_{kk}(t) + \alpha_{k'k'}(t) = \langle k|\hat{h}(t)|k\rangle + \langle k'|\hat{h}(t)|k'\rangle + \frac{2}{n_k(t)}\,\text{Re}\sum_{ijl}\tilde{\gamma}_{2,ijkl}(t)\langle\tilde{k}\tilde{l}|v_{\text{ee}}|\tilde{i}\,\tilde{j}\rangle. \tag{C8}$$

Equation (C8) reflects the freedom to distribute the global phase of $|i,i'\rangle - |i',i\rangle$ in (C1) among orbital i and orbital i'. Choosing

$$\alpha_{kk}(t) = \alpha_{k'k'}(t) - \langle k'|\hat{h}(t)|k'\rangle + \langle k|\hat{h}(t)|k\rangle, \tag{C9}$$

it is found that for both odd and even k the final result reads

$$\alpha_{kk}(t) = \frac{1}{n_k(t)}[\langle\tilde{k}|\hat{h}(t)|\tilde{k}\rangle + \text{Re}\sum_{ijl}\tilde{\gamma}_{2,ijkl}(t)\langle\tilde{k}\tilde{l}|v_{\text{ee}}|\tilde{i}\,\tilde{j}\rangle]. \tag{C10}$$

APPENDIX D: VARIATIONAL DETERMINATION OF THE SPIN-TRIPLET GROUND STATE

As in [25], we define an energy functional $\tilde{E}$ taking into account the constraints $\sum_i n_i = N = 2$, $\langle i|j\rangle = \delta_{ij}$, $n_i \geqslant 0$, $n_i \leqslant 1$ via the Lagrange parameters ϵ and λ_{ij} as well as the Karush-Kuhn-Tucker parameters [17,32] ϵ_i^0 and ϵ_i^1, respectively. Additionally, the degeneracy $n_i = n_{i'}$ is enforced via the Lagrange parameter ϵ_i^{d} for odd i. The functional $\tilde{E}$ reads

$$\tilde{E} = \sum_i\langle\tilde{i}|\hat{h}_0|\tilde{i}\rangle + \sum_{ijkl}\frac{\Gamma_{2,ijkl}}{\sqrt{\langle\tilde{i}|\tilde{i}\rangle\langle\tilde{k}|\tilde{k}\rangle}}\langle\tilde{k}\tilde{l}|v_{\text{ee}}|\tilde{i}\,\tilde{j}\rangle - \epsilon\left[\sum_i\langle\tilde{i}|\tilde{i}\rangle - 2\right] - \sum_i\sum_{j\neq i}\lambda_{ij}\langle\tilde{i}|\tilde{j}\rangle - \sum_i\left[\epsilon_i^0\langle\tilde{i}|\tilde{i}\rangle + \epsilon_i^1(1-\langle\tilde{i}|\tilde{i}\rangle)\right] - \sum_{i\ \text{odd}}\epsilon_i^{\text{d}}[\langle\tilde{i}|\tilde{i}\rangle - \langle\tilde{i}'|\tilde{i}'\rangle], \tag{D1}$$

where the slackness conditions [17] are $0 = \epsilon_i^0 n_i = \epsilon_i^1(1-n_i)$, and

$$\Gamma_{2,ijkl} = (-1)^{i-k}\frac{e^{i(\varphi_{i,0}-\varphi_{k,0})}}{2}\delta_{ij'}\delta_{kl'},$$

which is a constant regarding the variation of RNOs. Variation of the energy functional (D1) with respect to $\langle\tilde{m}|$ and $|\tilde{m}\rangle$ yields

$$\epsilon_m|\tilde{m}\rangle = \left\{\hat{h}_0 + 2\sum_{jl}\frac{\Gamma_{2,mjml}}{\langle\tilde{m}|\tilde{m}\rangle}\langle\tilde{l}|v_{\text{ee}}|\tilde{j}\rangle(x) - \frac{1}{\langle\tilde{m}|\tilde{m}\rangle}\,\text{Re}\left[\sum_{ijl}\frac{\Gamma_{2,ijml}}{\sqrt{\langle\tilde{i}|\tilde{i}\rangle\langle\tilde{m}|\tilde{m}\rangle}}\langle\tilde{m}\tilde{l}|v_{\text{ee}}|\tilde{i}\,\tilde{j}\rangle\right]\right\}|\tilde{m}\rangle + \sum_{i\neq m}\left\{2\sum_{jl}\frac{\Gamma_{2,ijml}}{\sqrt{\langle\tilde{i}|\tilde{i}\rangle\langle\tilde{m}|\tilde{m}\rangle}}\langle\tilde{l}|v_{\text{ee}}|\tilde{j}\rangle(x) - \lambda_{mi}\right\}|\tilde{i}\rangle \tag{D2}$$

and its Hermitian conjugate, respectively.

The orbital energies ϵ_m are defined as

$$\epsilon_m = \epsilon + \epsilon_m^0 - \epsilon_m^1 + \epsilon_m^{\text{d}}\delta_{m\ \text{odd}} - \epsilon_{m-1}^{\text{d}}\delta_{m\ \text{even}}.$$

The phases $\varphi_{i,0}$ in (31) are defined such that the ground-state NOs of the model system may be chosen real. Assuming real ground-state NOs, (D2) and its Hermitian conjugate yield

$$\epsilon_k = \frac{1}{n_k}\left[\langle\tilde{k}|\hat{h}_0|\tilde{k}\rangle + \sum_{ijl}\tilde{\gamma}_{2,ijkl}\langle\tilde{k}\tilde{l}|v_{\rm ee}|\tilde{i}\,\tilde{j}\rangle\right].$$

For correlated systems, i.e., in general noninteger ONs, we have $0=\epsilon_i^0=\epsilon_i^1$ so that $\epsilon_k=\epsilon+\epsilon_m^{\rm d}\delta_{m\ \rm odd}-\epsilon_{m-1}^{\rm d}\delta_{m\ \rm even}$. Hence, each sum of two associated orbital energies in the ground state fulfills

$$\epsilon_k+\epsilon_{k'}=2\epsilon.$$

Moreover, the set of ground-state RNOs is a stationary point of the imaginary-time propagation, as already pointed out for the singlet in [25].

APPENDIX E: NEWTON SCHEME FOR FINDING GROUND-STATE ONS

In this Appendix, a scheme for finding the correct ground-state ONs is presented when the phase convention of Sec. II E 1 is chosen. Section III A contains a brief discussion of why this "tuning" of ONs is necessary. The variational calculus in Appendix D shows that the converged RNOs associated with the correct ground-state ONs fulfill

$$\epsilon_k+\epsilon_{k'}=E=E_0. \tag{E1}$$

For $N_{\rm o}$ RNOs, due to the pairwise degeneracy of ONs and the constraint $\sum_k n_k=2$, there are $(N_{\rm o}/2-1)$ free parameters. With

$$n_1=n_2=1-\sum_{\text{odd } i\neq 1} n_i \tag{E2}$$

and

$$\boldsymbol{n}=(n_3,n_5,\ldots,n_{N_{\rm o}-1})^{\rm T},$$
$$\boldsymbol{F}(\boldsymbol{n})=(F_3(\boldsymbol{n}),F_5(\boldsymbol{n}),\ldots,F_{N_{\rm o}-1}(\boldsymbol{n}))^{\rm T},$$
$$F_m(\boldsymbol{n})=\epsilon_m+\epsilon_{m+1}-\epsilon_1-\epsilon_2,$$

the root of $\boldsymbol{F}$ fulfills (E1) for all k. We thus search the root of $\boldsymbol{F}$ using the Newton-Raphson scheme. One iteration step from configuration $\boldsymbol{n}^{(i)}$ to configuration $\boldsymbol{n}^{(i+1)}$ is performed according to

$$\boldsymbol{J}(\boldsymbol{n}^{(i+1)}-\boldsymbol{n}^{(i)})=-\boldsymbol{F}(\boldsymbol{n}^{(i)}),$$

where $\boldsymbol{J}=[J_{mn}]=[\partial_{n_n}F_m]$ (for odd $m\neq 1$ and odd $n\neq 1$) is the Jacobian matrix. The derivatives $\partial_{n_n}F_m$ are calculated using

$$\partial_{n_n}|\tilde{m}\rangle=|m\rangle\partial_{n_n}\sqrt{n_m}. \tag{E3}$$

In practice, also the converged NOs $|m_0(\boldsymbol{n})\rangle$ for a given ON configuration $\boldsymbol{n}$ change if the ON n_n (and thus also n_1, n_2, and $n_{n'}$) is modified. However, the approximation (E3) yields smooth convergence.

Because of (E2) $\partial_{n_n}n_1=-1$ for odd $n\neq 1$. Hence, for odd $n\neq 1$,

$$\partial_{n_n}\gamma_{2,ijkl}=[\delta_{ni}+\delta_{nj}+\delta_{nk}+\delta_{nl}]\frac{\gamma_{2,ijkl}}{2n_n}-[\delta_{1i}+\delta_{1j}+\delta_{1k}+\delta_{1l}]\frac{\gamma_{2,ijkl}}{2n_1}.$$

Assuming real NOs for the ground state, one finds for odd $m\neq 1$

$$F_m=\langle m|\hat{h}_0|m\rangle+\langle m'|\hat{h}_0|m'\rangle+2\sum_{ij}\frac{\gamma_{2,ijmm'}}{n_m}\langle mm'|v_{\rm ee}|ij\rangle-\langle 1|\hat{h}_0|1\rangle-\langle 2|\hat{h}_0|2\rangle-2\sum_{ij}\frac{\gamma_{2,ij12}}{n_1}\langle 12|v_{\rm ee}|ij\rangle.$$

The phases φ_i in $\gamma_{2,ijkl}$ can be set to the frozen phases $\varphi_{i,0}$ of the PINO phase convention (31) because the time-independent ground state is sought. For odd $n\notin\{1,m\}$, it follows that

$$\begin{aligned}\partial_{n_n}F_m=&\frac{1}{2(n_nn_m)^{3/2}}\langle\tilde{m}\tilde{m}'|v_{\rm ee}[|\tilde{n}\tilde{n}'\rangle-|\tilde{n}'\tilde{n}\rangle]\\&-\frac{e^{i\varphi_{m,0}}}{2(n_1n_m)^{3/2}}\langle\tilde{m}\tilde{m}'|v_{\rm ee}[|\tilde{1}\tilde{2}\rangle-|\tilde{2}\tilde{1}\rangle]\\&-\frac{e^{i\varphi_{n,0}}}{2(n_nn_1)^{3/2}}\langle\tilde{1}\tilde{2}|v_{\rm ee}[|\tilde{n}\tilde{n}'\rangle-|\tilde{n}'\tilde{n}\rangle]\\&-\sum_{\text{odd } i\neq 1}\frac{e^{i\varphi_{i,0}}}{2\sqrt{n_1^5n_i}}\langle\tilde{1}\tilde{2}|v_{\rm ee}[|\tilde{i}\tilde{i}'\rangle-|\tilde{i}'\tilde{i}\rangle];\end{aligned}$$

for the diagonal element,

$$\begin{aligned}\partial_{n_m}F_m=&-\sum_{\text{odd } i\neq m}\frac{e^{i[\varphi_{m,0}+\varphi_{i,0}]}}{2\sqrt{n_m^5n_i}}\langle\tilde{m}\tilde{m}'|v_{\rm ee}[|\tilde{i}\tilde{i}'\rangle-|\tilde{i}'\tilde{i}\rangle]\\&-\sum_{\text{odd } i\neq 1}\frac{e^{i\varphi_{i,0}}}{2\sqrt{n_1^5n_i}}\langle\tilde{1}\tilde{2}|v_{\rm ee}[|\tilde{i}\tilde{i}'\rangle-|\tilde{i}'\tilde{i}\rangle]\\&-\frac{e^{i\varphi_{m,0}}}{(n_1n_m)^{3/2}}\langle\tilde{m}\tilde{m}'|v_{\rm ee}[|\tilde{1}\tilde{2}\rangle-|\tilde{2}\tilde{1}\rangle].\end{aligned}$$

[1] A. Scrinzi, in *Attosecond and XUV Physics*, edited by Th. Schultz and M. Vrakking (Wiley-VCH, Weinheim, 2014), pp. 257–292.
[2] C. A. Coulson, Rev. Mod. Phys. **32**, 170 (1960).
[3] E. Runge and E. K. U. Gross, Phys. Rev. Lett. **52**, 997 (1984).
[4] C. A. Ullrich, *Time-Dependent Density Functional Theory, Concepts and Applications* (Oxford University Press, Oxford, UK, 2012).
[5] N. Helbig, J. Fuks, I. Tokatly, H. Appel, E. Gross, and A. Rubio, Chem. Phys. **391**, 1 (2011).
[6] M. Petersilka and E. K. U. Gross, Laser Phys. **9**, 105 (1999).
[7] F. Wilken and D. Bauer, Phys. Rev. Lett. **97**, 203001 (2006).
[8] F. Wilken and D. Bauer, Phys. Rev. A **76**, 023409 (2007).
[9] A. J. Coleman and V. I. Yukalov, *Reduced Density Matrices, Coulson's Challenge*, Lecture Notes in Chemistry Vol. 72 (Springer, Berlin Heidelberg, 2000).

[10] Edited by J. Cioslowski, *Many-electron Densities and Reduced Density Matrices*, Mathematical and Computational Chemistry Series (Kluwer/Plenum, New York, 2000).

[11] Edited by N. I. Gidopoulos and S. Wilson, *Electron Density, Density Matrix and Density Functional Theory in Atoms, Molecules and the Solid State*, Progress in Theoretical Chemistry and Physics (Kluwer, Dordrecht, 2003).

[12] Edited by D. A. Mazziotti, *Reduced-Density-Matrix Mechanics*, Advances in Chemical Physics Vol. 134 (Wiley, Hoboken, 2007).

[13] D. A. Mazziotti, Chem. Rev. **112**, 244 (2012).

[14] K. Pernal, O. Gritsenko, and E. J. Baerends, Phys. Rev. A **75**, 012506 (2007).

[15] H. Appel, Ph.D. thesis, Free University Berlin, 2007; http://www.diss.fu-berlin.de/diss/receive/FUDISS_thesis_000000003068.

[16] K. J. H. Giesbertz, E. J. Baerends, and O. V. Gritsenko, Phys. Rev. Lett. **101**, 033004 (2008).

[17] K. J. H. Giesbertz, Ph.D. thesis, Free University Amsterdam, 2010; http://dare.ubvu.vu.nl/handle/1871/16289.

[18] R. Requist and O. Pankratov, Phys. Rev. A **81**, 042519 (2010).

[19] H. Appel and E. K. U. Gross, Europhys. Lett. **92**, 23001 (2010).

[20] P.-O. Löwdin, Phys. Rev. **97**, 1474 (1955).

[21] P.-O. Löwdin and H. Shull, Phys. Rev. **101**, 1730 (1956).

[22] K. J. H. Giesbertz, Chem. Phys. Lett. **591**, 220 (2014).

[23] R. Grobe and J. H. Eberly, Phys. Rev. Lett. **68**, 2905 (1992); S. L. Haan, R. Grobe, and J. H. Eberly, Phys. Rev. A **50**, 378 (1994).

[24] D. Bauer, Phys. Rev. A **56**, 3028 (1997); D. G. Lappas and R. van Leeuwen, J. Phys. B: At. Mol. Opt. Phys. **31**, L249 (1998); D. Bauer and F. Ceccherini, Phys. Rev. A **60**, 2301 (1999); M. Lein, E. K. U. Gross, and V. Engel, Phys. Rev. Lett. **85**, 4707 (2000); M. Thiele, E. K. U. Gross, and S. Kümmel, *ibid.* **100**, 153004 (2008).

[25] M. Brics and D. Bauer, Phys. Rev. A **88**, 052514 (2013).

[26] A. J. Krueger and N. T. Maitra, Phys. Chem. Chem. Phys. **11**, 4655 (2009).

[27] K. J. H. Giesbertz, O. V. Gritsenko, and E. J. Baerends, J. Chem. Phys. **136**, 094104 (2012).

[28] R. van Meer, O. V. Gritsenko, K. J. H. Giesbertz, and E. J. Baerends, J. Chem. Phys. **138**, 094114 (2013).

[29] D. Hochstuhl, S. Bauch, and M. Bonitz, J. Phys.: Conf. Ser. **220**, 012019 (2010).

[30] M. Ruggenthaler and D. Bauer, Phys. Rev. Lett. **102**, 233001 (2009).

[31] R. Horn and C. Johnson, *Matrix Analysis*, 2nd ed. (Cambridge University Press, New York, 2012).

[32] J. Nocedal and S. Wright, *Numerical Optimization*, 2nd ed., Springer Series in Operations Research and Financial Engineering (Springer, New York, 2006).

2.3. Paper 3

Nonsequential double ionization with time-dependent renormalized-natural-orbital theory

Physical Review A 90, 053418:1–7 (2014)

DOI:http://dx.doi.org/10.1103/PhysRevA.90.053418

Author contributions

Martins Brics	Preparation of manuscript, programming, improvements to numerical scheme, calculations, figure preparations.
Julius Rapp	Contributed ideas in discussions, improvements to numerical scheme, proof reading.
Dieter Bauer	Finalization of manuscript, supervision.

PHYSICAL REVIEW A **90**, 053418 (2014)

Nonsequential double ionization with time-dependent renormalized-natural-orbital theory

M. Brics, J. Rapp, and D. Bauer
Institut für Physik, Universität Rostock, 18051 Rostock, Germany
(Received 12 September 2014; published 14 November 2014)

Recently introduced time-dependent renormalized-natural-orbital theory (TDRNOT) is tested on nonsequential double ionization (NSDI) of a numerically exactly solvable one-dimensional model He atom subject to few-cycle, 800-nm laser pulses. NSDI of atoms in strong laser fields is a prime example of nonperturbative, highly correlated electron dynamics. As such, NSDI is an important "worst-case" benchmark for any time-dependent few and many-body technique beyond linear response. It is found that TDRNOT reproduces the celebrated NSDI "knee," i.e., a many-order-of-magnitude enhancement of the double-ionization yield (as compared to purely sequential ionization) with only the ten most significant natural orbitals (NOs) per spin. Correlated photoelectron spectra—as "more differential" observables—require more NOs.

DOI: 10.1103/PhysRevA.90.053418 PACS number(s): 32.80.Rm, 31.15.ee, 31.70.Hq

I. INTRODUCTION

Nonsequential double ionization (NSDI) in intense laser pulses has been experimentally observed in measurements of ion yields as a function of the laser intensity, which deviate from the yields expected from a sequential ionization scenario, forming the so-called NSDI "knee" (see [1,2] for recent reviews). In fact, the multiple ionization yields are typically enhanced by several orders of magnitude. With ionization yields being rather integrated observables, the mechanism behind NSDI could not be unequivocally resolved until the measurement of ion spectra [3,4] and correlated photoelectron distributions has become feasible (see [5,6] for early and, e.g., [7] for very recent work). Meanwhile, NSDI is understood in terms of a recollision process: one electron is emitted but oscillates back to its parent ion to knock out the next electron. If the return energy is not sufficient for collisional ionization, the next electron might be excited and later emitted owing to the laser field [8].

The described recollision scenario poses a huge challenge for general many-body methods when applied to such a few-electron test case. For example, in time-dependent Hartree-Fock (TDHF) or time-dependent density functional theory (TDDFT) applied to He starting from the singlet ground state, there is only one spatial orbital describing both electrons (one spin-up, the other spin-down). Not surprisingly, it was found that such methods are not capable of describing NSDI [9], although formally for different reasons. TDHF, as a mean-field approach, does not incorporate correlation by definition. TDDFT is in principle exact, but only in the sense that it gives the exact time-dependent electron density. However, even if the exact time-dependent electron density was known from a TDDFT calculation employing the exact exchange-correlation potential [10], the exact double-ionization probability could still not be calculated because this observable is unknown as an explicit functional of the electron density, and simple approximations to it do not reproduce the NSDI knee [11,12].

Solving the full time-dependent Schrödinger equation (TDSE) for He in full dimensionality and in strong, long-wavelength (i.e., $\geqslant$800 nm) laser fields is still beyond what is possible with current supercomputer technology [13]. Therefore it is essential to develop practicable time-dependent many-electron methods beyond linear response that account for correlation. Time-dependent configuration interaction (TDCI) [14,15], multiconfigurational time-dependent Hartree (MCTDH) [16] or multiconfigurational TDHF (MCTDHF) [17–20] are exact in principle. However, the crucial question in practice is how many configurations or determinants are required to recover a certain strong correlation feature such as the NSDI knee. General conclusions are difficult to draw, as different TDCI and MCTDHF approaches may vary in the single-particle basis functions chosen. It has been shown that for He (or H_2) a time-dependent variational approach using a wave-function ansatz with two different single-particle orbitals (time-dependent extended Hartree-Fock) [9,21] or an *ad hoc* ansatz with an "inner" and an "outer" outer orbital [22] at least generate kneelike structures in the double-ionization yield. However, they are only in poor agreement with the exact numerical results available for low-dimensional models. To the best of our knowledge there are no systematic tests of computational approaches that demonstrate a convergence toward the exact NSDI knee. In fact, we are not aware of any work that accurately reproduces the NSDI knee using a many-body method that overcomes the "exponential wall" [23]. In this work, we will provide such an analysis for our recently introduced time-dependent renormalized-natural-orbital theory (TDRNOT) [24,25].

II. THEORY

Before we present results on the NSDI knee (Sec. III A) and on correlated photoelectron spectra (Sec. III B), we briefly introduce the He model, review the essentials of TDRNOT, particularly when applied to a two-electron system, and discuss the observables to be calculated. Atomic units (a.u.) are used unless otherwise indicated.

A. Model atom

The widely applied one-dimensional helium model atom [9,10,12,20,26–29] in a laser field has the Hamiltonian

$$\hat{H}^{(1,2)}(t) = \hat{h}^{(1)}(t) + \hat{h}^{(2)}(t) + v_{\mathrm{ee}}{}^{(1,2)}, \tag{1}$$

where upper indices indicate the action on either electron 1, electron 2, or both. The single-particle Hamiltonian reads

$\hat{h}(t) = \hat{H}_A + \hat{H}_L(t)$, with

$$\hat{H}_A = \frac{\hat{p}^2}{2} - \frac{2}{\sqrt{x^2 + \varepsilon_{\rm ne}}}, \tag{2}$$

$\hat{H}_L(t) = A(t)\hat{p}$ (dipole approximation and velocity gauge with the A^2 term transformed away), and the electron-electron interaction

$$v_{\rm ee}{}^{(1,2)} = \frac{1}{\sqrt{(x^{(1)} - x^{(2)})^2 + \varepsilon_{\rm ee}}}. \tag{3}$$

The electron-ion smoothing parameter $\varepsilon_{\rm ne} = 0.50$ is chosen such that the ground-state energy of He^+ $E_0^{\rm He^+} = -2.0$ is recovered. The electron-electron smoothing parameter $\varepsilon_{\rm ee} = 0.33$ is tuned to yield the neutral-He energy $E_0^{\rm He} = -2.9$.

B. Density matrices, renormalized natural orbitals, and their equations of motion

The Hamiltonian (1) does not act on the spin, which—in the two-particle case—allows one to factorize the wave function,

$$\langle 12|\Phi(t)\rangle = \Phi(12;t) = \Phi(x_1x_2;t)\Phi_{\sigma_1\sigma_2}. \tag{4}$$

Here 1 and 2 are shorthand notations for position and spin (x_1,σ_1) and (x_2,σ_2), respectively. The two- and one-body density matrices read

$$\gamma_2(12,1'2';t) = \Phi(12;t)\Phi^*(1'2';t), \tag{5}$$

$$\gamma_1(1,1';t) = 2\int d2\,\gamma_2(12,1'2;t). \tag{6}$$

Natural orbitals (NOs) $\phi_k(1;t) = \langle 1|k(t)\rangle$ are defined as eigenvectors of γ_1:

$$\gamma_1(1,1';t) = \sum_k n_k(t)\phi_k(1;t)\phi_k^*(1';t). \tag{7}$$

The corresponding eigenvalues $n_k(t) \in [0,1]$ are called occupation numbers (ONs). NOs and ONs were introduced a long time ago (see, e.g., [30–32]), but only recently has their usefulness for time-dependent few- and many-body problems been studied [33–38].

The coupled equations of motion for the ONs and the NOs can be unified by introducing renormalized NOs (RNOs) [24]

$$\langle 1|\tilde{k}(t)\rangle = \tilde{\phi}_k(1;t) = \sqrt{n_k(t)}\phi_k(1;t) \tag{8}$$

so that

$$n_k(t) = \langle\tilde{k}(t)|\tilde{k}(t)\rangle \tag{9}$$

and

$$\gamma_1(1,1';t) = \sum_k \tilde{\phi}_k(1;t)\tilde{\phi}_k^*(1';t). \tag{10}$$

The two-body density matrix expanded in RNOs reads

$$\gamma_2(12,1'2';t) = \sum_{ijkl} \tilde{\gamma}_{2,ijkl}(t)\tilde{\phi}_i(1;t)\tilde{\phi}_j(2;t)\tilde{\phi}_k^*(1';t)\tilde{\phi}_l^*(2';t). \tag{11}$$

The equation of motion (EOM) for the RNOs is [25]

$$i\partial_t|\tilde{n}\rangle = \hat{h}(t)|\tilde{n}\rangle + \boldsymbol{\mathcal{A}}_n(t)|\tilde{n}\rangle + \sum_{k\neq n}\boldsymbol{\mathcal{B}}_{nk}(t)|\tilde{k}\rangle + \sum_k \hat{\boldsymbol{\mathcal{C}}}_{nk}(t)|\tilde{k}\rangle \tag{12}$$

with

$$\boldsymbol{\mathcal{A}}_n(t) = -\frac{1}{n_n(t)}\,{\rm Re}\sum_{jkl}\tilde{\gamma}_{2,njkl}(t)\langle\tilde{k}\tilde{l}|v_{\rm ee}|\tilde{n}\tilde{j}\rangle, \tag{13}$$

$$\boldsymbol{\mathcal{B}}_{nk}(t) = \frac{2}{n_k(t) - n_n(t)}\sum_{jpl}[\tilde{\gamma}_{2,kjpl}(t)\langle\tilde{p}\tilde{l}|v_{\rm ee}|\tilde{n}\tilde{j}\rangle - \tilde{\gamma}_{2,plnj}(t)\langle\tilde{k}\tilde{j}|v_{\rm ee}|\tilde{p}\tilde{l}\rangle], \tag{14}$$

and

$$\hat{\boldsymbol{\mathcal{C}}}_{nk}(t) = 2\sum_{jl}\tilde{\gamma}_{2,kjnl}(t)\langle\tilde{l}|v_{\rm ee}|\tilde{j}\rangle. \tag{15}$$

One observes that the effective Hamiltonian in the TDSE-like equation (12) consists of the usual one-body operator $\hat{h}(t)$, a diagonal part $\boldsymbol{\mathcal{A}}_n(t) \in \mathbb{R}$, the part $\boldsymbol{\mathcal{B}}_{nk}(t) \in \mathbb{C}$ which couples RNOs, and the operator $\hat{\boldsymbol{\mathcal{C}}}_{nk}(t)$, which also couples RNOs. As the effective Hamiltonian in (12) is Hermitian, the corresponding time evolution of the RNOs is unitary.

In general, there are infinitely many NOs required to describe a correlated quantum system, even if it contains only two particles. Ordered decreasingly according to their ONs, the number of RNOs taken into account in an actual numerical implementation of (12) is necessarily truncated, which introduces errors in the propagation. The effect of this truncation will be seen in the results in Sec. III below.

In the two-particle case the expansion coefficients $\tilde{\gamma}_{2,ijkl}(t)$ are exactly known [25],

$$\tilde{\gamma}_{2,ijkl}(t) = (-1)^{i+k}\frac{e^{i[\varphi_i - \varphi_k]}}{2\sqrt{n_i(t)n_k(t)}}\delta_{i,j'}\delta_{k,l'}. \tag{16}$$

Here, the "prime operator" acts on the positive integer k according to

$$k' = \begin{cases} k+1 & \text{if } k \text{ odd} \\ k-1 & \text{if } k \text{ even,} \end{cases} \tag{17}$$

and the phase factors are [25]

$$e^{i\varphi_i^{(\rm S)}} = 2\delta_{k,1} + 2\delta_{k,2} - 1, \quad e^{i\varphi_i^{(\rm T)}} = 1 \tag{18}$$

in the spin-singlet and -triplet case, respectively. Note that the EOM for the RNOs (12) is given here for phase-including NOs [35] so that φ_i and φ_k in (16) do not depend on time. Employing the factorization (4) we can write

$$\gamma_2(12,1'2';t) = \Phi(x_1x_2;t)\Phi^*(x_1'x_2';t)\Phi_{\sigma_1\sigma_2}\Phi^*_{\sigma_1'\sigma_2'}, \tag{19}$$

$$\gamma_1(1,1';t) = \gamma_1(x_1,x_1';t)\sum_{\sigma_2}\Phi_{\sigma_1\sigma_2}\Phi^*_{\sigma_1'\sigma_2}, \tag{20}$$

where

$$\gamma_1(x_1,x_1';t) = 2\int dx_2\,\gamma_2(x_1x_2,x_1'x_2;t) = \sum_k \underline{n}_k(t)\underline{\phi}_k(x_1;t)\underline{\phi}_k^*(x_1';t) = \sum_k \tilde{\underline{\phi}}_k(x_1;t)\tilde{\underline{\phi}}_k^*(x_1';t), \tag{21}$$

$$\gamma_2(x_1x_2,x_1'x_2';t) = \Phi(x_1x_2;t)\Phi^*(x_1'x_2';t) = \sum_{ijkl}\tilde{\gamma}_{2,ijkl}(t)\tilde{\underline{\phi}}_i(x_1;t)\tilde{\underline{\phi}}_j(x_2;t) \times \tilde{\underline{\phi}}_k^*(x_1';t)\tilde{\underline{\phi}}_l^*(x_2';t). \tag{22}$$

Here and in the following, spatial RNOs and quantities calculated from them (e.g., $\underline{n}_i(t) = \langle\tilde{\underline{\phi}}_i(t)|\tilde{\underline{\phi}}_i(t)\rangle$) will be indicated by underlining them. How the RNOs can be written as a factorization in the spatial and the spin part is discussed in detail in [25]. In this work we will only consider results for the singlet configuration where the RNOs with $k = 1,2,3,\ldots$ can be arranged as

$$\langle x|\tilde{k}(t)\rangle = \begin{cases} |\uparrow\rangle\,\tilde{\underline{\phi}}_{k'/2}(x;t) & \text{if } k \text{ odd} \\ |\downarrow\rangle\,\tilde{\underline{\phi}}_{k/2}(x;t) & \text{if } k \text{ even} \end{cases} \tag{23}$$

so that any consecutive k-odd and $k+1$-even RNOs share the same spatial component $\tilde{\underline{\phi}}_{k'/2}(x;t)$.

C. Observables

We are interested in the double-ionization probability of the model He atom as a function of the laser intensity and in correlated photoelectron spectra, i.e., the probability to find one electron being emitted with momentum p_1 and the other with p_2, for laser intensities where NSDI occurs. Both should in principle be calculated via the projection of the wave function after the laser pulse on two-electron continuum states of asymptotic momenta p_1 and p_2. However, this approach is numerically unfeasible. We will shortly explain how the yields and spectra are calculated in a less rigorous but sufficiently accurate manner in this work.

1. Ionization probabilities

An efficient way to calculate ionization probabilities from the two-electron wave function $\Phi(x_1x_2)$ after the laser pulse is based on the integration of the probability density $|\Phi(x_1x_2)|^2$ over certain spatial regions,

$$P^0 = \iint_{|x_1|,|x_2|<a} dx_1dx_2\;\;|\Phi(x_1x_2)|^2\,, \tag{24}$$

$$P^{2+} = \iint_{|x_1|,|x_2|\geqslant a} dx_1dx_2\;\;|\Phi(x_1x_2)|^2\,, \tag{25}$$

$$P^{1+} = 1 - P^0 - P^{2+}, \tag{26}$$

where we made use of the fact that $P^0 + P^{1+} + P^{2+} = 1$. The parameter $a > 0$ should be sufficiently large such that the probabilities P^{1+} and P^{2+} are negligible for the ground-state and singly excited eigenstates. On the other hand, a should not be too large so that the probability density describing ionization does not need too much time to leave the neutral-He region $|x_1|\,,\,|x_2| < a$. For our model we chose $a = 6$.

As for a two-electron system $|\Phi(x_1x_2)|^2 = \gamma_2(x_1x_2,x_1x_2)$, Eqs. (24) and (25) are read in terms of RNOs:

$$P^0 = \sum_{ijkl}\tilde{\gamma}_{2,ijkl}\int_{-a}^{a} dx_1\,\tilde{\underline{\phi}}_i(x_1)\tilde{\underline{\phi}}_k^*(x_1) \times \int_{-a}^{a} dx_2\,\tilde{\underline{\phi}}_j(x_2)\tilde{\underline{\phi}}_l^*(x_2), \tag{27}$$

$$P^{2+} = \sum_{ijkl}\tilde{\gamma}_{2,ijkl}\int_{|x_1|\geqslant a} dx_1\,\tilde{\underline{\phi}}_i(x_1)\tilde{\underline{\phi}}_k^*(x_1) \times \int_{|x_2|\geqslant a} dx_2\,\tilde{\underline{\phi}}_j(x_2)\tilde{\underline{\phi}}_l^*(x_2). \tag{28}$$

Note that in the two-electron case this form is equivalent to first reconstructing the wave function (which is possible for two electrons [25]) and then using Eqs. (24) and (25).

2. Momentum distributions

A numerically efficient method to calculate correlated double-ionization photoelectron spectra is to multiply the two-electron wave function by a mask function $f(x_1x_2)$, which removes the parts representing He^+ and neutral He:

$$\Phi^{2+}(x_1x_2) \simeq f(x_1x_2)\Phi(x_1x_2).$$

Here, we chose $f(x_1x_2) = f(x_1)f(x_2)$, with $f(x) = 1/\sqrt{1+e^{-c(|x|-a)}}$ and $c = 1.25$ [29]. After Fourier transforming $\Phi^{2+}(x_1x_2)$ to momentum space,

$$\Phi^{2+}(p_1p_2) = \frac{1}{2\pi}\int dx_1\int dx_2\;\Phi^{2+}(x_1x_2)\,e^{-i(p_1x_1+p_2x_2)}, \tag{29}$$

the double-ionization photoelectron spectrum is obtained as

$$\rho^{2+}(p_1p_2) = 2|\Phi^{2+}(p_1p_2)|^2.$$

In our TDRNOT treatment we proceed analogously by first defining

$$\gamma_2^{2+}(x_1x_2,x_1'x_2') = f(x_1x_2)f^*(x_1'x_2')\gamma_2(x_1x_2,x_1'x_2'), \tag{30}$$

whose Fourier transform is $\gamma_2^{2+}(p_1p_2,p_1'p_2')$. Then,

$$\rho^{2+}(p_1p_2) = 2\gamma_2^{2+}(p_1p_2,p_1p_2),$$

which can be written as

$$\rho^{2+}(p_1p_2) \simeq 2\sum_{ijkl}\tilde{\gamma}_{2,ijkl}\tilde{\underline{\phi}}_i^+(p_1)\tilde{\underline{\phi}}_j^+(p_2)\{\tilde{\underline{\phi}}_k^+(p_1)\tilde{\underline{\phi}}_l^+(p_2)\}^*, \tag{31}$$

where

$$\underline{\phi}_i^+(p_j) = \frac{1}{\sqrt{2\pi}}\int dx_j\;f(x)\underline{\phi}_i(x_j)\,e^{-ix_jp_j}. \tag{32}$$

We thus have an explicit construction for $\rho^{2+}(p_1p_2)$ in terms of RNOs. Note that in TDDFT such a construction in terms of Kohn-Sham orbitals is unknown [29].

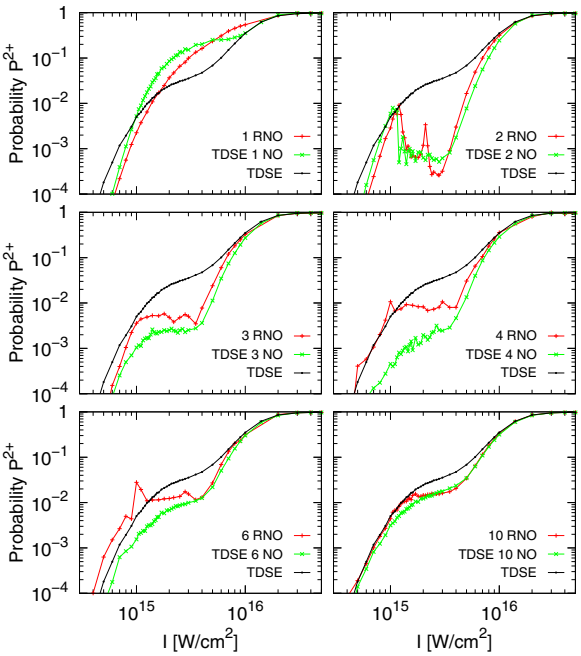

FIG. 1. (Color online) Double-ionization probability vs laser intensity. TDRNOT results with $N = 1,2,3,4,6,10$ spatial RNOs (red, +) are compared with the exact TDSE result (black, dots) and with the ionization probability reconstructed using the first N exact NOs calculated from the exact TDSE wave function (green, ×).

III. RESULTS AND DISCUSSION

We consider an 800-nm ($\omega = 0.058$) linearly polarized $N_{\rm cyc} = 3$-cycle $\sin^2$-shaped laser pulse of duration $T = 2\pi N_{\rm cyc}/\omega$. The vector potential in dipole approximation reads

$$A(t) = \hat{A} \sin^2\left(\frac{\omega t}{2N_{\rm cyc}}\right) \sin(\omega t) \quad \text{for } 0 \leqslant t \leqslant T \qquad (33)$$

and zero otherwise. The numerical grids for both the TDSE-benchmark and TDRNOT calculations covered ±1500 a.u. in the spatial directions.

A. Ionization yields

Figure 1 shows the double-ionization probability P^{2+} as a function of the laser intensity for different numbers of spatial RNOs N between 1 (upper-left panel) and 10 (lower-right panel). For comparison, the exact TDSE result is included in black in all panels. The nonmonotonic behavior of the first derivative of this exact P^{2+} curve in the region around 2×10^{15} W/cm^2 gives rise to the celebrated NSDI knee.

A TDRNOT calculation with $N = 1$ RNO per spin yields a featureless P^{2+} curve, as seen in the upper-left panel of Fig. 1. In fact, in the case of a two-electron spin-singlet system, a single NO per spin is equivalent to TDHF or TDDFT in exchange-only approximation, for which it is already known that the NSDI knee is not reproduced [9–12].

Truncating the number of RNOs in a TDRNOT calculation introduces an error in the propagation of the RNOs [25]. This error should be distinguished from the error that arises alone, due to the fact that only a finite number of NOs is taken into account for the calculation of an observable. We do this by determining all exact NOs from the exact TDSE wave function but consider only the N most dominant of them to calculate the observable P^{2+}. The respective results are also shown in Fig. 1. For $N = 1$ this procedure gives a result very different from the TDRNOT with $N = 1$. There is even already a knee in the TDSE-1-NO result, albeit a quantitatively wrong one. Both TDRNOT with a single RNO and the TDSE-1-NO curve show a wrong slope in the limit of low laser intensity.

For $N = 2$ NOs per spin (upper-right panel) a knee appears also in the TDRNOT result. It is exaggerated and jaggedly structured, and underestimates the P^{2+} yield. A similar behavior with two orbitals was observed in extended Hartree-Fock treatments [9,21] and with the so-called "crapola" model [22], where an "inner" and an "outer" orbital is postulated.

With increasing N the agreement between TDRNOT results and TDSE improves. For $N = 10$ the truncation error in the propagation of the RNOs is small enough to give almost the same probability P^{2+} as if it was calculated with the first $N = 10$ exact NOs.

Clearly, our TDRNOT approach is only attractive if N can be kept reasonably small. We have shown in Refs. [24,25] how, with a few RNOs, doubly excited states, autoionization, and Rabi flopping can be described using TDRNOT. Unfortunately, NSDI is more demanding in N, meaning that NSDI is highly correlated, and thus many more NOs than particles are required. Moreover, note that although NSDI is a huge effect on the P^{2+} level, it is a small effect compared to the probability for single-ionization P^{1+}, and small effects on an absolute scale are captured by NOs with small ONs. The dominant NOs are mainly "responsible" for single ionization, or no ionization at all. In that respect it is remarkable to achieve an agreement such as the one shown for $N = 10$ spatial RNOs in Fig. 1. We are not aware of any TDCI or TDMCHF calculation that achieved such an agreement, let alone with only ten basis functions.

B. Two-electron momentum distribution

Correlated photoelectron spectra contain more information than ionization probabilities. In general, the "more differential" an observable is, the harder it is to reproduce by some approximate method because the dynamic range to be accurately covered increases. An additional, conceptual challenge arises with TDDFT because $\rho^{2+}(p_1 p_2)$ is an unknown functional of the single-particle density, and simple approximations fail [29].

Figure 2 shows the TDSE benchmark result for $\rho^{2+}(p_1 p_2)$ at $I = 2.25 \times 10^{15}$ W/cm^2, i.e., in the NSDI intensity regime. The butterfly structure indicating electrons emitted into the same direction is characteristic of NSDI [1,2] and has been essential to identify rescattering as its origin.

From the TDSE benchmark we know that the first thousand exact NOs have ONs $> 10^{-15}$. The question is how many NOs are needed to recover the butterfly structure seen in Fig. 2. Figure 3 shows that with the first 15 exact NOs from the TDSE simulation the butterfly structure of Fig. 2 emerges, but details are still not accurately represented over the 4 orders of magnitude dynamic range shown. However, it is sufficient for

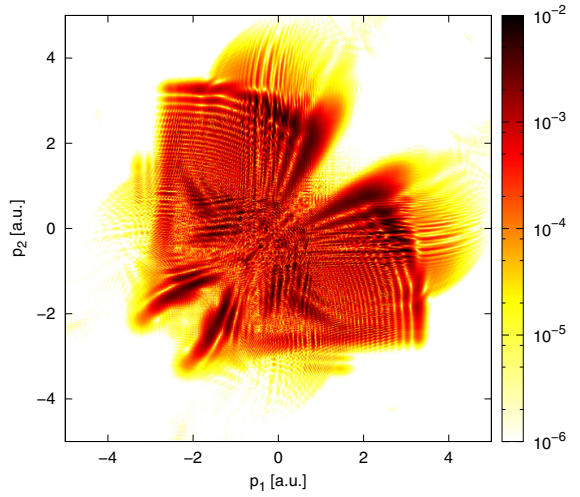

FIG. 2. (Color online) TDSE-benchmark two-electron photoelectron spectrum $\rho^{2+}(p_1 p_2)$ at $I = 2.25 \times 10^{15}$ W/cm^2.

the purpose of validating TDRNOT with a reasonably small number of RNOs. Up to $N = 5$, mainly uncorrelated, gridlike horizontal and vertical structures are visible. From $N = 6$ on, however, clear correlated structures appear, first in the first quadrant $p_1, p_2 > 0$.

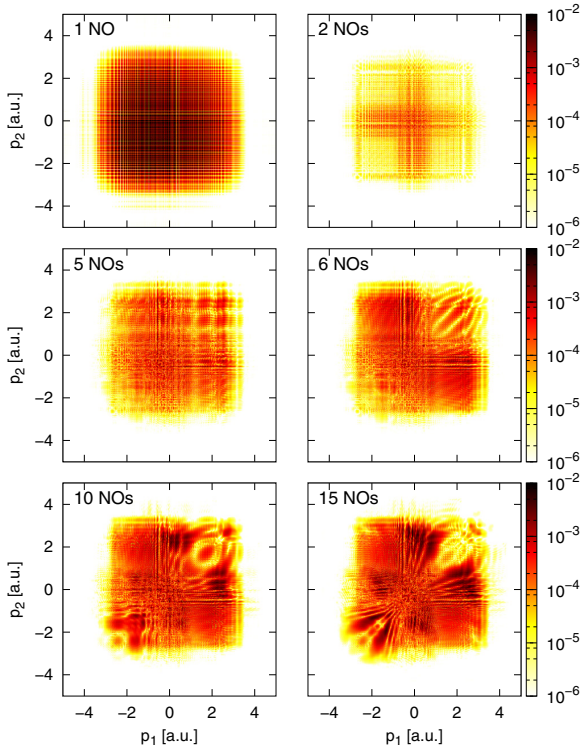

FIG. 3. (Color online) $\rho^{2+}(p_1 p_2)$ at $I = 2.25 \times 10^{15}$ W/cm^2 obtained from the $N = 1,2,5,6,10,15$ dominant, exact spatial NOs calculated from the exact TDSE wave function after the laser pulse.

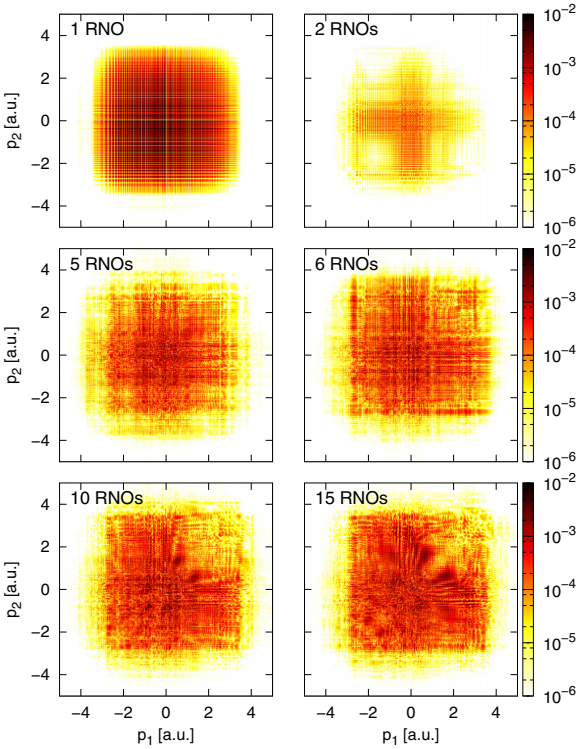

FIG. 4. (Color online) $\rho^{2+}(p_1 p_2)$ at $I = 2.25 \times 10^{15}$ W/cm^2 obtained from TDRNOT with $N = 1,2,5,6,10,15$ spatial RNOs.

Figure 4 shows the corresponding TDRNOT result with N RNOs per spin propagated. Again, the differences between the benchmark results in Fig. 3 and TDRNOT in Fig. 4 are due to the truncation error in the number of propagated RNOs. This truncation error severely spoils the correlation structure in the first quadrant; only for $N = 15$ does the structure start to emerge. In order to reproduce, say, the lower-right spectrum in Fig. 3, one would need to propagate about 50 RNOs in TDRNOT. This is prohibitive with our current implementation of solving the nonlinear EOM (12). We found, for instance, that apart from the expected increase of the numerical effort there is the additional complication that the time step needs to be reduced with increasing N.

Because of the truncation error, the Nth of the (according ON ordered) N dominant spatial RNOs is expected to be most defective. Thus it may make sense to propagate more RNOs than are actually used to calculate observables. Figure 5 shows results where $N = 15$ RNOs per spin were propagated but only $N = 5$ and 6 were used for the calculation of the photoelectron spectra. One sees that the agreement with the two corresponding middle-row spectra in Fig. 3 is much better than in Fig. 4.

C. Numerical effort

The computational time $\tau(N, N_x)$ required for a TDRNOT propagation using N NOs on N_x spatial grid points

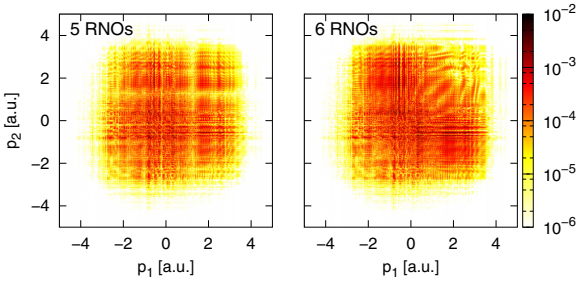

FIG. 5. (Color online) $\rho^{2+}(p_1 p_2)$ at $I = 2.25 \times 10^{15}$ W/cm^2 obtained from TDRNOT with $N = 15$ spatial RNOs propagated but only $N = 5$ and 6 used to calculate $\rho^{2+}(p_1 p_2)$.

scales as

$$\tau(N, N_x) \sim \alpha\, N^2\, N_x\, \log N_x + \beta\, N^3\, N_x \qquad (34)$$

for a fixed time step. The first term on the right-hand side arises from the calculation of the potentials in (15) using the fast Fourier transform, and the second term from the evaluation of the required matrix elements in (14) [39]. The computational costs of the corresponding operations are taken into account by the constant factors α and β.

The computational times $\tau(N) = \tau(N, 6000)$ required for one laser intensity using 1 (equivalent to TDHF), 2, and 6 NOs were $\tau(1) \approx 1.3$ min, $\tau(2) \approx 5.6$ min, and $\tau(6) \approx 40$ min, respectively, on a single core of an i5-3570 processor. This shows that the N^2 term in (34) is dominating. Compared to the TDSE calculation, where $\tau_{\mathrm{TDSE}} = 12$ h, TDRNOT thus performs faster by a factor of 550, 128, and 18, respectively.

Unfortunately, the time step in our present TDRNOT implementation needs to be decreased with increasing N to achieve converged results. For example, for $N = 10$ NOs, $\Delta t(10) = 0.001\,6$ was used, whereas in the TDSE simulation $\Delta t = 0.075$ was sufficient. This leads to a total computation time of $\tau(10) = 30$ h $> \tau_{\mathrm{TDSE}}$ and $\tau(15) = 22$ d. Hence, improving our TDRNOT scheme to allow for larger time steps is desirable. However, note that for more than two particles the small TDRNOT time step is harmless anyway compared to the exponential scaling of the TDSE wave function.

IV. CONCLUSION AND OUTLOOK

In summary, we reproduced the nonsequential double-ionization knee for a He-model atom starting from the spin-singlet ground state using the recently introduced time-dependent renormalized-natural-orbital theory. The equations of motion for the renormalized natural orbitals are exact in the two-electron case. This is because the expansion of the time-dependent two-body density matrix in natural orbitals is known exactly. Only the practical limitation in the number of spatial orbitals N forces us to restrict ourselves to $N < 20$. Correlated structures in the photoelectron spectra are also reproduced. However, a quantitative agreement with the benchmark spectra obtained from the solution of the corresponding two-electron time-dependent Schrödinger equation can only be achieved with more orbitals.

Current work is devoted to the application of time-dependent renormalized-natural-orbital theory to He in full dimensionality, to more electrons, and to the mitigation of the truncation error via better-suited boundary conditions.

ACKNOWLEDGMENT

This work was supported by the SFB 652 of the German Science Foundation (DFG).

[1] W. Becker, X. Liu, P. J. Ho, and J. H. Eberly, Rev. Mod. Phys. **84**, 1011 (2012).
[2] C. F. de Morisson Faria and X. Liu, J. Mod. Opt. **58**, 1076 (2011).
[3] T. Weber, M. Weckenbrock, A. Staudte, L. Spielberger, O. Jagutzki, V. Mergel, F. Afaneh, G. Urbasch, M. Vollmer, H. Giessen, and R. Dörner, Phys. Rev. Lett. **84**, 443 (2000).
[4] R. Moshammer, B. Feuerstein, W. Schmitt, A. Dorn, C. D. Schröter, J. Ullrich, H. Rottke, C. Trump, M. Wittmann, G. Korn, K. Hoffmann, and W. Sandner, Phys. Rev. Lett. **84**, 447 (2000).
[5] T. Weber, H. Giessen, M. Weckenbrock, G. Urbasch, A. Staudte, L. Spielberger, O. Jagutzki, V. Mergel, M. Vollmer, and R. Dörner, Nature (London) **405**, 658 (2000).
[6] B. Feuerstein, R. Moshammer, D. Fischer, A. Dorn, C. D. Schröter, J. Deipenwisch, J. R. Crespo Lopez-Urrutia, C. Höhr, P. Neumayer, J. Ullrich, H. Rottke, C. Trump, M. Wittmann, G. Korn, and W. Sandner, Phys. Rev. Lett. **87**, 043003 (2001).
[7] M. Kübel, K. J. Betsch, N. G. Kling, A. S. Alnaser, J. Schmidt, U. Kleineberg, Y. Deng, I. Ben-Itzhak, G. G. Paulus, T. Pfeifer, J. Ullrich, R. Moshammer, M. F. Kling, and B. Bergues, New J. Phys. **16**, 033008 (2014).
[8] A. Rudenko, K. Zrost, B. Feuerstein, V. L. B. de Jesus, C. D. Schröter, R. Moshammer, and J. Ullrich, Phys. Rev. Lett. **93**, 253001 (2004).
[9] N. E. Dahlen and R. van Leeuwen, Phys. Rev. A **64**, 023405 (2001).
[10] M. Lein and S. Kümmel, Phys. Rev. Lett. **94**, 143003 (2005).
[11] M. Petersilka and E. K. U. Gross, Laser Phys. **9**, 105 (1999).
[12] F. Wilken and D. Bauer, Phys. Rev. Lett. **97**, 203001 (2006).
[13] J. S. Parker, B. J. S. Doherty, K. T. Taylor, K. D. Schultz, C. I. Blaga, and L. F. DiMauro, Phys. Rev. Lett. **96**, 133001 (2006).
[14] N. Rohringer, A. Gordon, and R. Santra, Phys. Rev. A **74**, 043420 (2006).
[15] A. Karamatskou, S. Pabst, Y.-J. Chen, and R. Santra, Phys. Rev. A **89**, 033415 (2014).
[16] S. Sukiasyan, C. McDonald, C. Van Vlack, C. Destefani, T. Fennel, M. Ivanov, and T. Brabec, Phys. Rev. A **80**, 013412 (2009).
[17] J. Zanghellini, M. Kitzler, T. Brabec, and A. Scrinzi, J. Phys. B **37**, 763 (2004).
[18] J. Caillat, J. Zanghellini, M. Kitzler, O. Koch, W. Kreuzer, and A. Scrinzi, Phys. Rev. A **71**, 012712 (2005).

[19] O. Koch, W. Kreuzer, and A. Scrinzi, Appl. Mathematics and Computation **173**, 960 (2006).
[20] D. Hochstuhl, S. Bauch, and M. Bonitz, J. Phys.: Conf. Ser. **220**, 012019 (2010).
[21] N. A. Nguyen and A. D. Bandrauk, Phys. Rev. A **73**, 032708 (2006).
[22] J. B. Watson, A. Sanpera, D. G. Lappas, P. L. Knight, and K. Burnett, Phys. Rev. Lett. **78**, 1884 (1997).
[23] W. Kohn, Rev. Mod. Phys. **71**, 1253 (1999).
[24] M. Brics and D. Bauer, Phys. Rev. A **88**, 052514 (2013).
[25] J. Rapp, M. Brics, and D. Bauer, Phys. Rev. A **90**, 012518 (2014).
[26] D. Bauer, Phys. Rev. A **56**, 3028 (1997).
[27] D. G. Lappas and R. van Leeuwen, J. Phys. B **31**, L249 (1998).
[28] M. Lein, E. K. U. Gross, and V. Engel, Phys. Rev. Lett. **85**, 4707 (2000).
[29] F. Wilken and D. Bauer, Phys. Rev. A **76**, 023409 (2007).
[30] P.-O. Löwdin, Phys. Rev. **97**, 1474 (1955).
[31] A. J. Coleman, Rev. Mod. Phys. **35**, 668 (1963).
[32] A. Coleman and V. Yukalov, *Reduced Density Matrices, Coulson's Challenge*, Springer Lecture Notes in Chemistry Vol. 72 (Springer, Berlin, 2000).
[33] K. Pernal, O. Gritsenko, and E. J. Baerends, Phys. Rev. A **75**, 012506 (2007).
[34] H. Appel, Ph.D. thesis, Freie Universität Berlin, 2007.
[35] K. J. H. Giesbertz, Ph.D. thesis, Free University Amsterdam, 2010.
[36] H. Appel and E. K. U. Gross, Europhys. Lett. **92**, 23001 (2010).
[37] N. Helbig, J. Fuks, I. Tokatly, H. Appel, E. Gross, and A. Rubio, Chem. Phys. **391**, 1 (2011).
[38] K. J. H. Giesbertz, O. V. Gritsenko, and E. J. Baerends, J. Chem. Phys. **136**, 094104 (2012).
[39] Note that, thanks to the sparsity of $\gamma_{2,ijkl}$ in (16), not all combinations of NO indices contribute.

2.4. Paper 4

Strong-field absorption and emission of radiation in two-electron systems calculated with time-dependent natural orbitals

Physical Review A 93, 013404:1–8 (2016)

DOI:http://dx.doi.org/10.1103/PhysRevA.93.013404

Author contributions

Martins Brics	Preparation of manuscript, programming, improvements to numerical scheme, calculations, figure preparations.
Julius Rapp	Suggestion to derive again the EOM for complex potentials and check of the derivation, suggestion to apply an exponential filter for transient absorption spectra calculations, useful discussions.
Dieter Bauer	Finalization of manuscript, supervision.

PHYSICAL REVIEW A **93**, 013404 (2016)

Strong-field absorption and emission of radiation in two-electron systems calculated with time-dependent natural orbitals

M. Brics, J. Rapp, and D. Bauer
Institut für Physik, Universität Rostock, 18051 Rostock, Germany
(Received 6 October 2015; published 6 January 2016)

Recently introduced time-dependent renormalized-natural-orbital theory (TDRNOT) is based on the equations of motion for the so-called natural orbitals, i.e., the eigenfunctions of the one-body reduced density matrix. Exact TDRNOT can be formulated for any time-dependent two-electron system in either spin configuration. In this paper, the method is tested against high-order-harmonic generation (HHG) and Fano profiles in absorption spectra with the help of a numerically exactly solvable one-dimensional-model He atom, starting from the spin-singlet ground state. Such benchmarks are challenging because Fano profiles originate from transitions involving autoionizing states, and HHG is a strong-field phenomenon well beyond the linear response. TDRNOT with just one natural orbital per spin in the helium spin-singlet case is equivalent to time-dependent Hartree-Fock or time-dependent density functional theory (TDDFT) in the exact exchange-only approximation. It is not unexpected that TDDFT fails in reproducing Fano profiles due to the lack of doubly excited, autoionizing states. HHG spectra, on the other hand, are widely believed to be well captured by TDDFT. However, HHG spectra of helium may display a second plateau that originates from simultaneous HHG in He^+ and neutral He. It is found that TDRNOT with two natural orbitals per spin is already sufficient to capture this effect as well as the Fano profiles on a qualitative level. With more natural orbitals (6–8 per spin), quantitative agreement can be reached. Errors due to the truncation to a finite number of orbitals are identified.

DOI: 10.1103/PhysRevA.93.013404

I. INTRODUCTION

Time-dependent few- and many-body methods for driven quantum dynamics beyond linear response are urgently needed both to study the fundamental effects and for possible technological applications (involving strong light fields, for instance). Depending on the system studied, the "exact" solution would involve the numerical solution of the time-dependent Schrödinger, Pauli, Klein-Gordon, or Dirac equation, possibly with quantized electromagnetic field. Unfortunately, this is—in full dimensionality and with strong, long-wavelength lasers—even in the simplest case of the time-dependent Schrödinger equation (TDSE), possible only for (at most) two particles.

The most widely used and favorably scaling approach to electronic structure problems is density functional theory [1,2]. Its time-dependent version, i.e., time-dependent density functional theory (TDDFT) [3,4], often misses important correlation effects [5,6]. Other, more systematic approaches such as multiconfigurational time-dependent Hartree-Fock (MCTDHF) [7,8] and variants of it [9,10] or time-dependent configuration interaction (TDCI) [11–13] and related approaches [14,15] are (much) more demanding but capture correlation effects better [16,17]. Recently, we have introduced time-dependent renormalized-natural-orbital theory (TDRNOT) [18–20], which is based on equations of motion for the so-called natural orbitals (NOs), i.e., the eigenfunctions of the one-body reduced density matrix (1RDM) [21–25]. While the proof that the natural orbitals form the best basis is restricted to two electrons [26], the educated guess (and hope) is that TDRNOT calculations with a very limited number of NOs can well surpass TDDFT with relatively little computational overhead. In recent papers, we have already demonstrated that TDRNOT performs well in treating phenomena where TDDFT with known exchange-correlation potentials fails, e.g., autoionization [18], Rabi flopping [19], and nonsequential ionization [20]. In this work, we will continue along the same line by focusing on the emission and absorption of radiation. In fact, high-harmonic generation (HHG) and absorption spectroscopy (AS) are of eminent importance in strong-field laser physics. HHG is the basis of "attosecond science" [27,28], while transient AS provides an all-optical means to follow correlated processes in matter [29,30].

The paper is organized as follows. The theoretical methods and the way to calculate spectra are described in Sec. II. In Sec. III, we benchmark the performance of TDRNOT on HHG spectra and Fano profiles before we conclude and give an outlook in Sec. IV. Some of the detailed derivations are given in Appendices A and B.

Atomic units (a.u.) are used throughout, unless noted otherwise.

II. THEORETICAL METHODS

By numerically exactly solving the time-dependent Schrödinger equation (TDSE) for a one-dimensional helium atom in the laser field, we obtain a reference result for the corresponding TDRNOT calculation involving N NOs. With increasing N, the TDRNOT spectra should converge to the TDSE results, as the TDRNOT equations of motion (EOM) are exact for two electrons. In this section, the model atom, the EOM, and the method to calculate the absorption spectra are introduced.

A. Model helium atom

The Hamiltonian of the widely used [5,6,31–36] one-dimensional helium model atom is

$$\hat{H}^{(1,2)}(t) = \hat{h}^{(1)}(t) + \hat{h}^{(2)}(t) + \hat{v}_{ee}^{(1,2)} - i\hat{\Gamma}_e^{(1)} - i\hat{\Gamma}_e^{(2)}, \quad (1)$$

where upper indices indicate the action on either electron 1, electron 2, or both. The single-particle Hamiltonian reads $\hat{h}(t) = \hat{h}_\mathrm{A} + \hat{h}_\mathrm{L}(t)$ with

$$\hat{h}_\mathrm{A} = \frac{\hat{p}^2}{2} - \frac{2}{\sqrt{\hat{x}^2 + \varepsilon_\mathrm{ne}}}, \tag{2}$$

$$\hat{h}_\mathrm{L}(t) = E(t)\hat{x} \tag{3}$$

(dipole approximation and length gauge), the electron-electron interaction

$$\hat{v}_\mathrm{ee}^{(1,2)} = \frac{1}{\sqrt{(\hat{x}^{(1)} - \hat{x}^{(2)})^2 + \varepsilon_\mathrm{ee}}}, \tag{4}$$

and $-i\hat{\Gamma}_\mathrm{e}$ is an imaginary potential to absorb outgoing electron flux. The electron-ion smoothing parameter $\varepsilon_\mathrm{ne} = 0.50$ is chosen such that the ground-state energy of He^+, $E_0^{\mathrm{He}^+} = -2.0$, is recovered. The electron-electron smoothing parameter $\varepsilon_\mathrm{ee} = 0.33$ is tuned to yield the neutral-He energy $E_0^\mathrm{He} = -2.9$.

B. Equations of motion (EOM)

For a helium atom, the TDSE

$$i\frac{\partial}{\partial t}|\Phi(t)\rangle = \hat{H}^{(1,2)}(t)|\Phi(t)\rangle \tag{5}$$

describes the time evolution of the two-electron state $|\Phi(t)\rangle$. The starting point for TDRNOT in the two-electron case is the pure two-body density matrix (2DM),

$$\hat{\gamma}_2(t) = |\Phi(t)\rangle\langle\Phi(t)|. \tag{6}$$

From the TDSE (5), the EOM for the 2DM,

$$\begin{aligned} i\dot{\hat{\gamma}}_2(t) = &\big[\hat{h}^{(1)}(t) + \hat{h}^{(2)}(t) + \hat{v}_\mathrm{ee}^{(1,2)}, \hat{\gamma}_2(t)\big] \\ &- i\big[\hat{\Gamma}_\mathrm{e}^{(1)} + \hat{\Gamma}_\mathrm{e}^{(2)}, \hat{\gamma}_2(t)\big]_+, \end{aligned} \tag{7}$$

results. The 1RDM $\hat{\gamma}_1(t)$ reads

$$\hat{\gamma}_1(t) = \sum_{i=1}^{2} \mathrm{Tr}_i\, \hat{\gamma}_2(t) = 2\,\mathrm{Tr}_1\, \hat{\gamma}_2(t) = 2\,\mathrm{Tr}_2\, \hat{\gamma}_2(t), \tag{8}$$

where the partial trace Tr_i means tracing out all degrees of freedom of particle i. The EOM for $\hat{\gamma}_1$ can be derived by taking the time derivative of (8),

$$\begin{aligned} i\dot{\hat{\gamma}}_1(t) = &[\hat{h}(t), \hat{\gamma}_1(t)] + 2\mathrm{Tr}_2[\hat{v}_\mathrm{ee}, \hat{\gamma}_2(t)] - i[\hat{\Gamma}_\mathrm{e}, \hat{\gamma}_1(t)]_+ \\ &- 2i\mathrm{Tr}_2\big[\hat{\Gamma}_\mathrm{e}^{(2)}, \hat{\gamma}_2(t)\big]_+. \end{aligned} \tag{9}$$

The NOs $|k(t)\rangle$ and occupation numbers (ONs) $n_k(t)$ are defined as eigenstates and eigenvalues of the 1RDM, respectively,

$$\hat{\gamma}_1(t)|k(t)\rangle = n_k(t)|k(t)\rangle. \tag{10}$$

As $\hat{\gamma}_1(t)$ is Hermitian, the ONs $n_k(t)$ are real and the NOs $|k(t)\rangle$ form an orthonormal complete basis set. Renormalized NOs (RNOs) are defined as

$$|\tilde{k}(t)\rangle = \sqrt{n_k(t)}|k(t)\rangle, \tag{11}$$

so that

$$\hat{\gamma}_1(t) = \sum_k |\tilde{k}(t)\rangle\langle\tilde{k}(t)|, \tag{12}$$

and $\hat{\gamma}_2(t)$ can be expanded in RNOs as

$$\hat{\gamma}_2(t) = \sum_{ijkl} \tilde{\gamma}_{2,ijkl}(t)|\tilde{i}(t)\rangle|\tilde{j}(t)\rangle\langle\tilde{k}(t)|\langle\tilde{l}(t)|. \tag{13}$$

The EOM for the RNOs read

$$\begin{aligned} i\,\partial_t|\tilde{n}\rangle = &[\hat{h}(t) - i\hat{\Gamma}_\mathrm{e}]\,|\tilde{n}\rangle + \mathcal{A}_n(t)|\tilde{n}\rangle \\ &+ \sum_{k\neq n} \mathcal{B}_{nk}(t)|\tilde{k}\rangle + \sum_k \hat{\mathcal{C}}_{nk}(t)|\tilde{k}\rangle, \end{aligned} \tag{14}$$

with

$$\begin{aligned} \mathcal{A}_n(t) = &-\frac{1}{n_n(t)}\,\mathrm{Re}\sum_{jkl} \tilde{\gamma}_{2,njkl}(t)\langle\tilde{k}\tilde{l}|\hat{v}_\mathrm{ee}|\tilde{n}\tilde{j}\rangle \\ &- \frac{1}{2n_n(t)}(\langle\tilde{n}|\hat{h}(t)|\tilde{n}\rangle - \langle\tilde{n}'|\hat{h}(t)|\tilde{n}'\rangle) \\ &- 2i\sum_{jl} \tilde{\gamma}_{2,njnl}(t)\langle\tilde{l}|\hat{\Gamma}_\mathrm{e}|\tilde{j}\rangle, \end{aligned} \tag{15}$$

$$\begin{aligned} \mathcal{B}_{nk}(t) = &\frac{2}{n_k(t) - n_n(t)}\sum_{jpl}[\tilde{\gamma}_{2,kjpl}(t)\langle\tilde{p}\tilde{l}|\hat{v}_\mathrm{ee}|\tilde{n}\tilde{j}\rangle \\ &- \tilde{\gamma}_{2,plnj}(t)\langle\tilde{k}\tilde{j}|\hat{v}_\mathrm{ee}|\tilde{p}\tilde{l}\rangle] - 2i\frac{1}{n_n(t) - n_k(t)}\langle\tilde{k}|\hat{\Gamma}_\mathrm{e}|\tilde{n}\rangle \\ &- 4i\frac{n_n(t)}{n_n(t) - n_k(t)}\sum_{jl} \tilde{\gamma}_{2,kjnl}(t)\langle\tilde{l}|\hat{\Gamma}_\mathrm{e}|\tilde{j}\rangle, \\ &\qquad n_k(t) \neq n_n(t), \end{aligned} \tag{16}$$

$$\hat{\mathcal{C}}_{nk}(t) = 2\sum_{jl} \tilde{\gamma}_{2,kjnl}(t)\langle\tilde{l}|\hat{v}_\mathrm{ee}|\tilde{j}\rangle, \tag{17}$$

and the "prime operator" acting on a positive integer k as

$$k' = \begin{cases} k+1 & \text{if } k \text{ odd} \\ k-1 & \text{if } k \text{ even,} \end{cases} \qquad k > 0. \tag{18}$$

For derivations, see Appendices A and B. Also, note that the time argument of the RNOs is suppressed, and we can apply (16) only if at time t ON $n_k(t) \neq n_n(t)$ (otherwise, see Appendix A).

C. Absorption spectra

Let the classical electric field of a laser be polarized in the x direction and propagating in the y direction, $E_\mathrm{in}(t - y/c) = E_\mathrm{in}(t - \alpha y)$, and the atom be placed at the origin. The laser field E_in induces a dipole and the atom responds, generating a field $E_\mathrm{gen}(y,t)$ also polarized in the x direction. The spectral distribution $S(\omega)$ reads

$$S(\omega) = |E(\omega)|^2 = \frac{1}{2\pi}\left|\int_{-\infty}^{+\infty} dt\, E(y,t)e^{i\omega t}\right|^2, \tag{19}$$

where $E(y,t)$ is the total field and $E(\omega)$ is its Fourier transform at position y. The total electric field $E(y,t)$ is determined by the wave equation in the propagation direction with a polarization term as a source [37],

$$\left(\frac{\partial^2}{\partial y^2} - \frac{1}{c^2}\frac{\partial^2}{\partial t^2}\right)E(y,t) = \frac{1}{\epsilon_0 c^2}\frac{\partial^2}{\partial t^2}\langle d(t)\rangle\delta(y), \tag{20}$$

where $\langle d(t)\rangle$ is the expectation value of the x component of the atomic dipole, which is the quantum mechanical single-atom input obtained from the one-dimensional helium model. The dipole is $\langle d(t)\rangle = -\sum_i \langle x_i(t)\rangle$ with $\langle x_i(t)\rangle = \langle\Phi(t)|\hat{x}^{(i)}|\Phi(t)\rangle$.

The relevant solution of (20) consists of an incoming and two counterpropagating waves, generated by the induced dipole in the atom,

$$E(y,t) = E_{\rm in}(t-\alpha y) - 2\pi\alpha[\theta(y)\langle\dot{d}(t-\alpha y)\rangle + \theta(-y)\langle\dot{d}(t+\alpha y)\rangle], \quad (21)$$

where $\theta(\pm y)$ is the Heaviside step function and $\langle\dot{d}(t\pm\alpha y)\rangle$ is the expectation value of the dipole velocity. The generated wave traveling in the propagation direction of the incoming pulse $\langle\dot{d}(t-\alpha y)\rangle$ may interfere destructively with the latter (absorption). In order to identify what is absorbed and what is emitted, the spectrum of the incoming laser field $E_{\rm in}(\omega)$ is subtracted from the total one [37],

$$S_{\rm resp}(\omega) = S(\omega) - |E_{\rm in}(\omega)|^2 = \frac{4\pi^2\alpha^2}{\omega^2}|\ddot{d}(\omega)|^2 + \frac{4\pi\alpha}{\omega}\,{\rm Im}[E^*_{\rm in}(\omega)\ddot{d}(\omega)], \quad (22)$$

where $\ddot{d}(\omega)$ is the Fourier transform of the expectation value of the dipole acceleration. Positive values of $S_{\rm resp}(\omega)$ indicate emission; negative values indicate absorption.

If $|E_{\rm gen}| \ll |E_{\rm in}|$ in the frequency range where the incoming laser has components, one can approximate

$$S_{\rm resp}(\omega) \approx S^{\rm L}_{\rm resp}(\omega) = \frac{4\pi\alpha}{\omega}\,{\rm Im}[E^*_{\rm in}(\omega)\ddot{d}(\omega)]. \quad (23)$$

In HHG, we are rather interested in frequencies where the incoming laser has no or negligible components, i.e.,

$$S_{\rm resp}(\omega) \approx S^{\rm NL}_{\rm resp}(\omega) = \frac{4\pi^2\alpha^2}{\omega^2}|\ddot{d}(\omega)|^2. \quad (24)$$

Note that in the literature, one finds similar expressions derived using different approaches leading, however, to different prefactors and ω scaling. In [38,39], for instance, one finds that $S^{\rm L}_{\rm resp}(\omega) \sim \frac{1}{\omega^2}\,{\rm Im}\,[E^*_{\rm in}(\omega)\ddot{d}(\omega)]$. The "standard way" to calculate HHG spectra is via $S^{\rm NL}_{\rm resp}(\omega) \sim |\ddot{d}(\omega)|^2$ (derived from Larmor's formula). On the other hand, (24) is in agreement with quantum-electrodynamical calculations [40].

Numerically, it is advantageous to evaluate $\frac{d^2}{dt^2}\langle d\rangle$ using Ehrenfest's theorem,

$$\frac{d^2}{dt^2}\langle d\rangle = -2\left\langle\frac{d}{dx_i}\frac{2}{\sqrt{x_i^2+\varepsilon_{\rm ne}}}\right\rangle - 2\dot{A}(t) = 2\left\langle\frac{2x_i}{\left(x_i^2+\varepsilon_{\rm ne}\right)^{3/2}}\right\rangle + 2E(t). \quad (25)$$

III. RESULTS

Results from TDRNOT calculations for AS and HHG, together with the corresponding TDSE benchmarks, will be presented in this section. All results were obtained starting from the spin-singlet ground state, which was calculated via imaginary-time propagation. Real-time propagation was performed with enabled imaginary potential on a grid with 500 grid points (in each spatial direction) with a grid spacing of 0.4.

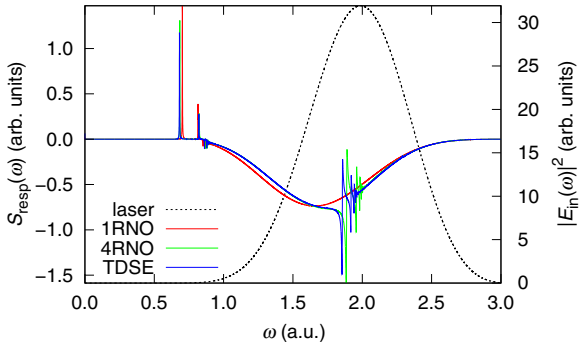

FIG. 1. Absorption spectra $S_{\rm resp}(\omega)$ (left vertical axis) calculated using TDSE and TDRNOT with one and four RNOs. The dashed curve indicates the spectrum $|E_{\rm in}(\omega)|^2$ of the incoming laser field (right vertical axis).

A. Fano profiles in absorption spectra

A 25-nm ($\omega = 1.84$) linearly polarized $N_{\rm cyc} = 3$-cycle $\sin^2$-shaped laser pulse of duration $T = 2\pi N_{\rm cyc}/\omega = 10.4 = 0.25$ fs was applied to the model helium atom. The vector potential in dipole approximation reads

$$A(t) = A_0 \sin^2\left(\frac{\omega t}{2N_{\rm cyc}}\right)\sin(\omega t) \quad \text{for } 0 \leqslant t \leqslant T, \quad (26)$$

and zero otherwise. The chosen peak intensity $I_0 = (\omega A_0)^2$ corresponds to $I_0 = 1.0\times10^{12}$ W/cm^2. In order to obtain a high-frequency resolution, the quantum propagation was continued for $T_{\rm free} = 10000$ after the laser pulse. An exponential decay $W(t) = e^{-\beta\theta(t-T)(t-T)}$ with $\beta = 2.5\times10^{-5}$ was multiplied to $\ddot{x}(t)$ in order to mimic the decay of the excited-state population due to spontaneous emission.

Figure 1 shows absorption spectra calculated with TDRNOT using one and four RNOs per spin, together with the exact TDSE benchmark result. The lines in the frequency interval [0.6,0.9] correspond to transitions between the ground state and singly excited states; the lines lying within [1.8,2.2] correspond to transitions involving doubly excited states where—in a single-particle picture—the lower-energetic electron is in the first excited level. Note that the strength of the lines in the frequency range [0.6,0.9] is sensitive to the choice of the damping coefficient β. However, for the purpose of benchmarking the TDRNOT results, that is not important as long as the same β is used for both TDSE and TDRNOT. While the lines involving singly excited states are already present in the 1RNO calculation, the Fano line shapes for $\omega \in [1.8,2.2]$ are only reproduced with more than one RNO per spin. This is not surprising, as one RNO per spin is equivalent to time-dependent Hartree-Fock, which is identical to TDDFT in the exact-exchange-only approximation. The latter is known to miss doubly excited states [41].

Figure 2 shows that the 2RNO result already reproduces the Fano profiles, but their positions are not yet satisfactory. We find that by adding more RNOs, the convergence to

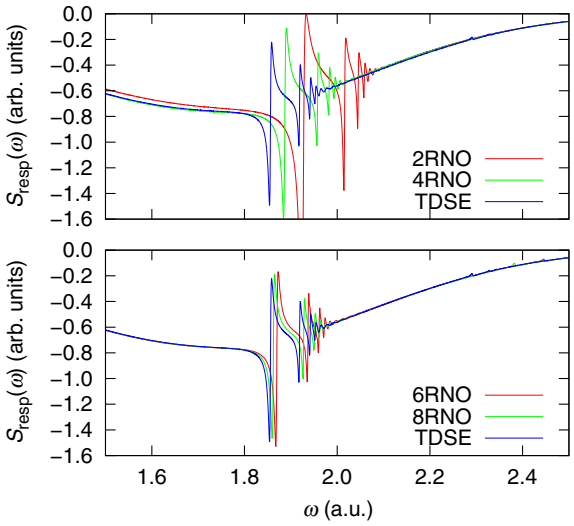

FIG. 2. Fano profiles due to doubly excited states calculated using TDSE and TDRNOT with two, four, six, and eight RNOs.

the TDSE result is "quasimonotonous," i.e., it transiently worsens for odd numbers of RNOs per spin but then improves for the subsequent even number. Six RNOs per spin give reasonable spectra if the lowest series of doubly excited states is relevant. We found that 14 RNOs are required if the next series (with the lower electron in the second excited level) is involved.

B. HHG spectra

One might expect that the calculation of HHG spectra is an easy task, even for TDDFT in the simple exact-exchange-only approximation. However, apart from possible correlation effects, one has to keep in mind that the celebrated HHG cutoff $3.17\,U_p + I_p$ (with $I_p = |E_0|$ the ionization potential and $U_p = A_0^2/4$ the ponderomotive energy) [42] involves I_p. Hence, a multiple steplike structure may arise because of the different I_p for different charge states in multielectron systems.

In this HHG part of our work, we applied a rather long ($N_{\rm cyc} = 15$), flat-top 800-nm ($\omega = 0.057$) pulse in order to generate well-defined, sharp harmonic lines. The up and down ramping was $\sin^2$ shaped over two cycles. The peak intensity of the laser pulse was $I_0 = 1.0\times10^{14}$ W/cm^2.

Figure 3 shows the HHG spectra obtained with TDRNOT using one, two, three, and six RNOs, together with the TDSE benchmark. The 1RNO result (i.e., TDHF or exact-exchange-only TDDFT) misses the proper extension of the plateau due to HHG in He^+. Instead, it gives an unphysical second plateau, which is a replica of the first plateau due to the nonlinearities in the EOM. Note that the laser parameters are not in the

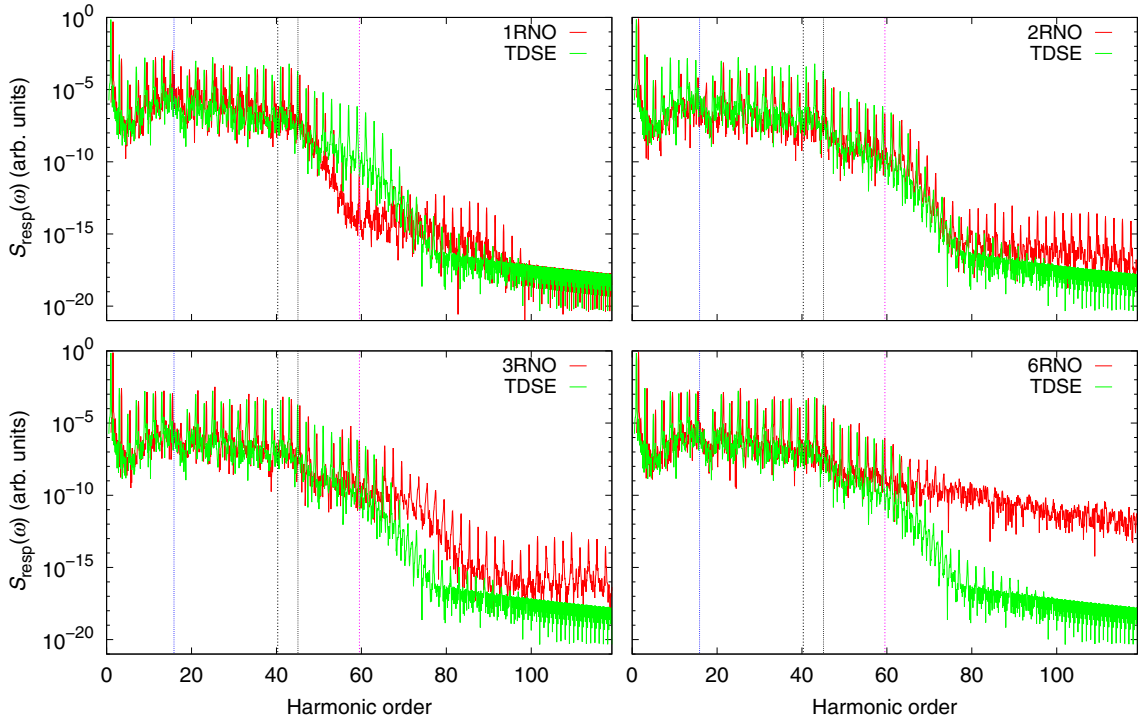

FIG. 3. Comparison of HHG spectra obtained with TDSE and TDRNOT with one, two, three, and six RNOs. For a better comparison, the TDRNOT spectra are shifted to the right by half a harmonic order. The vertical lines in each panel indicate (from left to right) the ionization potential I_p of neutral He, the cutoff $3.17\,U_p + I_p$, the corrected cutoff $3.17\,U_p + 1.3\,I_p$ obtained by Lewenstein *et al.* [42], and the He^+ cutoff $3.17\,U_p + I_p^{He^+}$.

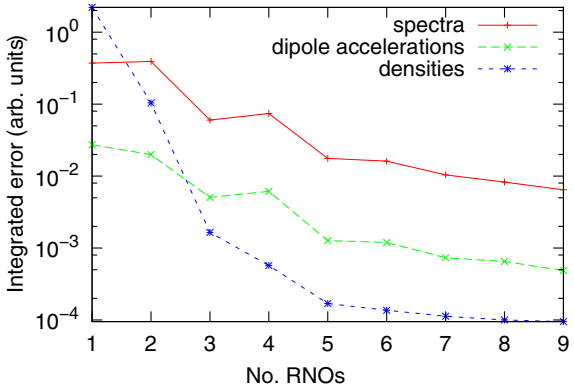

FIG. 4. Integrated error for HHG spectra, dipole accelerations $\langle \ddot{d} \rangle$, and densities in the TDRNOT results for one up to nine RNOs per spin.

regime where a second plateau due to single-photon double recombination occurs [43].

The 2RNO spectrum in Fig. 3 reproduces the He^+ cutoff very well. However, unphysical harmonic peaks emerge on a level of 10^{-13} well above even the 100th harmonic. The situation seems to worsen if more RNOs are added. The reason for these unphysical high harmonics is truncation. By adding more and more RNOs, TDRNOT is able to describe transitions to more and more doubly excited states. However, the energetic position of each new series of doubly excited states is never correct in the first place. It only converges to the right position if one adds even more RNOs (which bring new, initially poorly positioned series). These wrong states are responsible for the unphysical harmonics. Nevertheless the quantitative agreement improves with increasing number of RNOs because the harmonics up to the He^+ cutoff match better with the TDSE benchmark result. In fact, for six RNOs per spin, the TDRNOT and TDSE HHG peaks up to the 63rd harmonic agree very well. Figure 4 shows the error of the TDRNOT HHG spectra, i.e., the square of the difference between the TDRNOT and the TDSE spectrum, integrated over all frequencies. It is seen that the error decreases with number of RNOs, although not strictly monotonously. Similarly, the errors in the dipole acceleration $\langle \ddot{d} \rangle$ (integrated over the laser pulse duration) and in the density (integrated over space and the laser pulse duration) were calculated and are included in Fig. 4.

C. Computational effort

As already stated in [20], the computation time $\tau(N,N_x)$ required for a TDRNOT propagation using N NOs on N_x spatial grid points scales

$$\tau(N,N_x) = \alpha_1 N^2 N_x \log(N_x) + \alpha_2 N^3 N_x \qquad (27)$$

when using the same fixed time step $\Delta t \leqslant \Delta t_{\mathrm{conv}}$ small enough to yield converged results. However, for an increasing number N of NOs, one finds that the upper time-step limit $\Delta t_{\mathrm{conv}} = \Delta t_{\mathrm{conv}}(N)$ decreases. This unpleasant behavior originates from the minimal difference $\min |n_n - n_k|$ of ONs, which decreases with increasing N because the (small) ONs of the less significant NOs are more likely to come close on an absolute scale. Fortunately, computational effort can be saved thanks to the fact that any two ONs come close only occasionally during real-time propagation. Hence, using an adaptive time step, the scaling of the computation time becomes

$$\tau_{\mathrm{a}}(N,N_x) = [\alpha_3 N^2 N_x \log(N_x) + \alpha_4 N^3 N_x] F(N), \qquad (28)$$

with amended prefactors $\alpha_4 \ll \alpha_2$ and $\alpha_3 \ll \alpha_1$ and an additional factor $F(N)$, describing the varying number of time steps according to the adaptive scheme. We observed a speedup of at least one order of magnitude for $N > 6$ when using adaptive time steps and only a moderate increase of the average time step with increasing $N \in [1,9]$.

The computation times $\tau_{\mathrm{a}}(N) = \tau_{\mathrm{a}}(N,500)$ on a single core of an i5-3570 processor required to obtain the high-harmonic spectra using 1 to 9 RNOs were $\tau_{\mathrm{a}}(1) \simeq 6$, $\tau_{\mathrm{a}}(2) \simeq 14$, $\tau_{\mathrm{a}}(3) \simeq 27$, $\tau_{\mathrm{a}}(4) \simeq 45$, $\tau_{\mathrm{a}}(5) \simeq 71$, $\tau_{\mathrm{a}}(6) \simeq 169$, $\tau_{\mathrm{a}}(7) \simeq 241$, $\tau_{\mathrm{a}}(8) \simeq 352$, and $\tau_{\mathrm{a}}(9) \simeq 540$ seconds, while the TDSE calculation took $\tau_{\mathrm{TDSE}} \simeq 968$ seconds. Thus, 1RNO, 2RNO, 4RNO, and 8RNO perform faster by a factor 161, 60, 21, and 2.8. The computation times are too small for a thorough scaling analysis, but there are indications of cubic scaling, $\tau_{\mathrm{a}}(8)/\tau_{\mathrm{a}}(4) = 7.8 \simeq (8/4)^3$.

IV. CONCLUSION

In this work, we tested further the recently introduced time-dependent renormalized-natural-orbital theory (TDRNOT). The method is based on the equations of motion for the renormalized natural orbitals (RNOs), i.e., the time-dependent eigenfunctions of the one-body reduced density matrix, normalized to their eigenvalues. TDRNOT was applied again to a numerically exactly solvable model helium atom with the focus on the absorbed and emitted radiation. Both absorption and high-harmonic-generation (HHG) spectra are "simple observables" in the sense that the single-particle density is sufficient to calculate them. Hence, one could have expected that time-dependent density functional theory (TDDFT) in the exact-exchange-only approximation would work well. However, we showed that TDRNOT with just one RNO per spin (which equals TDDFT in exact-exchange-only approximation) fails to reproduce Fano line shapes in absorption spectra due to the absence of doubly excited states. Adding more RNOs, the Fano line shapes are captured well by TDRNOT. The 1RNO or TDDFT result for HHG spectra was qualitatively wrong because it lacked the correct cutoff originating from HHG in He^+, while predicting an unphysical second plateau. Again, with increasing number of RNOs, the agreement with the benchmark result from the exact numerical solution of the time-dependent Schrödinger equation improves. However, unphysical HHG peaks at high frequencies emerge because of the necessary truncation of the number of RNOs.

A TDRNOT implementation for helium in full dimensionality is under way. The computational effort can be kept manageable if the laser is restricted to linear polarization and the initial configuration is chosen with total magnetic quantum number $M = 0$ with respect to the polarization axis. Employing a spherical harmonics expansion with indices l and m under these restrictions, each time-dependent

three-dimensional (3D) RNO $|\tilde{n}(t)\rangle$ of helium contributes for exactly one value of $|m| = |m_n|$. For the ground state, one even finds a single well-defined $l = l_n$ for each RNO. It is an open question, though, as to how many RNOs are required to describe the particular phenomena of interest.

For more than two particles, approximations for the two-body reduced density matrix expansion coefficients $\tilde{\gamma}_{2,ijkl}(t)$ in (13) are required. Testing such approximations will be the subject of future work.

ACKNOWLEDGMENT

This work was supported by the Collaborative Research Center SFB 652 of the German Science Foundation (DFG).

APPENDIX A: DERIVATION OF EOM

Multiplying (9) from the right with $|\tilde{n}\rangle$ and using the 2DM expansion in RNOs (13), one obtains

$$\begin{aligned} i\dot{\tilde{\gamma}}_1(t)|\tilde{n}\rangle =& n_n(t)(\hat{h}(t) - i\hat{\Gamma}_e)|\tilde{n}\rangle - \sum_k \langle\tilde{k}|\hat{h}(t) + i\hat{\Gamma}_e|\tilde{n}\rangle|\tilde{k}\rangle \\ &+ 2n_n(t)\sum_{ijk}\tilde{\gamma}_{2,ijnk}(t)\langle\tilde{k}|\hat{v}_{ee}|\tilde{j}\rangle|\tilde{i}\rangle \\ &- 2\sum_{ijkl}\tilde{\gamma}_{2,ijkl}(t)\langle\tilde{k}\tilde{l}|\hat{v}_{ee}|\tilde{n}\,\tilde{j}\rangle|\tilde{i}\rangle \\ &- 4in_n(t)\sum_{ijl}\tilde{\gamma}_{2,ijnl}(t)\langle\tilde{l}|\hat{\Gamma}_e|\tilde{j}\rangle|\tilde{i}\rangle, \end{aligned} \tag{A1}$$

which multiplied from the left with $\langle\tilde{l}|$ leads to

$$\begin{aligned} i\langle\tilde{l}|\dot{\tilde{\gamma}}_1(t)|\tilde{n}\rangle =& (n_n(t) - n_l(t))\langle\tilde{l}|\hat{h}(t)|\tilde{n}\rangle \\ &- i(n_n(t) + n_l(t))\langle\tilde{l}|\hat{\Gamma}_e|\tilde{n}\rangle \\ &+ 2n_n(t)\sum_{ijk}\tilde{\gamma}_{2,ijnk}(t)\langle\tilde{l}\tilde{k}|\hat{v}_{ee}|\tilde{i}\,\tilde{j}\rangle \\ &- \left[2n_l(t)\sum_{ijk}\tilde{\gamma}_{2,ijlk}(t)\langle\tilde{n}\tilde{k}|\hat{v}_{ee}|\tilde{i}\,\tilde{j}\rangle\right]^* \\ &- 4in_n(t)n_l(t)\sum_{jk}\tilde{\gamma}_{2,ljnk}(t)\langle\tilde{k}|\hat{\Gamma}_e|\tilde{j}\rangle. \end{aligned} \tag{A2}$$

Multiplying

$$\dot{\tilde{\gamma}}_1(t) = \sum_k |\dot{\tilde{k}}\rangle\langle\tilde{k}| + \sum_k |\tilde{k}\rangle\langle\dot{\tilde{k}}| \tag{A3}$$

from the right with $|\tilde{n}\rangle$ and rearranging terms, one obtains

$$n_n(t)|\dot{\tilde{n}}\rangle = \dot{\tilde{\gamma}}_1(t)|\tilde{n}\rangle - \langle\dot{\tilde{n}}|\tilde{n}\rangle|\tilde{n}\rangle - \sum_{k\neq n}\langle\dot{\tilde{k}}|\tilde{n}\rangle|\tilde{k}\rangle. \tag{A4}$$

Using the time derivative of the orthogonality relation $\langle\tilde{l}(t)|\tilde{n}(t)\rangle = \delta_{l,n}n_n(t)$,

$$\langle\dot{\tilde{l}}|\tilde{n}\rangle + \langle\tilde{l}|\dot{\tilde{n}}\rangle = \delta_{l,n}\dot{n}_n(t), \tag{A5}$$

allows us to rewrite (A4) as

$$|\dot{\tilde{n}}\rangle = \dot{\tilde{\gamma}}_1(t)|\tilde{n}\rangle + \langle\tilde{n}|\dot{\tilde{n}}\rangle|\tilde{n}\rangle - \dot{n}_n|\tilde{n}\rangle + \sum_{k\neq n}\langle\tilde{k}|\dot{\tilde{n}}\rangle|\tilde{k}\rangle, \tag{A6}$$

which is still implicit. However, multiplying (A6) from the left with $\langle\tilde{l}|$ for $\langle\tilde{l}| = \langle\tilde{n}|$,

$$\begin{aligned} \dot{n}_n(t) =& \frac{1}{n_n(t)}\langle\tilde{n}|\dot{\tilde{\gamma}}_1(t)|\tilde{n}\rangle \\ =& 4\,\mathrm{Im}\sum_{ijl}\tilde{\gamma}_{2,ijnl}(t)\langle\tilde{n}\tilde{l}|\hat{v}_{ee}|\tilde{i}\,\tilde{j}\rangle - 2\langle\tilde{n}|\hat{\Gamma}_e|\tilde{n}\rangle \\ &- 4n_n(t)\sum_{jl}\tilde{\gamma}_{2,njnl}(t)\langle\tilde{l}|\hat{\Gamma}_e|\tilde{j}\rangle, \end{aligned} \tag{A7}$$

for $n_l(t) \neq n_n(t)$ at time t, results in

$$\langle\tilde{l}|\dot{\tilde{n}}\rangle = -\langle\dot{\tilde{l}}|\tilde{n}\rangle = \frac{\langle\tilde{l}|\dot{\tilde{\gamma}}_1(t)|\tilde{n}\rangle}{n_n(t) - n_l(t)}, \tag{A8}$$

and, for $n_l(t) = n_n(t)$ at time t if $l \neq n$, results in

$$\langle\tilde{l}|\dot{\tilde{\gamma}}_1(t)|\tilde{n}\rangle = 0. \tag{A9}$$

The last expression, with (A2), yields a conservation rule at time t for $n_l(t) = n_n(t)$ and $\langle l|n\rangle = 0$:

$$\begin{aligned} &\sum_{ijk}\tilde{\gamma}_{2,ijnk}(t)\langle\tilde{l}\tilde{k}|\hat{v}_{ee}|\tilde{i}\,\tilde{j}\rangle - 2i\langle\tilde{l}|\hat{\Gamma}_e|\tilde{n}\rangle \\ &= \sum_{ijk}\tilde{\gamma}_{2,lkij}(t)\langle\tilde{i}\,\tilde{j}|\hat{v}_{ee}|\tilde{n}\tilde{k}\rangle + 4in_n(t)\sum_{jk}\tilde{\gamma}_{2,ljnk}(t)\langle\tilde{k}|\hat{\Gamma}_e|\tilde{j}\rangle. \end{aligned} \tag{A10}$$

The condition $n_l(t) = n_n(t)$ for $\langle l|n\rangle = 0$ means that these orbitals at time t are degenerate, and one may choose any orthogonal pair from the subspace they span.

The term $\langle\tilde{n}|\dot{\tilde{n}}\rangle$ depends on the phase choice for the RNOs. In principle, one can use any value, keeping in mind that $\tilde{\gamma}_{2,ijnk}(t)$ will depend on the choice. For the phase convention introduced in [19] (with slight modifications to ensure that during imaginary-time propagation, the norms of RNOs $|\tilde{n}\rangle$ and $|\tilde{n}'\rangle$ remain the same; see Appendix B),

$$\begin{aligned} i\langle\tilde{n}|\dot{\tilde{n}}\rangle =& \frac{1}{2}\langle\tilde{n}|\hat{h}|\tilde{n}\rangle + \frac{1}{2}\langle\tilde{n}'|\hat{h}|\tilde{n}'\rangle \\ &+ \mathrm{Re}\sum_{ijk}\tilde{\gamma}_{2,ijnk}\langle\tilde{n}\tilde{k}|\hat{v}_{ee}|\tilde{i}\,\tilde{j}\rangle + i\frac{\dot{n}_n}{2}. \end{aligned} \tag{A11}$$

Inserting (A1), (A11), (A7), and (A8) with (A2) into (A6), one obtains the explicit EOM for the RNOs (14)–(17).

Note that we can use (16) to calculate $\mathcal{B}_{nk}(t)$ only if at time t we have $n_k(t) \neq n_n(t)$. Otherwise,

$$\begin{aligned} \mathcal{B}_{nk}(t) =& \frac{i}{n_n(t)}\langle\tilde{k}|\dot{\tilde{n}}\rangle - \frac{\langle\tilde{k}|h(t)|\tilde{n}\rangle}{n_n(t)} \\ &- 2\sum_{ijl}\frac{\tilde{\gamma}_{2,kijl}(t)\langle\tilde{j}\tilde{l}|\hat{v}_{ee}|\tilde{n}\tilde{i}\rangle}{n_n(t)} - i\frac{\langle\tilde{k}|\hat{\Gamma}_e|\tilde{n}\rangle}{n_n(t)} \\ &- 4i\sum_{jl}\tilde{\gamma}_{2,kjnl}(t)\langle\tilde{l}|\hat{\Gamma}_e|\tilde{j}\rangle, \end{aligned} \tag{A12}$$

if $n_k(t) = n_n(t)$. Without the imaginary potential, it is always possible to choose such linear combination that $\mathcal{B}_{nk}(t) = 0$. However, with the imaginary potential, the situation is more complicated. For two-electron systems, one can still set $\mathcal{B}_{nn'}(t) = 0$ but, in general, it is advisable to use (A12) with some value for $\langle\tilde{k}|\dot{\tilde{n}}\rangle$ which does not change $\gamma_{2,ijnk}(t)$, e.g., 0.

APPENDIX B: RNO PHASE CONVENTION AND PROOF OF (A11)

The two-electron state within a particular phase convention for the RNOs can be written as [19]

$$|\Phi(t)\rangle = \sum_{i \text{ odd}} \tilde{g}_i(t)[|\tilde{i}\tilde{i}'\rangle - |\tilde{i}'\tilde{i}\rangle], \quad \tilde{g}_i(t) = \frac{e^{i\varphi_i}}{\sqrt{2n_i(t)}}. \tag{B1}$$

The phase factors $e^{i\varphi_i}$ for the helium singlet can be chosen,

$$e^{i\varphi_i} = 2\delta_{k,1} - 1, \quad k \text{ odd}, \tag{B2}$$

leading to real expansion coefficients

$$\begin{aligned}\tilde{\gamma}_{2,ijkl}(t) &= \tilde{g}_i(t)\tilde{g}_k(t)\delta_{i,j'}\delta_{k,l'} \\ &= (-1)^{i-k}\frac{e^{i[\varphi_i-\varphi_k]}}{2\sqrt{n_i(t)n_k(t)}}\delta_{i,j'}\delta_{k,l'}.\end{aligned} \tag{B3}$$

Inserting (B1) into the left-hand side of the TDSE (5) leads to

$$\begin{aligned}\hat{H}^{(1,2)}(t)|\Phi(t)\rangle = i\sum_{i \text{ odd}} \dot{\tilde{g}}_i(t)[|\tilde{i}\tilde{i}'\rangle - |\tilde{i}'\tilde{i}\rangle] \\ + i\sum_{i \text{ odd}} \tilde{g}_i(t)[|\dot{\tilde{i}}\tilde{i}'\rangle + |\tilde{i}\dot{\tilde{i}}'\rangle - |\dot{\tilde{i}}'\tilde{i}\rangle - |\tilde{i}'\dot{\tilde{i}}\rangle].\end{aligned} \tag{B4}$$

Multiplying from the left by $2\tilde{g}_k(t)\langle\tilde{k}\tilde{k}'|$ for an odd k and making use of $2\tilde{g}_k^2(t)n_k(t) = 1$ gives

$$\begin{aligned}2\tilde{g}_k(t)\langle\tilde{k}\tilde{k}'|\hat{H}(t)|\Phi(t)\rangle &= i\frac{\dot{\tilde{g}}_k(t)}{\tilde{g}_k(t)}n_k(t) + i(\langle\tilde{k}|\dot{\tilde{k}}\rangle + \langle\tilde{k}'|\dot{\tilde{k}}'\rangle) \\ &= i\left(\langle\tilde{k}|\dot{\tilde{k}}\rangle + \langle\tilde{k}'|\dot{\tilde{k}}'\rangle - \frac{\dot{n}_k(t)}{2}\right).\end{aligned} \tag{B5}$$

Inserting (B1) into the right-hand side of (B5) gives

$$\begin{aligned}2\tilde{g}_k(t)\langle\tilde{k}\tilde{k}'|\hat{H}(t)|\Phi(t)\rangle \\ = \langle\tilde{k}|\hat{h}(t) - i\hat{\Gamma}_e|\tilde{k}\rangle + \langle\tilde{k}'|\hat{h}(t) - i\hat{\Gamma}_e|\tilde{k}'\rangle \\ + 2\sum_{i \text{ odd}} \tilde{g}_i(t)\tilde{g}_k(t)[\langle\tilde{k}\tilde{k}'|\hat{v}_{ee}|\tilde{i}\tilde{i}'\rangle + \langle\tilde{k}\tilde{k}'|\hat{v}_{ee}|\tilde{i}'\tilde{i}\rangle],\end{aligned} \tag{B6}$$

which, using (A7) and (B3), simplifies to

$$\begin{aligned}2\tilde{g}_k(t)\langle\tilde{k}\tilde{k}'|\hat{H}(t)|\Phi(t)\rangle \\ = \langle\tilde{k}|\hat{h}(t)|\tilde{k}\rangle + \langle\tilde{k}'|\hat{h}(t)|\tilde{k}'\rangle \\ + 2\,\mathrm{Re}\sum_{ijl} \tilde{\gamma}_{2,ijkl}\langle\tilde{k}\tilde{l}|\hat{v}_{ee}|\tilde{i}\,\tilde{j}\rangle + i\frac{\dot{n}_k(t)}{2}.\end{aligned} \tag{B7}$$

Combining (B5) and (B7), one arrives at

$$\begin{aligned}i\langle\tilde{n}|\dot{\tilde{n}}\rangle + i\langle\tilde{n}'|\dot{\tilde{n}}'\rangle = \langle\tilde{n}|\hat{h}(t)|\tilde{n}\rangle + \langle\tilde{n}'|\hat{h}(t)|\tilde{n}'\rangle \\ + 2\,\mathrm{Re}\sum_{ijl} \tilde{\gamma}_{2,ijnl}\langle\tilde{n}\tilde{l}|\hat{v}_{ee}|\tilde{i}\,\tilde{j}\rangle + i\dot{n}_n(t).\end{aligned} \tag{B8}$$

There is the freedom to distribute the right-hand side between $i\langle\tilde{n}|\dot{\tilde{n}}\rangle$ and $i\langle\tilde{n}'|\dot{\tilde{n}}'\rangle$. We deviate slightly from the choice in [19] and set

$$\begin{aligned}i\langle\tilde{n}|\dot{\tilde{n}}\rangle &= i\langle\tilde{n}'|\dot{\tilde{n}}'\rangle \\ &= \frac{1}{2}\langle\tilde{n}|\hat{h}(t)|\tilde{n}\rangle + \frac{1}{2}\langle\tilde{n}'|\hat{h}(t)|\tilde{n}'\rangle \\ &\quad + \mathrm{Re}\sum_{ijl} \tilde{\gamma}_{2,ijnl}\langle\tilde{n}\tilde{l}|\hat{v}_{ee}|\tilde{i}\,\tilde{j}\rangle + i\frac{\dot{n}_n(t)}{2},\end{aligned} \tag{B9}$$

which has the advantage that the ONs of RNOs $|n\rangle$ and $|n'\rangle$ remain automatically equal during imaginary-time propagation.

[1] W. Kohn, Nobel lecture: Electronic structure of matter–wave functions and density functionals, Rev. Mod. Phys. **71**, 1253 (1999).

[2] R. M. Dreizler and E. K. U. Gross, *Density Functional Theory* (Springer Science + Business Media, New York, 1990).

[3] C. A. Ullrich, *Time-Dependent Density-Functional Theory* (Oxford University Press, Oxford, 2011).

[4] C. A. Ullrich and Z.-H. Yang, A brief compendium of time-dependent density functional theory, Braz. J. Phys. **44**, 154 (2014).

[5] F. Wilken and D. Bauer, Momentum distributions in time-dependent density-functional theory: Product-phase approximation for nonsequential double ionization in strong laser fields, Phys. Rev. A **76**, 023409 (2007).

[6] M. Ruggenthaler and D. Bauer, Rabi Oscillations and Few-level Approximations in Time-Dependent Density Functional Theory, Phys. Rev. Lett. **102**, 233001 (2009).

[7] J. Zanghellini, M. Kitzler, T. Brabec, and A. Scrinzi, Testing the multi-configuration time-dependent Hartree-Fock method, J. Phys. B **37**, 763 (2004).

[8] D. Hochstuhl, S. Bauch, and M. Bonitz, Multiconfigurational time-dependent Hartree-Fock calculations for photoionization of one-dimensional helium, J. Phys. Conf. Ser. **220**, 012019 (2010).

[9] T. Sato and K. L. Ishikawa, Time-dependent complete-active-space self-consistent-field method for multielectron dynamics in intense laser fields, Phys. Rev. A **88**, 023402 (2013).

[10] T. Sato and K. L. Ishikawa, Time-dependent multiconfiguration self-consistent-field method based on the occupation-restricted multiple-active-space model for multielectron dynamics in intense laser fields, Phys. Rev. A **91**, 023417 (2015).

[11] L. Greenman, P. J. Ho, S. Pabst, E. Kamarchik, D. A. Mazziotti, and R. Santra, Implementation of the time-dependent configuration-interaction singles method for atomic strong-field processes, Phys. Rev. A **82**, 023406 (2010).

[12] S. Pabst and R. Santra, Strong-Field Many-Body Physics and the Giant Enhancement in the High-Harmonic Spectrum of Xenon, Phys. Rev. Lett. **111**, 233005 (2013).

[13] A. Karamatskou, S. Pabst, Y.-J. Chen, and R. Santra, Calculation of photoelectron spectra within the time-dependent configuration-interaction singles scheme, Phys. Rev. A **89**, 033415 (2014).

[14] D. Hochstuhl and M. Bonitz, Time-dependent restricted-active-space configuration-interaction method for the photoionization of many-electron atoms, Phys. Rev. A **86**, 053424 (2012).

[15] S. Bauch, L. K. Sørensen, and L. B. Madsen, Time-dependent generalized-active-space configuration-interaction approach to

photoionization dynamics of atoms and molecules, Phys. Rev. A **90**, 062508 (2014).

[16] K. Ishikawa and T. Sato, A review on ab initio approaches for multielectron dynamics, IEEE J. Sel. Top. Quantum Electron. **21**, 1 (2015).

[17] D. Hochstuhl, C. Hinz, and M. Bonitz, Time-dependent multiconfiguration methods for the numerical simulation of photoionization processes of many-electron atoms, Eur. Phys. J. Spec. Top. **223**, 177 (2014).

[18] M. Brics and D. Bauer, Time-dependent renormalized natural orbital theory applied to the two-electron spin-singlet case: Ground state, linear response, and autoionization, Phys. Rev. A **88**, 052514 (2013).

[19] J. Rapp, M. Brics, and D. Bauer, Equations of motion for natural orbitals of strongly driven two-electron systems, Phys. Rev. A **90**, 012518 (2014).

[20] M. Brics, J. Rapp, and D. Bauer, Nonsequential double ionization with time-dependent renormalized-natural-orbital theory, Phys. Rev. A **90**, 053418 (2014).

[21] P.-O. Löwdin, Quantum theory of many-particle systems. i. physical interpretations by means of density matrices, natural spin-orbitals, and convergence problems in the method of configurational interaction, Phys. Rev. **97**, 1474 (1955).

[22] A. Coleman and V. Yukalov, *Reduced Density Matrices: Coulson's Challenge*, Lecture Notes in Chemistry (Springer, Berlin, Heidelberg, 2000).

[23] H. Appel, Time-Dependent Quantum Many-Body Systems: Linear Response, Electronic Transport, and Reduced Density Matrices, Ph.D. thesis, Freie Universität, Berlin, 2007.

[24] K. J. H. Giesbertz, Time-Dependent One-Body Reduced Density Matrix Functional Theory, Ph.D. thesis, Free University, Amsterdam, 2010.

[25] T. Sato and K. L. Ishikawa, The structure of approximate two electron wavefunctions in intense laser driven ionization dynamics, J. Phys. B **47**, 204031 (2014).

[26] K. Giesbertz, Are natural orbitals useful for generating an efficient expansion of the wave function? Chem. Phys. Lett. **591**, 220 (2014).

[27] F. Krausz and M. Ivanov, Attosecond physics, Rev. Mod. Phys. **81**, 163 (2009).

[28] T. Schultz and M. Vrakking, *Attosecond and XUV Spectroscopy: Ultrafast Dynamics and Spectroscopy* (Wiley, New York, 2013).

[29] C. Ott, A. Kaldun, P. Raith, K. Meyer, M. Laux, J. Evers, C. H. Keitel, C. H. Greene, and T. Pfeifer, Lorentz meets fano in spectral line shapes: A universal phase and its laser control, Science **340**, 716 (2013).

[30] Z. Liu, S. M. Cavaletto, C. Ott, K. Meyer, Y. Mi, Z. Harman, C. H. Keitel, and T. Pfeifer, Phase Reconstruction of Strong-Field Excited Systems by Transient-Absorption Spectroscopy, Phys. Rev. Lett. **115**, 033003 (2015).

[31] R. Grobe and J. H. Eberly, Photoelectron Spectra for a Two-Electron System in a Strong Laser Field, Phys. Rev. Lett. **68**, 2905 (1992).

[32] S. L. Haan, R. Grobe, and J. H. Eberly, Numerical study of autoionizing states in completely correlated two-electron systems, Phys. Rev. A **50**, 378 (1994).

[33] D. Bauer, Two-dimensional, two-electron model atom in a laser pulse: Exact treatment, single-active-electron analysis, time-dependent density-functional theory, classical calculations, and nonsequential ionization, Phys. Rev. A **56**, 3028 (1997).

[34] D. G. Lappas and R. van Leeuwen, Electron correlation effects in the double ionization of He, J. Phys. B **31**, L249 (1998).

[35] M. Lein and S. Kümmel, Exact Time-Dependent Exchange-Correlation Potentials for Strong-Field Electron Dynamics, Phys. Rev. Lett. **94**, 143003 (2005).

[36] F. Wilken and D. Bauer, Adiabatic Approximation of the Correlation Function in the Density-Functional Treatment of Ionization Processes, Phys. Rev. Lett. **97**, 203001 (2006).

[37] J. C. Baggesen and L. B. Madsen, On the dipole, velocity and acceleration forms in high-order harmonic generation from a single atom or molecule, J. Phys. B **44**, 115601 (2011).

[38] M. B. Gaarde, C. Buth, J. L. Tate, and K. J. Schafer, Transient absorption and reshaping of ultrafast xuv light by laser-dressed helium, Phys. Rev. A **83**, 013419 (2011).

[39] Z. Q. Yang, D. F. Ye, T. Ding, T. Pfeifer, and L. B. Fu, Attosecond xuv absorption spectroscopy of doubly excited states in helium atoms dressed by a time-delayed femtosecond infrared laser, Phys. Rev. A **91**, 013414 (2015).

[40] D. J. Diestler, Harmonic generation: Quantum-electrodynamical theory of the harmonic photon-number spectrum, Phys. Rev. A **78**, 033814 (2008).

[41] N. T. Maitra, F. Zhang, R. J. Cave, and K. Burke, Double excitations within time-dependent density functional theory linear response, J. Chem. Phys. **120**, 5932 (2004).

[42] M. Lewenstein, P. Balcou, M. Y. Ivanov, A. L'Huillier, and P. B. Corkum, Theory of high-harmonic generation by low-frequency laser fields, Phys. Rev. A **49**, 2117 (1994).

[43] P. Koval, F. Wilken, D. Bauer, and C. H. Keitel, Nonsequential Double Recombination in Intense Laser Fields, Phys. Rev. Lett. **98**, 043904 (2007).

2.5. Paper 5

Time-dependent renormalized-natural-orbital theory applied to laser-driven H_2^+.

Physical Review A 93, 043414:1–8 (2016)

DOI:http://dx.doi.org/10.1103/PhysRevA.93.043414

Author contributions

Adrian Hanusch	Theory extension, preparation of manuscript, programming, calculations, figure preparations.
Julius Rapp	Supervision, technical advices.
Martins Brics	Check of EOM, suggestions.
Dieter Bauer	Finalization of manuscript, co-supervision.

PHYSICAL REVIEW A **93**, 043414 (2016)

Time-dependent renormalized-natural-orbital theory applied to laser-driven H_2^+

A. Hanusch, J. Rapp, M. Brics, and D. Bauer*
Institut für Physik, Universität Rostock, 18051 Rostock, Germany
(Received 5 February 2016; published 19 April 2016)

Recently introduced time-dependent renormalized-natural-orbital theory (TDRNOT) is extended towards a multicomponent approach in order to describe H_2^+ beyond the Born-Oppenheimer approximation. Two kinds of natural orbitals, describing the electronic and the nuclear degrees of freedom are introduced, and the exact equations of motion for them are derived. The theory is benchmarked by comparing numerically exact results of the time-dependent Schrödinger equation for an H_2^+ model system with the corresponding TDRNOT predictions. Ground-state properties, linear-response spectra, fragmentation, and high-order harmonic generation are investigated.

DOI: 10.1103/PhysRevA.93.043414

I. INTRODUCTION

Simulating laser-driven N-particle systems truly *ab initio*, i.e., by solving the time-dependent Schrödinger equation (TDSE), is only possible for very small N. As more and more experiments are performed in the intense-laser, ultrashort-pulse regime [1,2], efficient time-dependent many-body methods, applicable beyond linear response, are needed. A widely used approach is time-dependent density functional theory (TDDFT) [3–5], in which the single-particle density $n(\vec{r},t)$ is used as the basic variable. This quantity is, in principle, sufficient to calculate every observable of a time-dependent quantum system [3,6]. However, while the scaling of the computational effort is favorable for TDDFT, a generally unknown exchange-correlation (XC) functional is involved that needs to be approximated. Especially, the often-used adiabatic XC functionals often miss correlation effects [7–9]. Additionally, not all observables are known as functionals of $n(\vec{r},t)$ (an example being correlated photoelectron spectra [10]), meaning that even if the exact single-particle density $n(\vec{r},t)$ was reproduced by TDDFT, the interesting observables measured in nowadays intense-laser matter experiments could not be reproduced. Other approaches, e.g., multiconfigurational time-dependent Hartree-Fock (MCTDHF) [11,12] or time-dependent configuration interaction (TDCI) [13–17] do not suffer from these difficulties, however, at a price of much higher computational cost.

When applying many-body methods to molecular systems, the Born-Oppenheimer (BO) approximation is often employed, or the nuclei are even treated classically. However, for an accurate description of molecules in, e.g., strong laser fields, the nuclei should be treated fully quantum mechanically beyond BO. Especially in the case of fragmentation of molecules in intense laser fields the adiabatic BO approximation may break down as electronic and nuclear energy scales are not well separated at avoided crossings or conical intersections. Several approaches aiming at the description of correlated electron-nuclear dynamics beyond the BO approximation were presented in the last few years, e.g., the exact factorization of the molecular wave function [18–20], a multiconfigurational time-dependent Hartree (Fock) approach [MCTDH(F)] [21–23], or a multicomponent extension of (TD)DFT [MC(TD)DFT] [24–26], which, besides the single-particle electron density, also takes the diagonal of the nuclear density matrix into account.

In this paper, we extend the recently introduced time-dependent renormalized-natural-orbital theory (TDRNOT) [27–30] towards the simplest molecular system, H_2^+, taking both the electronic and nuclear degrees of freedom fully quantum mechanically into account. We restrict ourselves to a low-dimensional H_2^+ model system [20,23,26,31–34] in order to have the TDSE benchmark results readily available. However, the TDRNOT equations derived in this work are easily generalized to the real, three-dimensional (3D) H_2^+.

The basic quantities of our theory are the so-called natural orbitals (NOs), introduced by Löwdin as the eigenfunctions of the one-body reduced density matrix (1-RDM) [35]. Equations of motion (EOM) for the NOs can be derived. However, as each NO is defined up to a phase factor only, the EOM are not unique. This phase freedom can be employed to the computational benefit and to remove seeming singularities. Renormalizing NOs amounts to normalizing them to their eigenvalues, which simplifies an exactly unitary propagation [28]. TDRNOT has been applied to a model two-electron atom and performed well in treating phenomena where TDDFT with known and practicable XC functionals fails [28–30]. As the NOs are proven to form the best possible basis for two-electron systems [36], the hope is that TDRNOT provides a means to treat bigger systems in a computationally economic way as well.

The paper is structured as follows. The H_2^+ model system and the basic properties of the reduced density matrices and NOs of a two-component system are introduced in Sec. II. The EOM for the NOs are presented in Sec. III. In Sec. IV we benchmark TDRNOT by first calculating ground-state properties and linear-response spectra. Second, the interaction with intense laser pulses is simulated, with the focus on the fragmentation dynamics and high-order harmonic generation (HHG). Finally, in Sec. V we give a conclusion.

Atomic units (a.u.) are used throughout unless noted otherwise.

*Corresponding author: dieter.bauer@uni-rostock.de

II. NATURAL-ORBITAL THEORY FOR A TWO-COMPONENT SYSTEM

A. Model system

We apply TDRNOT to the widely used one-dimensional H_2^+ model system [20,23,26,31–34]. This collinear model utilizes the fact that the ionization and dissociation dynamics of H_2^+ is predominantly constrained to the polarization direction when interacting with a strong, linearly polarized laser field. The reduced dimensionality permits the exact numerical solution of the TDSE at relatively low computational cost, and thus efficient benchmarking of TDRNOT.

The Hamiltonian of the H_2^+ model system (in dipole approximation and length gauge) reads

$$\hat{H}(x,R,t) = \hat{h}_\mathrm{e} + \hat{h}_\mathrm{n} + V_\mathrm{en}(x,R), \tag{1}$$

where

$$\hat{h}_\mathrm{e}(x,t) = -\frac{1}{2\,\mu_\mathrm{e}}\,\partial_x^2 + q_e\,x\,E(t) \tag{2}$$

$$\hat{h}_\mathrm{n}(R) = -\frac{1}{2\,\mu_\mathrm{n}}\,\partial_R^2 + V_\mathrm{nn}(R). \tag{3}$$

x and R denote the electron coordinate and the internuclear distance, respectively. We introduce $\hat{h}_\mathrm{e}$ and $\hat{h}_\mathrm{n}$ as the single-particle Hamiltonians for the electronic and nuclear degree of freedom, respectively. Furthermore, $\mu_\mathrm{e} = 2\,M/(2\,M+1)$ (with the proton mass $M \simeq 1836$) and $\mu_\mathrm{n} = M/2$ denote the reduced masses of the electron and the nuclei, respectively, and $q_\mathrm{e} = (2\,M+2)/(2\,M+1)$ is the reduced charge.

The interaction potentials are modeled by soft-core potentials in order to eliminate the singularities:

$$V_\mathrm{en}(x,R) = -\frac{1}{\sqrt{\left(x-\frac{R}{2}\right)^2+\varepsilon_\mathrm{en}^2}} - \frac{1}{\sqrt{\left(x+\frac{R}{2}\right)^2+\varepsilon_\mathrm{en}^2}}, \tag{4}$$

$$V_\mathrm{nn}(R) = \frac{1}{\sqrt{R^2+\varepsilon_\mathrm{nn}^2}}. \tag{5}$$

The softening parameters are set to $\varepsilon_\mathrm{en}^2 = 1$ and $\varepsilon_\mathrm{nn}^2 = 0.03$.

To describe the model system in terms of NOs it is useful to expand the wave function in orthonormal single-particle wave functions describing the electronic and nuclear degree of freedom. The Schmidt decomposition [37] ensures that only a single summation is necessary for this expansion,

$$\Psi(x,R,t) = \sum_k c_k(t)\,\varphi_k(x,t)\,\eta_k(R,t). \tag{6}$$

B. Density matrices and natural orbitals

Let us start from the pure density matrix

$$\hat{\gamma}_{1,1}(t) = |\Psi(t)\rangle\,\langle\Psi(t)|\,. \tag{7}$$

Unlike in the two-electron case [28] the pure two-body density matrix (2-DM) is a multicomponent object in the case of H_2^+. Due to the two distinguishable degrees of freedom, different 1-RDMs are obtained, depending on which degree of freedom is traced out,

$$\hat{\gamma}_{1,0}(t) = \mathrm{Tr}_\mathrm{n}\,\hat{\gamma}_{1,1}(t), \tag{8}$$

$$\hat{\gamma}_{0,1}(t) = \mathrm{Tr}_\mathrm{e}\,\hat{\gamma}_{1,1}(t). \tag{9}$$

As the NOs and occupation numbers (ONs) are defined as the eigenstates and eigenvalues of the 1-RDM, respectively, two different kinds of orbitals are expected:

$$\hat{\gamma}_{1,0}(t)\,|k(t)\rangle = n_k(t)\,|k(t)\rangle \tag{10}$$

$$\hat{\gamma}_{0,1}(t)\,|K(t)\rangle = N_K(t)\,|K(t)\rangle. \tag{11}$$

Throughout this paper, we will use lowercase letters for electronic NOs and uppercase for nuclear NOs.

Inserting Eq. (6) into Eqs. (7)–(11) leads to the conclusion that the single-particle wave functions in Eq. (6) are the electronic and nuclear NOs,

$$\varphi_k(x,t) = \langle x|k(t)\rangle\,, \qquad \eta_k(R,t) = \langle R|K(t)\rangle\,, \tag{12}$$

respectively. The expansion coefficients in Eq. (6) can be expressed in terms of the ONs,

$$c_k(t) = \sqrt{n_k(t)}\,e^{i\phi_k(t)}, \tag{13}$$

i.e., they are defined up to a phase factor. Additionally, one finds the constraint

$$n_k(t) = N_K(t). \tag{14}$$

Hence, ONs of each pair of electronic and nuclear NOs have to be equal at any time, despite their distinguishability.

For a numerical propagation it is beneficial to introduce renormalized natural orbitals (RNOs)

$$|\tilde{k}(t)\rangle = \sqrt{n_k(t)}\,|k(t)\rangle\,, \quad |\tilde{K}(t)\rangle = \sqrt{N_K(t)}\,|K(t)\rangle \tag{15}$$

in order to unify the coupled equations of motion for the ONs and NOs and thus propagate only one combined quantity. In terms of RNOs

$$\hat{\gamma}_{1,0}(t) = \sum_k |\tilde{k}(t)\rangle\,\langle\tilde{k}(t)|\,. \tag{16}$$

In the same way $\hat{\gamma}_{0,1}(t)$ can be expanded in nuclear RNOs. The multicomponent 2-DM $\hat{\gamma}_{1,1}$ expanded in RNOs reads

$$\hat{\gamma}_{1,1}(t) = \sum_{iJkL} \tilde{\gamma}_{iJkL}(t)\,|\tilde{i}(t),\tilde{J}(t)\rangle\,\langle\tilde{k}(t),\tilde{L}(t)|. \tag{17}$$

The expansion coefficients $\tilde{\gamma}_{iJkL}(t)$ are exactly known in the case of a two-particle system like helium [28]. But also for any other systems with two degrees of freedom

$$\tilde{\gamma}_{iJkL}(t) = \frac{1}{\sqrt{n_i(t)\,n_k(t)}}\,\delta_{i,J}\,\delta_{k,L} \tag{18}$$

holds.

By definitions (10), (11) the NOs are determined only up to an orbital-dependent factor. Assuming the NOs to be normalized (e.g., to unity) there remains still the freedom to choose an orbital-dependent phase factor. Such a choice, however, will affect the phase factors $e^{i\phi_k(t)}$ in the expansion (6) of $\Psi(x,R,t)$. The phase freedom of the NOs thus allows for a phase transformation leading to tunable, constant phases (for more details see Ref. [28]), and all time dependencies are then incorporated in the so-called phase-including natural orbitals (PINOs) [38–40]. Moreover, as already noted in Ref. [28], even after shifting all time dependencies from the phase factor to the NOs there is still the freedom to distribute this phase arbitrarily between each pair of orbitals in the product $\varphi_k(x,t)\,\eta_k(R,t)$.

The time evolution of the electronic NOs can be formally expanded as

$$i\,\partial_t\,|k(t)\rangle = \sum_m \alpha_{km}(t)\,|m(t)\rangle \tag{19}$$

(analogously for the nuclear NOs). Different phase choices translate to different diagonal elements $\alpha_{kk}(t)$ and $\alpha_{KK}(t)$.

III. EQUATIONS OF MOTION

Starting from the EOM of the 2-DM and with the knowledge of the expansions of the 1-RDM and 2-DM in RNOs, exact equations of motion for the two types of RNOs can be derived. The electronic RNOs evolve (all time arguments are suppressed for the sake of brevity) according to

$$i\,\partial_t\,|\tilde{n}\rangle = \hat{h}_\mathrm{e}\,|\tilde{n}\rangle + \mathcal{A}_n\,|\tilde{n}\rangle + \sum_{k\neq n}\mathcal{B}_{nk}\,|\tilde{k}\rangle + \sum_k \hat{\mathcal{C}}_{nk}\,|\tilde{k}\rangle \tag{20}$$

with the coefficients

$$\mathcal{A}_n = \frac{\beta_n - 1}{n_n}\,\mathrm{Re}\sum_{pJL}\tilde{\gamma}_{nJpL}\,\langle\tilde{p}\tilde{L}|\hat{V}_\mathrm{en}|\tilde{n}\tilde{J}\rangle\,, \tag{21a}$$

$$\mathcal{B}_{nk} = \frac{1}{n_n - n_k}\sum_{pJL}[\tilde{\gamma}_{pLnJ}\,\langle\tilde{k}\tilde{J}|\hat{V}_\mathrm{en}|\tilde{p}\tilde{L}\rangle - \tilde{\gamma}_{kJpL}\,\langle\tilde{p}\tilde{L}|\hat{V}_\mathrm{en}|\tilde{n}\tilde{J}\rangle], \tag{21b}$$

$$\hat{\mathcal{C}}_{nk} = \sum_{JL}\tilde{\gamma}_{kJnL}\,\langle\tilde{L}|\hat{V}_\mathrm{en}|\tilde{J}\rangle\,, \tag{21c}$$

while the EOM for the nuclear RNOs is of a similar form:

$$i\,\partial_t\,|\tilde{N}\rangle = \hat{h}_\mathrm{n}\,|\tilde{N}\rangle + \mathcal{A}_N\,|\tilde{N}\rangle + \sum_{K\neq N}\mathcal{B}_{NK}\,|\tilde{K}\rangle + \sum_K \hat{\mathcal{C}}_{NK}\,|\tilde{K}\rangle \tag{22}$$

with

$$\mathcal{A}_N = -\frac{\beta_n}{N_N}\,\mathrm{Re}\sum_{ijL}\tilde{\gamma}_{iNjL}\,\langle\tilde{j}\tilde{L}|\hat{V}_\mathrm{en}|\tilde{i}\tilde{N}\rangle\,, \tag{23a}$$

$$\mathcal{B}_{NK} = \frac{1}{N_N - N_K}\sum_{ijL}[\tilde{\gamma}_{jLiN}\,\langle\tilde{i}\tilde{K}|\hat{V}_\mathrm{en}|\tilde{j}\tilde{L}\rangle - \tilde{\gamma}_{iKjL}\,\langle\tilde{j}\tilde{L}|\hat{V}_\mathrm{en}|\tilde{i}\tilde{N}\rangle], \tag{23b}$$

$$\hat{\mathcal{C}}_{NK} = \sum_{ij}\tilde{\gamma}_{iKjN}\,\langle\tilde{j}|\hat{V}_\mathrm{en}|\tilde{i}\rangle\,. \tag{23c}$$

In order to fulfill the constraint given in Eq. (14) at any time also $\dot{n}_i(t) = \dot{N}_I(t)$ has to hold. While this condition is automatically fulfilled during real-time propagation, the distribution of the phase between each pair of orbitals has to be chosen in a particular way during imaginary-time propagation in order to find the true ground state of the system. To that end the parameters

$$\beta_n = \frac{1}{2}\,\mathrm{Re}\left[\frac{\langle\tilde{N}|\hat{h}_\mathrm{n}|\tilde{N}\rangle - \langle\tilde{n}|\hat{h}_\mathrm{e}|\tilde{n}\rangle}{\sum_{k,K}\frac{1}{\sqrt{n_n n_k}}\,\langle\tilde{n}\tilde{N}|\hat{V}_{en}|\tilde{k}\tilde{K}\rangle\,\delta_{k,K}} + 1\right] \tag{24}$$

during imaginary-time propagation are introduced (arbitrary real β_n can be chosen during real-time propagation; we simply took $\beta_n = 1/2$).

The EOM are exact for an infinite number of RNOs. However, in a numerical implementation it is necessary to restrict the number of orbitals to a finite value N_o. This truncation introduces errors in the propagation. We will therefore analyze the effect of the truncation by comparing to the corresponding exact results obtained by propagating the full many-body wave function according to the TDSE. In particular, we may extract the correct, truncation-free NOs by diagonalizing the exact 1-RDMs.

IV. RESULTS

In this section, we first benchmark ground-state results for the $H_2{}^+$ model obtained with TDRNOT in imaginary time against the TDSE result. Second, as the simplest real-time propagation application, linear-response spectra are calculated for different N_o and compared to the reference TDSE result. Finally, we consider the interaction with a short, intense laser pulse.

A. Ground state

The ground-state energies obtained from a TDRNOT imaginary-time propagation of N_o orbitals per degree of freedom are presented in Table I, together with the exact value from the TDSE.

Clearly, the TDRNOT ground-state energy converges to the exact value for increasing N_o, and only a few RNOs are needed to obtain excellent agreement. The ONs show a behavior expected for the ground state: The first orbital is highly occupied with an ON close to one while the ONs for higher orbitals decrease rapidly with increasing orbital index.

Using only one orbital per degree of freedom ($N_\mathrm{o} = 1$) TDRNOT corresponds to an uncorrelated time-dependent Hartree (TDH) approach [41]. The ground-state energy is already reasonably accurate. However, it is known that the TDH approach fails to describe dissociation, as the nuclear potential is only well approximated around the equilibrium internuclear distance [23,26,41].

Not only the ground-state energy but also the correlated ground-state probability density is in excellent agreement if enough RNOs are taken into account, as shown in Fig. 1.

TABLE I. Energies and ONs of the ground state obtained from imaginary-time propagation using different N_o. The exact TDSE results are presented for comparison. With increasing N_o the values converge to the exact results.

	Total energy	Dominant occupation numbers			
N_o	E_0 [a.u.]	n_1	$n_2\,/10^{-3}$	$n_3\,/10^{-6}$	$n_4\,/10^{-8}$
1	−0.774 84	1.000 00			
2	−0.776 36	0.997 75	2.255		
4	−0.776 38	0.997 70	2.291	8.330	4.685
8	−0.776 38	0.997 70	2.291	8.332	4.746
TDSE	−0.776 38	0.997 70	2.291	8.332	4.746

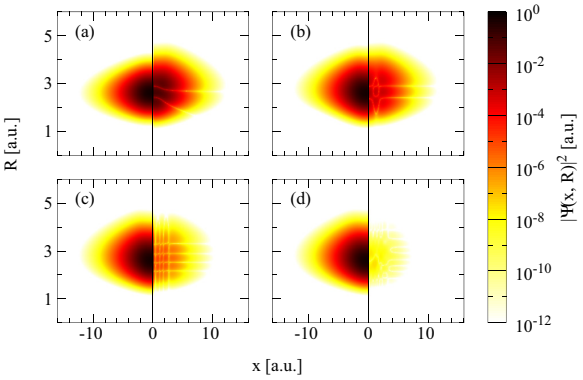

FIG. 1. Plot of the correlated ground-state probability density $|\Psi(x,R)|^2$ for (a) $N_o = 1$, (b) $N_o = 2$, (c) $N_o = 4$, and (d) $N_o = 8$ for negative values of x. For $x > 0$ the absolute difference to the exact probability density is plotted.

A gridlike structure is apparent in the differences between the TDRNOT ground-state probability densities and the exact TDSE density. This structure is related to the location of the nodal lines of the most significant RNO not included in the TDRNOT calculation.

B. Linear-response spectrum

In order to obtain linear-response spectra, the initial ground-state RNOs are propagated in real time for $t_{max} = 2000$ after a kick with a small electric field ($E = 0.0001$). An imaginary potential is enabled to prevent reflection of the density at the boundaries of the grid. Fourier transforming the time-dependent dipole expectation value $d(t)$,

$$d(t) = -\langle\Psi(t)|q_e\hat{x}|\Psi(t)\rangle = -\sum_n q_e \langle\tilde{n}(t)|\hat{x}|\tilde{n}(t)\rangle, \quad (25)$$

leads to a spectrum which exhibits peaks at energy differences $E - E_0$ of dipole-allowed transitions. The resulting spectra calculated from TDRNOT propagations with different N_o as well as the reference spectrum from a TDSE calculation are depicted in Fig. 2.

A severe difference between the exact and the TDRNOT result is apparent. As the electronic first excited state (in the BO picture) is dissociative, a broad continuous feature is visible in the exact spectrum. This is also the case for other electronic transitions. In contrast to HD^+ [26], vibrational excitations have vanishing dipole oscillator strengths. Hence, no excitations at low energies are visible. The results from the TDRNOT calculations show a different behavior: Discrete peaks are observed instead of a continuum. The number of peaks increases with the number of RNOs used in the calculation. In contrast to the helium model atom—where including more RNOs leads to the appearance of peaks describing series of doubly excited states [28]—in the molecular case several of the emerging discrete peaks can be assigned to the same electronic transition. The increasing number of discrete transitions should finally result in a continuous spectrum if enough orbitals are taken into account. For the TDH case $N_o = 1$ this behavior has already been observed [23,26,41]. Using the

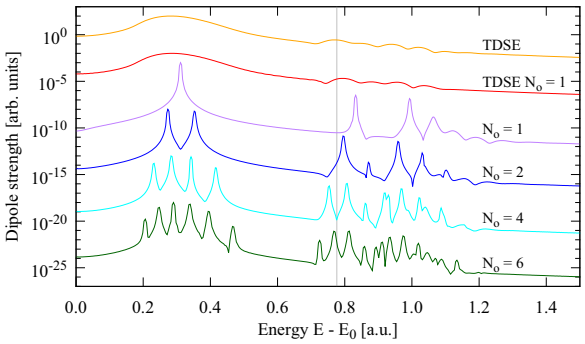

FIG. 2. Linear-response spectra obtained from TDRNOT calculations with different numbers of RNOs N_o compared to the exact TDSE result. Each spectrum is normalized to one, and the spectra are shifted vertically by factors of 10^{-5} in order to make them distinguishable.

Hartree approximation, only one sharp peak—corresponding to a transition to a bound state—appears in the spectrum for the first electronic transition. The reason for this erroneous behavior is the wrong shape of the nuclear potential in this case (see, e.g., Refs. [26,41]).

As stated before, the restriction to a finite number of RNOs introduces a truncation error. Truncation-error-free reference results for a given N_o can be obtained by diagonalization of the exact 1-RDM (from the TDSE). The resulting spectrum from only one truncation-error-free NO (labeled with TDSE $N_o = 1$) is also shown in Fig. 2. It almost completely coincides with the full exact result. One thus can conclude that almost all important information is already included in the first dominant RNO. However, due to the coupling between RNOs in the TDRNOT EOM all other RNOs are important during the propagation.

C. H_2^+ in intense laser fields

Many different processes influence the fragmentation dynamics of molecules subjected to intense laser fields, e.g., bond softening [42], above-threshold dissociation (ATD) [43], bond hardening or vibrational trapping [44], charge-resonance-enhanced ionization [45], and the retroaction due to the long-range Coulomb potential [46]. We want to further benchmark TDRNOT by investigating its ability to describe nonperturbative phenomena far from equilibrium. As the theory is aiming to describe strong-field laser-matter interaction, we study the fragmentation of H_2^+ upon the interaction with a short, intense laser pulse. Furthermore, HHG spectra are calculated.

1. Dissociation and ionization

An infrared 800-nm four-cycle pulse with a $\sin^2$ envelope and a peak intensity of $I_0 = 10^{14}\,\mathrm{W/cm^2}$ was applied to the H_2^+ model system. Upon the interaction with an intense laser pulse, fragmentation can occur due to dissociation or dissociative ionization (DI). In the latter case the removal of the electron leads to Coulomb explosion as the nuclei fly apart due to their Coulomb repulsion. In order to judge whether the different fragmentation processes can be reproduced with TDRNOT, we analyze the time-dependent nuclear probability

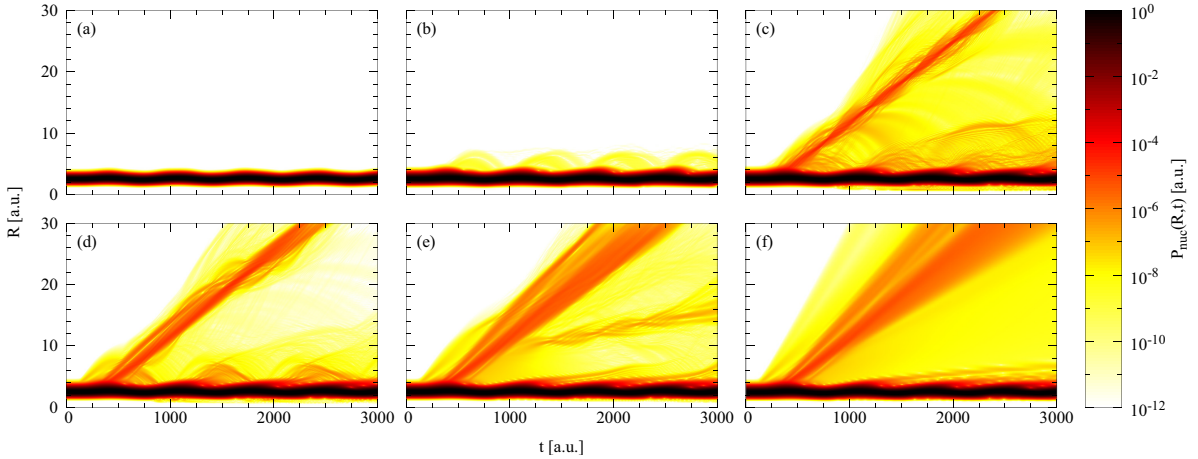

FIG. 3. Time-dependent nuclear probability density upon the interaction with an 800-nm four-cycle pulse with $I_0 = 10^{14}\,\mathrm{W/cm^2}$. Again different numbers of orbitals were used: (a) $N_o = 1$, (b) $N_o = 2$, (c) $N_o = 4$, (d) $N_o = 8$, and (e) $N_o = 10$. With more RNOs included, the agreement with the exact result of the TDSE, given in (f), is considerably improved.

density,

$$P_{\mathrm{nuc}}(R,t) = \int \mathrm{d}x\, |\Psi(x,R,t)|^2 = \sum_k |\tilde{\eta}_k(R,t)|^2. \qquad (26)$$

Figure 3 shows the logarithmically scaled, time-dependent nuclear probability density $P_{\mathrm{nuc}}(R,t)$ resulting from TDRNOT calculations. The TDSE reference result is included for comparison in Fig. 3(f). In the latter figure a many-fold jetlike structure becomes apparent, which can be attributed to dissociation. Due to ATD—the absorption of more photons than needed—dissociation channels with different kinetic energies of the fragments appear. In the TDH case $N_o = 1$, however, the time-dependent nuclear probability density shows no indication of dissociation at all [Fig. 3(a)]. This erroneous behavior is due to the wrong shape of the effective nuclear potential again (see Fig. 1 in Ref. [41]). Vibrations around the equilibrium internuclear distance are already reproduced though. A TDRNOT calculation with $N_o = 2$ does not lead to a much improved result. However, four RNOs are sufficient for reproducing dissociation, as the most prominent jet is clearly visible, although the broadening is not yet in good agreement with $P_{\mathrm{nuc}}(R,t)$ obtained from the TDSE. As expected, including more orbitals leads to a better agreement with the exact result. A second jet corresponding to dissociation upon the absorption of a different number of photons is already clearly visible in the $N_o = 8$ density, and with two more orbitals the broadening improves. However, an erroneous structure emerges at intermediate internuclear distances $10 < R < 20$, which vanishes with even more RNOs (not shown).

The kinetic energy release (KER) in the nuclear fragments for dissociation and DI can be calculated from the RNOs by means of the virtual-detector method [33,47]. To that end we reconstruct the wave function from the RNOs and then follow Ref. [33]. The resulting KER spectra obtained with ten RNOs per degree of freedom are compared with the corresponding TDSE benchmark results in Fig. 4(a).

Regarding dissociation, multiple peaks at energies $E_{\mathrm{kin}} < 0.2$ are observed. The most distinct peaks are separated by roughly the photon energy and can be assigned to three- and four-photon ATD, respectively. These processes were found to be dominant also for longer pulses of the same wavelength and intensity [48]. The expected positions of the peaks (using the BO-approximation and assuming the vibrational ground state) in the spectrum can be calculated using a simple energy conservation formula [32]. These positions are depicted as vertical gray lines in Fig. 4(a). The spectrum obtained from the TDRNOT calculation has a structure similar to the exact one—heights and positions of the peaks coincide approximately with the exact results.

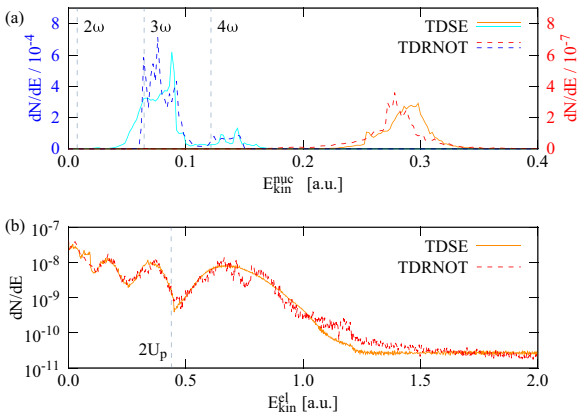

FIG. 4. Energy spectra for nuclei and photoelectrons, calculated using the (extended) virtual-detector method. The laser parameters are the same as in Fig. 3. (a) Kinetic-energy spectra of the nuclei for dissociation (blue) and DI (red). The vertical gray lines denote 2ω, 3ω, and 4ω absorption from the vibrational ground state. (b) TDRNOT photoelectron spectrum for 10 RNOs per degree of freedom (red, dashed) compared to the exact result from the TDSE (orange, solid).

However, in the TDRNOT spectrum several discrete peaks are visible for the three-photon dissociation instead of the broad, continuous energy distribution in the exact spectrum. Moreover, there are discrepancies for lower energies, and the two-photon dissociation is missing completely.

The KER spectrum in the case of DI is, as the Coulomb energy is released, centered around higher energies $E_{\mathrm{kin}} > 0.2$. Note the different scaling of the ordinate as the ionization yield is several orders of magnitude below the dissociation yield. There are slight deviations of TDRNOT from the exact result—the spectrum obtained from TDRNOT is shifted towards lower energies—but the general structure of the spectrum is reproduced.

Furthermore, in the case of DI, we calculate electronic kinetic-energy spectra using the extended virtual-detector method [49]. Starting from the virtual detectors, classical trajectories are calculated in order to obtain the final momentum of the electron at the end of the laser pulse. The results are presented in Fig. 4(b). For both the TDRNOT and the TDSE results, a modulation in the yield, depending on $E_{\mathrm{kin}}^{\mathrm{el}}$, is visible. This can be attributed to the interference of quantum trajectories starting at different ionization times, which lead to the same final momentum [50,51]. In the case of the electronic kinetic-energy spectrum, the agreement between the results from a TDRNOT calculation with $N_{\mathrm{o}} = 10$ and the exact result is clearly better than for the KER spectra. This shows that different minimum numbers of RNOs are required, depending on the observable to calculate.

2. *HHG spectra*

Harmonic spectra are obtained by Fourier transforming the time-dependent dipole acceleration $\ddot{d}(t)$ [52], which is given by

$$\frac{\mu_{\mathrm{e}}}{q_{\mathrm{e}}}\,\ddot{d}(t) = \int dx \int dR\,|\Psi(x,R,t)|^2\,\frac{\partial V_{\mathrm{en}}}{\partial x} + q_{\mathrm{e}}\,E(t). \quad (27)$$

An 800-nm 10-cycle pulse with $\sin^2$-shaped on and off ramping over two cycles was employed. The peak intensity of the laser pulse was $I_0 = 3.0 \times 10^{14}\,\mathrm{W/cm^2}$. In Fig. 5, TDRNOT HHG spectra, calculated using 1–8 RNOs per degree of freedom, are compared to the exact TDSE spectrum. In the inset, a part of the spectrum is plotted on a linear scale.

With only one RNO the position of the cutoff is already in good agreement with the exact result. However, the shape of individual peaks, especially at high harmonic order, is completely wrong. The TDRNOT calculation with $N_{\mathrm{o}} = 2$ exhibits erroneous peaks in addition to the peaks at the odd harmonics, especially pronounced in the region beyond the cutoff. When adding more RNOs the quantitative agreement improves, and the wrong peaks vanish. A similar improvement with increasing number of single-particle functions has been reported for calculations using an MCTDH approach [23]. For $N_{\mathrm{o}} = 8$ the height and the shape of the peaks are well reproduced up to the 60th harmonic order. At very high harmonic orders some deviations in the spectra are still visible, and the noise level of the TDRNOT results is two orders of magnitude higher than for the TDSE. A similar behavior was observed for HHG in a model He atom [30]. On a linear scale, as often used in experiments, the agreement is excellent and clearly improves with increasing N_{o} (see insets in Fig. 5).

V. CONCLUSION

We have investigated the performance of time-dependent renormalized-natural-orbital theory (TDRNOT) when applied to the simplest multicomponent system exhibiting electron-nuclear correlation, i.e., $H_2{}^+$. Different types of renormalized natural orbitals (RNOs), describing the electronic and the nuclear component, were introduced, and their coupled equations of motion derived. As in the case of helium investigated earlier no approximations concerning the expansion of the time-dependent two-body density matrix need to be made.

In order to benchmark the theory the ground state of a one-dimensional $H_2{}^+$ model system and linear-response spectra were calculated using TDRNOT. While an excellent agreement with the exact ground-state energy was achieved with very few

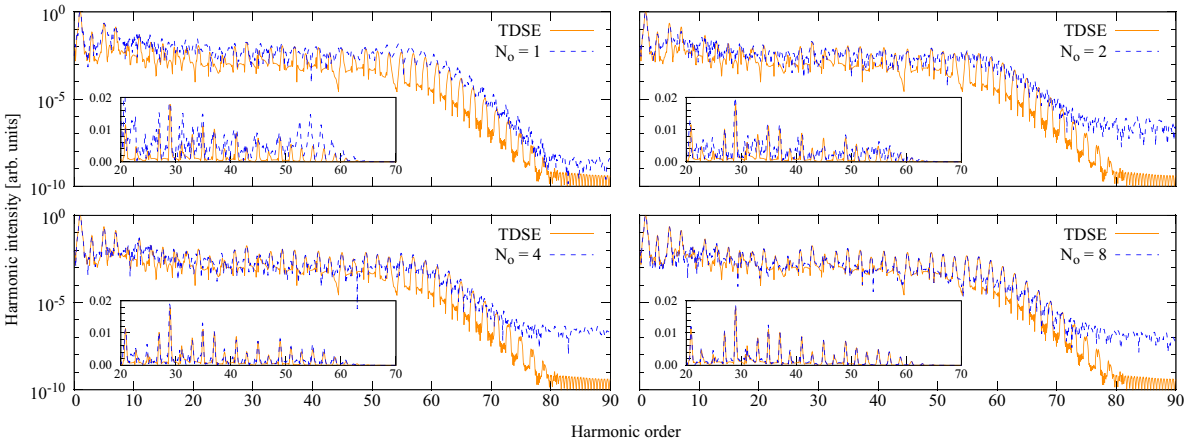

FIG. 5. HHG spectra for an 800-nm 10-cycle flat-top pulse with $I_0 = 3.0 \times 10^{14}\,\mathrm{W/cm^2}$ calculated with TDRNOT using 1, 2, 4, and 8 RNOs per degree of freedom compared to the exact spectrum obtained from the TDSE. The insets show a section of each spectrum plotted on a linear scale.

orbitals, the linear-response spectra were plagued by multiple sharp peaks that only for very many orbitals would reproduce the correct, broad structure caused by bound-continuum transitions. This unpleasant feature is caused by the restriction to a finite number of orbitals, which introduces a truncation error. Future work will be devoted to improve on that aspect of TDRNOT.

Finally, TDRNOT was applied to H_2^+ interacting with a short, intense laser pulse. The time evolution of the nuclear probability density was studied, and features indicating different fragmentation processes were identified. It was found that TDRNOT is able to reproduce dissociation and Coulomb explosion and the corresponding kinetic-energy-release spectra if enough RNOs are taken into account. The same applies to high-harmonics spectra where eight RNOs were found to yield very good agreement with the benchmark result from the time-dependent Schrödinger equation.

ACKNOWLEDGMENTS

This work was supported by the Collaborative Research Center SFB 652 of the German Science Foundation (DFG).

[1] *Attosecond and XUV Spectroscopy: Ultrafast Dynamics and Spectroscopy*, edited by T. Schultz and M. Vrakking (Wiley-VCH, Weinheim, 2014).

[2] *Progress in Ultrafast Intense Laser Science IX*, edited by K. Yamanouchi and K. Midorikawa (Springer, Heidelberg, 2013).

[3] C. A. Ullrich, *Time-Dependent Density-Functional Theory: Concepts and Applications* (Oxford University Press, Oxford, 2011).

[4] M. A. L. Marques, C. A. Ullrich, F. Nogueira, A. Rubio, K. Burke, and E. K. U. Gross, *Time-Dependent Density Functional Theory*, Lect. Notes Phys., Vol. 706 (Springer, Berlin Heidelberg, 2006).

[5] K. Burke, J. Werschnik, and E. K. U. Gross, Time-dependent density functional theory: Past, present, and future, J. Chem. Phys. **123**, 062206 (2005).

[6] E. Runge and E. K. U. Gross, Density-Functional Theory for Time-Dependent Systems, Phys. Rev. Lett. **52**, 997 (1984).

[7] F. Wilken and D. Bauer, Adiabatic Approximation of the Correlation Function in the Density-Functional Treatment of Ionization Processes, Phys. Rev. Lett. **97**, 203001 (2006).

[8] M. Ruggenthaler and D. Bauer, Rabi Oscillations and Few-Level Approximations in Time-Dependent Density Functional Theory, Phys. Rev. Lett. **102**, 233001 (2009).

[9] N. Helbig, J. Fuks, I. Tokatly, H. Appel, E. K. U. Gross, and A. Rubio, Time-dependent density-functional and reduced density-matrix methods for few electrons: Exact versus adiabatic approximations, Chem. Phys. **391**, 1 (2011).

[10] F. Wilken and D. Bauer, Momentum distributions in time-dependent density-functional theory: Product-phase approximation for nonsequential double ionization in strong laser fields, Phys. Rev. A **76**, 023409 (2007).

[11] D. L. Yeager and P. Jørgensen, A multiconfigurational time-dependent hartree-fock approach, Chemical Physics Letters **65**, 77 (1979).

[12] J. Zanghellini, M. Kitzler, T. Brabec, and A. Scrinzi, Testing the multi-configuration time-dependent hartree–fock method, J. Phys. B: At., Mol. Opt. Phys. **37**, 763 (2004).

[13] P. Krause, T. Klamroth, and P. Saalfrank, Time-dependent configuration-interaction calculations of laser-pulse-driven many-electron dynamics: Controlled dipole switching in lithium cyanide, J. Chem. Phys. **123**, 074105 (2005).

[14] N. Rohringer, A. Gordon, and R. Santra, Configuration-interaction-based time-dependent orbital approach for *ab initio* treatment of electronic dynamics in a strong optical laser field, Phys. Rev. A **74**, 043420 (2006).

[15] P. Krause, T. Klamroth, and P. Saalfrank, Molecular response properties from explicitly time-dependent configuration interaction methods, J. Chem. Phys. **127**, 034107 (2007).

[16] L. Greenman, P. J. Ho, S. Pabst, E. Kamarchik, D. A. Mazziotti, and R. Santra, Implementation of the time-dependent configuration-interaction singles method for atomic strong-field processes, Phys. Rev. A **82**, 023406 (2010).

[17] A. Karamatskou, S. Pabst, Y.-J. Chen, and R. Santra, Calculation of photoelectron spectra within the time-dependent configuration-interaction singles scheme, Phys. Rev. A **89**, 033415 (2014).

[18] A. Abedi, N. T. Maitra, and E. K. U. Gross, Exact Factorization of the Time-Dependent Electron-Nuclear Wave Function, Phys. Rev. Lett. **105**, 123002 (2010).

[19] A. Abedi, N. T. Maitra, and E. K. U. Gross, Correlated electron-nuclear dynamics: Exact factorization of the molecular wavefunction, J. Chem. Phys. **137**, 22A530 (2012).

[20] Y. Suzuki, A. Abedi, N. T. Maitra, K. Yamashita, and E. K. U. Gross, Electronic Schrödinger equation with nonclassical nuclei, Phys. Rev. A **89**, 040501 (2014).

[21] M. Nest, The multi-configuration electron–nuclear dynamics method, Chem. Phys. Lett. **472**, 171 (2009).

[22] I. S. Ulusoy and M. Nest, The multi-configuration electron-nuclear dynamics method applied to LiH, J. Chem. Phys. **136**, 054112 (2012).

[23] C. Jhala and M. Lein, Multiconfiguration time-dependent hartree approach for electron-nuclear correlation in strong laser fields, Phys. Rev. A **81**, 063421 (2010).

[24] T. Kreibich and E. K. U. Gross, Multicomponent Density-Functional Theory for Electrons and Nuclei, Phys. Rev. Lett. **86**, 2984 (2001).

[25] T. Kreibich, R. van Leeuwen, and E. K. U. Gross, Multicomponent density-functional theory for electrons and nuclei, Phys. Rev. A **78**, 022501 (2008).

[26] O. Butriy, H. Ebadi, P. L. de Boeij, R. van Leeuwen, and E. K. U. Gross, Multicomponent density-functional theory for time-dependent systems, Phys. Rev. A **76**, 052514 (2007).

[27] M. Brics and D. Bauer, Time-dependent renormalized natural orbital theory applied to the two-electron spin-singlet case: Ground state, linear response, and autoionization, Phys. Rev. A **88**, 052514 (2013).

[28] J. Rapp, M. Brics, and D. Bauer, Equations of motion for natural orbitals of strongly driven two-electron systems, Phys. Rev. A **90**, 012518 (2014).

[29] M. Brics, J. Rapp, and D. Bauer, Nonsequential double ionization with time-dependent renormalized-natural-orbital theory, Phys. Rev. A **90**, 053418 (2014).

[30] M. Brics, J. Rapp, and D. Bauer, Strong-field absorption and emission of radiation in two-electron systems calculated with time-dependent natural orbitals, Phys. Rev. A **93**, 013404 (2016).

[31] K. C. Kulander, F. H. Mies, and K. J. Schafer, Model for studies of laser-induced nonlinear processes in molecules, Phys. Rev. A **53**, 2562 (1996).

[32] S. Chelkowski, C. Foisy, and A. D. Bandrauk, Electron-nuclear dynamics of multiphoton H_2^+ dissociative ionization in intense laser fields, Phys. Rev. A **57**, 1176 (1998).

[33] B. Feuerstein and U. Thumm, Fragmentation of $H_2{}^+$ in strong 800-nm laser pulses: Initial-vibrational-state dependence, Phys. Rev. A **67**, 043405 (2003).

[34] V. Mosert and D. Bauer, Dissociative ionization of $H_2{}^+$: Few-cycle effect in the joint electron-ion energy spectrum, Phys. Rev. A **92**, 043414 (2015).

[35] P.-O. Löwdin, Quantum theory of many-particle systems. I. Physical interpretations by means of density matrices, natural spin-orbitals, and convergence problems in the method of configurational interaction, Phys. Rev. **97**, 1474 (1955).

[36] K. J. H. Giesbertz, Are natural orbitals useful for generating an efficient expansion of the wave function?, Chem. Phys. Lett. **591**, 220 (2014).

[37] A. Pathak, *Elements of Quantum Computation and Quantum Communication* (CRC Press/Taylor and Francis, Boca Raton, FL, 2013), p. 92.

[38] K. J. H. Giesbertz, Ph.D. thesis, Free University Amsterdam, 2010; http://dare.ubvu.vu.nl/handle/1871/16289.

[39] K. J. H. Giesbertz, O. V. Gritsenko, and E. J. Baerends, Response calculations based on an independent particle system with the exact one-particle density matrix: Excitation energies, J. Chem. Phys. **136**, 094104 (2012).

[40] R. van Meer, O. V. Gritsenko, K. J. H. Giesbertz, and E. J. Baerends, Oscillator strengths of electronic excitations with response theory using phase including natural orbital functionals, J. Chem. Phys. **138**, 094114 (2013).

[41] T. Kreibich, R. van Leeuwen, and E. K. U. Gross, Time-dependent variational approach to molecules in strong laser fields, Chem. Phys. **304**, 183 (2004).

[42] P. H. Bucksbaum, A. Zavriyev, H. G. Muller, and D. W. Schumacher, Softening of the H_2^+ Molecular Bond in Intense Laser Fields, Phys. Rev. Lett. **64**, 1883 (1990).

[43] A. Giusti-Suzor, X. He, O. Atabek, and F. H. Mies, Above-Threshold Dissociation of H_2^+ in Intense Laser Fields, Phys. Rev. Lett. **64**, 515 (1990).

[44] A. Giusti-Suzor and F. H. Mies, Vibrational trapping and suppression of dissociation in intense laser fields, Phys. Rev. Lett. **68**, 3869 (1992).

[45] T. Zuo and A. D. Bandrauk, Charge-resonance-enhanced ionization of diatomic molecular ions by intense lasers, Phys. Rev. A **52**, R2511 (1995).

[46] M. Waitz, D. Aslitürk, N. Wechselberger, H. K. Gill, J. Rist, F. Wiegandt, C. Goihl, G. Kastirke, M. Weller, T. Bauer, D. Metz, F. P. Sturm, J. Voigtsberger, S. Zeller, F. Trinter, G. Schiwietz, T. Weber, J. B. Williams, M. S. Schöffler, L. P. H. Schmidt, T. Jahnke, and R. Dörner, Electron localization in dissociating $H_2{}^+$ by Retroaction of a Photoelectron Onto its Source, Phys. Rev. Lett. **116**, 043001 (2016).

[47] B. Feuerstein and U. Thumm, On the computation of momentum distributions within wavepacket propagation calculations, J. Phys. B.: At., Mol. Opt. Phys. **36**, 707 (2003).

[48] L.-Y. Peng, I. D. Williams, and J. F. McCann, Dissociation of H_2^+ from a short, intense, infrared laser pulse: proton emission spectra and pulse calibration, J. Phys. B.: At., Mol. Opt. Phys. **38**, 1727 (2005).

[49] X. Wang, J. Tian, and J. H. Eberly, Extended Virtual Detector Theory for Strong-Field Atomic Ionization, Phys. Rev. Lett. **110**, 243001 (2013).

[50] D. B. Milošević, G. G. Paulus, D. Bauer, and W. Becker, Above-threshold ionization by few-cycle pulses, J. Phys. B.: At., Mol. Opt. Phys. **39**, R203 (2006).

[51] D. G. Arbó, K. L. Ishikawa, K. Schiessl, E. Persson, and J. Burgdörfer, Intracycle and intercycle interferences in above-threshold ionization: The time grating, Phys. Rev. A **81**, 021403 (2010).

[52] K. Burnett, V. C. Reed, J. Cooper, and P. L. Knight, Calculation of the background emitted during high-harmonic generation, Phys. Rev. A **45**, 3347 (1992).

List of contributions

Publications

1. **M. Brics**, R. Mahnke, and R. Kühne, "Model of Vehicular Traffic by Hilliges and Weidlich Revisited", Proceedings of the conference *Traffic and Granular Flow '11*, 27–33, (2013). [cited 0 times]
2. **M. Brics**, J. Kaupuzs, and R. Mahnke, "Scaling Behavior of an Airplane Boarding Model", *Phys. Rev. E* **87**, 042117:1–5, (2013). [cited 7 times]
3. **M. Brics**, J. Kaupuzs, and R. Mahnke, "How to Solve Fokker–Planck Equation Treating Mixed Eigenvalue Spectrum?", *Condensed Matter Physics* **16**, 13002:1–13, (2013). [cited 5 times]
4. **M. Brics** and D. Bauer, "Time-dependent renormalized natural orbital theory applied to the two-electron spin-singlet case: ground state, linear response, and autoionization", *Phys. Rev. A* **88** 052514:1–14, (2013) . [cited 13 times]
5. J. Rapp, **M. Brics**, and D. Bauer, "Equations of motion for natural orbitals of strongly driven two-electron systems", *Phys. Rev. A* **90**, 012518:1–11, (2014). [cited 8 times]
6. **M. Brics**, J. Rapp, and D. Bauer, "Non-sequential double ionization with time-dependent renormalized natural orbital theory", *Phys. Rev. A* **90**, 053418:1–7, (2014). [cited 6 times]
7. R. Mahnke, J. Kaupuzs, and **M. Brics**, "Air Traffic, Boarding and Scaling Exponents", Proceedings of the conference *Traffic and Granular Flow '13*, 305–314, (2015). [cited 1 times]
8. **M. Brics**, J. Rapp, and D. Bauer, "Strong-field absorption and emission of radiation in two-electron systems calculated with time-dependent natural orbitals", *Phys. Rev. A* **93**, 053418:1–8, (2016). [cited 1 time]
9. A. Hanusch, J. Rapp, **M. Brics**, and D. Bauer, "Time-dependent renormalized-natural-orbital theory applied to laser-driven H_2^+", *Phys. Rev. A* **93**, 043414:1–8, (2016). [cited 0 times]

Conference talks

1. **M. Brics**, J. Rapp, and D. Bauer, "Time-dependent renormalized natural orbital theory applied to correlated two-electron dynamics", *DPG-Frühjahrstagung 2014*, Berlin, March 17–21, 2014
2. **M. Brics**, J. Rapp, and D. Bauer, 'Nonsequential double ionization and radiation/absorption spectra with time-dependent renormalized-natural-orbital theory ", *DPG-Frühjahrstagung 2015*, Heidelberg, March 23–27, 2015

Presented posters

1. **M. Brics** and D. Bauer, "Time-dependent reduced density matrix functional theory applied to laser driven, correlated two-electron dynamics", *DPG-Frühjahrstagung 2013*, Hannover, March 18–22, 2013
2. **M. Brics** and D. Bauer, "Time-dependent renormalized natural orbital theory" , Rostock, September 8–13, 2013
3. **M. Brics** and D. Bauer, "Time-dependent renormalized natural orbital theory applied to the two-electron spin-singlet case: ground state, linear response, and autoionization", *International Workshop on ATOMIC PHYSICS* , Dresden, November 25–29, 2013
4. **M. Brics**, J. Rapp, and D. Bauer, "Non-sequential double ionization with time-dependent renormalized natural orbital theory", *International Workshop on ATOMIC PHYSICS* , Dresden, November 24–28, 2014
5. **M. Brics**, J. Rapp, A. Hanusch, and D. Bauer, "Photoelectrons and light from laser-driven 1D helium using TDRNOT", Ψ_k*-2015 Conference* , Donostia-San Sebastián, September 6–10, 2015
6. **M. Brics**, J. Rapp, A. Hanusch, and D. Bauer, "Photoelectrons and light from laser-driven 1D helium using TDRNOT", *3rd International Conference on Correlation Effects in Radiation Fields 2015*, Rostock, September 13–18, 2015
7. **M. Brics**, J. Rapp, A. Hanusch, and D. Bauer, "Photoelectrons and light from laser-driven 1D helium using TDRNOT", *DPG-Frühjahrstagung 2015*, Heidelberg, February 29 – March 4, 2016
8. **M. Brics**, J. Rapp, A. Hanusch, and D. Bauer, "Time-dependent renormalized natural orbital theory for intense laser-atom interaction", *International workshop on: Reduced Density Matrices in Quantum Physics and Role of Fermionic Exchange Symmetry*, University of Oxford (Oxford), United Kingdom, April 12–15, 2016

Acknowledgment

Firstly, I would like to express gratitude to my supervisor Dieter Bauer, to whom I have to thank for finding an interesting topic, financial support, motivation, patience, fruitful discussions, teaching me English grammar, ... There are so many things that it is hard even to list them.

Secondly, I have to express my thanks to Julius Rapp for answering my endless questions and for fruitful discussions. He also checked my derivations and corrected mistakes in them. Thanks also to various proofreadings and for correcting my grammar mistakes.

Also, extra gratitude is provided to Jānis Aizezers, Vents Valle, Reinhard Mahnke, who visited me in the hospital after a "small" traffic accident at 02.04.2012, which actually was supposed to be the official date for the beginning of the PhD. Their visits made the time in the hospital much more bearable. Reinhard Mahnke deserves special thanks, as he is still helping to manage my doctor's appointments.

I am also very thankful for a great atmosphere in our group. Dieter, Julius, Volker, Thomas, Tatyana, Yaroslav, Adel, Adrian, Marina, thanks for that!

Finally, I have to say sorry to all the people that I did not mention here explicitly but who supported me. I know that my bad memory is not an excuse. I really have to thank, way much more often.

Erklärung

Ich versichere hiermit an Eides statt, dass ich die vorliegende Arbeit selbstständig angefertigt und ohne fremde Hilfe verfasst habe, keine außer den von mir angegebenen Hilfsmitteln und Quellen dazu verwendet habe und die den benutzten Werken inhaltlich und wörtlich entnommenen Stellen als solche kenntlich gemacht habe.

Rostock, den 24.08.2016

Mārtiņš Brics

A. Appendix

A.1. EOM for NOs and ONs

EOMs for NOs and ONs are derived by inserting (1.28) and (1.26) into (1.22), obtaining

$$\begin{aligned} & i\sum_m \Big(\dot{n}_m(t)|m\rangle\langle m| + n_m(t)|m\rangle\langle\dot{m}| + n_m(t)|\dot{m}\rangle\langle m|\Big) \\ =&\sum_m n_m(t)\Big(\hat{h}(t)|m\rangle\langle m| - |m\rangle\langle m|\hat{h}(t)\Big) + 2\sum_{ijklm}\langle m|\left[\hat{V}_{\mathrm{ee}}, \gamma_{2,ijkl}(t)|ij\rangle\langle kl|\right]|m\rangle\,. \end{aligned} \tag{A.1}$$

Multiplying from right with $|n\rangle$ one gets

$$\begin{aligned} i n_n(t)|\dot{n}\rangle =& n_n(t)\hat{h}(t)|n\rangle - i\dot{n}_n(t)|n\rangle - \sum_k n_k(t)\Big(\langle k|\,\hat{h}(t)\,|n\rangle + i\langle\dot{k}|n\rangle\Big)|k\rangle \\ &+ 2\sum_{ijl}\gamma_{2,ijnl}(t)\,\langle l|\,\hat{V}_{\mathrm{ee}}\,|j\rangle\,|i\rangle - 2\sum_{ijkl}\gamma_{2,ijkl}(t)\,\langle kl|\,\hat{V}_{\mathrm{ee}}\,|nj\rangle\,|i\rangle, \end{aligned} \tag{A.2}$$

which is already an implicit EOM for NOs. To write it in explicit form multiply (A.2) from left with $\langle m|$, which gives

$$\begin{aligned} i n_n(t)\langle m|\dot{n}\rangle =& n_n(t)\,\langle m|\,\hat{h}(t)\,|n\rangle - i\dot{n}_n(t)\delta_{mn} - n_m(t)\Big(\langle m|\,\hat{h}(t)\,|n\rangle + i\langle\dot{m}|n\rangle\Big) \\ &+ 2\sum_{ijl}\gamma_{2,ijnl}(t)\,\langle ml|\,\hat{V}_{\mathrm{ee}}\,|ij\rangle - 2\sum_{jkl}\gamma_{2,mjkl}(t)\,\langle kl|\,\hat{V}_{\mathrm{ee}}\,|nj\rangle\,. \end{aligned} \tag{A.3}$$

Taking the time derivative of $\langle m|k\rangle = \delta_{mn}$ one finds $\langle\dot{m}|n\rangle = -\langle m|\dot{n}\rangle$, with which

$$\begin{aligned} -i n_n(t)\langle\dot{m}|n\rangle =& n_n(t)\,\langle m|\,\hat{h}(t)\,|n\rangle - i\dot{n}_n(t)\delta_{mn} - n_m(t)\Big(\langle m|\,\hat{h}(t)\,|n\rangle + i\langle\dot{m}|n\rangle\Big) \\ &+ 2\sum_{jpl}\Big(\gamma_{2,pjnl}(t)\,\langle ml|\,\hat{V}_{\mathrm{ee}}\,|pj\rangle - \gamma_{2,mjpl}(t)\,\langle pl|\,\hat{V}_{\mathrm{ee}}\,|nj\rangle\Big) \end{aligned} \tag{A.4}$$

follows. Further, for $m = n$ one obtains EOM for ONs:

$$\dot{n}_n(t) = 4\,\mathrm{Im}\sum_{ijl}\gamma_{2,ijnl}(t)\,\langle nl|\,\hat{V}_{\mathrm{ee}}\,|ij\rangle\,, \tag{A.5}$$

and for $m \neq n$, assuming $n_n(t) \neq n_m(t)$,

$$\langle m|\,\hat{h}(t)\,|n\rangle + i\langle\dot{m}|n\rangle = -2\sum_{jpl}\frac{\gamma_{2,pjnl}(t)\,\langle ml|\,\hat{V}_{\mathrm{ee}}\,|pj\rangle - \gamma_{2,mjpl}(t)\,\langle pl|\,\hat{V}_{\mathrm{ee}}\,|nj\rangle}{n_n(t) - n_m(t)}. \tag{A.6}$$

By inserting (A.5) and (A.6) into (A.4) one obtains

$$i\partial_t|n(t)\rangle = \hat{h}(t)|n(t)\rangle + \underline{\mathcal{A}}_n(t)|n(t)\rangle + \sum_{k\neq n}\mathcal{B}_{nk}(t)|k(t)\rangle + \sum_k\hat{\mathcal{C}}_{nk}(t)|k(t)\rangle, \tag{A.7}$$

with

$$\underline{\mathcal{A}}_n(t) = i\langle n|\dot{n}\rangle - \langle n|\,\hat{h}(t)\,|n\rangle - \frac{2}{n_n(t)}\sum_{jkl}\gamma_{klnj}(t)\,\langle nj|\,\hat{V}_{\mathrm{ee}}\,|kl\rangle\,, \tag{A.8}$$

$$\mathcal{B}_{nk}(t) = \frac{2}{n_n(t)}\sum_{jpl}\frac{n_k(t)\gamma_{2,pjnl}(t)\,\langle kl|\,\hat{V}_{\mathrm{ee}}\,|pj\rangle - n_n(t)\gamma_{2,kjpl}(t)\,\langle pl|\,\hat{V}_{\mathrm{ee}}\,|nj\rangle}{n_n(t) - n_k(t)}, \tag{A.9}$$

for $n_n(t) \neq n_m(t)$, and

$$\hat{\mathcal{C}}_{nk}(t) = \frac{2}{n_n(t)}\sum_{jl}\gamma_{2,kjnl}(t)\,\langle l|\,\hat{V}_{\mathrm{ee}}\,|j\rangle\,. \tag{A.10}$$

A phase convention for the NOs amounts to assigning a real number (or possibly time-dependent function) to $i\langle n|\dot{n}\rangle$. One particularly useful phase convention in the two-electron case reads

$$in_n(t)\langle n|\dot{n}\rangle = n_n(t)\,\langle n|\,\hat{h}(t)\,|n\rangle + \Re\sum_{jpl}\gamma_{2,plnj}(t)\,\langle nj|\,\hat{V}_{\mathrm{ee}}\,|pl\rangle\,, \tag{A.11}$$

which inserted in (A.7) delivers the EOMs for NOs and ONs

$$\begin{aligned} i\partial_t|n(t)\rangle &= \hat{h}(t)|n(t)\rangle + \mathcal{A}_n(t)|n(t)\rangle + \sum_{k\neq n}\mathcal{B}_{nk}(t)|k(t)\rangle + \sum_k\hat{\mathcal{C}}_{nk}(t)|k(t)\rangle, \\ i\dot{n}_k(t) &= 4\sum_{ijl}\gamma_{2,ijnl}(t)\,\langle nl|\,\hat{V}_{\mathrm{ee}}\,|ij\rangle\,, \end{aligned} \tag{A.12}$$

with

$$\mathcal{A}_n(t) = -\frac{1}{n_n(t)} \sum_{jkl} \left(2\gamma_{2,klnj}(t) \langle nj| \hat{V}_{\mathrm{ee}} |kl\rangle - \Re\gamma_{2,klnj}(t) \langle nj| \hat{V}_{\mathrm{ee}} |kl\rangle \right). \tag{A.13}$$

This phase convention leads to an adiabatic expression for expansion coefficients $\gamma_{2,ijkl}(t)$, depending only on the ONs at time t.

A.2. EOM from variation principle of NOs

The EOM for the two-electron case can be also derived via the variation of the action [33]. The two-electron state expanded in NOs reads

$$|\Phi\rangle = \sum_i d_i(t)|ii'\rangle, \tag{A.14}$$

where the expansion coefficients

$$d_i(t) = \sqrt{\frac{n_i(t)}{2}} \mathrm{e}^{i\phi_i(t)} = -d_{i'}(t) \tag{A.15}$$

are connected to ONs via:

$$d_i(t)d_i^*(t) = \frac{n_i(t)}{2} = d_{i'}(t)d_{i'}^*(t) = \frac{n_{i'}(t)}{2}. \tag{A.16}$$

Here, the explicit time dependence in states and NOs is suppressed. Since it is known how to express the two-electron state in NOs, one can express also the Lagrangian in NOs, which reads

$$\begin{aligned} L &= \langle \Phi| \, i\frac{\partial}{\partial t} - \hat{H}(t) \, |\Phi\rangle \\ &= \sum_{ij} \langle jj' d_j(t)| \, i\frac{\partial}{\partial t} - \hat{H}(t) \, |d_i(t) ii'\rangle \\ &= \sum_{ij} \left(i d_i(t) d_j^*(t) \langle jj'| \, \frac{\partial}{\partial t} \, |ii'\rangle + i\dot{d}_i(t) d_j^*(t) \langle jj'|ii'\rangle - d_i(t) d_j^*(t) \langle jj'| \, \hat{H}(t) \, |ii'\rangle \right) \\ &= \sum_i \left(i\dot{d}_i(t) d_i^*(t) + i n_i(t) \langle i|\dot{i}\rangle - n_i(t) \langle i| \, \hat{h}(t) \, |i\rangle \right) - \sum_{ij} d_i(t) d_j^*(t) \langle jj'| \, \hat{V}_{\mathrm{ee}} \, |ii'\rangle \, . \end{aligned} \tag{A.17}$$

The Lagrangian which takes into account that NOs are orthonormal via the Lagrange multipliers $\lambda_{ij}(t)$ then is

$$\begin{aligned} L[|k\rangle, d_k(t), \langle k|, d_k^*(t)] = &\sum_i i\dot{d}_i(t)d_i^*(t) + in_i(t)\langle i|\dot{i}\rangle - n_i(t)\,\langle i|\,\hat{h}(t)\,|i\rangle \\ &- \sum_{ij} d_i(t)d_j^*(t)\,\langle jj|\,\hat{V}_{\mathrm{ee}}\,|ii\rangle - \sum_{i,j}\lambda_{ij}(t)\,(\langle i|j\rangle - \delta_{ij})\,, \end{aligned} \tag{A.18}$$

and the action is defined as the time integral

$$A = \int_0^T \mathrm{d}t\, L[|k\rangle, d_k(t), \langle k|, d_k^*(t)]. \tag{A.19}$$

The variation of the action with respect to $\langle k|$ gives

$$\begin{aligned} 0 &= \frac{\partial A}{\partial\langle k|} \\ &= in_k(t)|\dot{k}\rangle - n_k(t)\hat{h}(t)|k\rangle - \sum_i 2d_i(t)d_k^*(t)\,\langle k'|\,\hat{V}_{\mathrm{ee}}\,|i'\rangle\,|i\rangle - \sum_i \lambda_{ki}(t)|i\rangle, \end{aligned} \tag{A.20}$$

thus leading to

$$in_k(t)|\dot{k}\rangle = n_k\hat{h}(t)|k\rangle + \sum_i 2d_i(t)d_k^*(t)\,\langle k'|\,\hat{V}_{\mathrm{ee}}\,|i'\rangle\,|i\rangle + \sum_i \lambda_{ki}(t)|i\rangle. \tag{A.21}$$

Multiplying from the left with $\langle l|$ and rearranging terms yields

$$\lambda_{kl}(t) = in_k(t)\langle l|\dot{k}\rangle - n_k(t)\,\langle l|\,\hat{h}(t)\,|k\rangle - \sum_i 2d_i(t)d_k^*(t)\,\langle lk'|\,\hat{V}_{\mathrm{ee}}\,|ii'\rangle\,. \tag{A.22}$$

The variation of action with respect to $|k\rangle$ leads to

$$\begin{aligned} 0 =& \frac{\partial A}{\partial|k\rangle} - \frac{d}{dt}\frac{\partial A}{\partial|\dot{k}\rangle} \\ =& - i\dot{n}_k(t)\langle k| - in_k(t)\langle\dot{k}| - n_k(t)\langle k|\hat{h}(t) - \sum_i 2d_i^*(t)d_k(t)\,\langle i'|\,\hat{V}_{\mathrm{ee}}\,|k'\rangle\,\langle i| \\ &- \sum_i \lambda_{ik}(t)\langle i|. \end{aligned} \tag{A.23}$$

Complex conjugation gives

$$\begin{aligned} in_k(t)|\dot{k}\rangle =& - i\dot{n}_k(t)|k\rangle + n_k(t)\hat{h}(t)|k\rangle + \sum_i 2d_i(t)d_k^*(t)\,\langle k'|\,\hat{V}_{\rm ee}\,|i'\rangle\,|i\rangle \\ &+ \sum_i \lambda_{ik}^*(t)|i\rangle. \end{aligned} \tag{A.24}$$

Comparing (A.21) and (A.24), one notices that

$$\lambda_{kk}(t) = -i\dot{n}_k(t) + \lambda_{kk}^*(t), \tag{A.25}$$

and for $l \neq k$

$$\lambda_{ik}(t) = \lambda_{ki}^*(t). \tag{A.26}$$

Inserting (A.22) into (A.25) one gets

$$\begin{aligned} & in_k(t)\langle k|\dot{k}\rangle - n_k(t)\,\langle k|\,\hat{h}(t)\,|k\rangle - \sum_i 2d_i(t)d_k^*(t)\,\langle kk'|\,\hat{V}_{\rm ee}\,|ii'\rangle \\ =& - i\dot{n}_k(t) - in_k(t)\langle\dot{k}|k\rangle - n_k(t)\,\langle k|\,\hat{h}(t)\,|k\rangle - \sum_i 2d_i^*(t)d_k(t)\,\langle ii'|\,\hat{V}_{\rm ee}\,|kk'\rangle\,, \end{aligned} \tag{A.27}$$

which, using that $\langle l|\dot{k}\rangle = -\langle\dot{l}|k\rangle$, leads to

$$\dot{n}_k(t) = 4\,\mathrm{Im}\sum_i d_i(t)d_k^*(t)\,\langle kk'|\,\hat{V}_{\rm ee}\,|ii'\rangle\,. \tag{A.28}$$

Inserting (A.22) into (A.26) one gets for $l \neq k$, assuming that $n_k(t) \neq n_l(t)$,

$$\begin{aligned} \lambda_{kl}(t) &= in_k(t)\langle l|\dot{k}\rangle - n_k(t)\,\langle l|\,\hat{h}(t)\,|k\rangle - \sum_i 2d_i(t)d_k^*(t)\,\langle lk'|\,\hat{V}_{\rm ee}\,|ii'\rangle \\ &= in_l\langle l|\dot{k}\rangle - n_l(t)\,\langle l|\,\hat{h}\,|k\rangle - \sum_i 2d_i^*(t)d_l(t)\,\langle ii'|\,\hat{V}_{\rm ee}\,|kl'\rangle\,, \end{aligned} \tag{A.29}$$

$$i\langle l|\dot{k}\rangle = \langle l|\,\hat{h}\,|k\rangle + 2\sum_i \frac{d_i(t)d_k^*(t)\,\langle lk|\,\hat{V}_{\rm ee}\,|ii\rangle - d_i^*(t)d_l(t)\,\langle ii'|\,\hat{V}_{\rm ee}\,|kl'\rangle}{n_k(t) - n_l(t)}, \tag{A.30}$$

$$\lambda_{kl} = 2\sum_i \frac{n_l(t)d_i(t)d_k^*(t)\,\langle lk'|\,\hat{V}_{\rm ee}\,|ii'\rangle - n_k(t)d_i^*(t)d_l(t)\,\langle ii'|\,\hat{V}_{\rm ee}\,|kl'\rangle}{n_k(t) - n_l(t)} \tag{A.31}$$

Inserting (A.22) and (A.29) into (A.20) one recovers (A.7) with $\gamma_{2,ijkl} = d_i(t)d_k^*(t)\delta_{ij'}\delta_{kl'}$.

The variation of action with respect to $d_k^*(t)$ and $d_k(t)$ yields

$$\begin{aligned} 0 &= \frac{\partial A}{\partial d_k^*(t)} \\ &= i\dot{d}_k(t) + 2id_k(t)\langle k|\dot{k}\rangle - 2d_k(t)\,\langle k|\,\hat{h}(t)\,|k\rangle - \sum_i d_i(t)\,\langle kk'|\,\hat{V}_{\mathrm{ee}}\,|ii'\rangle\,, \end{aligned} \tag{A.32}$$

and its complex conjugate, respectively. The EOM for expansion coefficients $d_k(t)$ is

$$i\dot{d}_k(t) = -2id_k(t)\langle k|\dot{k}\rangle + 2d_k(t)\,\langle k|\,\hat{h}(t)\,|k\rangle + \sum_i d_i(t)\,\langle kk'|\,\hat{V}_{\mathrm{ee}}\,|ii'\rangle\,. \tag{A.33}$$

By choosing some real expression for $i\langle n|\dot{n}\rangle$ e.g. zero as was done in [82], one can propagate NOs and expansion coefficients $d_n(t)$ by solving the system of coupled equations

$$\begin{aligned} i\partial_t|n(t)\rangle &= \hat{h}(t)|n(t)\rangle + \underline{\mathcal{A}}_n(t)|n(t)\rangle + \sum_{k\neq n}\mathcal{B}_{nk}(t)|k(t)\rangle + \sum_k \hat{\mathcal{C}}_{nk}(t)|k(t)\rangle, \\ i\dot{d}_n(t) &= -2id_n(t)\langle n|\dot{n}\rangle + 2d_n(t)\,\langle n|\,\hat{h}(t)\,|n\rangle + \sum_i d_i(t)\,\langle nn'|\,\hat{V}_{\mathrm{ee}}\,|ii'\rangle\,. \end{aligned} \tag{A.34}$$

One can obtain the groundstate of the system via propagation in imaginary time although a smaller time step than for RNO propagation is required.

It is also possible to choose a phase convention for NOs such that the phases $\mathrm{e}^{i\phi_i(t)}$ for the expansion coefficients do not change in time. In this case

$$\dot{d}_k(t) = \frac{1}{2}\frac{\dot{n}_k(t)}{n_k(t)}d_k(t). \tag{A.35}$$

Inserting this into (A.33) one gets

$$2id_k\langle k|\dot{k}\rangle = -i\frac{1}{2}\frac{\dot{n}_k(t)}{n_k(t)}d_k(t) + 2d_k(t)\,\langle k|\,\hat{h}(t)\,|k\rangle + \sum_i d_i\,\langle kk'|\,\hat{V}_{\mathrm{ee}}\,|ii\rangle\,. \tag{A.36}$$

Multiplying with $d_k(t)$ and using that $2d_k^*(t)d_k(t) = n_k(t)$ we get

$$\begin{aligned} in_k(t)\langle k|\dot{k}\rangle =& -i\frac{\dot{n}_k(t)}{4} + n_k(t)\,\langle k|\,\hat{h}(t)\,|k\rangle + \sum_i d_i(t)d_k^*(t)\,\langle kk'|\,\hat{V}_{\rm ee}\,|ii'\rangle \\ =& -i\,\mathrm{Im}\sum_i d_i(t)d_k^*(t)\,\langle kk'|\,\hat{V}_{\rm ee}\,|ii'\rangle + n_k(t)\,\langle k|\,\hat{h}(t)\,|k\rangle \\ &+ \sum_i d_i(t)d_k^*(t)\,\langle kk'|\,\hat{V}_{\rm ee}\,|ii'\rangle \\ =& n_k(t)\,\langle k|\,\hat{h}(t)\,|k\rangle + \Re\sum_i d_i(t)d_k^*(t)\,\langle kk'|\,\hat{V}_{\rm ee}\,|ii'\rangle\,. \end{aligned} \tag{A.37}$$

For this phase convention one obtains (A.12) with $\gamma_{2,ijkl}(t) = d_i(t)d_k^*(t)\delta_{ij'}\delta_{kl'}$. Unfortunately, the ONs then do not change in imaginary time so that in order to find the groundstate one has to combine imaginary-time propagation with methods for searching ONs [77].

In terms of RNOs, however, using

$$|\dot{\tilde{k}}\rangle = \sqrt{n_k(t)}|\dot{k}\rangle + \frac{\dot{n}_k(t)}{2\sqrt{n_k(t)}}|k\rangle = \sqrt{n_k(t)}|\dot{k}\rangle + \frac{\dot{n}_k(t)}{2n_k(t)}|\tilde{k}\rangle \tag{A.38}$$

leads to (1.35) with $\tilde{\gamma}_{2,ijkl}(t) = \tilde{d}_i(t)\tilde{d}_k^*(t)\delta_{ij'}\delta_{kl'}$, and the groundstate can be obtained via imaginary-time propagation.

A.3. Improved figures of Paper 3 [13]

Results of higher resolution in momentum space for the TDSE calculation and with more RNOs for TDRNOT than those shown in Paper 3 [13] are presented. Conclusions made in [13] are unaltered.

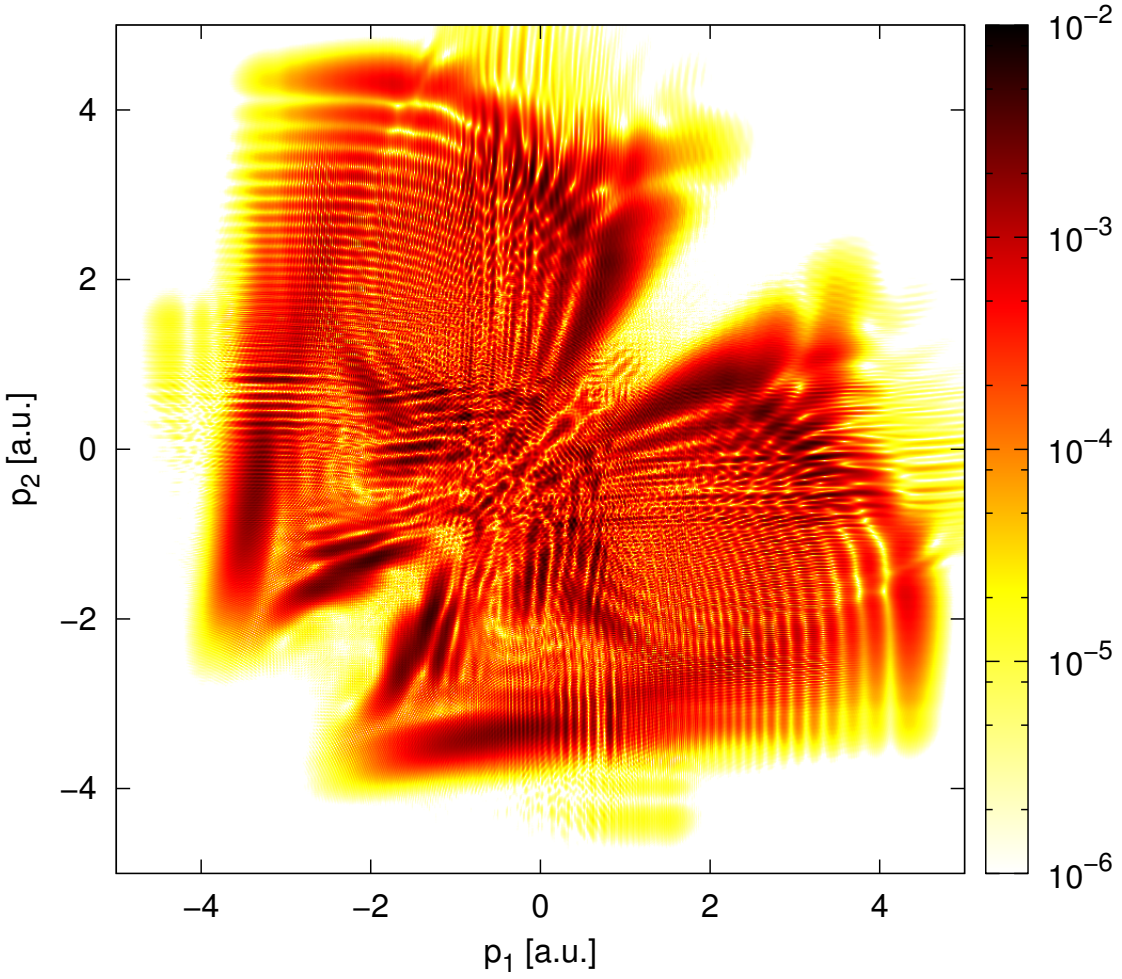

Figure A.1.: Improved Fig. 2 of [13]. The part of two-electron momentum distribution when both electrons are ionized $\rho^{2+}(p_1 p_2)$ obtained from TDSE in logarithmic scale over 4 orders of magnitude.

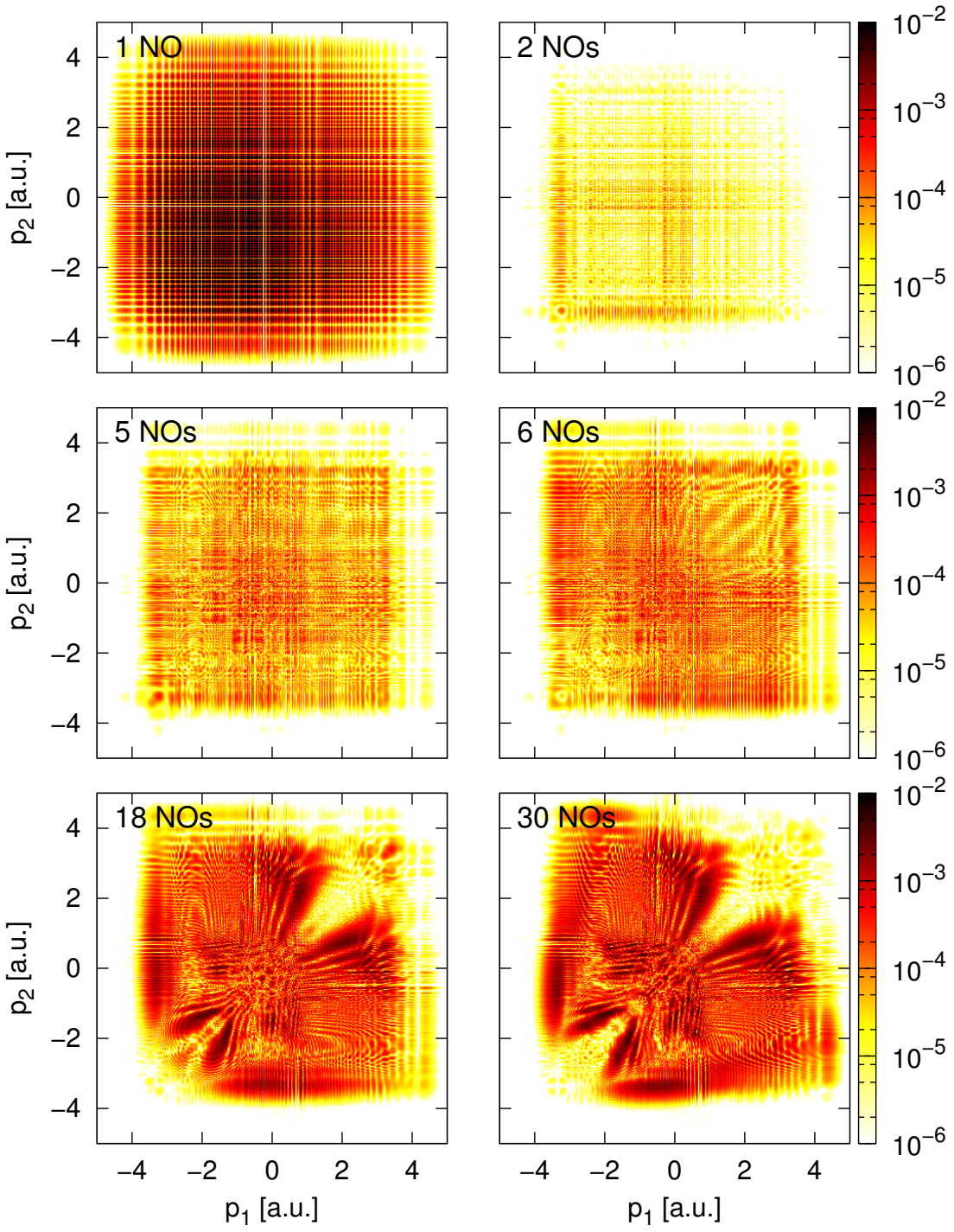

Figure A.2.: Improved Fig. 3 of [13]. The part of two-electron momentum distribution when both electrons left atom $\rho^{2+}(p_1 p_2)$ obtained from first 30 NOs (not all are shown) calculated from TDSE wavefunction after laser pulse in logarithmic scale over 4 orders of magnitude.

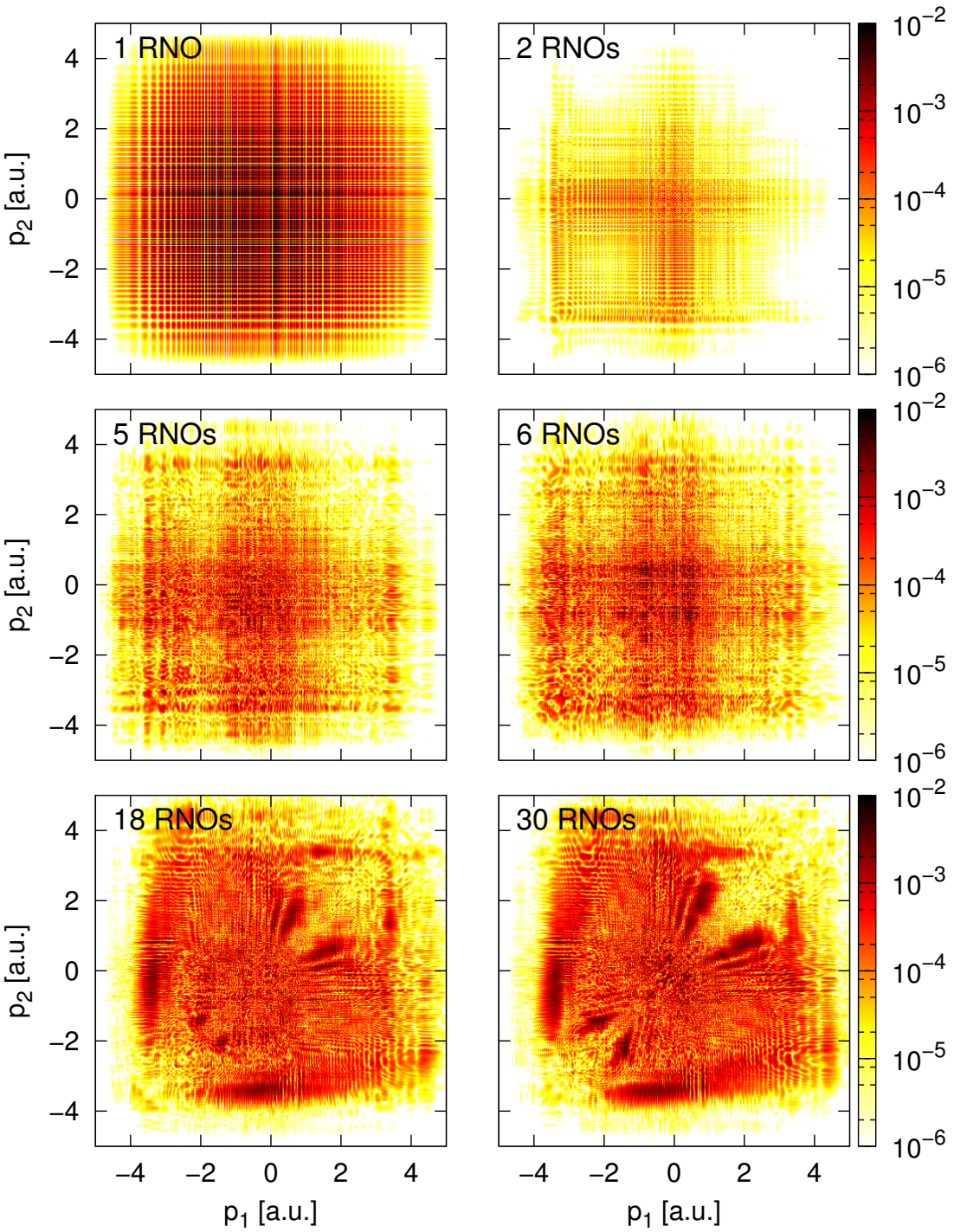

Figure A.3.: Improved Fig. 4 of [13]. The part of two-electron momentum distribution when both electrons are ionized $\rho^{2+}(p_1 p_2)$ obtained by TDRNOT with 1-30 RNO (not all are shown) in logarithmic scale over 4 orders of magnitude.

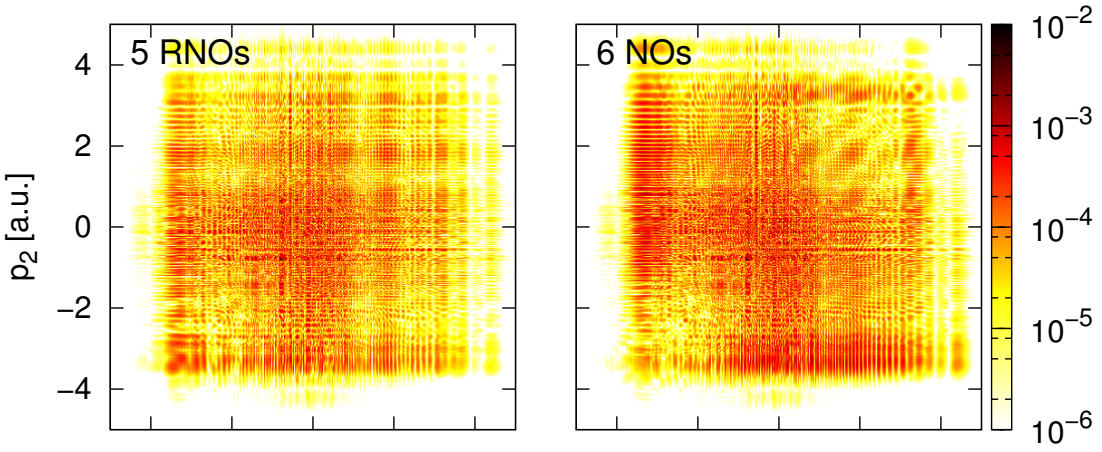

Figure A.4.: Improved Fig. 5 of [13]. The part of two-electron momentum distribution when both electrons are ionized $\rho^{2+}(p_1 p_2)$ obtained by TDRNOT propagation with 30 RNO when only first 5 and 6 RNOs were used for variable calculation in logarithmic scale over 4 orders of magnitude.

Bibliography

[1] AKBARI, A. ; HASHEMI, M. J. ; RUBIO, A. ; NIEMINEN, R. M. ; LEEUWEN, R. van: Challenges in truncating the hierarchy of time-dependent reduced density matrices equations. In: Phys. Rev. B 85 (2012), Jun, S. 235121. – URL http://link.aps.org/doi/10.1103/PhysRevB.85.235121

[2] APPEL, H. ; GROSS, E. K. U.: Time-dependent natural orbitals and occupation numbers. In: Europhys. Lett. 92 (2010), Nr. 2, S. 23001. – URL http://stacks.iop.org/0295-5075/92/i=2/a=23001

[3] APPEL, Heiko: Time-Dependent Quantum Many-Body Systems: Linear Response, Electronic Transport, and Reduced Density Matrices. Berlin, Freie Universität Berlin, Dissertation, 2007

[4] AYRES, R. U.: Variational Approach to the Many-Body Problem. In: Phys. Rev. 111 (1958), Sep, S. 1453–1460. – URL http://link.aps.org/doi/10.1103/PhysRev.111.1453

[5] BADER, Philipp ; BLANES, Sergio ; CASAS, Fernando: Solving the Schrödinger eigenvalue problem by the imaginary time propagation technique using splitting methods with complex coefficients. In: J. Chem. Phys. 139 (2013), Nr. 12. – URL http://scitation.aip.org/content/aip/journal/jcp/139/12/10.1063/1.4821126

[6] BAUCH, S. ; SØRENSEN, L. K. ; MADSEN, L. B.: Time-dependent generalized-active-space configuration-interaction approach to photoionization dynamics of atoms and molecules. In: Phys. Rev. A 90 (2014), Dec, Nr. 6, S. 062508. – URL http://dx.doi.org/10.1103/PhysRevA.90.062508. – ISSN 1094-1622

[7] BAUER, D.: Two-dimensional, two-electron model atom in a laser pulse: Exact treatment, single-active-electron analysis, time-dependent density-functional theory, classical calculations, and nonsequential ionization. In: Phys. Rev. A 56 (1997), Oct, S. 3028–3039. – URL http://link.aps.org/doi/10.1103/PhysRevA.56.3028

[8] BOGOLIUBOV, N. N.: Kinetic Equations. In: J. Phys. USSR 10 (1946), S. 265–274

[9] BOGOLIUBOV, N. N. ; GUROV, K. P.: Kinetic Equations in Quantum Mechanics. In: J. Exp. Theor. Phys. (in Russian) 17 (1947), S. 614–628

[10] BOPP, Fritz: Ableitung der Bindungsenergie von N-Teilchen-Systemen aus 2-Teilchen-Dichtematrizen. In: Z. Physik 156 (1959), Sep, Nr. 3, S. 348–359. – URL http://dx.doi.org/10.1007/BF01461233. – ISSN 1434-601X

[11] BORN, M. ; GREEN, H. S.: A General Kinetic Theory of Liquids. I. The Molecular Distribution Functions. In: Proceedings of the Royal Society of London A: Mathematical, Physical and Engineering Sciences 188 (1946), Nr. 1012, S. 10–18. – URL http://rspa.royalsocietypublishing.org/content/188/1012/10. – ISSN 0080-4630

[12] BRICS, M. ; BAUER, D.: Time-dependent renormalized natural orbital theory applied to the two-electron spin-singlet case: Ground state, linear response, and autoionization. In: Phys. Rev. A 88 (2013), Nov, S. 052514. – URL http://link.aps.org/doi/10.1103/PhysRevA.88.052514

[13] BRICS, M. ; RAPP, J. ; BAUER, D.: Nonsequential double ionization with time-dependent renormalized-natural-orbital theory. In: Phys. Rev. A 90 (2014), Nov, S. 053418. – URL http://link.aps.org/doi/10.1103/PhysRevA.90.053418

[14] BRICS, M. ; RAPP, J. ; BAUER, D.: Strong-field absorption and emission of radiation in two-electron systems calculated with time-dependent natural orbitals. In: Phys. Rev. A 93 (2016), Jan, S. 013404. – URL http://link.aps.org/doi/10.1103/PhysRevA.93.013404

[15] BUIJSE, M. A. ; BAERENDS, E. J.: An approximate exchange-correlation hole density as a functional of the natural orbitals. In: Mol. Phys. 100 (2002), Feb, Nr. 4, S. 401–421. – URL http://dx.doi.org/10.1080/00268970110070243. – ISSN 1362-3028

[16] CASSING, W. ; NIITA, K. ; WANG, S. J.: Dynamical aspects of intermediate-energy nucleus-nucleus collisions. In: Zeitschrift für Physik A Atomic Nuclei 331 (1988), Nr. 4, S. 439–449. – URL http://dx.doi.org/10.1007/BF01291902. – ISSN 0939-7922

[17] CASSING, W. ; PFITZNER, A.: Correlation dynamics of finite fermion systems. In: Zeitschrift für Physik A Atomic Nuclei 337 (1990), Nr. 2, S. 175–183. – URL http://dx.doi.org/10.1007/BF01294289. – ISSN 0939-7922

[18] CASSING, W. ; PFITZNER, A.: Self-consistent truncation of the BBGKY hierarchy on the two-body level. In: Zeitschrift für Physik A Hadrons and Nuclei 342 (1992), Nr. 2, S. 161–167. – URL http://dx.doi.org/10.1007/BF01288464. – ISSN 0939-7922

[19] CASSING, W. ; WANG, S. J.: Numerical study of a selfconsistent two-body theory for colliding ions in a one-dimensional model. In: Zeitschrift für Physik A Atomic Nuclei 328 (1987), Nr. 4, S. 423–429. – URL http://dx.doi.org/10.1007/BF01289628. – ISSN 0939-7922

[20] COLEMAN, A. J.: Structure of Fermion Density Matrices. In: Rev. Mod. Phys. 35 (1963), Jul, S. 668–686. – URL http://link.aps.org/doi/10.1103/RevModPhys.35.668

[21] COLEMAN, A.J. ; YUKALOV, V.I.: Reduced Density Matrices: Coulson's Challenge. Berlin : Springer Berlin Hpageselberg, 2000 (Lecture Notes in Chemistry). – URL http://www.springer.com/us/book/9783540671480. – ISBN 9783540671480

[22] CRANK, J. ; NICOLSON, P.: A practical method for numerical evaluation of solutions of partial differential equations of the heat-conduction type. In: Adv Comput Math 6 (1996), Dec, Nr. 1, S. 207–226. – URL http://dx.doi.org/10.1007/BF02127704. – ISSN 1572-9044

[23] DORMAND, J.R. ; PRINCE, P.J.: A family of embedded Runge-Kutta formulae. In: J. Comput. Appl. Math. 6 (1980), Nr. 1, S. 19 – 26. – URL http://www.sciencedirect.com/science/article/pii/0771050X80900133. – ISSN 0377-0427

[24] DREIZLER, Reiner M. ; GROSS, Eberhard K. U.: Density Functional Theory. Berlin : Springer Science + Business Media, 1990. – URL http://dx.doi.org/10.1007/978-3-642-86105-5. – ISBN http://id.crossref.org/isbn/978-3-642-86105-5

[25] ELLIOTT, Peter ; MAITRA, Neepa T.: Density-matrix propagation driven by semiclassical correlation. In: Int. J. Quantum Chem. 116 (2016), Nr. 10, S. 772–783. – URL http://dx.doi.org/10.1002/qua.25087. – ISSN 1097-461X

[26] FEIT, M.D ; FLECK, J.A ; STEIGER, A: Solution of the Schrödinger equation by a spectral method. In: J. Comp. Phys. 47 (1982), Sep, Nr. 3, S. 412–433. – URL http://dx.doi.org/10.1016/0021-9991(82)90091-2. – ISSN 0021-9991

[27] FRANK, Rupert L. ; LIEB, Elliott H. ; SEIRINGER, Robert ; SIEDENTOP, Heinz: Müller's exchange-correlation energy in density-matrix-functional theory. In: Phys. Rev. A 76 (2007), Nov, S. 052517. – URL http://link.aps.org/doi/10.1103/PhysRevA.76.052517

[28] FRIESECKE, G.: On the Infinitude of Non-Zero Eigenvalues of the Single-Electron Density Matrix for Atoms and Molecules. In: Proceedings: Mathematical, Physical

and Engineering Sciences 459 (2003), Nr. 2029, S. 47–52. – URL http://www.jstor.org/stable/3655030. – ISSN 13645021

[29] FUKS, J. I. ; ELLIOTT, P. ; RUBIO, A. ; MAITRA, N. T.: Dynamics of Charge-Transfer Processes with Time-Dependent Density Functional Theory. In: J. Phys. Chem. Lett. 4 (2013), Nr. 5, S. 735–739. – URL http://dx.doi.org/10.1021/jz302099f. – PMID: 26281927

[30] FUKS, J. I. ; HELBIG, N. ; TOKATLY, I. V. ; RUBIO, A.: Nonlinear phenomena in time-dependent density-functional theory: What Rabi oscillations can teach us. In: Phys. Rev. B 84 (2011), Aug, S. 075107. – URL http://link.aps.org/doi/10.1103/PhysRevB.84.075107

[31] FUKS, Johanna I. ; MAITRA, Neepa T.: Challenging adiabatic time-dependent density functional theory with a Hubbard dimer: the case of time-resolved long-range charge transfer. In: Phys. Chem. Chem. Phys. 16 (2014), S. 14504–14513. – URL http://dx.doi.org/10.1039/C4CP00118D

[32] GARROD, Claude ; PERCUS, Jerome K.: Reduction of the N-Particle Variational Problem. In: J. Math. Phys. 5 (1964), Nr. 12, S. 1756–1776. – URL http://scitation.aip.org/content/aip/journal/jmp/5/12/10.1063/1.1704098

[33] GIESBERTZ, K. J. H.: Time-Dependent One-Body Reduced Density Matrix Functional Theory. Amsterdam, Free University Amsterdam, Dissertation, 2010

[34] GIESBERTZ, K. J. H.: Invertibility of retarded response functions for Laplace transformable potentials: Application to one-body reduced density matrix functional theory. In: J. Chem. Phys. 143 (2015), Nr. 5, S. 054102. – URL http://scitation.aip.org/content/aip/journal/jcp/143/5/10.1063/1.4927075

[35] GIESBERTZ, K.J.H.: Are natural orbitals useful for generating an efficient expansion of the wave function? In: Chem. Phys. Lett. 591 (2014), Jan, S. 220–226. – URL http://dx.doi.org/10.1016/j.cplett.2013.11.038. – ISSN 0009-2614

[36] GILBERT, T. L.: Hohenberg-Kohn theorem for nonlocal external potentials. In: Phys. Rev. B 12 (1975), Sep, S. 2111–2120. – URL http://link.aps.org/doi/10.1103/PhysRevB.12.2111

[37] GOEDECKER, S. ; UMRIGAR, C. J.: Natural Orbital Functional for the Many-Electron Problem. In: Phys. Rev. Lett. 81 (1998), Jul, S. 866–869. – URL http://link.aps.org/doi/10.1103/PhysRevLett.81.866

[38] GREENMAN, Loren ; HO, Phay J. ; PABST, Stefan ; KAMARCHIK, Eugene ; MAZZIOTTI, David A. ; SANTRA, Robin: Implementation of the time-dependent configuration-interaction singles method for atomic strong-field processes. In: Phys. Rev. A 82 (2010), Aug, Nr. 2, S. 023406. – URL http://dx.doi.org/10.1103/PhysRevA.82.023406. – ISSN 1094-1622

[39] GRITSENKO, Oleg ; PERNAL, Katarzyna ; BAERENDS, Evert J.: An improved density matrix functional by physically motivated repulsive corrections. In: J. Chem. Phys. 122 (2005), Nr. 20, S. 204102. – URL http://scitation.aip.org/content/aip/journal/jcp/122/20/10.1063/1.1906203

[40] GROBE, R. ; EBERLY, J. H.: Photoelectron spectra for a two-electron system in a strong laser field. In: Phys. Rev. Lett. 68 (1992), May, S. 2905–2908. – URL http://link.aps.org/doi/10.1103/PhysRevLett.68.2905

[41] HAAN, S. L. ; GROBE, R. ; EBERLY, J. H.: Numerical study of autoionizing states in completely correlated two-electron systems. In: Phys. Rev. A 50 (1994), Jul, Nr. 1, S. 378–391. – URL http://dx.doi.org/10.1103/PhysRevA.50.378. – ISSN 1094-1622

[42] HANUSCH, A. ; RAPP, J. ; BRICS, M. ; BAUER, D.: Time-dependent renormalized-natural-orbital theory applied to laser-driven H_2^+. In: Phys. Rev. A xx (2016), XX, S. XX. – URL http://link.aps.org/doi/10.1103/PhysRevA.XX

[43] HELBIG, N. ; FUKS, J.I. ; TOKATLY, I.V. ; APPEL, H. ; GROSS, E.K.U. ; RUBIO, A.: Time-dependent density-functional and reduced density-matrix methods for few electrons: Exact versus adiabatic approximations. In: Chem. Phys. 391 (2011), Nr. 1, S. 1–10. – URL http://www.sciencedirect.com/science/article/pii/S0301010411002485. – ISSN 0301-0104

[44] HINZ, C M. ; BAUCH, S ; BONITZ, M: Instabilities and inaccuracies of multi-configuration time-dependent Hartree-Fock. In: Journal of Physics: Conference Series 696 (2016), Nr. 1, S. 012009. – URL http://stacks.iop.org/1742-6596/696/i=1/a=012009

[45] HOCHSTUHL, D. ; HINZ, C.M. ; BONITZ, M.: Time-dependent multiconfiguration methods for the numerical simulation of photoionization processes of many-electron atoms. In: Eur. Phys. J. Spec. Top. 223 (2014), Jan, Nr. 2, S. 177–336. – URL http://dx.doi.org/10.1140/epjst/e2014-02092-3. – ISSN 1951-6401

[46] HOCHSTUHL, David ; BAUCH, Sebastian ; BONITZ, Michael: Multiconfigurational time-dependent Hartree-Fock calculations for photoionization of one-dimensional Helium. In: J. Phys. Conf. Ser. 220 (2010), Nr. 1, S. 012019. – URL http://stacks.iop.org/1742-6596/220/i=1/a=012019

[47] HOCHSTUHL, David ; BONITZ, Michael: Time-dependent restricted-active-space configuration-interaction method for the photoionization of many-electron atoms. In: Phys. Rev. A 86 (2012), Nov, Nr. 5, S. 86.053424. – URL http://dx.doi.org/10.1103/PhysRevA.86.053424. – ISSN 1094-1622

[48] HOHENBERG, P. ; KOHN, W.: Inhomogeneous Electron Gas. In: Phys. Rev. 136 (1964), Nov, S. B864–B871. – URL http://link.aps.org/doi/10.1103/PhysRev.136.B864

[49] ISHIKAWA, Kenichi ; SATO, Takeshi: A Review on Ab Initio Approaches for Multielectron Dynamics. In: IEEE J. Sel. Topics Quantum Electron. 21 (2015), Jun, Nr. 5, S. 1–1. – URL http://dx.doi.org/10.1109/JSTQE.2015.2438827. – ISSN 1558-4542

[50] KARAMATSKOU, Antonia ; PABST, Stefan ; CHEN, Yi-Jen ; SANTRA, Robin: Calculation of photoelectron spectra within the time-dependent configuration-interaction singles scheme. In: Phys. Rev. A 89 (2014), Mar, Nr. 3, S. 033415. – URL http://dx.doi.org/10.1103/PhysRevA.89.033415. – ISSN 1094-1622

[51] KIRKWOOD, John G.: The Statistical Mechanical Theory of Transport Processes I. General Theory. In: J. Chem. Phys. 14 (1946), Nr. 3, S. 180–201. – URL http://scitation.aip.org/content/aip/journal/jcp/14/3/10.1063/1.1724117

[52] KIRKWOOD, John G.: The Statistical Mechanical Theory of Transport Processes II. Transport in Gases. In: J. Chem. Phys. 15 (1947), Nr. 1, S. 72–76. – URL http://scitation.aip.org/content/aip/journal/jcp/15/1/10.1063/1.1746292

[53] KLYACHKO, Alexander A.: Quantum marginal problem and N-representability. In: Journal of Physics: Conference Series 36 (2006), Nr. 1, S. 72. – URL http://stacks.iop.org/1742-6596/36/i=1/a=014

[54] KOHN, W.: Nobel Lecture: Electronic structure of matter¯wave functions and density functionals. In: Rev. Mod. Phys. 71 (1999), Oct, S. 1253–1266. – URL http://link.aps.org/doi/10.1103/RevModPhys.71.1253

[55] KOHN, W. ; SHAM, L. J.: Self-Consistent Equations Including Exchange and Correlation Effects. In: Phys. Rev. 140 (1965), Nov, S. A1133–A1138. – URL http://link.aps.org/doi/10.1103/PhysRev.140.A1133

[56] KRAUSE, Jeffrey L. ; SCHAFER, Kenneth J. ; KULANDER, Kenneth C.: Calculation of photoemission from atoms subject to intense laser fields. In: Phys. Rev. A 45 (1992), Apr, S. 4998–5010. – URL http://link.aps.org/doi/10.1103/PhysRevA.45.4998

[57] KUMMER, Hans: n-Representability Problem for Reduced Density Matrices. In: J. Math. Phys. 8 (1967), Nr. 10, S. 2063–2081. – URL http://scitation.aip.org/content/aip/journal/jmp/8/10/10.1063/1.1705122

[58] KURZWEIL, Yair ; BAER, Roi: Quantum memory effects in the dynamics of electrons in gold clusters. In: Phys. Rev. B 73 (2006), Feb, S. 075413. – URL http://link.aps.org/doi/10.1103/PhysRevB.73.075413

[59] KURZWEIL, Yair ; BAER, Roi: Adapting approximate-memory potentials for time-dependent density functional theory. In: Phys. Rev. B 77 (2008), Feb, S. 085121. – URL http://link.aps.org/doi/10.1103/PhysRevB.77.085121

[60] LACKNER, Fabian ; BŘEZINOVÁ, Iva ; SATO, Takeshi ; ISHIKAWA, Kenichi L. ; BURGDÖRFER, Joachim: Propagating two-particle reduced density matrices without wave functions. In: Phys. Rev. A 91 (2015), Feb, S. 023412. – URL http://link.aps.org/doi/10.1103/PhysRevA.91.023412

[61] LAPPAS, Demetris G. ; LEEUWEN, Robert van: Electron correlation effects in the double ionization of He. In: J. Phys. B 31 (1998), Mar, S. L249. – URL http://iopscience.iop.org/0953-4075/31/6/001/

[62] LEEUWEN, Robert van: Mapping from Densities to Potentials in Time-Dependent Density-Functional Theory. In: Phys. Rev. Lett. 82 (1999), May, S. 3863–3866. – URL http://link.aps.org/doi/10.1103/PhysRevLett.82.3863

[63] LEIN, Manfred ; KÜMMEL, Stephan: Exact Time-Dependent Exchange-Correlation Potentials for Strong-Field Electron Dynamics. In: Phys. Rev. Lett. 94 (2005), Apr, Nr. 14, S. 143003. – URL http://dx.doi.org/10.1103/PhysRevLett.94.143003. – ISSN 1079-7114

[64] LOPEZ, Xabier ; PIRIS, Mario ; RUIPÉREZ, Fernando ; UGALDE, Jesus M.: Performance of PNOF6 for Hydrogen Abstraction Reactions. In: J. Phys. Chem. A 119 (2015), Nr. 27, S. 6981–6988. – URL http://dx.doi.org/10.1021/acs.jpca.5b01585. – PMID: 26065935

[65] LÖWDIN, Per-Olov: Quantum Theory of Many-Particle Systems. I. Physical Interpretations by Means of Density Matrices, Natural Spin-Orbitals, and Convergence Problems in the Method of Configurational Interaction. In: Phys. Rev. 97 (1955), Mar, Nr. 6, S. 1474–1489. – URL http://dx.doi.org/10.1103/PhysRev.97.1474. – ISSN 0031-899X

[66] MAITRA, N. T. ; TODOROV, T. N. ; WOODWARD, C. ; BURKE, K.: Density-potential mapping in time-dependent density-functional theory. In: Phys. Rev. A 81 (2010), Apr, S. 042525. – URL http://link.aps.org/doi/10.1103/PhysRevA.81.042525

[67] MAITRA, Neepa T.: Memory: History , Initial-State Dependence , and Double-Excitations. In: MARQUES, Miguel A. (Hrsg.) ; MAITRA, Neepa T. (Hrsg.) ; NOGUEIRA, Fernando M. (Hrsg.) ; GROSS, E.K.U. (Hrsg.) ; RUBIO, Angel (Hrsg.): Fundamentals of Time-Dependent Density Functional Theory. Springer Science + Business Media, 2012 (Lecture Notes in Physics), S. 167–184. – URL http://dx.doi.org/10.1007/978-3-642-23518-4_8. – ISBN http://id.crossref.org/isbn/978-3-642-23518-4

[68] MAITRA, Neepa T. ; ZHANG, Fan ; CAVE, Robert J. ; BURKE, Kieron: Double excitations within time-dependent density functional theory linear response. In: J. Chem. Phys. 120 (2004), Nr. 13, S. 5932. – URL http://dx.doi.org/10.1063/1.1651060. – ISSN 0021-9606

[69] MAYER, Joseph E.: Electron Correlation. In: Phys. Rev. 100 (1955), Dec, S. 1579–1586. – URL http://link.aps.org/doi/10.1103/PhysRev.100.1579

[70] MAZZIOTTI, David A.: Two-Electron Reduced-Density-Matrix Theory: With Application to Many-Electron Atoms and Molecules. Hoboken, New Jersy : John Wiley & Sons, Inc., Mar 2007 (Advances in Chemical Physics). – URL http://dx.doi.org/10.1002/0470106603. – ISBN http://id.crossref.org/isbn/9780471790563

[71] MAZZIOTTI, David A.: Structure of Fermionic Density Matrices: Complete N-Representability Conditions. In: Phys. Rev. Lett. 108 (2012), Jun, S. 263002. – URL http://link.aps.org/doi/10.1103/PhysRevLett.108.263002

[72] MIZUNO, Yukio ; IZUYAMA, Takeo: Remarks on Mayer's Reduced Density Matrix Method. In: Prog. Theor. Phys. 18 (1957), Jul, Nr. 1, S. 33–38. – URL http://dx.doi.org/10.1143/PTP.18.33. – ISSN 0033-068X

[73] MÜLLER, A.M.K.: Explicit approximate relation between reduced two- and one-particle density matrices. In: Phys. Lett. A 105 (1984), Nr. 9, S. 446 – 452. – URL http://www.sciencedirect.com/science/article/pii/037596018491034X. – ISSN 0375-9601

[74] PABST, Stefan ; SANTRA, Robin: Strong-Field Many-Body Physics and the Giant Enhancement in the High-Harmonic Spectrum of Xenon. In: Phys. Rev. Lett. 111 (2013), Dec, Nr. 23, S. 233005. – URL http://dx.doi.org/10.1103/PhysRevLett.111.233005. – ISSN 1079-7114

[75] PERDEW, John P. ; PARR, Robert G. ; LEVY, Mel ; BALDUZ, Jose L.: Density-Functional Theory for Fractional Particle Number: Derivative Discontinuities of the Energy. In: Phys. Rev. Lett. 49 (1982), Dec, S. 1691–1694. – URL http://link.aps.org/doi/10.1103/PhysRevLett.49.1691

[76] PIRIS, M. ; MATXAIN, J. M. ; LOPEZ, X.: The intrapair electron correlation in natural orbital functional theory. In: J. Chem. Phys. 139 (2013), Nr. 23, S. 234109. – URL http://scitation.aip.org/content/aip/journal/jcp/139/23/10.1063/1.4844075

[77] RAPP, J. ; BRICS, M. ; BAUER, D.: Equations of motion for natural orbitals of strongly driven two-electron systems. In: Phys. Rev. A 90 (2014), Jul, S. 012518. – URL http://link.aps.org/doi/10.1103/PhysRevA.90.012518

[78] ROSINA, M.: Untitled. In: COLEMAN, A. J. (Hrsg.) ; ERDAHL, R. M. (Hrsg.): Reduced Density Operators with Application to Physical and Chemical Systems Bd. 11. Queen's University, Kingston, Ontario, 1968

[79] RUGGENTHALER, M. ; BAUER, D.: Rabi Oscillations and Few-Level Approximations in Time-Dependent Density Functional Theory. In: Phys. Rev. Lett. 102 (2009), Jun, S. 233001. – URL http://link.aps.org/doi/10.1103/PhysRevLett.102.233001

[80] RUNGE, Erich ; GROSS, E. K. U.: Density-Functional Theory for Time-Dependent Systems. In: Phys. Rev. Lett. 52 (1984), Mar, S. 997–1000. – URL http://link.aps.org/doi/10.1103/PhysRevLett.52.997

[81] SAND, Andrew M. ; MAZZIOTTI, David A.: Enhanced computational efficiency in the direct determination of the two-electron reduced density matrix from the anti-Hermitian contracted Schrödinger equation with application to ground and excited states of conjugated π-systems. In: J. Chem. Phys. 143 (2015), Nr. 13, S. 134110. – URL http://scitation.aip.org/content/aip/journal/jcp/143/13/10.1063/1.4931471

[82] SATO, Takeshi ; ISHIKAWA, Kenichi L.: Time-dependent complete-active-space self-consistent-field method for multielectron dynamics in intense laser fields. In: Phys. Rev. A 88 (2013), Aug, Nr. 2, S. 023402. – URL http://dx.doi.org/10.1103/PhysRevA.88.023402. – ISSN 1094-1622

[83] SATO, Takeshi ; ISHIKAWA, Kenichi L.: The structure of approximate two electron wavefunctions in intense laser driven ionization dynamics. In: J. Phys. B 47 (2014), Oct, Nr. 20, S. 204031. – URL http://dx.doi.org/10.1088/0953-4075/47/20/204031. – ISSN 1361-6455

[84] SATO, Takeshi ; ISHIKAWA, Kenichi L.: Time-dependent multiconfiguration self-consistent-field method based on the occupation-restricted multiple-active-space model for multielectron dynamics in intense laser fields. In: Phys. Rev. A 91 (2015), Feb, Nr. 2, S. 023417. – URL http://dx.doi.org/10.1103/PhysRevA.91.023417. – ISSN 1094-1622

[85] SCHULTZ, Thomas ; VRAKKING, Marc: Attosecond and XUV Spectroscopy: Ultrafast Dynamics and Spectroscopy. Weinheim : John Wiley & Sons, Jan 2014. – URL http://dx.doi.org/10.1002/9783527677689. – ISBN http://id.crossref.org/isbn/9783527411245

[86] SCRINZI, Armin: Infinite-range exterior complex scaling as a perfect absorber in time-dependent problems. In: Phys. Rev. A 81 (2010), May, S. 053845. – URL http://link.aps.org/doi/10.1103/PhysRevA.81.053845

[87] SHARMA, S. ; DEWHURST, J. K. ; LATHIOTAKIS, N. N. ; GROSS, E. K. U.: Reduced density matrix functional for many-electron systems. In: Phys. Rev. B 78 (2008), Nov, S. 201103. – URL http://link.aps.org/doi/10.1103/PhysRevB.78.201103

[88] SHUN-JIN, Wang ; CASSING, W: Explicit treatment of N-body correlations within a density-matrix formalism. In: Annals of Physics 159 (1985), Nr. 2, S. 328 – 350. – URL http://www.sciencedirect.com/science/article/pii/0003491685901162. – ISSN 0003-4916

[89] SURJÁN, Péter R.: An Introduction to the Theory of Geminals. S. 63–88. In: SURJÁN, Péter R. (Hrsg.) ; BARTLETT, R. J. (Hrsg.) ; BOGÁR, F. (Hrsg.) ; COOPER, D. L. (Hrsg.) ; KIRTMAN, B. (Hrsg.) ; KLOPPER, W. (Hrsg.) ; KUTZELNIGG, W. (Hrsg.) ; MARCH, N. H. (Hrsg.) ; MEZEY, P. G. (Hrsg.) ; MÜLLER, H. (Hrsg.) ; NOGA, J. (Hrsg.) ; PALDUS, J. (Hrsg.) ; PIPEK, J. (Hrsg.) ; RAIMONDI, M. (Hrsg.) ; RØEGGEN, I. (Hrsg.) ; SUN, J. Q. (Hrsg.) ; SURJÁN, P. R. (Hrsg.) ; VALDEMORO, C. (Hrsg.) ; VOGTNER, S. (Hrsg.): Correlation and Localization. Berlin, Heidelberg : Springer Berlin Heidelberg, 1999. – URL http://dx.doi.org/10.1007/3-540-48972-X_4. – ISBN 978-3-540-48972-6

[90] THEOPHILOU, Iris ; LATHIOTAKIS, Nektarios N. ; MARQUES, Miguel A. L. ; HELBIG, Nicole: Generalized Pauli constraints in reduced density matrix functional theory. In: The Journal of Chemical Physics 142 (2015), Nr. 15, S. 154108. – URL http://scitation.aip.org/content/aip/journal/jcp/142/15/10.1063/1.4918346

[91] TREDGOLD, R. H.: Density Matrix and the Many-Body Problem. In: Phys. Rev. 105 (1957), Mar, S. 1421–1423. – URL http://link.aps.org/doi/10.1103/PhysRev.105.1421

[92] ULLRICH, Carsten A.: Time-Dependent Density-Functional Theory: Concepts and Applications. Oxford : Oxford University Press, Dec 2011. – URL http://dx.doi.org/10.1093/acprof:oso/9780199563029.001.0001. – ISBN http://id.crossref.org/isbn/9780199563029

[93] ULLRICH, Carsten A. ; BANDRAUK, André D.: Atoms and Molecules in Strong Laser Fields. In: MARQUES, Miguel A. (Hrsg.) ; MAITRA, Neepa T. (Hrsg.) ; NOGUEIRA, Fernando M. (Hrsg.) ; GROSS, E.K.U. (Hrsg.) ; RUBIO, Angel (Hrsg.): Fundamentals of Time-Dependent Density Functional Theory. Springer Science + Business Media, 2012 (Lecture Notes in Physics), S. 351–371. – URL http://dx.doi.org/10.1007/978-3-642-23518-4_18. – ISBN http://id.crossref.org/isbn/978-3-642-23518-4

[94] ULLRICH, Carsten A. ; YANG, Zeng-Hui: A Brief Compendium of Time-Dependent Density Functional Theory. In: Braz. J. Phys. 44 (2013), Jul, Nr. 1, S. 154–188. – URL http://dx.doi.org/10.1007/s13538-013-0141-2. – arXiv:1305.1388. – ISSN 1678-4448

[95] WIJEWARDANE, H. O. ; ULLRICH, C. A.: Time-Dependent Kohn-Sham Theory with Memory. In: Phys. Rev. Lett. 95 (2005), Aug, S. 086401. – URL http://link.aps.org/doi/10.1103/PhysRevLett.95.086401

[96] WIJEWARDANE, H. O. ; ULLRICH, C. A.: Real-Time Electron Dynamics with Exact-Exchange Time-Dependent Density-Functional Theory. In: Phys. Rev. Lett. 100 (2008), Feb, S. 056404. – URL http://link.aps.org/doi/10.1103/PhysRevLett.100.056404

[97] WILKEN, F. ; BAUER, D.: Adiabatic Approximation of the Correlation Function in the Density-Functional Treatment of Ionization Processes. In: Phys. Rev. Lett. 97 (2006), Nov, S. 203001. – URL http://link.aps.org/doi/10.1103/PhysRevLett.97.203001

[98] WILKEN, F. ; BAUER, D.: Momentum distributions in time-dependent density-functional theory: Product-phase approximation for nonsequential double ionization in strong laser fields. In: Phys. Rev. A 76 (2007), Aug, S. 023409. – URL http://link.aps.org/doi/10.1103/PhysRevA.76.023409

[99] YANG, Zeng-hui ; MAITRA, Neepa T. ; BURKE, Kieron: Effect of Cusps in Time-Dependent Quantum Mechanics. In: Phys. Rev. Lett. 108 (2012), Feb, S. 063003. – URL http://link.aps.org/doi/10.1103/PhysRevLett.108.063003

[100] YVON, J.: La Théorie Statistique des Fluides et l'Équation d'Etat, Actualités Scientifiques et Industrialles. Bd. 203. Paris : Hermann, 1935

[101] ZANGHELLINI, Jürgen ; KITZLER, Markus ; BRABEC, Thomas ; SCRINZI, Armin: Testing the multi-configuration time-dependent Hartree–Fock method. In: J. Phys. B 37 (2004), Nr. 4, S. 763. – URL http://stacks.iop.org/0953-4075/37/i=4/a=004

[102] ZIELINSKI, Alejandro ; MAJETY, Vinay P. ; SCRINZI, Armin: Double photoelectron momentum spectra of helium at infrared wavelength. In: Phys. Rev. A 93 (2016), Feb, S. 023406. – URL http://link.aps.org/doi/10.1103/PhysRevA.93.023406

[103] ZIESCHE, P.: On relations between correlation, fluctuation and localization. In: J. Mol, Struct. 527 (2000), Nr. 1–3, S. 35 –50. – URL http://www.sciencedirect.com/science/article/pii/S0166128000004760. – ISSN 0166-1280